Effect of elevated strain rates on the mechanical performance of polyethylene structures

J P J Coulton

A thesis submitted for the degree of Doctor of Philosophy

Department of Engineering
University of Warwick

May 1996

Summary

The theme of this research was the development of an integrated approach to establish how the stiffness of a thermoplastic material could be measured and modelled for use in impact simulations. By undertaking this an understanding was obtained of how thermoplastic materials behave and the structures that are made from them perform when subjected to mechanical impact loads.

A series of tensile tests was undertaken using three control methods to establish a tensile test control method suitable for a wide range of strain rates. The effect of applied strain rate on the mechanical performance of High Density Polyethylene (HDPE), as illustrated by the tensile stress-strain curve, was investigated. Tests were performed at various elongation rates and temperatures to simulate different practical operating conditions. Extensive use of the finite element method was made in simulating the mechanical impact performance of various beam, disc and automotive fuel tank structures with the predictions of these analyses being correlated with experimental test data.

The research is novel and of direct practical relevance as indicated by the prediction and correlation with experimental data, of the impact performance of a HDPE fuel tank, which to the author's knowledge has not been previously done. The demonstrated methodology thus provides a significant advance in the prediction of the impact performance of components made from polymers, whose mechanical performance is strain rate sensitive.

Index

List of Contents

List of Figures

List of Tables

Acknowledgements

I would like to thank my supervisor Dr G Smith for his guidance during my studies and in the preparation of this thesis. Special thanks are also due to Dr J Wallbank for his valuable advice .

This thesis is based upon research undertaken by the author in work package 2a "non-linear design behaviour and the effect of elevated strain rates" of the EPIC (Engineering Polymers - Integrated Capability) programme. This programme was a club based research consortium based at the Manufacturing Group, University of Warwick. Costing £2.6 m over 3 years and part funded by the DTI under the general collaborative programme, it produced significant technological innovations in six closely linked areas associated with the use of engineering polymers and polymer composites in high volume structural components. The collaborative partners of work package 2a were The Rover Group and Ove Arup and Partners for whose support the author is indebted. I would also like to express my thanks to the following BASF, Wilmid and Solvay Automotive for their support in the supply of materials.

Finally I would like to thank my wife Joy for all her support and encouragement.

Declaration

I declare that all the work described in this report was undertaken by myself (unless otherwise acknowledged in the text) and that none of the work has been previously submitted for any academic degree. All sources of quoted information have been acknowledged by means of references.

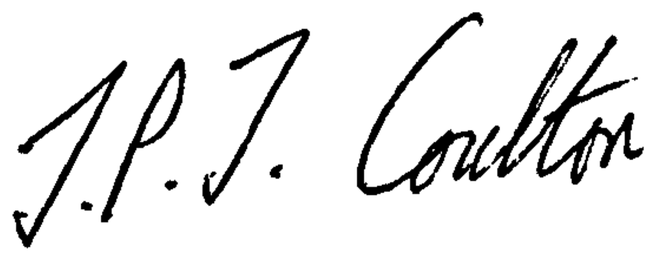

J P J Coulton

May 1996

Abbreviations

ATC	Advanced Technology Centre
CAD	Computer aided design
CAMPUS	Computer aided material preselection by uniform standards
C/H	Crosshead
DMA	Dynamic mechanic analysis
GPIB	General purpose interface bus
HDPE	High density polyethylene
HSR	High Strain Rate
IMC	International Manufacturing Centre
LDPE	Low density polyethylene
LVDT	Linear-variable Displacement Transducer
MDPE	Medium density polyethylene
NPL	National Physical Laboratory
PC	Personal Computer
SHPB	Split Hopkins pressure bar
SSR	Slow Strain Rate
SSRN	Sample Strain Resolution

Variables

f_n	Resonant frequency
l	Deformation
m_1	Initial bi-linear curve fit modulus
m_2	Secondary bi-linear curve fit modulus
p	Load
t	Time
tan δ	Damping loss factor where δ is the phase angle between stress and strain
A	Cross sectional area
E	Initial low strain material modulus
E_a	Activation energy
F	Force
H	Enthalpy
R	Universal gas constant
T	Temperature
$\dot{\delta}$	Crosshead deformation rate
ε	Strain
ε_{eng}	Engineering strain
$\dot{\varepsilon}$	Strain rate
$\dot{\varepsilon}_o$	Strain rate constant for Eyring flow theory
ε_n	Strain to onset of neck formation
σ	Stress
σ_{eng}	Engineering stress

σ_f	Flow stress
σ_n	Stress at the onset of neck formation
σ_{vm}	Von Mises equivalent stress
σ_y	Yield stress as determined by a bi-linear curve fit
τ	Shear stress
υ	Poisson's Ratio
ω	Frequency
Δ	Logarithmic decay rate of mechanical damping

Chapter 1

Introduction

The first mass produced passenger vehicle which used a thermoplastic fuel tank, made from high density polyethylene (HDPE), was the VW Passat in November 1973. Since then the use of thermoplastics for fuel tanks has increased to approximately 70%, 25% and 5% respectively of current (1992) European, US and Japanese passenger vehicle production [1] and this growth is expected to continue [2]. In 1969 before thermoplastic fuel tanks were used in production vehicles, guidelines were published by the German authorities to ensure their safety [3]. As it was known that thermoplastics became brittle at low temperatures subject to impact loadings, the 6 m drop test used to qualify thermoplastic chemical drums was carried over and incorporated into the safety regulations [3]. This was despite the fact that the 6 m drop test at -40° C is not representative of the in-service conditions. At this time it was not feasible to undertake structural analyses of the impact performance of thermoplastic fuel tanks; thus tanks were developed on a "make and test" principle.

Thermoplastic materials do not have a constant Young's modulus or yield point, as they are dependent of loading rate, thus all design analyses must include loading rate effects. As the stiffness of thermoplastic materials is much less than that of metals it is necessary to load these materials to higher strains than the equivalent metal counterparts in order to effectively utilise them for structural applications. At large strains their stress-strain behaviour is distinctly nonlinear with thermoplastic components exhibiting membrane stiffening and large displacement effects. It is therefore necessary to include these nonlinear effects into design analyses in order to accurately predict the performance of thermoplastic components.

Previous techniques developed at the University of Warwick's Advanced Technology Centre (ATC) [4,5] for using rate dependent non-linear material stiffness to predict the performance of thermoplastic components were based on the "anticipated" strain rate and are therefore limited. To overcome this limitation a snapshot analysis method based on the use of creep data was developed [6]. However this approach is limited to steady state load cases and can not predict the unloading event. However, this method has been successfully used by the author to determine the long term deformation behaviour of automotive radiator header and fuel tanks under load [7].

Prior to making a thermoplastic component it would be a strategic economic advantage if the proposed component's response to impact events could be predicted. Although this has not been done in the past, because of the lack of suitable computer hardware and software [8], this has now become feasible and is demonstrated herein.

1.1 The growing importance of impact analysis

Crashworthiness predictions are of strategic advantage to automotive manufacturers and these predictions will become increasingly important if the concept of the ultra light vehicle is to become a reality. This is because presently occupant crash protection is greater in larger vehicles than smaller vehicles and it is desirable to design light weight vehicles with greater occupant crash protection than today's large cars [9].

To achieve the goals of the American "Partnership for a new Generation of Vehicle" [10] and its European Equivalent [11] it will be necessary to develop tools to

predict the crash performance of an ultra light weight vehicle and hence the occupants crash protection. It is envisaged that this and other vehicles will use significant quantities of polymers and polymeric composites. To utilise these materials effectively as part of a comprehensive energy absorbing impact resistant structure they must be sufficiently characterised for use in structural performance predictions. Some generic tools are already available but the development of polymeric and composite material models still poses a difficulty and requires additional work [12].

1.2 Information required for an impact analysis

Prediction of crash worthiness of a component or assembly is an area in which not all the parameters are known and there are many gaps in fundamental knowledge. These are summarised as [13]:

1) penetration mechanics;

2) collision mechanics;

3) stress analysis and numerical modelling;

4) residual strength of impact-damaged structures;

5) material performance at high strain rates;

To undertake a structural simulation of a proposed thermoplastic component, subject to an impact event, the following precursors are necessary:

1) definition of the components geometry;

2) definition of the components wall thicknesses and distribution;

3) material properties of the thermoplastic for the proposed environment and at the expected strain rates;

4) definition of the loading event;

5) suitable software and hardware to undertake the analysis.

Current available computer aided design (CAD) software can readily model the complicated geometrical shapes that are usually required to define a component's geometry. This geometry can then be used to generate the tool paths required to manufacture the mould. In the case of injection moulded thermoplastic components as both of the mould surfaces are defined the wall thickness of the component is known prior to manufacture. An important number of thermoplastic components are not made by injection moulding but by blow moulding and for these components the wall thickness is not predefined by the twin surfaces of a mould. The majority of large pressure vessels such as automotive thermoplastic fuel tanks are made by the blow moulding process with the rest being rotationally moulded. Although the moulds for rotational moulding are cheaper and the process produces a more consistent wall thickness, blow moulding is quicker and a cheaper method for mass production and the polymer grade that is used has superior mechanical performance. Thus the majority of tanks are made by blow moulding and the definition of the tank's wall thicknesses would need to be determined by a numerical simulation of this process. It is known that two major material suppliers, BASF [14] and Solvay [15], have developed and use blow moulding simulation tools to predict wall thickness and that the software company AC Technology are preparing to launch C-PITA, a simulation tool [16].

For an impact analysis a knowledge of the whole of the true stress-strain curve to failure is necessary. This is known to be strain rate, temperature and history dependent. Currently it is not known how accurate the measurements have to be and how to collate the information into a suitable material model for an impact analysis. Consequently the problem of material property measurement and use in impact analyses has been identified as an area suitable for research [13,17].

The definition of loading in an impact event is normally one where either the component, travelling at a known velocity strikes a very much more massive object or is struck by an object of known stiffness, mass and energy. Typical impact loading events for thermoplastic components on vehicles can be identified from all current known and proposed international standards and legislation e.g.[3,18].

There is a wide range of available software that could be used for the non-linear analysis of the impact events, e.g. OASYS LS-DYNA3D [19], PAMCRASH [20] or ABAQUS explicit [21]. However the limiting factor in the choice of software would be the availability of suitable material models or the ability to create suitable material models within the software.

1.3 Aims of this thesis

Having established that there is a need to ascertain how the mechanical characteristics of thermoplastics should be measured and modelled for inclusion in impact simulations [12,13,17], this thesis endeavours to establish how the material stiffness can be measured and collated into a material model for use in impact simulations. As there

are a wide variety of thermoplastic materials for which an exhaustive survey would take a prohibitively long time, this work has concentrated on one specific type of thermoplastic material, high density polyethylene (HDPE), which is widely used in a range of structural applications such as automotive fuel tanks, gas and water pipes. The temperature and strain rate ranges of consideration are -40 to 23° C and $1x10^{-4}$ to 20 s^{-1}.

Before considering how the material behaviour of thermoplastic materials should be modelled, it is necessary to understand typical material measurement techniques which could be used to determine the effect of strain rate and temperature on the mechanical performance of thermoplastics. Through understanding the test measurement techniques the test results can be assessed to establish how ambient temperature and applied strain rate effect the mechanical performance of thermoplastics. Only then can the analytical simulation of elevated strain rate events, as applied to thermoplastic components, be examined to establish what material modelling techniques have been used and whether these were appropriate or not.

Chapter 2

Review of material testing techniques

The testing of thermoplastics to obtain data for the simulation of the in-service mechanical performance of thermoplastic components and the correlation with test results is not well understood by the majority of the thermoplastics industry. This has resulted in the majority of mechanical testing being done to compare materials and not to supply data for design purposes. Thus despite there being a past conference targeted to solve this problem [22] the role of materials testing within the design and development process is still being debated [23]. Documents such as those supplied by BASF and Hoechst Celanese [24,25] provide an insight into material testing methods and basic design methods for thermoplastic parts [25,26,27,28]. These however do not provide quantitative information on how to predict the impact performance of thermoplastic components.

The required material properties for an impact simulation of a thermoplastic component are those which can be used to define a three dimensional material model describing the stress-strain curve to failure. However there is no one single test configuration which is suitable for testing materials in all three orthogonal axes and in both tension and compression. Furthermore it is normal to characterise the stress-strain curve of a material by a number of nominal parameters, for example initial low strain elastic modulus (E), stress at the onset of neck formation (σ_n) and strain to onset of neck formation (ε_n) [25]. The ideal test method would be: quick, accurate, insensitive to sample preparation and low cost. However all test methods have limitations and prior to using material stiffness and strength measurements it is necessary to understand how they were measured. In general there are three basic methods for measuring polymeric material stiffness and strength: quasi static,

creep/relaxation and dynamic which are reviewed briefly. For all tests it should be noted that although it is desired that test samples are normally subjected to one dimensional quasi static loads both test samples and test equipment are three dimensional objects and have distributed mass, stiffness and damping. Thus there are always the potential undesired complications due to deviations from one dimensional to three dimensional specimen loading and quasi static to dynamic loading of both specimen and test equipment.

2.1 Definition of stress and strain

There are several commonly used definitions of stress and strain [29]. During the early 1980's it was the author's experience that the aerospace industry would only undertake linear analyses to predict the static and dynamic performance of structures. If it was predicted that either the applied load exceeded the proportional limit of the material or the deformation of the structure was gross and thus likely to be non-linear then the design was deemed to have "failed" by exceeding the design brief. This design brief was set as non-linear analyses could not be achieved within the available cost and design cycle time scales. Thus when it was necessary to characterise new material only the linear elastic material properties were measured with the onset of non-linearity being defined as failure (non acceptable material behaviour). The most common mechanical test undertaken for material samples is the tensile test. As this test has been developed for metals the common measurements from this test reflect the small strain nature of the properties that the test definers desired to measure. The standard way of converting load and deformation, in the tensile test, to stress and strain is to divide the load by the original cross sectional area of the specimen to

obtain stress and divide the extension of the specimen by the original gauge length over which it was measured to obtain strain. These are known as the engineering or Cauchy definitions of stress and strain.

$$\sigma_{eng} = \frac{F}{A_o} \quad ; \quad \epsilon_{eng} = \frac{l - l_o}{l_o} = \frac{\Delta l}{l_o} \tag{1}$$

Figure 2.1 shows the typical engineering stress-strain curves measured, using a screw driven tensile test machine, for ductile and high strength concrete reinforcing bars.

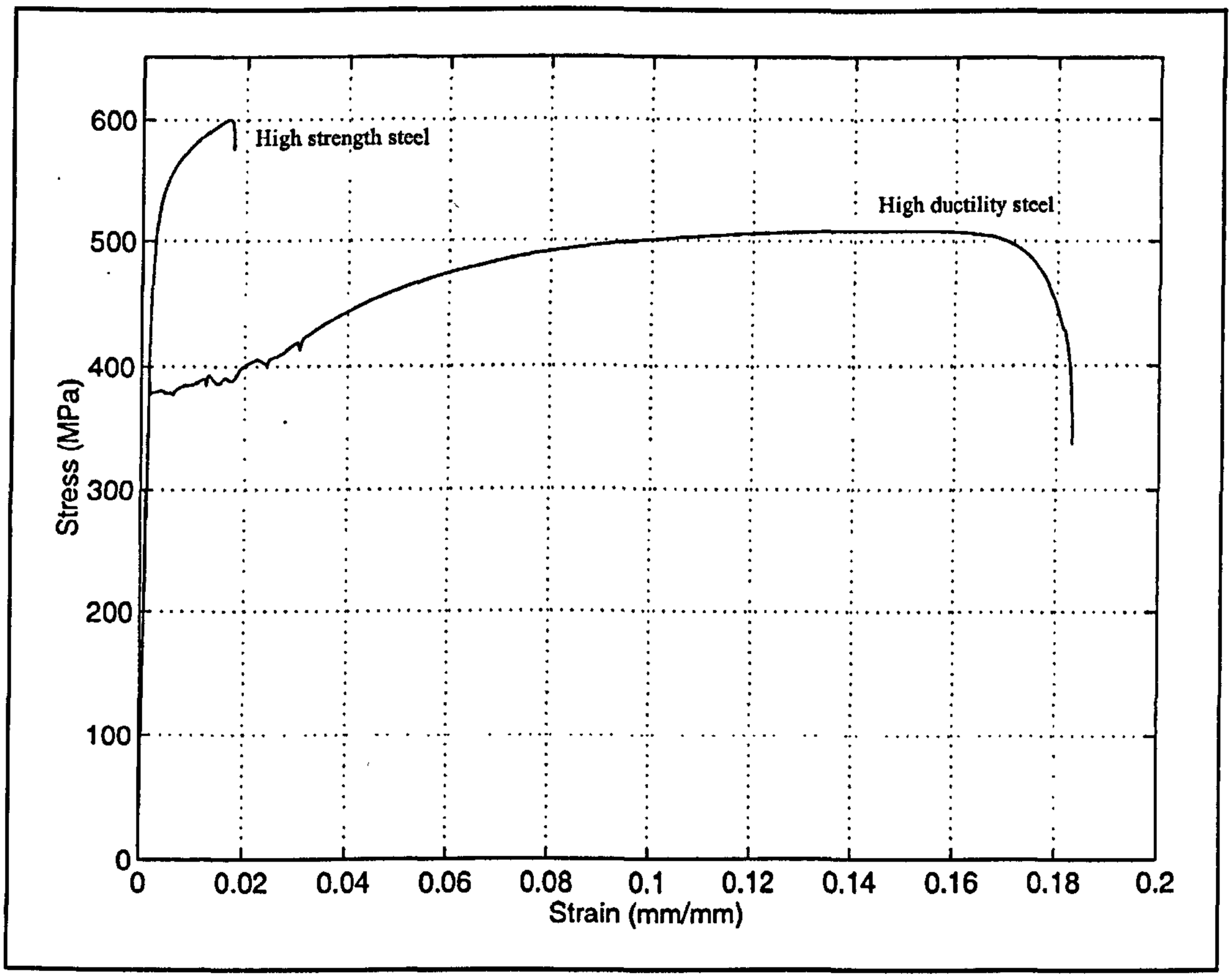

Figure 2.1 Typical steel stress-strain curves

Below the onset of yield the material stiffness is normally described by a modulus of elasticity defined as follows: "The modulus of elasticity, or Young's modulus, is the

slope of the stress-strain curve in the elastic region. This relationship is Hooke's law" [30].

$$E = \frac{\Delta \sigma_{eng}}{\Delta \epsilon_{eng}} \tag{2}$$

Likewise the lateral strains induced in the tensile test are characterised by Poisson's ratio defined as the ratio of "longitudinal elastic deformation produced by a simple tensile or compressive stress to the lateral deformation that must simultaneously occur" [30].

$$\nu = \frac{-\epsilon_{lateral}}{\epsilon_{longnitudinal}} \tag{3}$$

It should be noted that these are engineering measures and only applicable to small strain theory. If it is wished to go beyond small strain theory, which is generally the case when using thermoplastics, then the definition of stress and strain must be redefined to be mathematically correct. These are known as the true or Hencky definitions of stress and strain [29].

$$\sigma = \frac{F}{A} \quad ; \quad \epsilon = \int_{l_o}^{l} \frac{d\,l}{l} = \ln\left(\frac{l}{l_0}\right) \tag{4}$$

Similarly redefining of modulus of elasticity allows it to be non-linear and non-elastic.

$$E = \frac{d\,\sigma}{d\,\epsilon} \tag{5}$$

As the applied strain approaches zero, the true definitions for stress, strain and modulus approach their engineering definitions.

2.2 Quasi static tests

In quasi static testing it is desired to keep the strain rate of the material constant such that inertial disturbance effects are negligible. The most widely used quasi static methods are the tensile, bending and compression methods. By varying the ambient temperature and applied deformation rate the effect of these parameters on the material stiffness and strength can be investigated.

2.2.1 Tensile

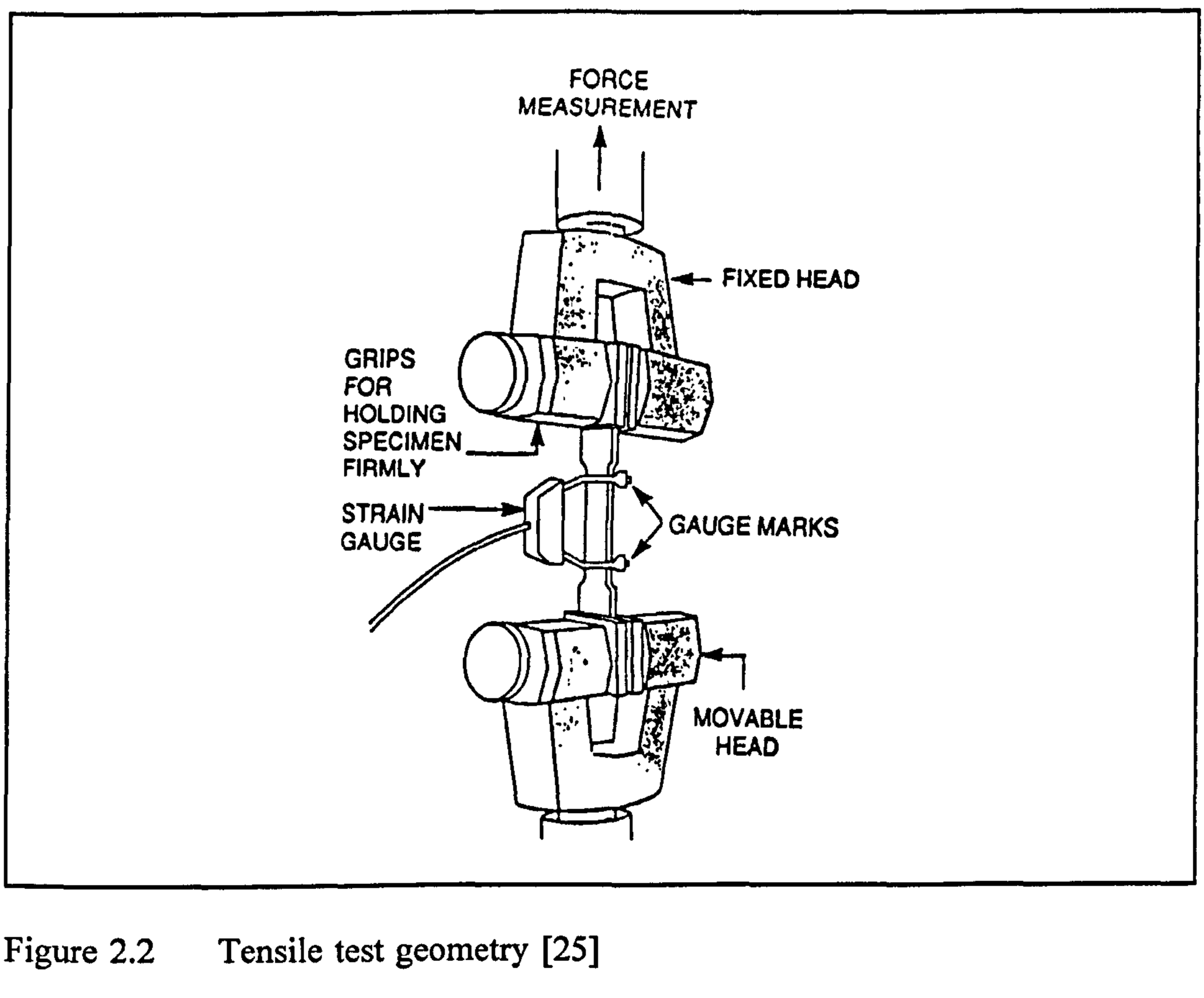

Figure 2.2 Tensile test geometry [25]

Illustrated in Figure 2.2 this is the most widely used method to mechanically test materials. Capable of recording the whole of the engineering stress-strain curve, the standard output parameters that are quoted from this test are the engineering measures

of E, σ_n and ε_n [31]. A wide range of test strain rates can be achieved by the use of electric motors and screw drives or hydraulic actuator drive mechanisms. Running servohydraulic testing machines at increasing strain rates has several notable drawbacks. At high strain rates, e.g. above 20 s^{-1}, there is a likelihood of producing erroneous data due to "inertial effects and load cell ringing" [32]. Thus instead of measuring a quasi static event the experimenter measures the inertia response of the test equipment. In this test the sample shape has been designed to minimise the effects of holding the sample such that the desired applied stress field in the gauge length is approximately constant. As the cross-head displacement is not necessarily the same as the sample strain it is necessary to instrument the specimen and use this in a closed loop control circuit to achieve a constant strain rate. Instrumentation on the gauge length of a thermoplastic test sample is difficult as contacting extensometers can cause premature failure of the sample at their attachment points, non-contacting extensometers may have insufficient resolution to accurately determine low strain modulus and strain gauges may adhere poorly due to the low surface activity of the thermoplastics. In the current national standard [31], the material properties that are normally evaluated are initial low strain secant modulus, and engineering stress and strain at the point of maximum load during the test. At the point of maximum load the material sample begins to neck and the stress-strain field in the gauge length becomes nonuniform. To measure the stress and strain beyond this point is extremely difficult and not normally done. Attempting to reconcile the difference between one dimensional and three dimensional stress-strain fields, noncontacting video cameras have been used to determine the shape of the neck zone and hence deduce the stress and strain in the neck [33,34] by applying three dimensional stress concentration

factors and calculating an equivalent one dimensional stress from the three dimensional neck zone. This approach is potentially flawed as a prior knowledge of the stress concentrations and relationship between one and three dimensional behaviour is required.

2.2.2 Compression

For this test, cubes or disks of material are compressed whilst recording the applied load and resultant displacements. The dimensions of the samples are selected to avoid geometric buckling and the contact surfaces between the test sample and the test jig must be lubricated to minimise barrelling caused by the strain discontinuity between the test specimen and jig. Capable of recording the whole of the engineering stress-strain curve, the sample failure mode is different to the tensile test as material voids are closed by the applied load with the material failing through shear yielding.

2.2.3 Bending

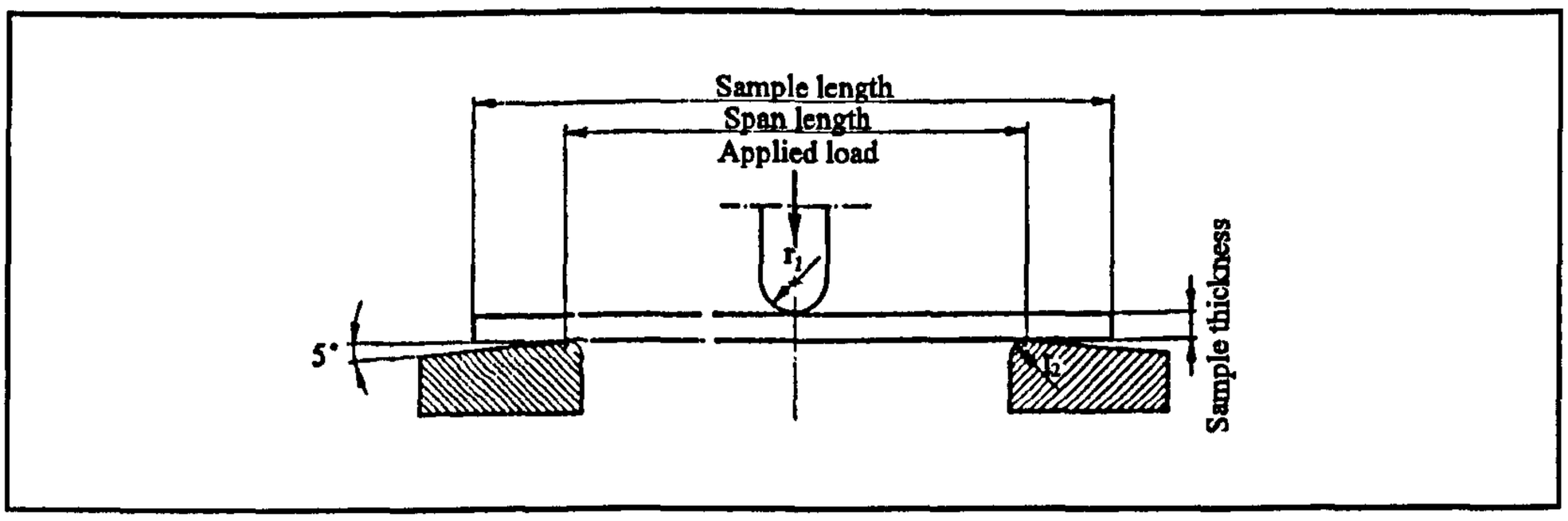

Figure 2.3 Bending test geometry [42]

Illustrated in Figure 2.3 [35] the standard output parameters that are quoted from this test are the apparent bending modulus, and the flexural stress and deflection at

rupture. Unlike the tensile test the bending test is only suitable for small strain testing of thermoplastics as large displacements induce non-linear stiffening effects and the method does not induce a uniform stress field in the specimen.

2.3 Creep/relaxation

These tests are variations of the quasi static tensile test and use the same geometry but in general measure the response of a sample to constant load or elongation. In the case of the creep test [36] the sample is loaded in tension to a finite engineering stress and the increase of engineering strain with time is recorded. For the relaxation test the sample is elongated in tension to a finite engineering strain and the decrease in engineering stress with time is recorded. The isochronous stress-strain curves recorded by the creep and relaxation tests, at various constant temperatures, should in theory be interchangeable. By subjecting the samples to stress jumps, both positive and negative, the response of the material to proposed creep models can be assessed. These models can then be used to predict the long term deformation of thermoplastic components

2.4 Dynamic tests

In most conventional dynamic fracture tests little attempt is made to measure or control the deformation of the specimen and the strain rate achieved is not measured or controlled. The Tensile Impact, Charpy, Izod and Instrumented Puncture tests do not control the strain rate and are normally used to measure the energy to break samples at high strain rates. The results are then used to grade materials relatively and

are test geometry dependent. Other methods such as ultrasonic wave velocity measurements and dynamic mechanical analysis testing, in which the applied strain rate is controlled are more useful for measuring the low strain, high strain rate modulus of thermoplastics. As with quasi static tests by varying the ambient temperature and applied deformation rate the effect of these parameters on the material stiffness and strength can be investigated.

2.4.1 Tensile impact test

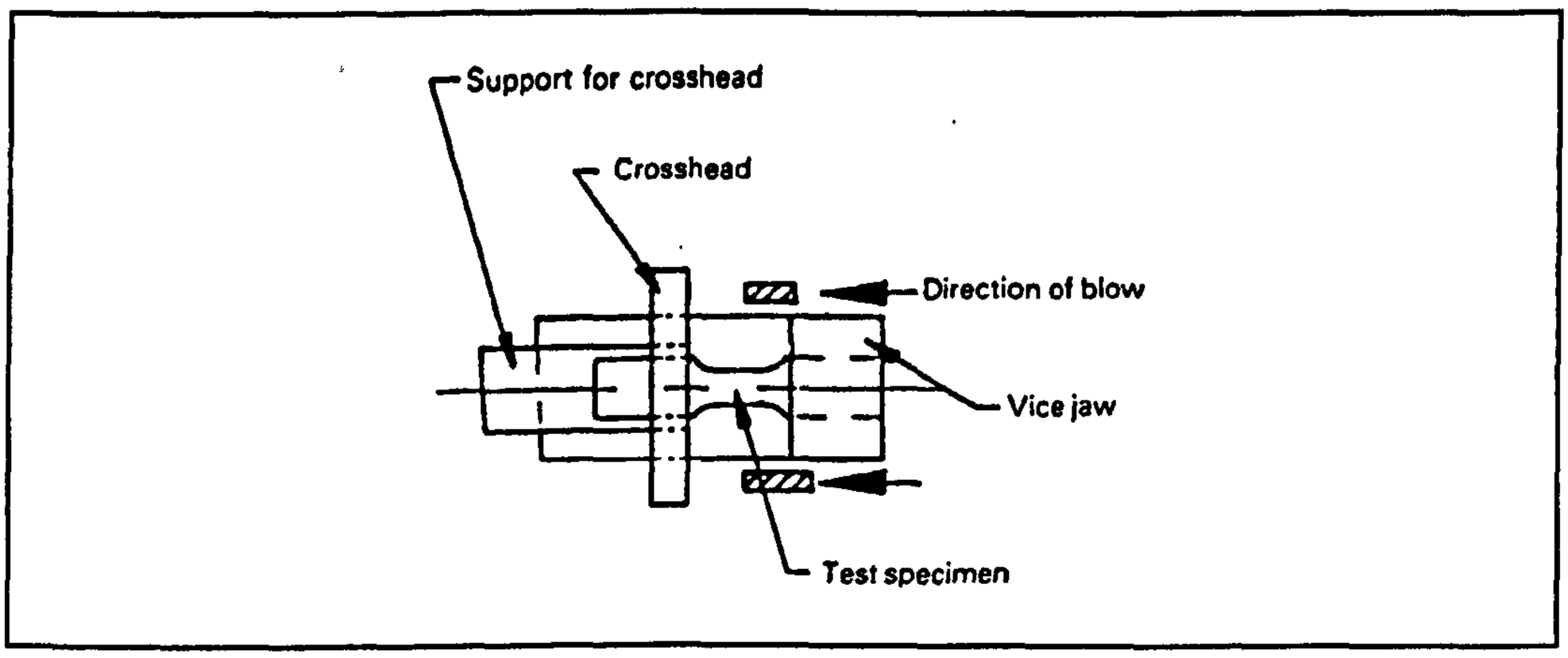

Figure 2.4 Tensile impact test geometry [37]

Illustrated in Figure 2.4 the tensile impact test [37] is little used. The single measurement of the test is the amount of energy used to break the sample and the results can only be used to subjectively compare materials.

2.4.2 Compressive split Hopkins pressure bar (SHPB)

Recording the whole of the engineering stress-strain curve the output parameters that are quoted from this test are the post yield stress-strain curves. By using the propagation of a wave along a bar, a disk specimen sandwiched between two bars, can

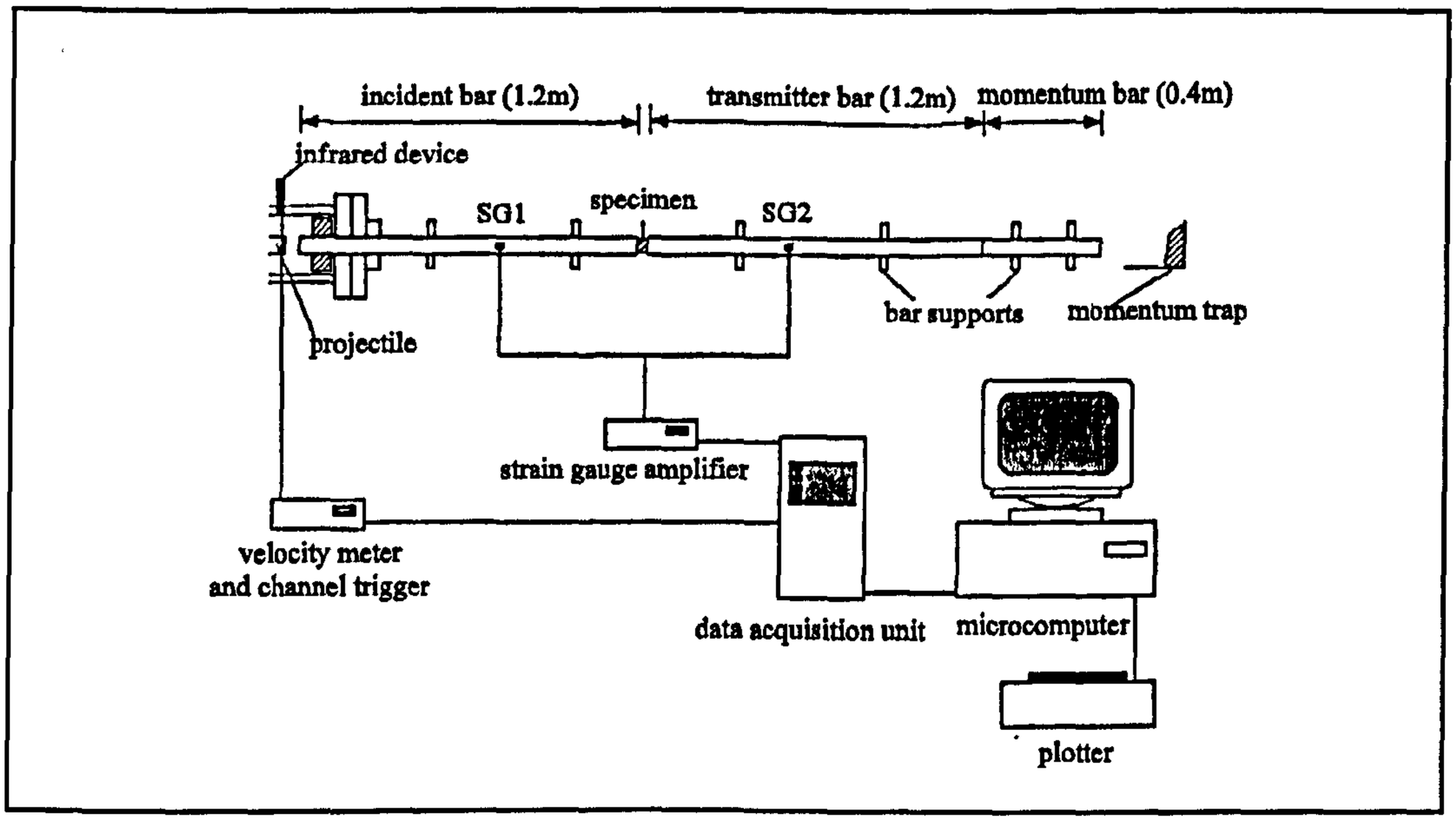

Figure 2.5 SHPB test configuration [38]

be subjected to a high strain rate compressive load as shown in Figure 2.5 . Whereas SHPB testing may be used to test materials at high strain rates in compression and tension the following points must be noted [32]:

1) the data obtained is only valid after some degree of uniformity is obtained;

2) this uniformity is not obtained at the beginning of the test and hence precludes its use for determining material behaviour in the elastic region;

3) the strain rate is not constant.

Providing that suitable sample dimensions are used, to limit inertial effects, this method is suitable to obtain the high strain rate/large strain behaviour of samples but the resolution is not sufficient to determine low strain modulus values [38]. The compressive SHPB test may be modified to load the specimen in tension. However the tensile SHPB results are extremely difficult to interpret after necking has begun [39]. During plastic deformation the point of maximum load has been associated with the onset of necking which is itself associated with local instabilities including

shear yielding, adiabatic heating effects, and the drawing of amorphous material to form a fibrous structure.

2.4.3 Bending tests

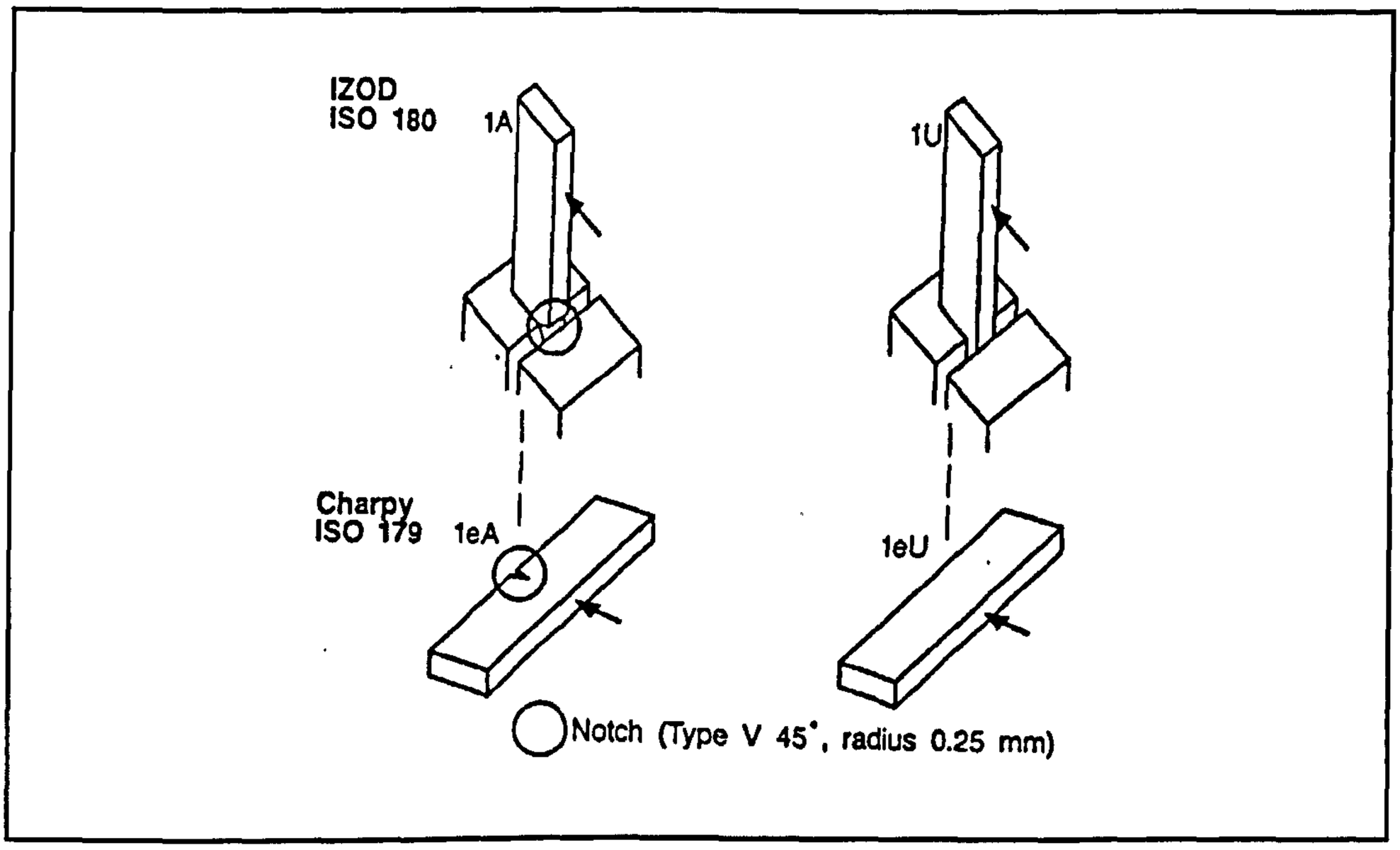

Figure 2.6 Charpy and Izod test geometry [24]

The most commonly used methods to test thermoplastics at high strain rates are the Charpy and Izod methods. The geometry of these tests are notched beams which are shown in Figure 2.6. The single measurement of the test is the amount of energy used to break the sample [40,41]. This is geometry and size dependent. Although novel dynamic bending tests can be used to determine the modulus of un-notched beam samples at high strain rates [42] this modulus is still an apparent bending modulus and is dependent upon an assumed idealised material model and specimen stress-strain distribution.

2.4.4 Instrumented puncture test

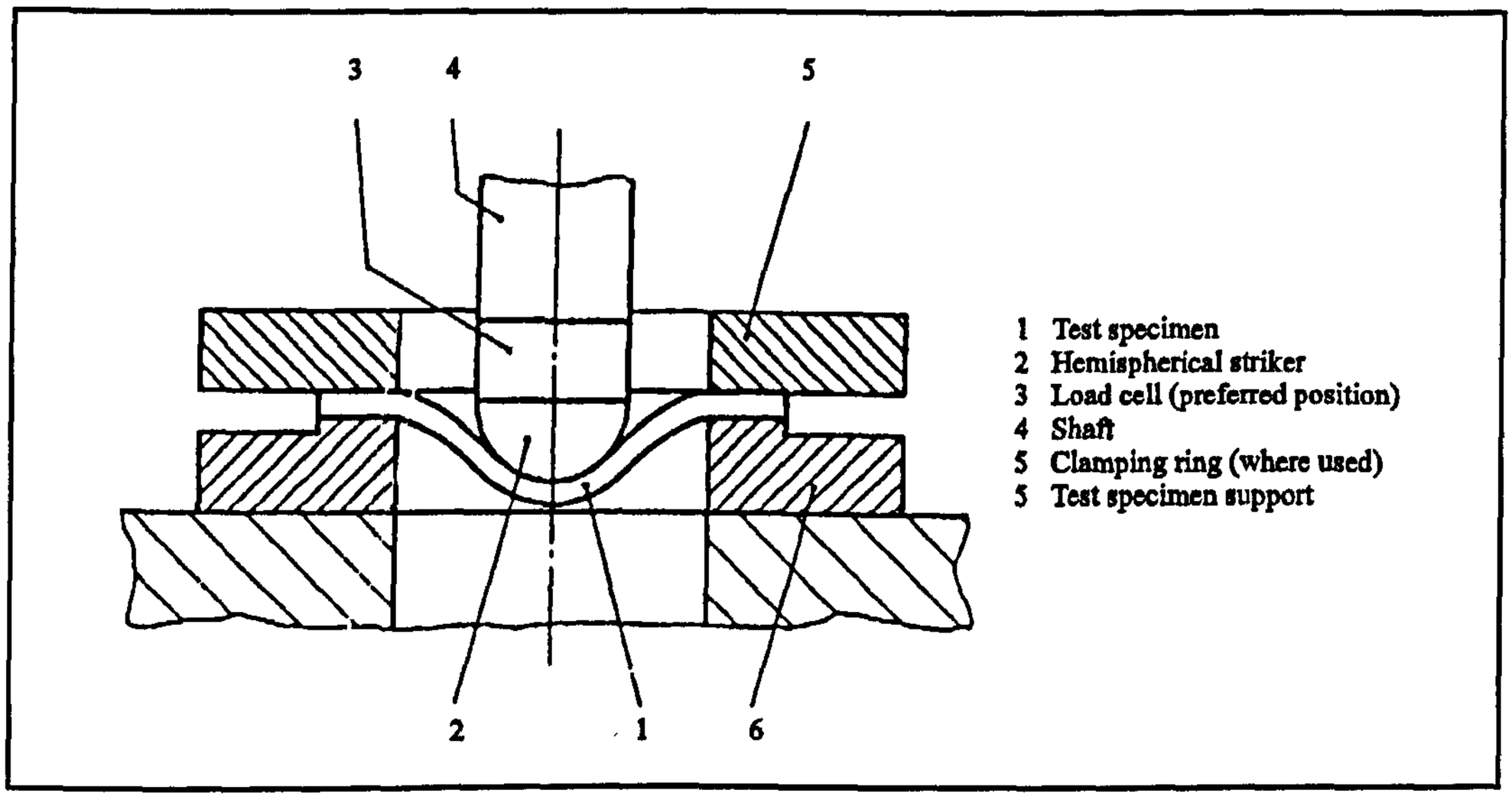

Figure 2.7 Instrumented puncture test geometry [43]

Illustrated in Figure 2.7 the energy for this test is obtained by either a falling weight or mechanical means e.g. a pneumatic ram. The impact speed is typically about 4 m/s and approximately constant during the impact event depending upon the relative energies of the impacting system and energy absorbed by the test sample. During the test, a load cell is used to measure the force generated in the hemispherical striker with respect to time. The quantities that are recorded are: peak force, deformation at peak force, energy to peak force and total penetration energy [43]. Typical analyses of the results assume that both the test sample and instrumentation can be treated as quasi static systems. However this is not strictly true with the test results being misleading as confirmed by statistical studies [44]. As for the Charpy and Izod tests the results are size and geometry dependent.

2.4.5 Ultrasonic wave velocity methods

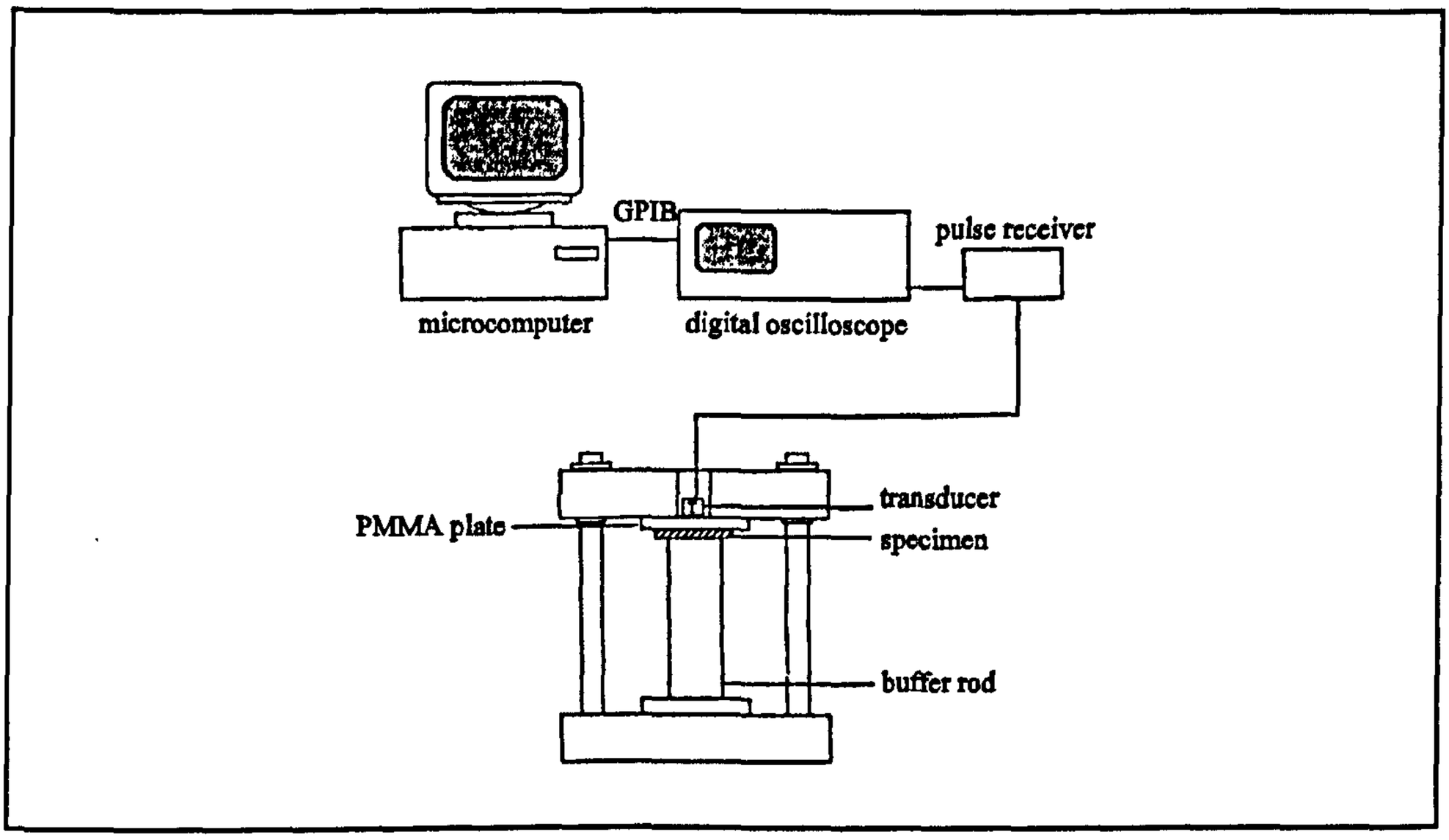

Figure 2.8 Direct excitation ultrasonic test configuration [46]

By exciting a sample ultrasonically it is possible to measure longitudinal and lateral wave propagation speeds and, knowing the density of the material and sample geometry, calculate the low strain/high strain rate modulae of the material. A review of the methods used is given in [45] which discusses direct excitation and indirect excitation. Extreme care must be taken in interpreting the results if the sample density is not uniform due to processing. An example of the test set up is shown in Figure 2.8 [46]. As the material stiffness of thermoplastics are sensitive to strain rate effects the results are frequency and amplitude dependent.

2.4.6 Dynamic mechanical analysis (DMA)

DMA tests [47] can be performed on a number of sample geometries subjecting the specimen to low strain sinusoidal tensile, shear bending or compound loads [48,49]. Examples of the type of geometries used are illustrated in Figure 2.9. Unfortunately

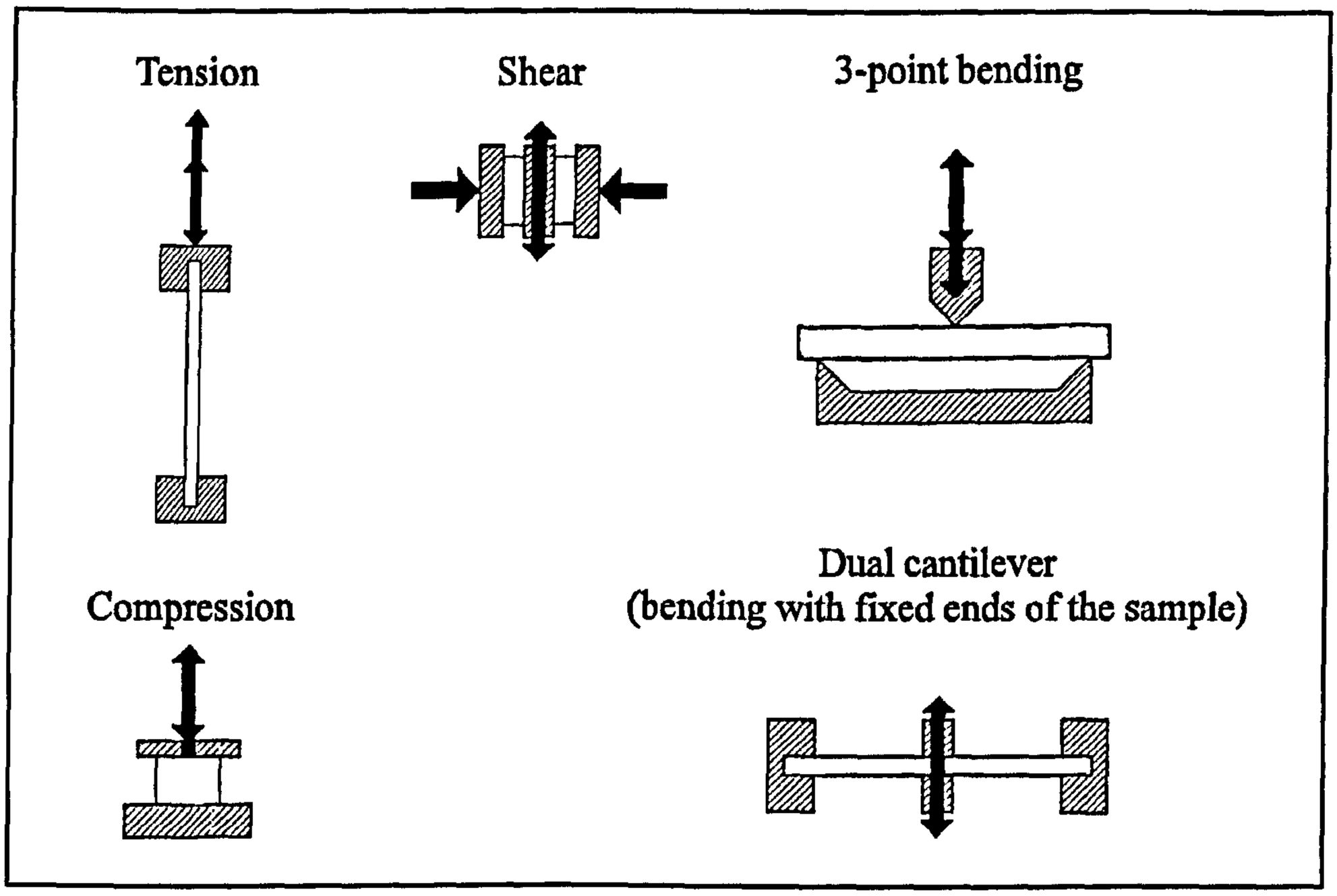

Figure 2.9 DMA test geometries [34]

tests on the same sample by different equipment suppliers have differing results [48]. By subjecting the test sample to a constant low strain excitation an indication of the effect of temperature on the material sample may be obtained by scanning in the temperature domain.

2.5 Three dimensional behaviour

In describing the three dimensional behaviour of thermoplastics the following assumptions are known not to be true but are still normally used in structural analyses [50]:

1) isotropy;

2) no dependence of behaviour on the hydrostatic component of stress;

3) identical yield behaviour in tension and compression.

Most material tests try to load the sample in a single axis. However real components and test samples have three dimensions. The relationship between the behaviour in one dimensional strain and three dimensional strain is normally achieved by the measurement of Poisson's ratios ν_{12}, ν_{23} ν_{13}. These are defined as the ratio of strain in two mutually perpendicular axis and can be measured during tensile tests by the use of extensometers or strain gauges. To determine relationships between one dimensional and three dimensional failure criteria it is normal to use the concept of equivalent principal stress.

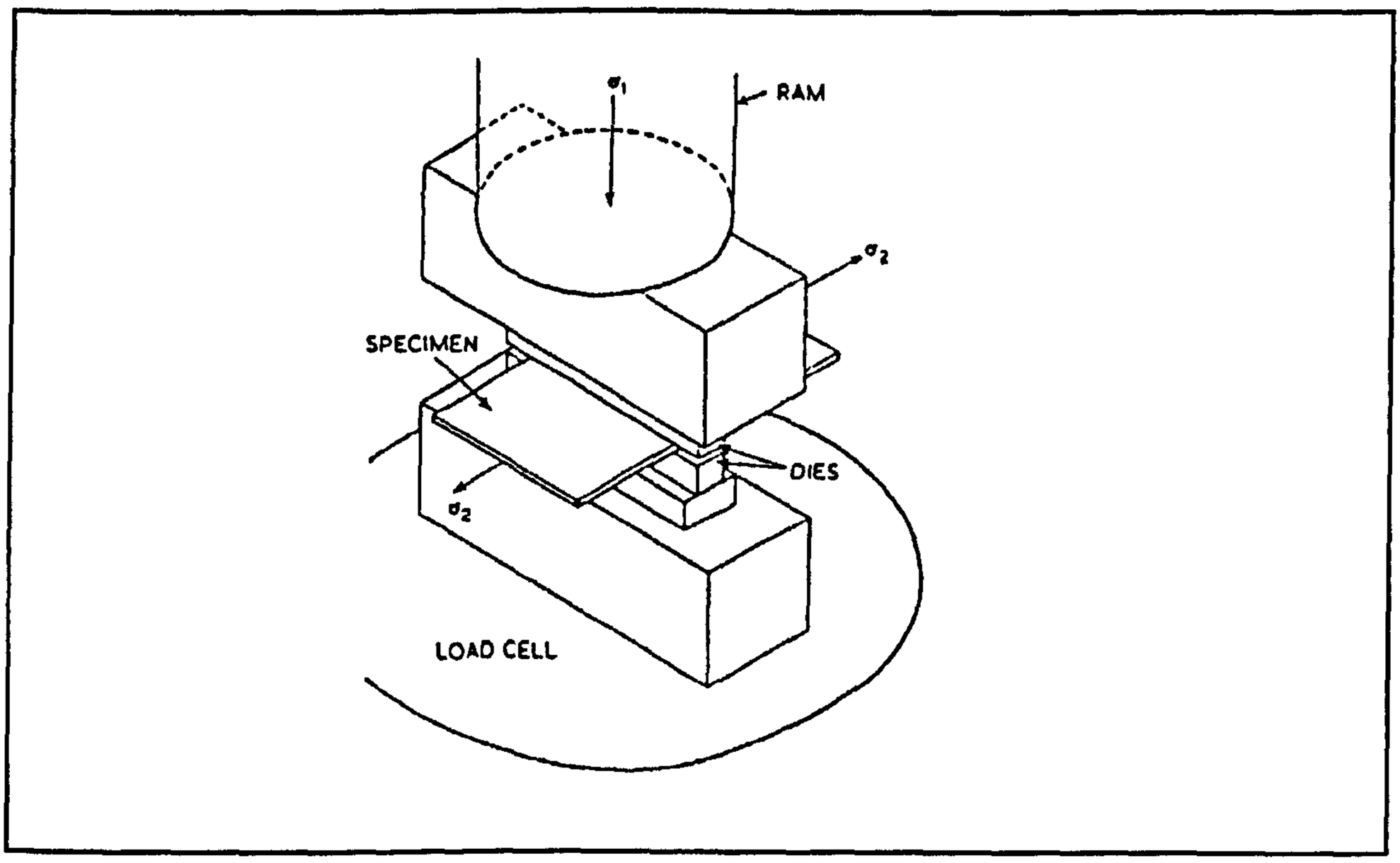

Figure 2.10 Plane strain compression test [50]

The determination of the strain relationship between one and three dimensional load requires the application of load in more than one axis. Examples of this are the combined tension and torsion test and the plane strain compression test (shown in Figure 2.10) [50]. Although it has been widely documented that the yield of thermoplastics does not comply with the equivalent stress as defined by the von Mises

criterion [26,50], this is still presented as the most commonly used theory for describing three dimensional material behaviour of thermoplastics [51,52,53].

$$\sigma_{vm}=\frac{1}{\sqrt{2}}[(\sigma_{11}-\sigma_{22})^2+(\sigma_{22}-\sigma_{33})^2+(\sigma_{33}-\sigma_{11})^2+6\tau_{12}^2+6\tau_{23}^2+6\tau_{31}^2]^{1/2} \quad (6)$$

The failure of thermoplastics is thought to be a process whereby two modes are possible, shear yielding or crazing [54] and depending on the applied stress field one of the two mechanisms may be dominant. No full three dimensional description of crazing is yet available [53] but if plane stress conditions are assumed the craze is proposed to occur if:

$$|\sigma_1-\sigma_2| = A-\frac{B}{\sigma_1+\sigma_2} \quad (7)$$

(where A and B are material constants which are functions of temperature and strain rate.)

2.6 Summary of material testing techniques

A summary of typical material stiffness and strength measurements are given in Table 2.1. As the mechanical performance of thermoplastics are well known to be strain rate sensitive, the control of load/strain rate in thermoplastics during mechanical testing is of critical importance. All the stiffness tests reviewed above, with the exception of tensile testing with closed loop strain rate control, do not have a constant controlled strain rate during the test. Thus it is very difficult to define a true material property or constant determined from any of these tests. If any of the tests listed in Table 2.1 is used to investigate the effect of strain rate on the mechanical performance of a

thermoplastic then it is important that a consistent normalised strain rate response is obtained from the test configuration. If this is not done then the results will be dominated by the control of the test equipment and will not be a true measure of the effect of applied strain rate. Hence some tests, for example the Charpy and Izod impact tests, are clearly limited in their approach, and should only be used for quality control or limited grading of materials.

Test	Standard parameters measured	Control parameter
Quasi static		
Tensile [31]	Secant modulus, stress and strain at peak load	$\dot{\varepsilon}$
Bending [35]	Apparent modulus, bending stress and deflection at break	$\dot{\varepsilon}$
Compression	Secant modulus, stress and strain at peak load	$\dot{\varepsilon}$
Creep		
Tensile creep [36]	1% strain Modulus at 1 and 100 hours, Isochronous stress-strain curves	σ_{eng}
Dynamic		
Tensile impact [37]	Tensile-impact energy to break	-
Bending rebound [42]	Apparent bending modulus	$\dot{\varepsilon} =$ a sin ωt
Compression SHPB [38]	Stress-strain curve	-
Charpy/Izod [40,41]	Bending-impact energy to break	-
Puncture [43]	Peak force, deformation at peak force, energy to peak force, total penetration energy	-
Ultrasonic [45]	Tensile and shear moduli corresponding to wave speed used	$\dot{\varepsilon} =$ a sin ωt
DMA [48,49]	Tensile and shear moduli corresponding to test amplitude , frequency and sample size used	$\dot{\varepsilon} =$ a sin ωt

Table 2.1 Material stiffness and strength measurements

Chapter 3

Review of material property trends for polyethylene

A typical engineering stress-strain curve to failure for HDPE, subjected to a tensile test, is shown in Figure 3.1. At the point of maximum load the material starts to neck and standard test instrumentation is unable to determine the true stress-strain behaviour of the material beyond this point.

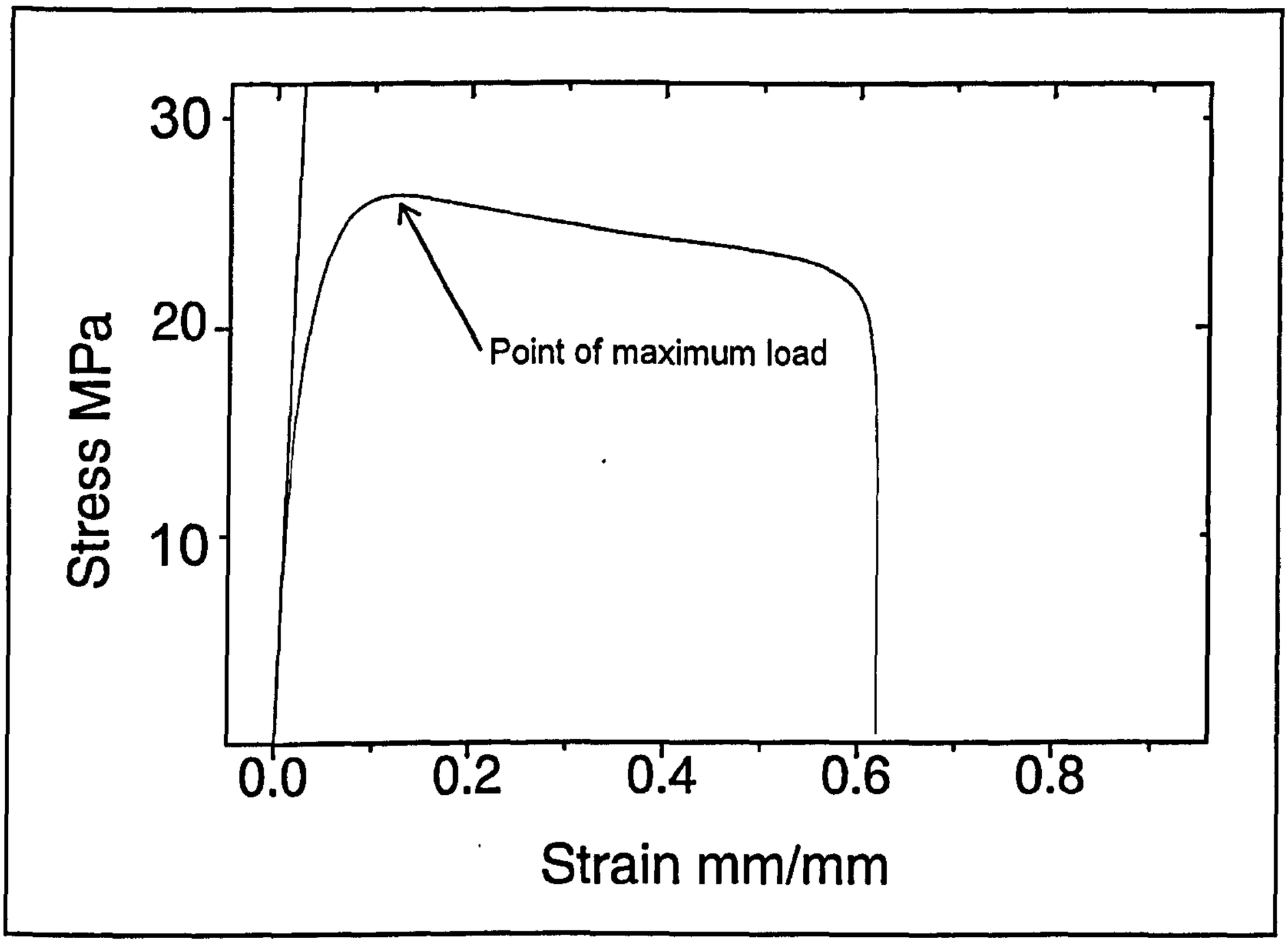

Figure 3.1 Typical tensile test data for HDPE

When subject to high strain rates and low temperatures, thermoplastics are generally stiffer and more likely to fail in a brittle manner than when they are subject to low strain rates and high temperatures. If there is a clear trend of material stiffness and strength with respect to both strain rate and temperature it is important to establish this so that test methods may be optimised and erroneous test results avoided.

Previous work has shown that for Medium Density Polyethylene (MDPE) and HDPE the large strain post yield behaviour can be described as a simple Eyring model [38] i.e.

$$\frac{\sigma}{T} = \frac{R}{E_a}\left\{\frac{\Delta H}{RT} + \ln\frac{2\dot{\epsilon}}{\dot{\epsilon}_0}\right\} \quad (8)$$

Similar results have been measured for the low strain bending modulus of both Polypropylene and Low Density Polyethylene (LDPE) with respect to the applied strain rate [55]. It is necessary to understand the effect of both strain rate and temperature on the whole of the stress-strain curve such that the material behaviour can be characterised for all impact simulations.

3.1 Strain rate trends

3.1.1 Shape of the stress-strain curve

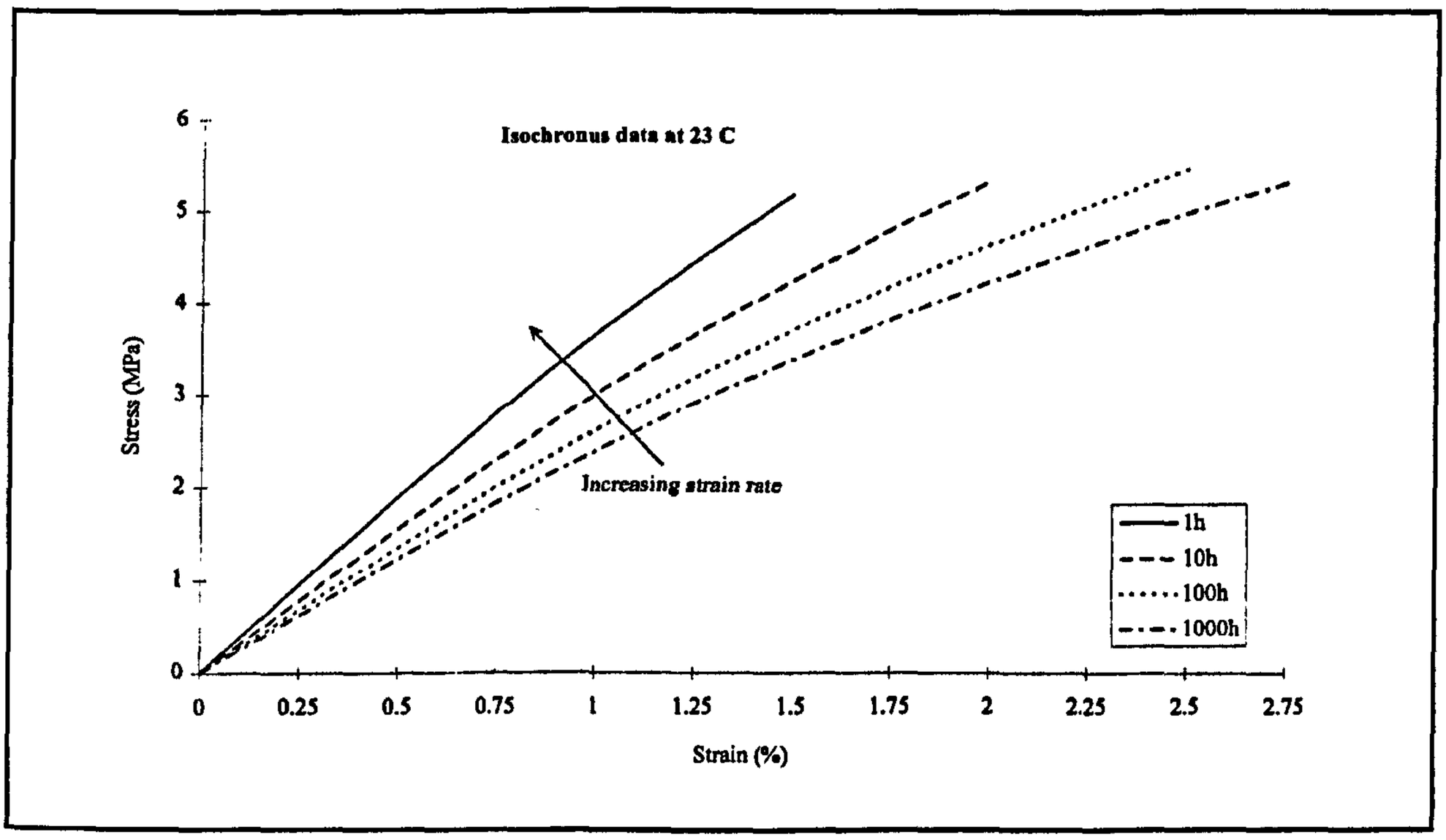

Figure 3.2 Low strain rate creep of HDPE [56]

The effect of strain rate on the shape of the isochronous stress-strain curve can be seen by examining the creep behaviour of HDPE (Lupolen 4261A supplied by BASF) [56] as shown in Figure 3.2 . This shows a very important trend, that as strain rate increases the initial part of the stress-strain curve becomes increasingly linear. As the applied testing strain rate is increased this trend continues. This is demonstrated by the results of medium strain rate tensile testing shown in Figure 3.3 [57].

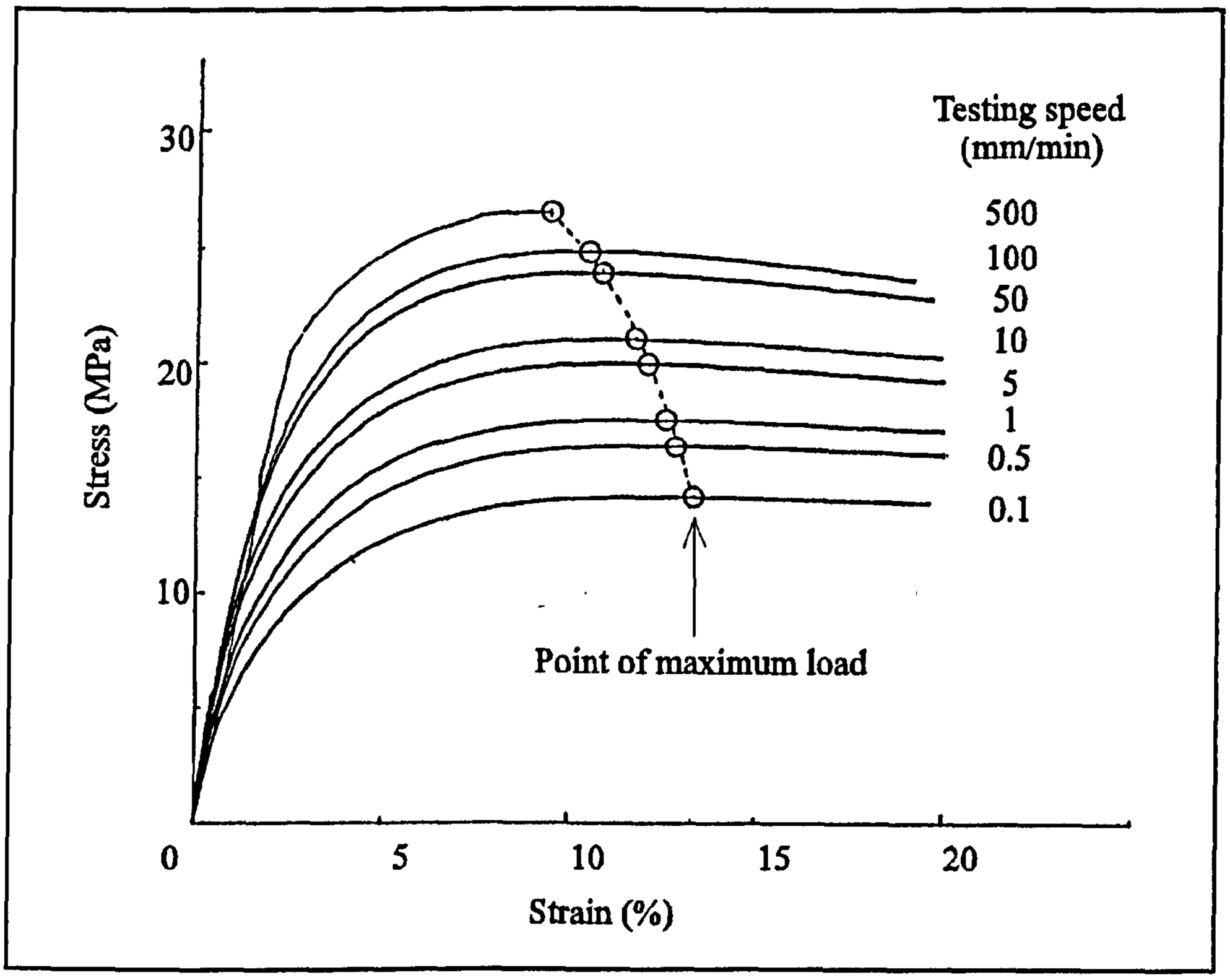

Figure 3.3 Medium strain rate tensile testing of HDPE [57]

The effect of increasing strain rate on the shape of the tensile stress-strain curve is duplicated in the compressive stress-strain curve. Compression testing and compressive SHPB testing give similar results [38] and are shown in Figure 3.4.

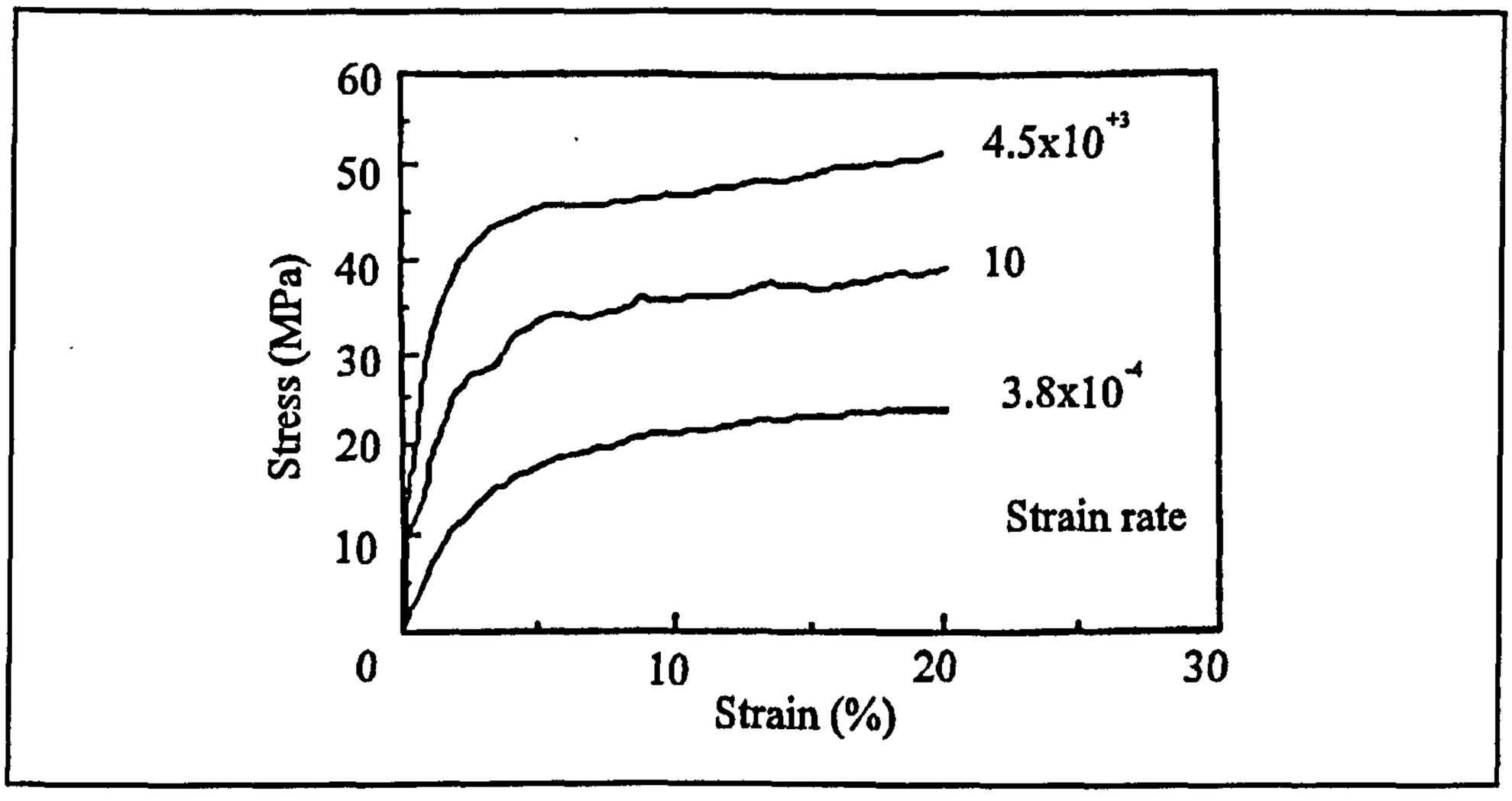

Figure 3.4 Effect of strain rate on the compression testing of HDPE [38]

3.1.2 Initial low strain material stiffness

Figure 3.5 shows that, as indicated by the shape of the stress-strain curves, an increasing strain rate increases the initial material stiffness [57] with a logarithmic relationship. This trend is confirmed by rate dependent bending and stress relaxation data for LDPE [55], and high strain rate rebound test data [42]. Although a trend of increasing modulus with strain rate is reported, the increase in strain rate sensitivity at high strain rates measured by the rebound technique is probably due to deviations between the analytical assumptions and the physical tests e.g. non-ideal boundary conditions, wave propagation effects and nonuniform strain rates. Other workers using wave propagation methods have demonstrated that if the underlying assumptions are not fully adhered to e.g. inappropriate choice of specimen thickness in the SHPB compression test, this can result in erroneous data being published [38].

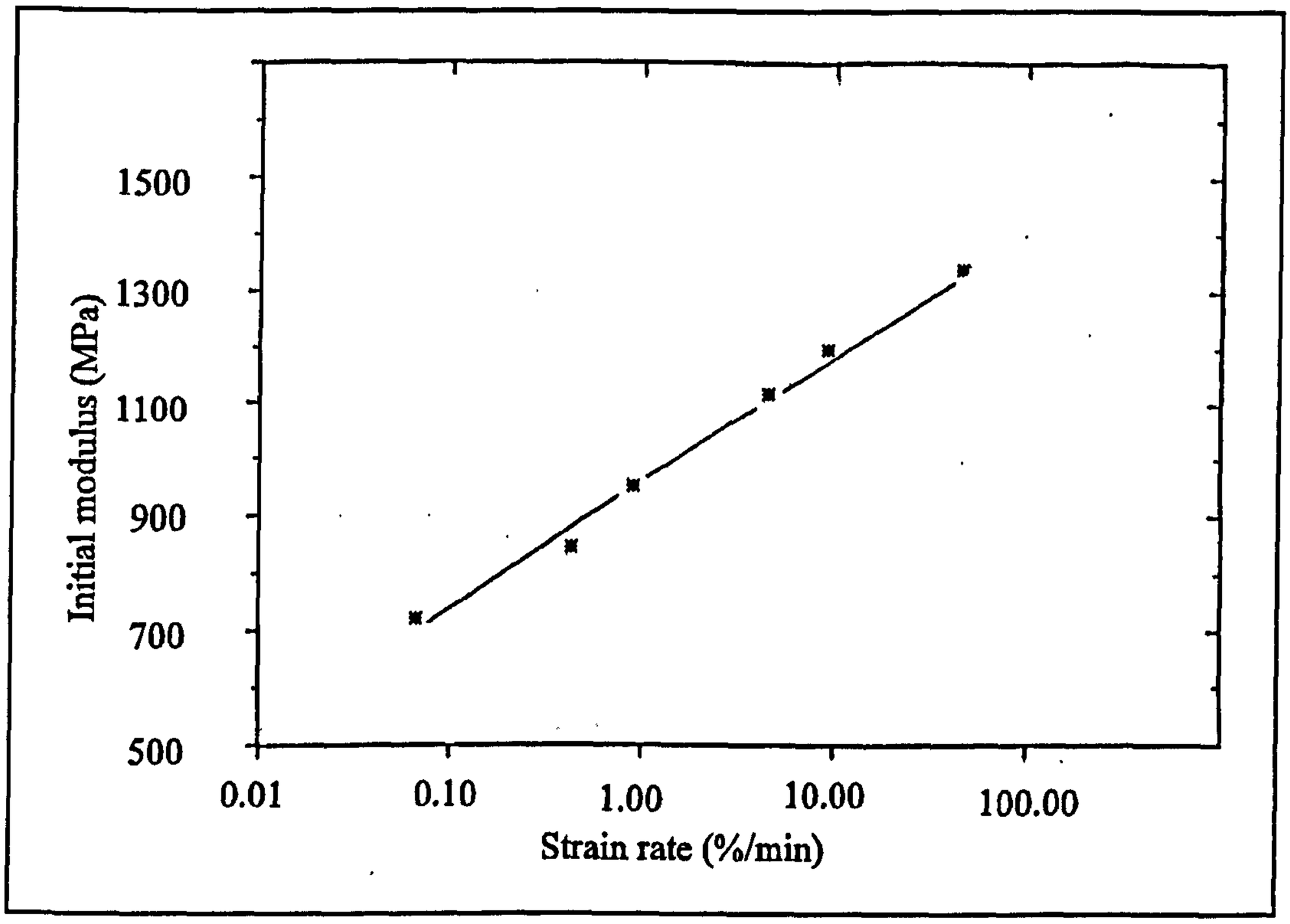

Figure 3.5 Effect of strain rate on HDPE initial modulus [57]

3.1.3 Initial low strain material damping

To accurately measure the low strain dynamic response of a material and decouple the elastic and viscous parts requires a high level of test accuracy. Accurate measurements are notoriously difficult to make due to the problems of decoupling the dynamic mechanical and electrical response of the test apparatus and that of the test specimen. Indeed typical DMA test equipment testing samples using the same test geometries and theories to determine material properties could result in differing test results [48]. Precision torsional test results made on custom built equipment indicate that, because commercial thermoplastics have a broad range of molecular weights, the effective material damping is approximately constant with frequency [58]. This is shown in Figure 3.6 and has important consequences as it indicates that the standard theoretical models i.e. the Maxwell model, Kelvin-Voigt model and standard linear solid, which

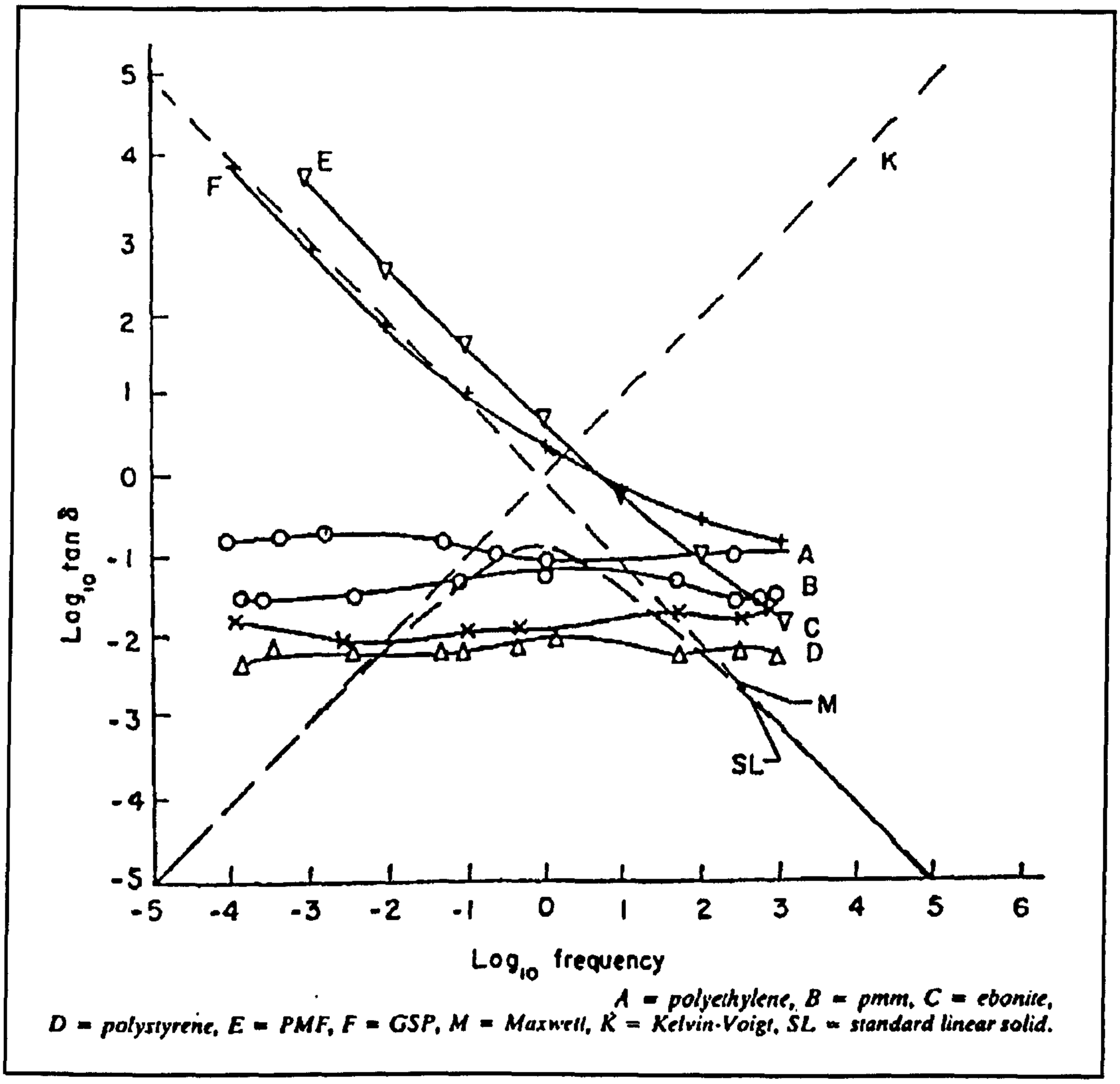

Figure 3.6 Measured torsional damping of thermoplastics compared with standard material models [58]

are used by commercial DMA systems, are not suitable models for characterising the structural response of thermoplastics. This is because they can not accurately represent the damping of these materials over a wide range of frequencies.

3.1.4 Point of neck formation

Figures 3.7 and 3.8 [57] show that as the applied strain rate is increased the material becomes stronger (neck point stress increases) and less ductile (strain to neck point decreases).

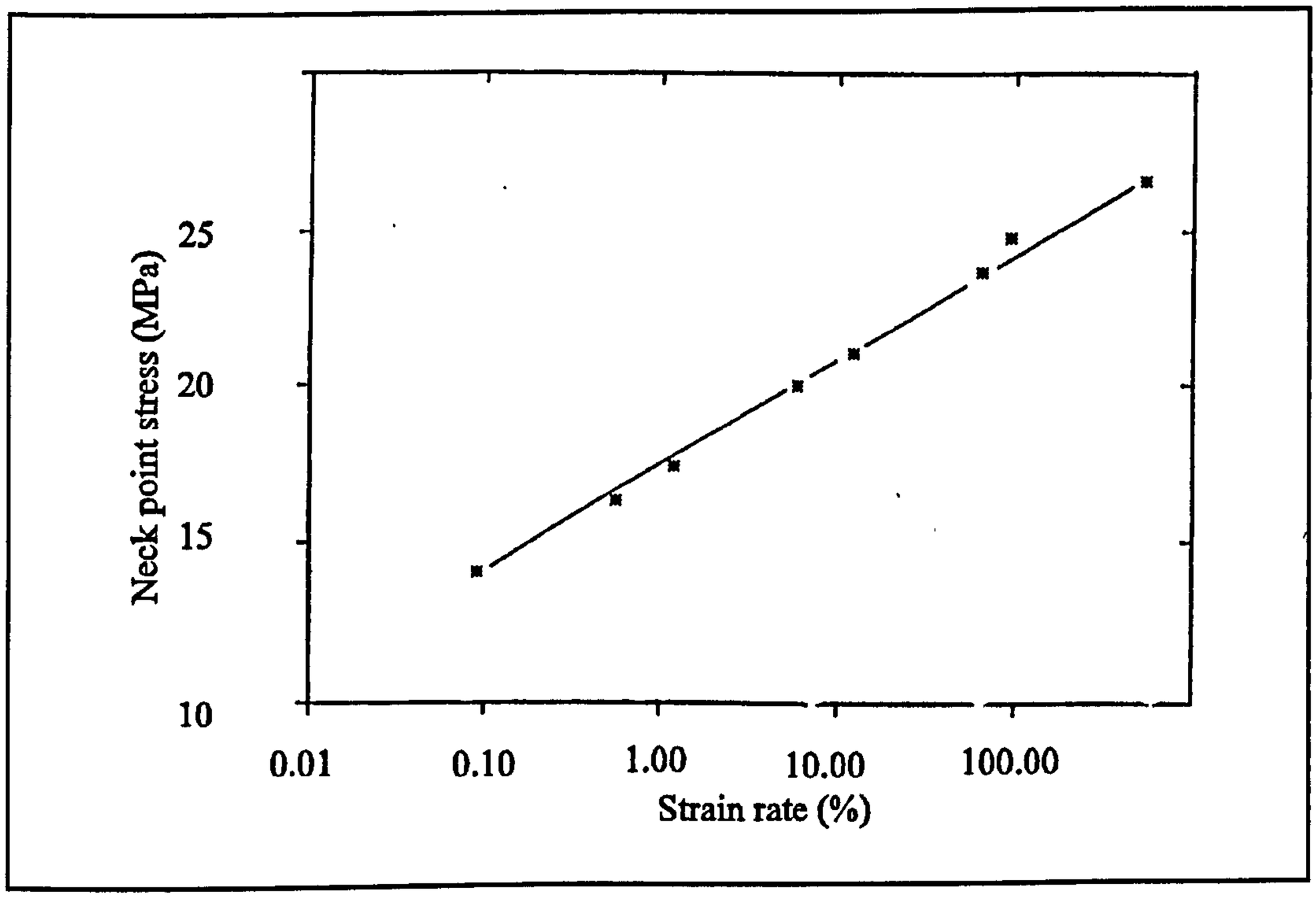

Figure 3.7 Effect of strain rate on σ_n [57]

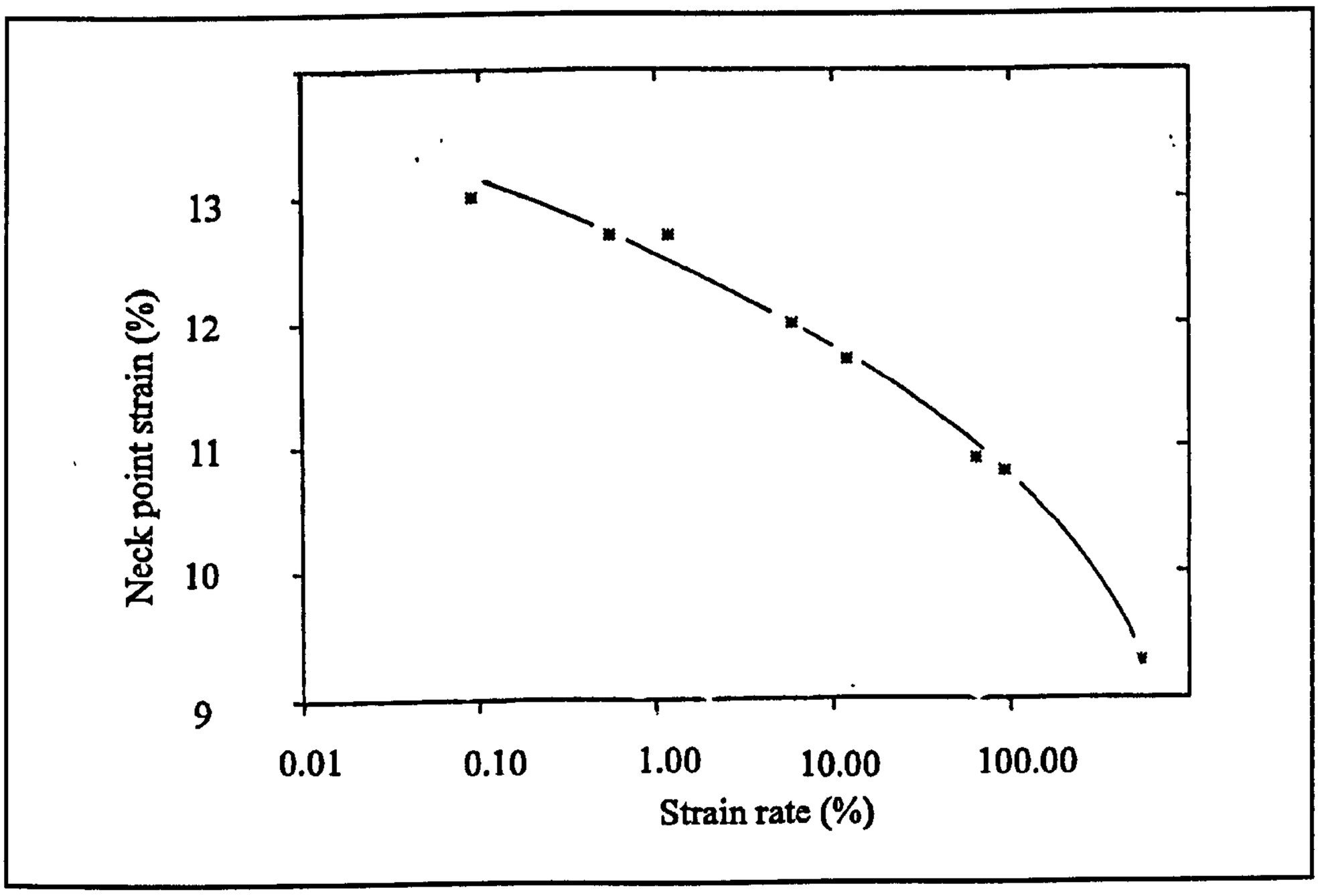

Figure 3.8 Effect of strain rate on ε_n [57]

3.2 Temperature trends

As well as considering the effect of strain rate on the material properties of thermoplastics it is necessary to review the effect of ambient temperature. As indicated in Equation 8 [38] there should be a direct relationship between temperature and mechanical performance according to the Eyring model.

3.2.1 Shape of the stress-strain curve

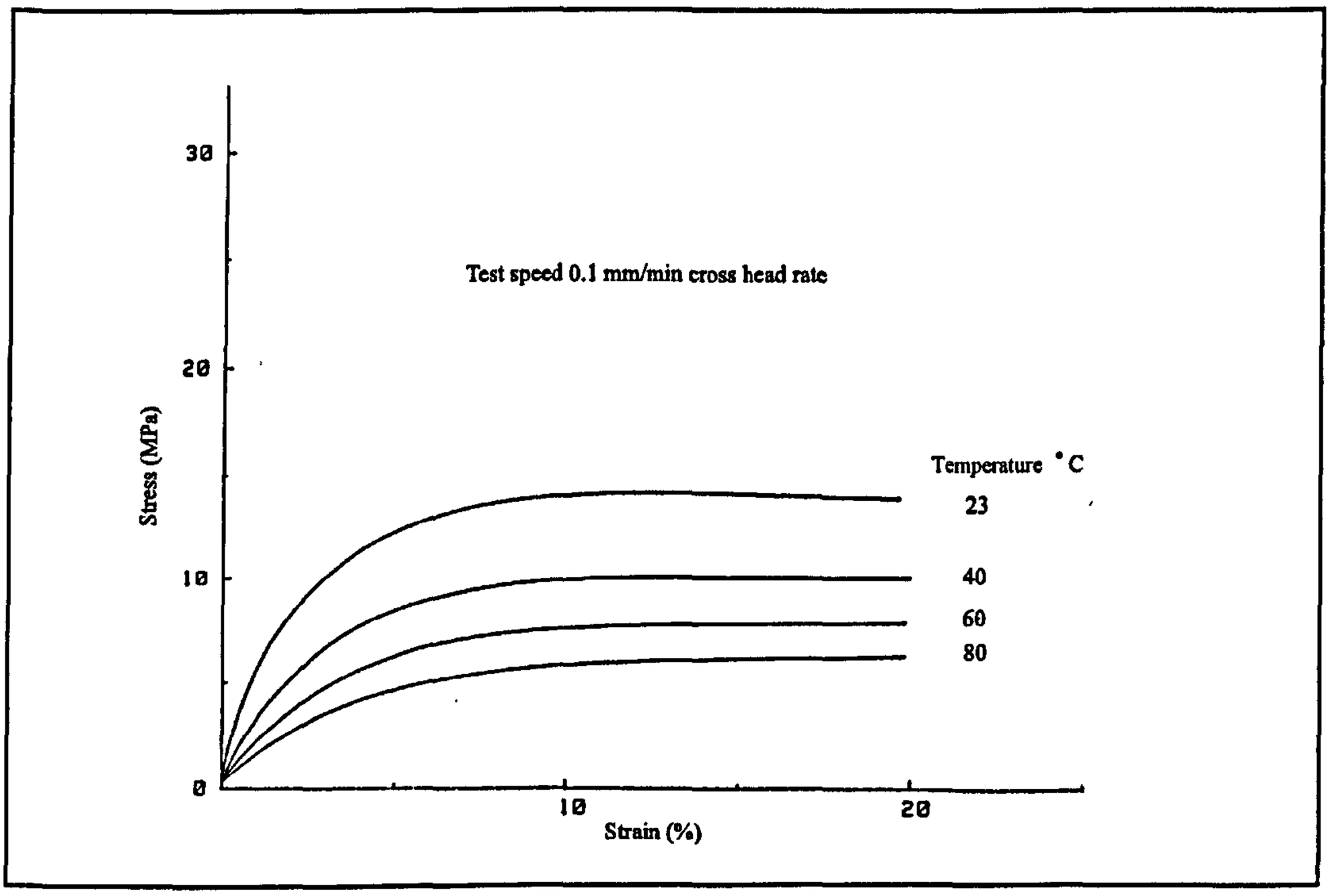

Figure 3.9 Stress-strain curve of HDPE at different temperatures [57]

The effect of temperature on the shape of the stress-strain curve can be seen in Figures 3.9 [57] and 3.10 [56]. As the temperature decreases the initial part of the stress-strain curve becomes more linear.

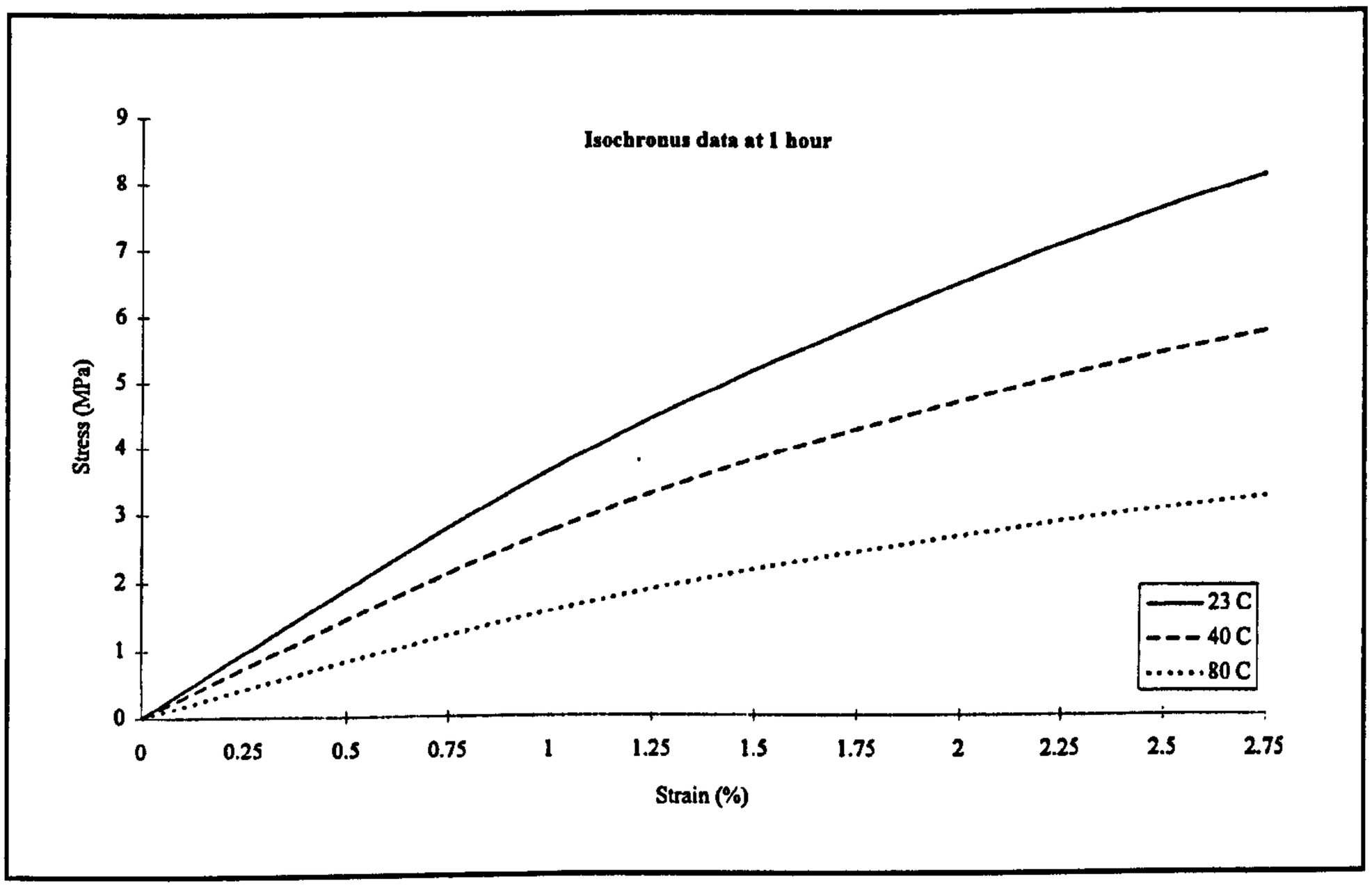

Figure 3.10 Creep stress-strain curve of HDPE at different temperatures [56]

3.2.2 Initial low strain material stiffness

Figure 3.11 shows the effect of decreasing temperature on the increasing initial low strain modulus of elasticity for HDPE as measured by the tensile test [59]. This trend is confirmed at high strain rates in Figure 3.12 showing the effect of decreasing temperature on the increasing low strain ultrasonic dynamic modulus [38].

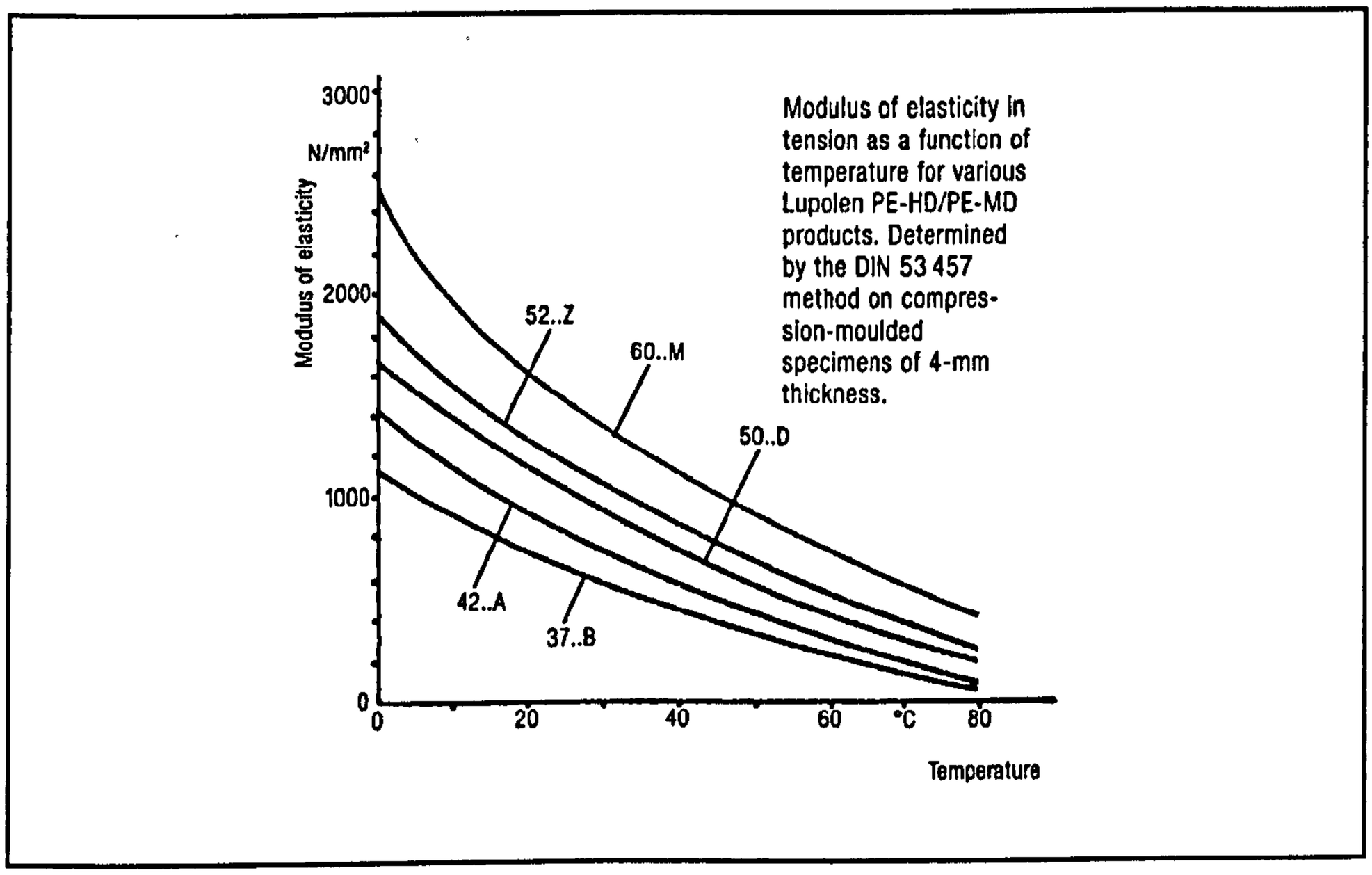

Figure 3.11 Effect of temperature on tensile test modulus of elasticity [59]

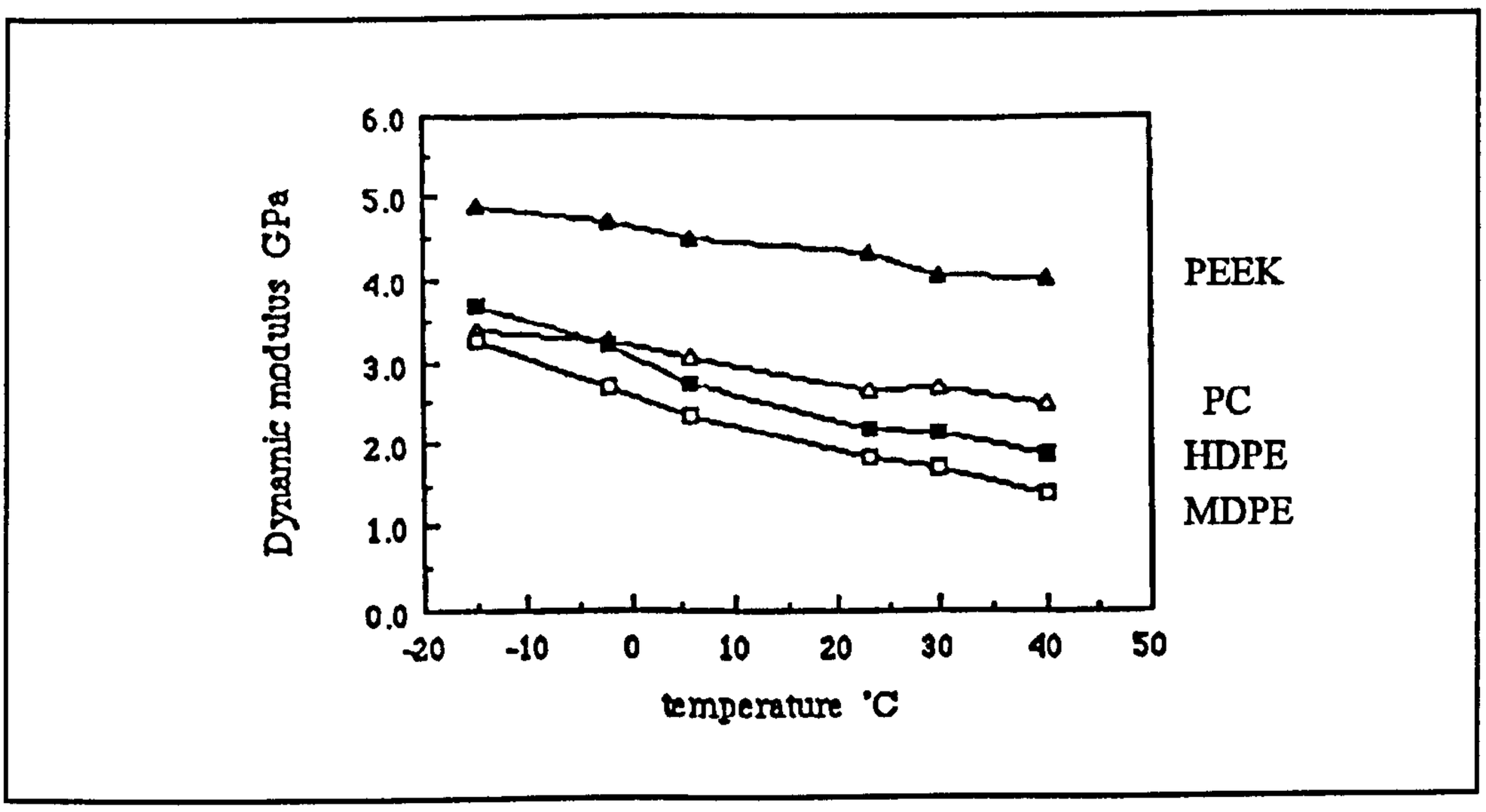

Figure 3.12 Effect of temperature on ultrasonic dynamic modulus [38]

3.2.3 Point of neck formation

Figure 3.13 shows the effect of temperature on the stress at maximum load of the tensile test. This Figure shows that as the temperature decreases the material becomes stronger (neck point stress increases).

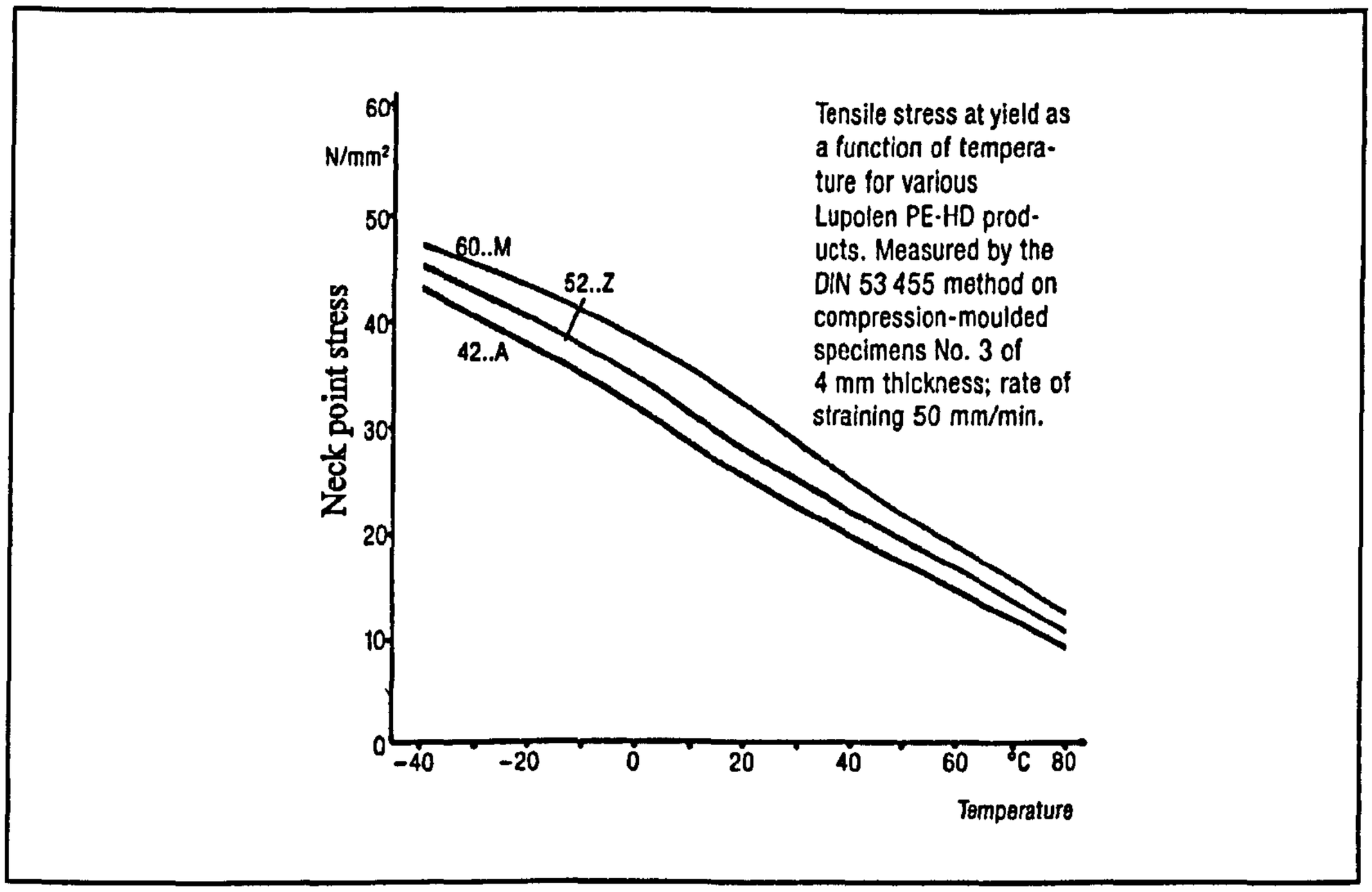

Figure 3.13 Effect of temperature on σ_n of HDPE [59]

3.2.4 Initial low strain material damping

Although there is data for the effect of temperature on the low strain material damping of thermoplastics e.g. Figure 3.14 [59], the reported trends are suspect due to limitations of the test methodology and equipment (see section 3.1.3).

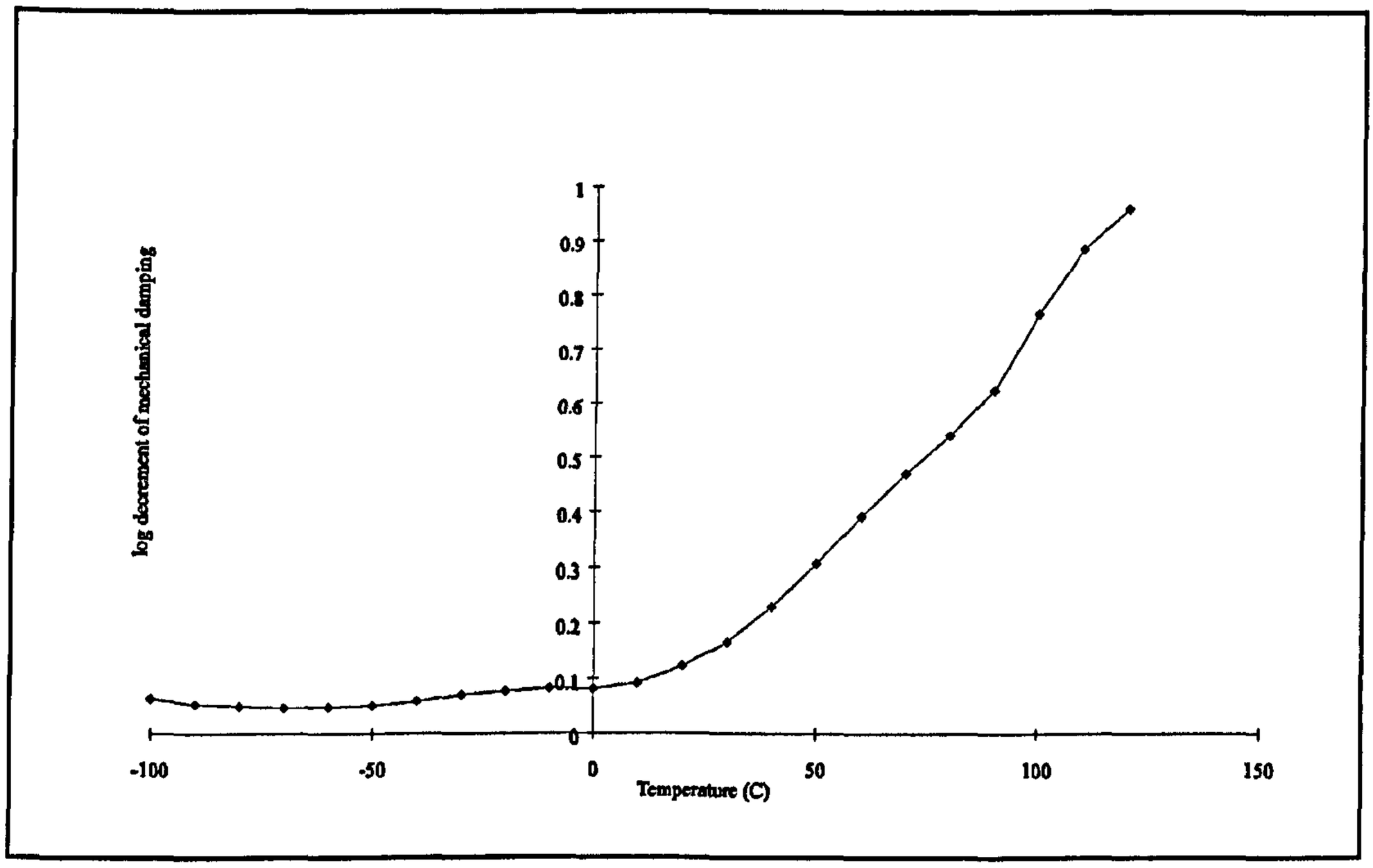

Figure 3.14 Effect of temperature on DMA shear damping of HDPE [59]

3.3 Summary of material property trends

The effects of strain rate and temperature on the initial material stiffness and point of neck formation are summarised in Table 3.1.

Material property	Effect of $\dot{\varepsilon}$	Approximate relationship	Effect of T	Approximate relationship
E	Increase	$\propto \ln \dot{\varepsilon}$	Decrease	$\propto -T$
σ_n	Increase	$\propto \ln \dot{\varepsilon}$	Decrease	$\propto -T$
ε_n	Decrease	$\propto -\ln \dot{\varepsilon}$	Increase	$\propto T$

Table 3.1 Effects of strain rate and temperature

Previous work [38] has shown that the effect of strain rate on large strain post yield compressive behaviour of a material can be described as a simple Eyring model for

the strain range of 10^{-4} to 10^{+4} s^{-1} and the temperature range of -20 to 23° C. In addition it appears that the low strain elastic stiffness also follows a similar trend with respect to both temperature and the natural logarithm of strain rate [56,59,55]. The effect of increasing strain rate and decreasing temperature is to increase the linearity of the stress-strain curve. It can thus be concluded that there are definite material stiffness trends with respect to both strain rate and temperature which indicate that both the low strain modulus and material neck point appear to follow an Eyring rule for both strain rate and temperature. Thus it is probable that the shape of the stress-strain curve also follows this rule.

Chapter 4

High strain rate events and their simulation

Despite the fact that polymeric materials have been used for impact resistant applications for many years, the expertise to characterise the mechanical behaviour of these types of materials for use in the simulation of high strain rate events is not well developed. The nonlinear effects that occur in impact events may be broadly characterised as:

1) boundary (opening/closing of gaps, contact, follower force);

2) geometry - stress stiffening (membranes);

3) geometry - gross deformation with large rotations (snap through buckling);

4) geometry - large strains (engineering versus true stress and strain);

5) material - stiffness (plasticity, creep, viscoelasticity);

6) material - damage and failure (brittle, ductile).

Whereas the first three of these have been addressed in many commercial software analysis packages [17,20,21] there are no universally accepted models for the strain rate dependent nonlinear behaviour of thermoplastic materials. A successful implementation of a material model is defined by:

1) its ability to simulate the tests whereby the material properties were determined;

2) its use to satisfactorily predict the performance of complicated three dimensional objects.

In the case of most materials this means simulating the test whereby the true stress-strain curve was obtained. To determine adequacy of a three dimensional structural prediction it is necessary to establish the sensitivity of the numerical prediction and the degree of correlation with experimental test results. Although there are many papers detailing the determination of material models with strain rate and thermal

effects [60,61,62,63,64] these have generally been applied to the modelling of tensile test and fracture mechanics test samples and not to the prediction of complicated three dimensional objects.

In general the analysis of impact events applied to polymeric materials assume that the material properties are independent from the strain rate and the thermomechanical effects, which are known to occur. Typical of the material models used are the linear elastic orthotropic model used to model glass reinforced polymeric materials [51,65] and the multi-linear elastic-plastic isotropic model used to model thermoplastic materials [51,66,67]. These approaches are potentially flawed if the material in question has a strain rate dependent stiffness. In Nimmer's approach [51] it is suggested that a strain rate independent material stiffness can be used based on the maximum strain rate expected in the component. Despite reporting good results it is known that this approach is limited and can result in wrong predictions [45]. It is also known that the accuracy of predictions is strongly dependent on the material model used [58].

In approaching the modelling of polymeric material stiffness and failure the incorporation of nonlinear effects must follow the logical sequence as dictated by the loading of a material from zero strain to failure. Thus the sequence of nonlinear material effects that should be considered is:

1) strain rate/temperature dependent modulus;

2) nonlinearity of the stress-strain curve;

3) thermal softening;

4) damage and failure mechanisms.

4.1 Material testing configurations

4.1.1 Tensile test

A requirement of an analysis package, that can be used to simulate the impact performance of polymers; is that it uses the true stress and strain measures [68]. The reason for this is that to effectively use low modulus thermoplastics it is necessary to use the whole of the stress-strain curve by loading the material to strains at which the difference between engineering and true measures become significant. The simulation of the test illustrates some of the competing deformation modes within polymers. It has been documented [51,53] that there are two competing failure modes in polymers. These are described as shear yielding and crazing which infer that there should be a fundamental difference between tensile and compression yield of polymers. In the case of tensile loading existing voids may be encouraged to increase in size to form crazes whereas in the case of compressive loading these same voids are closed. This has been confirmed by experimental and theoretical studies [34]. During the tensile test the material softens i.e. $d\sigma/d\varepsilon$ decreases, up to the point of maximum test load, which is associated with shear yielding and ductile drawing. As the applied displacement increases the measured load decreases. Upon the formation of a stable neck in the tensile specimen and the response hardens i.e. $d\sigma/d\varepsilon$ increases, as the material crazes with polymers being drawn into a highly orientated state producing a fibrous material [69]. The use of bi-linear or creep models [70,64] cannot predict the formation of necking and tri-linear [51] or other [63] material models have been

proposed to model the unstable creation and subsequent stabilisation of the necking process. Whereas the tri-linear approach of Nimmer [51] has successfully been used to investigate the localisation and formation of necks within the tensile test, Nimmer's work has not embraced the questions of thermal softening and strain rate dependency.

4.1.2 Split Hopkins Pressure Bar test

In varying the thickness of the specimen size in the SHPB test it has been shown that for MDPE and HDPE the observed apparent increase in strain rate sensitivity is due to specimen geometry effects [71]. In analyzing the results of the SHPB tests both closed form wave propagation and three dimensional finite volume calculations were used. The material model used was a bi-linear representation with the elastic modulus determined from ultrasonic tests and the yield point and plastic modulus determined from the SHPB tests [38]. As the aim of the analyses was to investigate the effect of strain rate on the flow stress (σ_f) of polyethylene this could be readily achieved by these analyses. However as the applied strain rate in the SHPB test is nonuniform and changes rapidly prior to yield in the specimen, an investigation into the effect of strain rate on the initial modulus was not appropriate.

4.1.3 High speed double torsion test

In developing the high speed double torsion test geometry to measure the small strain shear modulus of polyethylene at the high strain rates appropriate to rapid crack propagation, both steady state and fully dynamic numerical models were used to calculate the fracture resistance of each test [45]. Both linear elastic and elastic/plastic rate independent material models were used, with modulus values determined from

ultrasonic tests, to compare test and analysis data. Despite the use of a nonlinear elastic-plastic material model it was concluded that the non inclusion of strain rate effects resulted in excessively high loads being predicted.

4.2 Instrumented puncture test

Before considering the analysis of this configuration it is necessary to understand how the discs are tested and what measurements are made.

4.2.1 Test configuration

In general the disc will be impacted in a similar configuration to the British Standard [41] and that the force time history trace of the piezo electric load cell will be compared with the predicted force between the hemispherical striker and the disc. Although it is assumed that the force recorded in the test is also that sustained by the specimen [72] this is not always true. The remotely measured response of the load cell is not necessarily that experienced by the specimen due to mechanical oscillations and wave propagation effects within the hemispherical striker. It is also important to note that the recorded response may be heavily filtered [72] by the physical characteristics of the measurement transducer, electronic circuitry and time domain aliassing. Hence experimental results can be very misleading [73]. If a well conditioned test is conducted, in which the transient dynamic effects of the impacting hemispherical striker and measurement load cell can be neglected, then characteristics of the force time history can be attributed to a quasi static large deformation and contact problem [51,73,74]. If the material has a strain rate dependent stiffness then

the measured response is a function of incident energy and velocity [72]. Failure to include strain rate dependency of the material stiffness can result in poor correlation between test and analyses [75].

4.2.2 Analyses

Although finite element analyses have been carried out on the instrumented puncture test configuration [51,73,74,75,76] these have assumed that the materials have the following characteristics:

1) isotropic;

2) no dependence of behaviour on the hydrostatic component of stress;

3) identical yield behaviour in tension and compression;

4) no strain rate dependency or thermal effects;

5) material's one dimensional stiffness can be defined by a bi-linear [74,75] or tri-linear stress-strain curve idealisation.

Although the tri-linear elastic-plastic approach by Nimmer et al. [51,73] appears to be successful, the analyses are "speculative" as the basis of Nimmer's material model has not been rigorously proved, thus the good correlation may have been achieved by chance. In particular Nimmer's approach of using the von Mises equivalent stress to define ductile failure has been proved wrong for modelling the impact response and ductile failure of strain rate dependent aluminium discs [77]. Although strain rate dependent material models which include thermomechanical effects have been proposed for the analysis of the instrumented puncture test [76], sufficient material data has not been collated to characterise the materials and they not been implemented in numerical analyses of complicated components. The use of an effective stress based

failure criterion has been discounted as a suitable approach for modelling ductile failure [51,74,77] with the suggestion that failure modelling needs to be characterised by a fracture mechanics [74] or damage approach [77]. This is dramatically illustrated in Figure 4.1 which shows the effect of surface finish (and hence surface damage) on impact resistance [78].

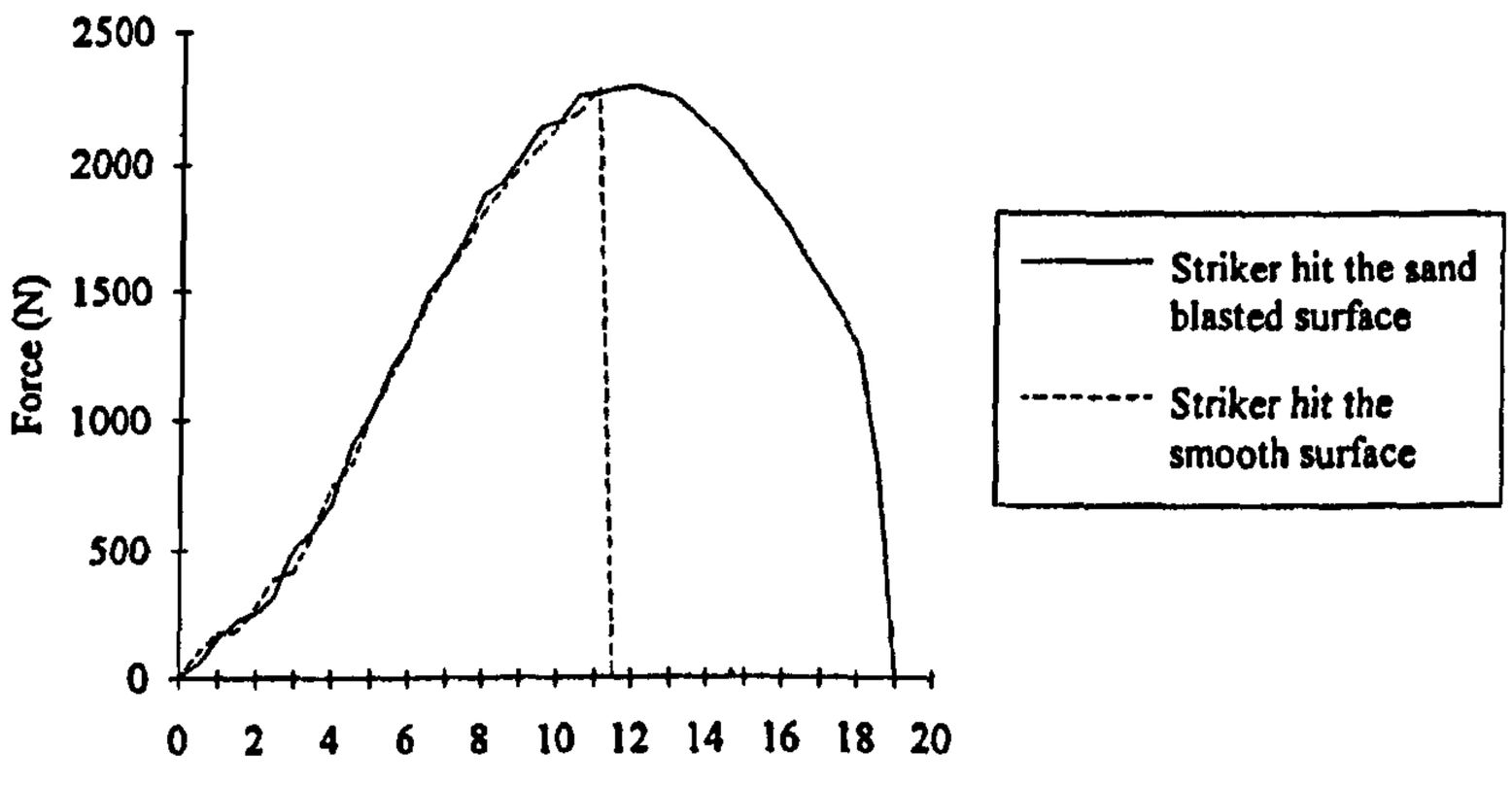

Force as a function of deformation of a medium impact resistant PP-copolymer when the striker hit the sandblasted surface and the smooth surface opposite to the sand blasted surface. Test temperature 0°C.

Figure 4.1 Effect of surface preparation on impact resistance [78]

4.2.3 Attributed effects

From experimental studies an insight has been obtained into the mechanisms involved. The initial measured response is due to the hemispherical striker and the load cell responding as a single degree of freedom system. Damage initiates very early under the nose of the impacting striker [72,79] is localised [73] and progressive throughout the test [72]. The peak force is associated with the onset of specimen collapse and the penetration of the hemispherical striker [72]. Correlation of quasi-static analysis with

test results indicate that the elastic response of the material accounts for little of the measured response [51] with the response being dominated by a small zone under the striker nose which is subject to very large strains. The stages of the predicted force time history in Figure 4.1 are:

1) initial elastic response (0-2 mm);

2) material yield under the nose of the striker and nonlinear geometrical stiffening (2-10 mm);

3) material softening and drawing under the nose of the striker (10-12 mm);

4) rapid thinning and perforation of the disc (12 mm and onwards).

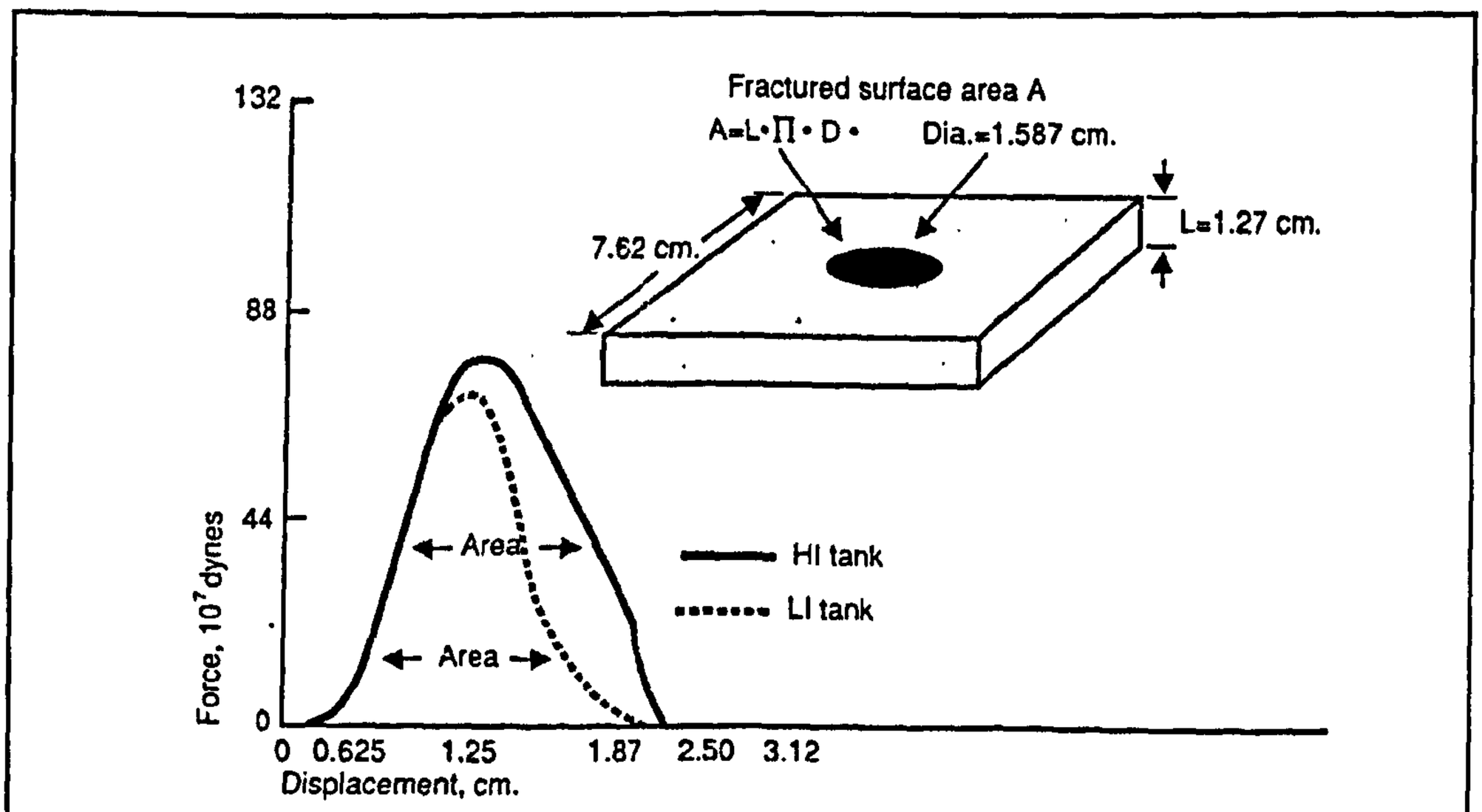

Dart impact strength of specimens from high-impact (HI) and low-impact (LI) high density polyethylene gasoline tanks.

Figure 4.2 Instrumented puncture test results for HDPE [80]

Figure 4.2 [80] shows that the difference between a high and low impact strength HDPE can be differentiated using the instrumented puncture test. Showing identical

characteristics for stages one to two, the third and fourth stages differentiate the material grades.

4.3 Polymeric materials in vehicles

Historically thermoplastic polymers have initially been used as nonstructural materials in vehicles and applied in areas where stiffness and strength were not important. As such it has not been necessary to determine their structural performance to impact loads. The author has been working for a number of years predicting the performance of thermoplastic pressure vessels for the Rover Group [81,82,83,84] and has achieved good correlation with experimental results for the long term deformation of these types of components. Polymeric materials can be used for safety critical applications where the absorption of impact energy is required. Examples of this are the HDPE blow moulded bumper armature developed for the Mazda MX-5 [85] and the XENOY bumper armature [67]. Unfortunately no details of the structural performance of the HDPE bumper armature have been published. In their paper on the XENOY bumper armature [67] Nimmer et al. concluded from their sizing calculations that transient dynamic effects would be negligible. The armature was analyzed using nonlinear static analysis and details were discussed in reference [51]. The following assumptions were made in the analysis: the material was idealised using a multi-linear isotropic elastic-plastic model using the von Mises yield equivalent stress, large deformations and effect of gaps were included. It is not reported whether a sensitivity analysis of the finite element modelling approach was undertaken and hence it is not possible to identify what aspect of the analytical modelling resulted in the quoted excellent correlation with full scale test results.

4.4 Liquid containing vessels

There is very little information available on this subject. Indeed following detailed discussions with two of the major European material suppliers (BASF and Solvay) it became clear that no one was currently working on the prediction of the impact performance of thermoplastic components. This implies that significant development risks are being taken, as in automotive applications thermoplastic fuel tanks are required to be subjected to full scale impact qualification tests [3]. In the sphere of military applications implicit codes such as ANSYS and explicit analysis codes such as LS-DYNA3D are being used to analyze fluid filled containers [86] and the crash performance of whole helicopters (containing fluid filled containers) [87]. In the case of the fluid filled container [86] a fragility criterion was assumed. The requirement was that the container (an aluminium transformer housing) should be able to withstand an equivalent 40g quasi static acceleration. The analysis consisted of two stages: establishing the equivalent fluid load at 40g and applying this to the transformer casing. No correlation with any test results was quoted.

The helicopter analysis [87] was a more rigorous approach and modelled the airframe structure and tank, filled with fluid, subjected to a 65 ft drop test. No details of how the fuel tank (reinforced Firestone 1550-1) was modelled were given but it was stated that the fuel load was modelled using solid elements with an elastic-plastic hydrodynamic model. The analysis predicted the pressure time profile in the fuel tank and this was shown to compare well with test data. The analysis concluded: "The impact of the fuel tank with the ground initially induces a short wave propagation mode during which high internal pressures are generated, which is followed by a large

deformation mode, due to inertial effects. Since the deformations associated with the shortwave propagation are relatively small, the design loads should be primarily based on the large deformation interaction pressures due to inertial effects." From this it can be deduced that the potential failure of a fuel tank could be due to two different phenomena. The first could be a brittle failure, associated with very high strain rates with failure initiating at a surface flaw in the tank; and the second could be a ductile failure as the tank grossly deforms at a high strain rate. For the first failure mode (brittle) nonlinear finite element impact simulations are not suitable for reducing the design development risk as the failure occurs at high strain rates but low strains. For this type of failure a fracture mechanics approach is necessary. Nonlinear impact simulations are suitable for reducing the design development risk if the potential failure is associated with gross deformations (large strains) of the tank.

4.5 Summary of previous material modelling experience

It was found that although the effect of strain rate and temperature on the stiffness of polymers was significant, models containing these had not been used to simulate the impact performance of complicated thermoplastic components subject to elevated strain rate events. If the expected component strain rate and temperature are known to be uniform then a strain rate and temperature independent multi-linear elastic-plastic material approach can be used [51]. If not then it is necessary for the material model to include strain rate and temperature effects otherwise inaccurate predictions will be made [45]. Although material models which include strain rates effects have been

used to model the creep stiffness of polymers [70] these models need to be verified with respect to a wide range of strain rates and have not been used in high strain rate impact analyses. Most models cannot represent material behaviour beyond the necking point in the tensile test. Above this point a fracture mechanics or damage material model is required [51]. Both multi-linear [51] and non-linear time dependent [70] material modelling approaches have been shown to successfully model the stiffness behaviour of thermoplastics, however they have not been used to model whole components.

Chapter 5

Proposed hypothesis and evaluation plan

Having established that there is a need to ascertain how the mechanical characteristics of thermoplastics should be measured and modelled for inclusion in impact simulations [12,13,17] (Chapter 1), previous work has been reviewed to establish how material properties have been measured (Chapter 2) and what the known effects of temperature and strain rate have on the stiffness of HDPE (Chapter 3). It was concluded that there are definite material stiffness trends with respect to both strain rate and temperature. The impact simulation of thermoplastic components was then investigated to establish what material models previous workers had used (Chapter 4). It was found that although the effect of strain rate and temperature on the stiffness of thermoplastics was significant, material models containing these effects had not been used to simulate the impact performance of complicated thermoplastic components subject to elevated strain rate events. This is acceptable if the strain rate and temperature in a component are known and remain relatively constant. However there still remains the need to develop a consistent methodology of how the strain rate dependent stiffness of polymeric materials should be measured, modelled and used in the impact simulation of a complicated thermoplastic components subject to elevated nonuniform strain rate events.

5.1 Hypothesis

It was proposed that:

1) below the tensile test neck point, the material stiffness of thermoplastics can be characterised by a bi-linear curve fit idealization;

2) measurements for the stiffness data can be made at slow strain rates and the bi-linear idealization extrapolated to high strain rates;

3) using this bi-linear idealization for the stress-strain curve and including the effects of the variable strain rate, the impact performance of thermoplastic components subject to nonuniform elevated strain rates may be simulated.

5.2 Evaluation plan

This hypothesis was evaluated in four principal stages:

1) establish a suitable method for determining the strain rate dependent stress-strain curve of HDPE such that the measured data would be suitable for use in impact simulations;

2) measure the strain rate dependent stiffness of HDPE and compare it with measurements made at high strain rates;

3) establish the suitability of this methodology for predicting the impact performance of simple structures such as beams and discs;

4) establish the suitability of this methodology for predicting the impact performance of complicated structures such as a blow moulded fuel tank.

Chapter 6

Stress-strain measurements and the effect of displacement control

If the effect of applied deformation rate on the mechanical performance of a thermoplastic is to be investigated, over a wide range of strain rates, then more than one test machine will generally be required. Thus it is important that a consistent loading methodology is used otherwise the test results will be dependent on the different loading methodologies used for the different tests. To investigate the effect of test loading methodology a series of tests was undertaken, using the three control methods available for an Instron 4505 tensile tester at the University of Warwick's International Manufacturing Centre (IMC). The aim was to compare the effect of tensile test control methods on the material properties that the test methods propose to measure such as those defined in [31] i.e. the engineering measures of 0.2% secant modulus (E) and Poisson's ratio (υ) and the stress (σ_n) and strain (ε_n) at maximum load.

6.1 Manufacture of tensile test samples

The test samples were prepared from a rotationally moulded JCB fuel tank, supplied by Wilmid plc. The fuel tank material was a linear polyethylene for rotational moulding (NCPE 8627/NCPE 8628 supplied by NESTE Chemicals). Rectangular plaques were cut from the tanks and then annealed whilst being held flat to remove residual stresses. This was done by heating overnight in an oven at 110° C and then slowly cooling the oven during the following day at 10° C/hour. Test specimens were cut from these plaques and filed to shape. The test specimen geometry used for the samples is defined as method 320C of BS 2782 part 3 [31].

6.2 Testing of samples

Due to problems with temperature stability of the IMC engineering hall, all the test samples were held at a constant temperature of 35° C in a thermal chamber during the testing. During the tests the load, tensile and lateral displacements of the samples were recorded via the tensile testing machines IEEE488 GPIB (general purpose interface bus) using the default PC based data acquisition software supplied by Instron.

6.2.1 Strain rate control methods

There were three available methods of machine control: "position", (closed loop) "control" and "pacing". The control signals used for the three methods are shown in Table 6.1.

Control method	Control signal
Crosshead	$\dot{\delta}$
Pacing	ε, p
"Closed loop" Control	$\dot{\varepsilon}$, $\dot{p}$

Table 6.1 Control method - control signals

For the "control" method the user can change the tensile tester's control parameters, but for the "position" and "pacing" methods the user can not. The default method is "position" control of the tensile tester's crosshead. In this method the tensile tester's controller attempts to maintain a constant crosshead displacement rate ($\dot{\delta}$), as determined by the twin crosshead screw encoders, by changing the motor speed. This method does not attempt to control the straining or loading rate of the test sample. The second method type is "pacing" control using the data logging PC to calculate a

load or strain (ε, p) drive signal which is supplied at 50 Hz to the controller via the GPIB link. The tensile tester's controller then attempts to match this demand signal by changing the motor speed. The third method type is (closed loop) "control" using the load/strain hardware option within the tensile tester's advanced functions panel to control the test strain or loading rate (έ, ṕ). This is a closed loop method in which the proportional, differential and integral terms of the control system can be changed to optimise the system response.

6.2.2 Data sampling and strain rate limits

To compare the three different methods it is necessary to run comparative tests at similar strain rates and data acquisition rates for the three different methods. Thus the range of comparable test strain rates is limited by the common ability of all the three methods. Table 6.2 lists the documented strain rate and crosshead rates for the three available control methods.

Control method	Deformation rate range (mm/min)
Crosshead	0.001 to 1000
Pacing	0.0025 to ? or 1% of extensometer full scale deflection to ?
Control (Closed loop)	none specified

Table 6.2 Control method deformation rate limits

As there were no specified limits for the "control" (closed loop) method, the minimum controllable test strain rate was determined by the gauge length of the sample

extensometer (50 mm) and by generating a large enough signal for the "pacing" method control system (0.5 mm/min, 1%/min). The maximum possible test strain rate for all methods was determined by the maximum achievable crosshead rate of the tester and the test sample dimensions. For a standard thermoplastic test sample, such as that defined by method 320C of BS 2782 part 3 [31], a crosshead rate of 1000 mm/min corresponds to a sample strain rate of ≈800%/min. A further factor in determining the desired test strain rates was the ability of the data acquisition (DAQ) system to record the test results at the required strain resolution. The sample strain resolution (SSRN) is defined as:

$$SSRN\ (\%) = \frac{crosshead\ rate * gauge\ length\ factor * 100}{gauge\ length * 60 * sampling\ rate} \qquad (9)$$

The frequency of tensile tester control system was 250 Hz and the maximum available data sampling rate (set by the Instron software) was 50 Hz. Table 6.3 lists the available sampling rates for the three control methods.

Control method	Data sampling rate range (Hz)
Crosshead	50/i (i=1 to 3333)
Pacing	5/i (i=1 to ? by data reduction)
Control (Closed loop)	50/i (i=1 to 3333)

Table 6.3 Control method sampling rate limits

For the "pacing" method the sampling rate was fixed at 5 Hz but this could be reduced by data reduction. i.e. only recording the data every i^{th} sample number. By assuming the following data for Equation 9:

1) crosshead rate = 1000 mm/min;

2) gauge length factor = 0.6 (gauge length sample deformation / crosshead deformation);

3) gauge length = 50 mm;

4) sampling rate = 50 Hz;

the resulting sample strain resolution would be 0.4% . A sample strain resolution of 0.4% is clearly inadequate if the 0.2% secant modulus is required [31]. It should also be noted that for the "pacing" and "control" methods to work, the desired rate must be significantly below the maximum achievable strain rate for the controller to be able to decrease or increase the motor speed to achieve the desired rate. Table 6.4 lists the five test strain rates, corresponding crosshead rates and data sampling rates that were chosen. It should be noted that the "pacing" method was not appropriate above $\dot{\varepsilon}$ = 24 %/min as the data acquisition rate was limited to 5 Hz and thus limiting the strain resolution. Hence the "pacing" method has a limited strain rate range and is not considered a suitable method for determining the effect of strain rate on material parameters.

Crosshead		Pacing		Control		ε (%) resolution
$\dot{\delta}$ (mm/min)	DAQ rate (Hz)	$\dot{\varepsilon}$ (%/min)	DAQ rate (Hz)	$\dot{\varepsilon}$ (%/min)	DAQ rate (Hz)	
200	50			240	50	0.08
65	25			78	25	0.052
20	5	24	5	24	5	0.08
6.5	2.5	7.8	2.5	7.8	22.5	0.052
2	0.5	2.4	0.5	2.4	0.5	0.08

Table 6.4 Chosen test strain and data sampling rates

6.3 Results

Having recorded the displacement and load during the tests these were converted into engineering stress and strain using the MATLAB mathematical analysis program [88]. The test time was implicitly known as a constant data sampling rate was used and hence the tensile strain rate could be calculated. Figure 6.1 shows the typical stress-strain curves that were measured and the effect of the applied deformation rate. The results from the three sets of test are listed in Tables A1 to A3 of Appendix A.

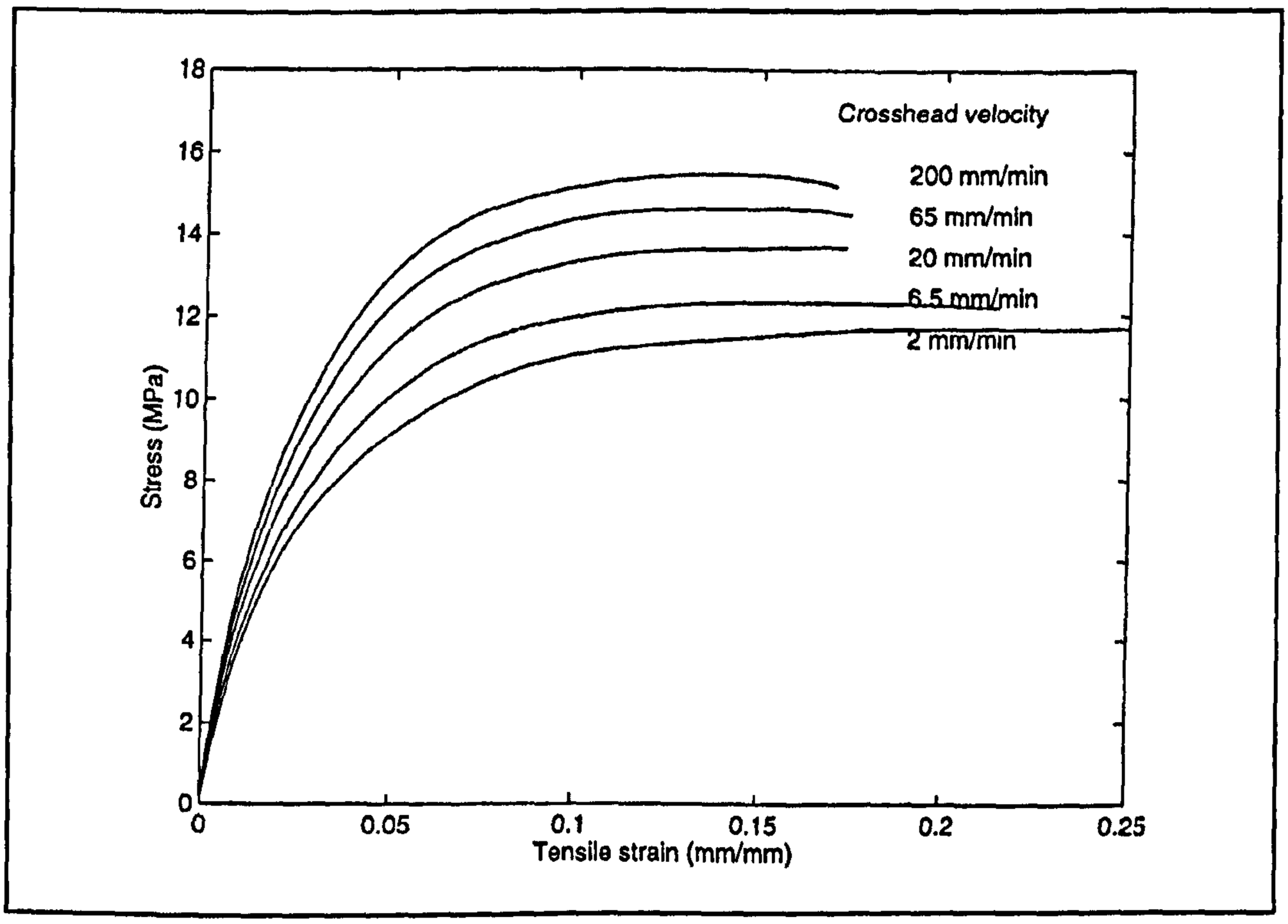

Figure 6.1 Crosshead method - effect of test crosshead rate

6.3.1 Strain rate profile

Figures 6.2 to 6.4 show the typical normalised strain rate response of the three different methods and how the effect of desired deformation rate affects the strain rate

response of the tensile test specimen. Figure 6.2 shows the effect of desired deformation rate has little effect on the normalised strain rate response of the tensile test specimen for the "crosshead" method. Figures 6.3 and 6.4 clearly show that as the desired deformation rate is increased the system's ability to achieve this, for the "pacing" and "control" methods, decreases. At the slowest deformation rate used (2.4 %/min) the erratic strain rate response of the tensile test specimen indicated that the "pacing" method was struggling with the small control signal.

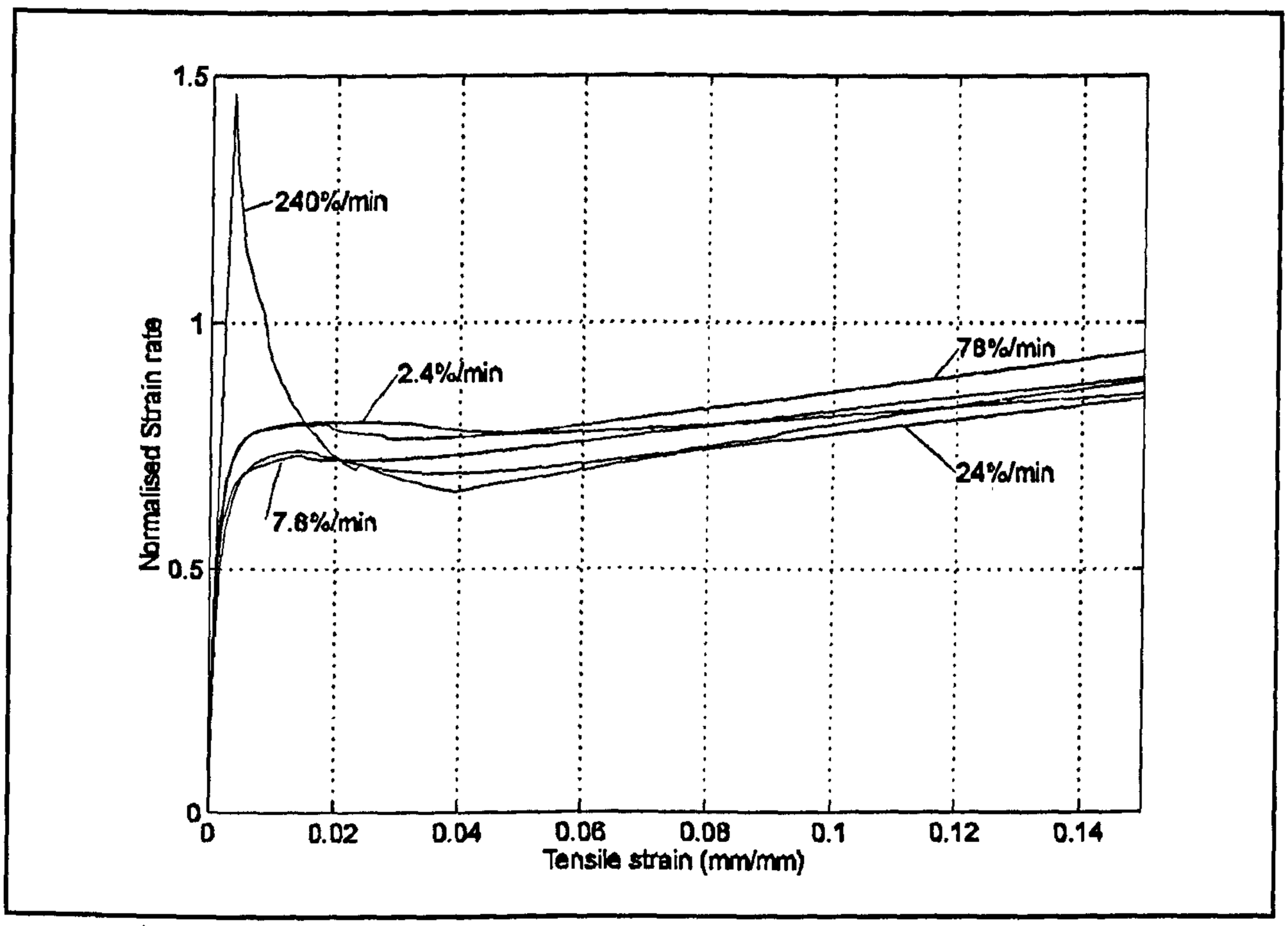

Figure 6.2 Crosshead method - effect of desired deformation rate

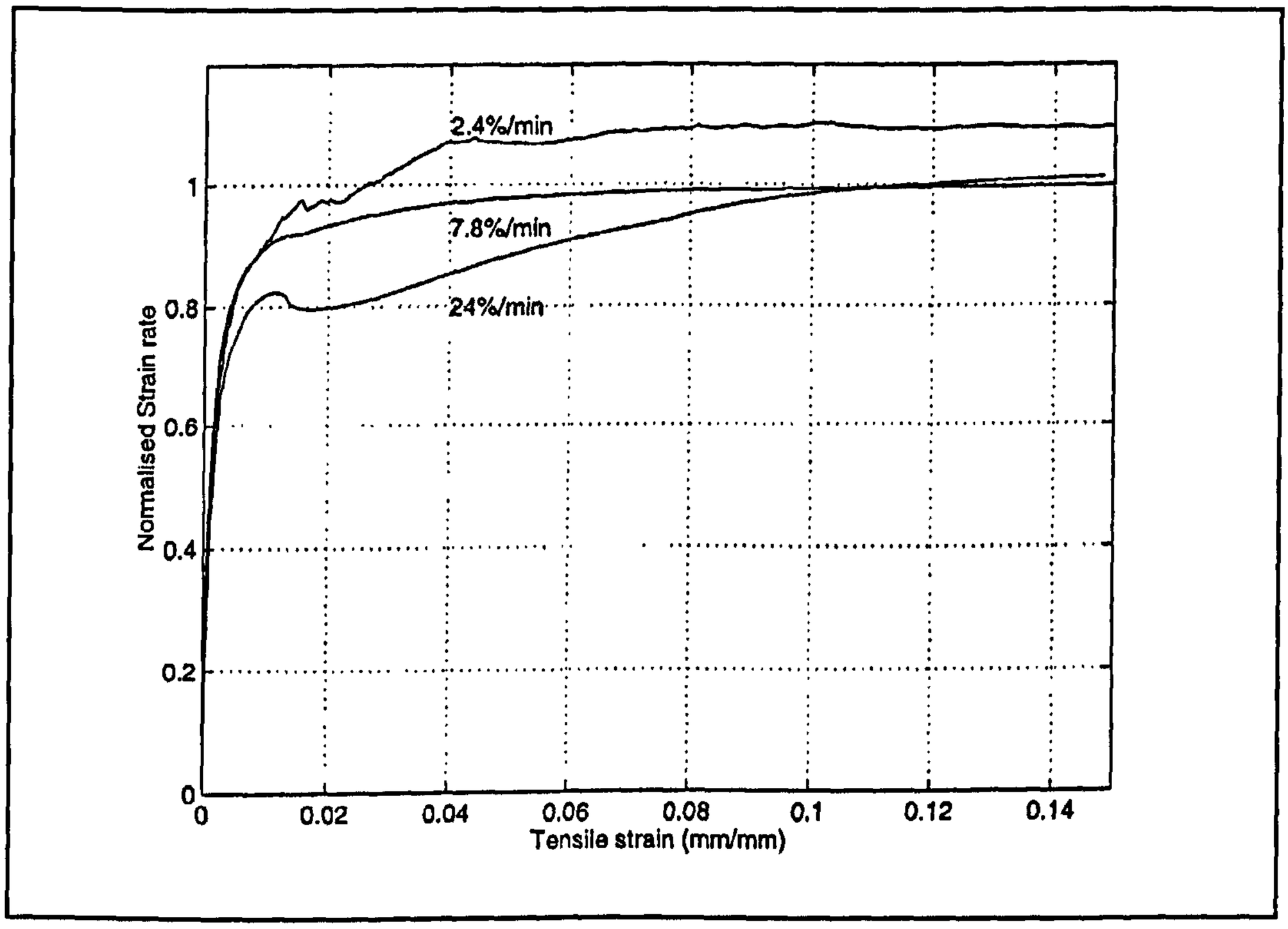

Figure 6.3 Pacing method - effect of desired deformation rate

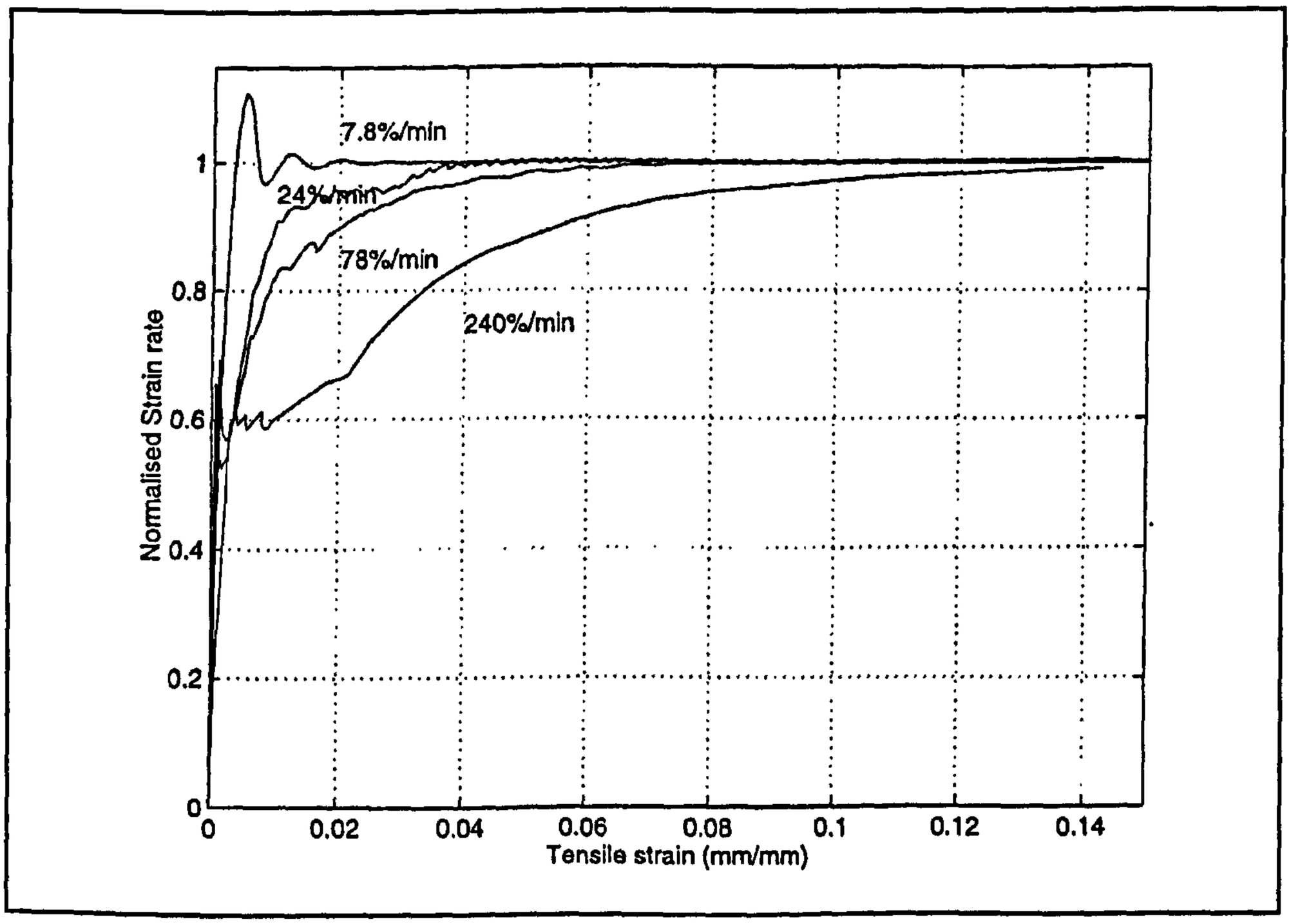

Figure 6.4 Control method - effect of desired deformation rate

For the "control" (closed loop) method the control parameters were set up for the fastest deformation rate. The gain was set just below that at which a noticeable resonance could be heard from the test machine. These control parameters were held constant for four of the tests ($\dot{\varepsilon}$ = 240, 78, 24, 7.8 %/min). However for the slowest test ($\dot{\varepsilon}$ = 2.4 %/min) the gain setting needed to be reduced due to noticeable under damping of the system response. Figure 6.4 indicates that although it was thought that the gain setting had been chosen to avoid exciting any dynamic system resonances, dynamic resonant responses can clearly be seen on some of the strain rate plots for the tensile test specimens. In trying to identify at what frequency the system was vibrating it should be noted that the test data sampling rate and number of data samples limits the frequency content and resolution of the measured response due to aliassing [89]. (The frequency range of the spectrum is 0 to the Nyquist frequency and the resolution of the spectrum is the sampling rate divided by the total number of data samples.) From counting the number of vibration cycles with respect to the time axis the system resonant frequency was estimated to be at approximately 3½ to 4 Hz.

Figures A1 to A5 in Appendix A show comparisons of the different test methods for the same five nominal test strain rates (0.0004 to 0.04 s^{-1}). For all the comparisons the crosshead method shows that after an initial transient, the tensile strain rate increases continuously whereas for the other two methods the strain rate responses converge on a constant value. At the slowest test deformation rate (0.0004 s^{-1}) there was negligible difference between the closed loop and pacing control methods but as the desired strain rate is increased the "control" (closed loop) method performs better than the "pacing" method. Figures A1 to A5 show that all three methods fail to result

in a constant strain rate during the tensile test. In theory the "control" (closed loop) method, with optimised control settings, should produce the best strain rate response during the tensile test at a given strain rate, however due to hardware limitations this could not be achieved.

6.3.2 Material properties

The effect of test deformation control methods on the following parameters: E, υ, σ_n, ε_n are shown in Figures 6.5 to 6.8 and Table 6.5 shows how the test methods affected the curve fits of the material properties measured with respect to the natural logarithm of strain rate.

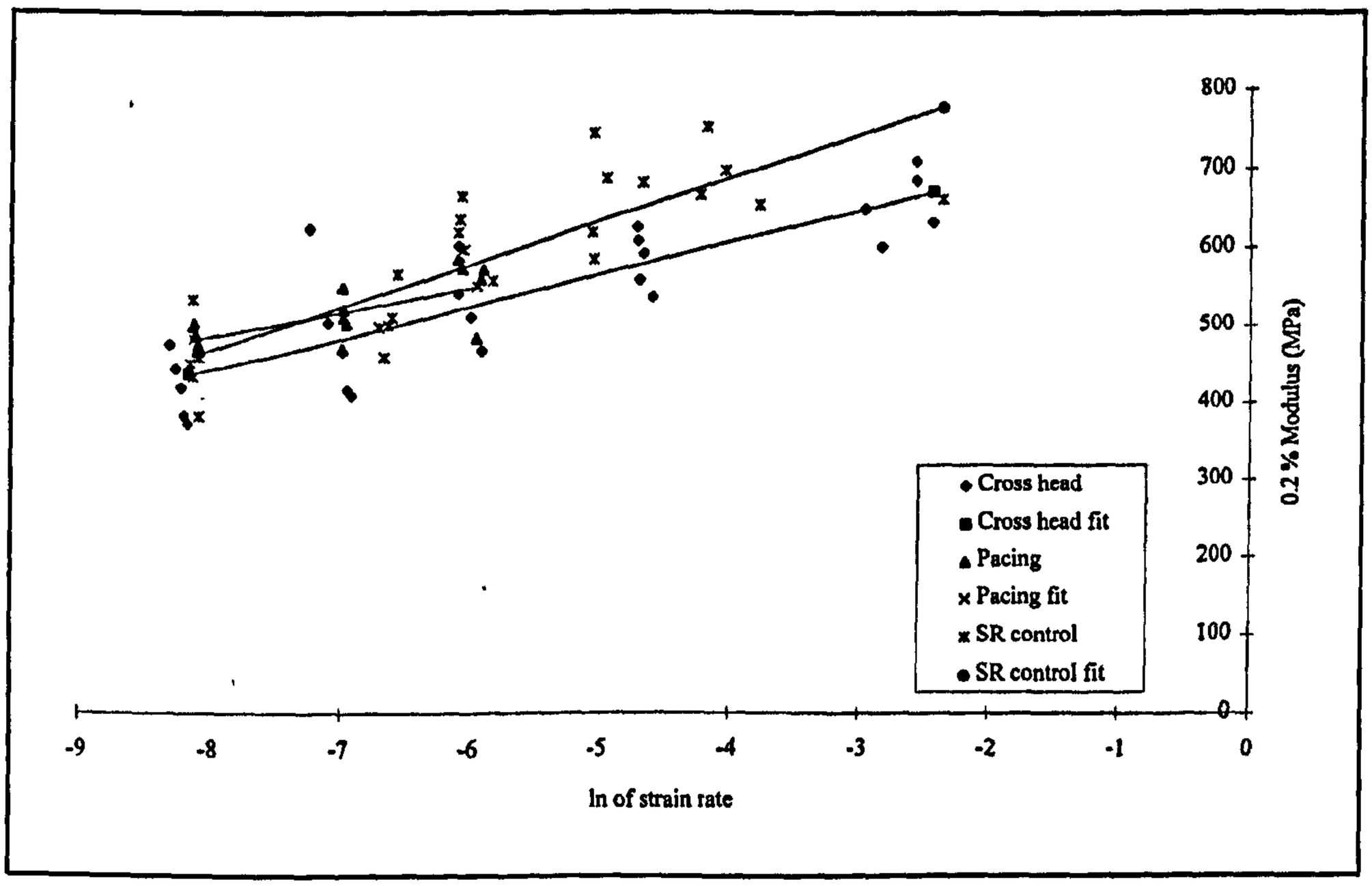

Figure 6.5 Effect of strain rate on 0.2% modulus

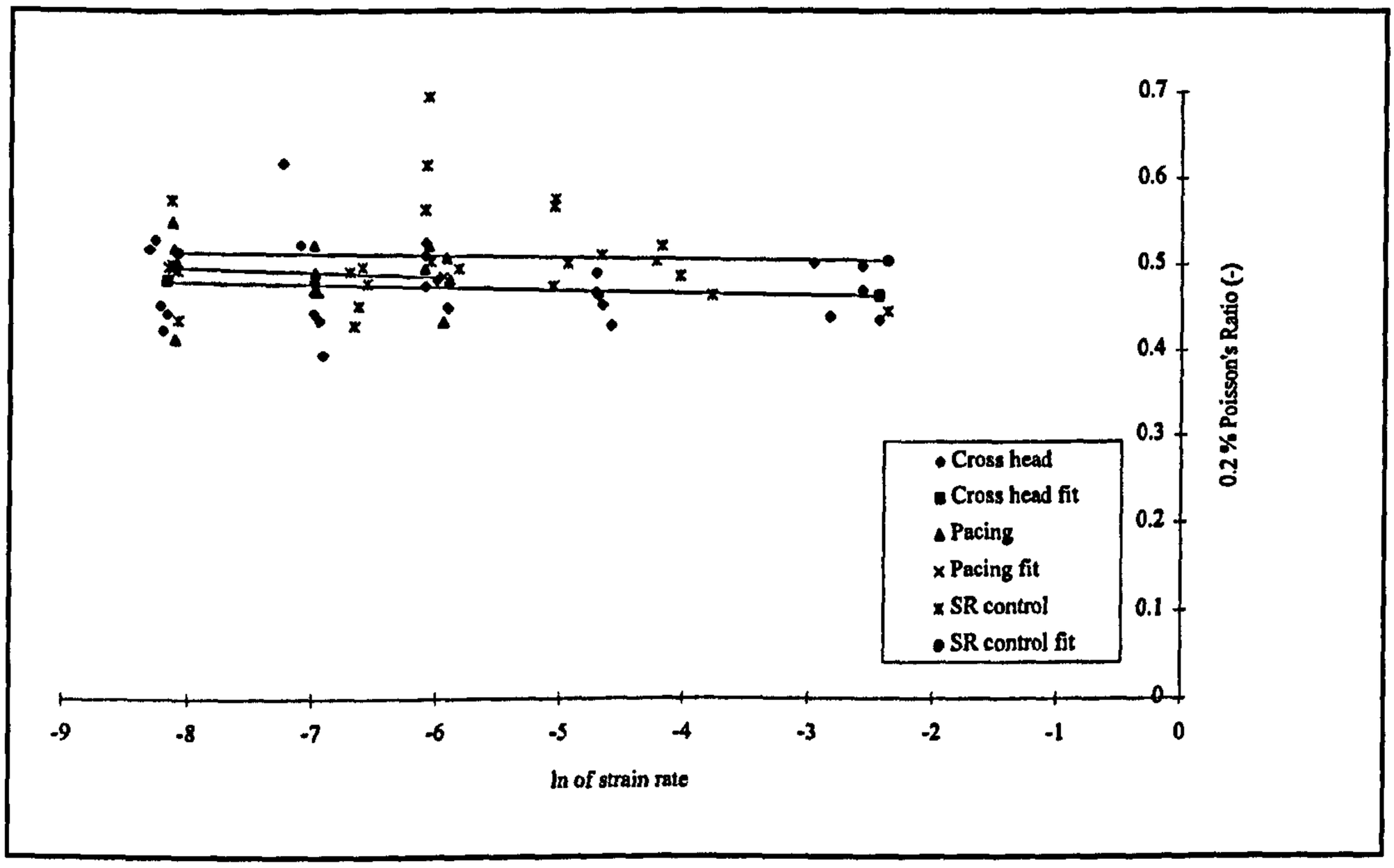

Figure 6.6 Effect of strain rate on 0.2% strain Poisson's Ratio

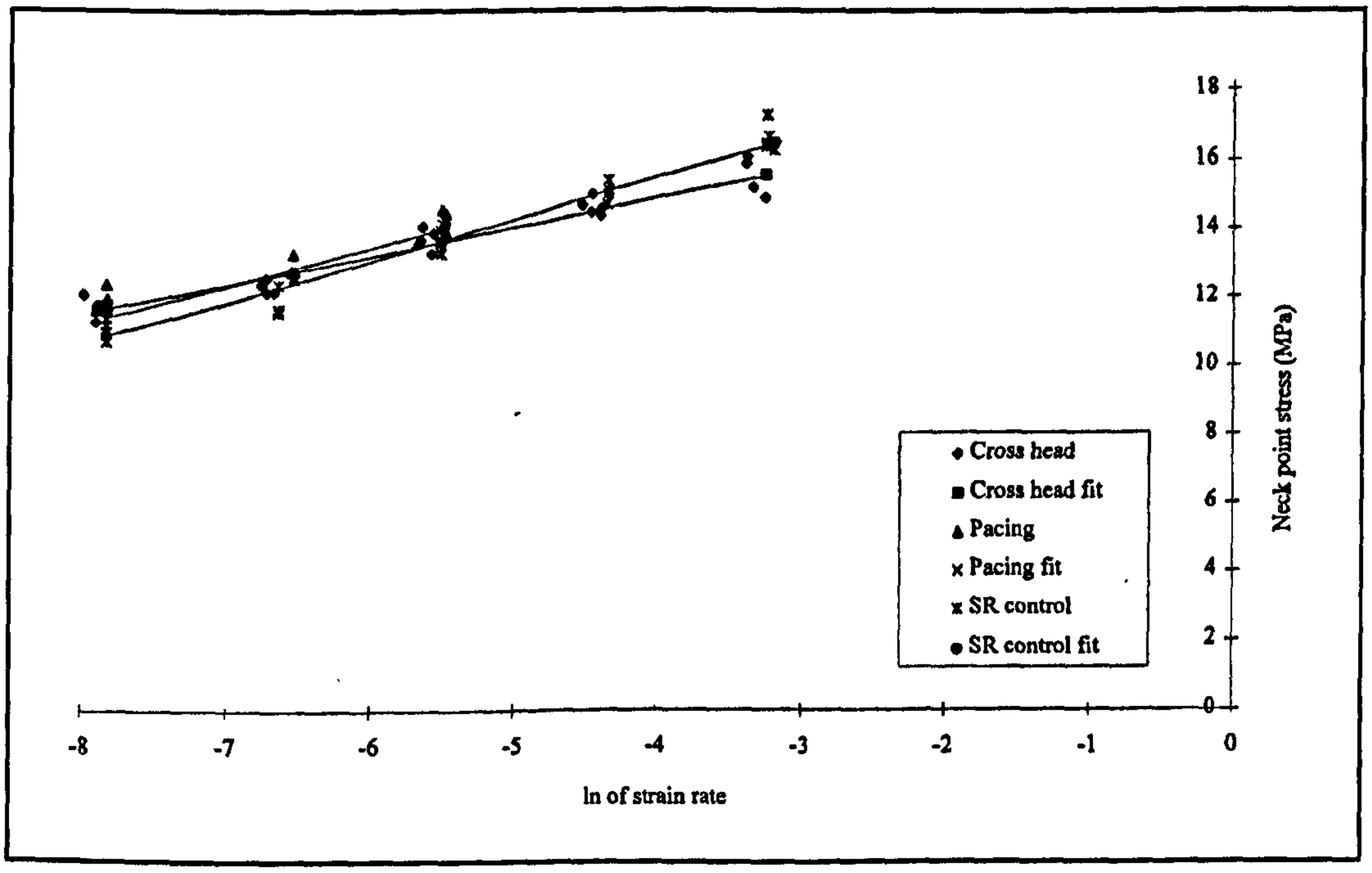

Figure 6.7 Effect of strain rate on neck point stress

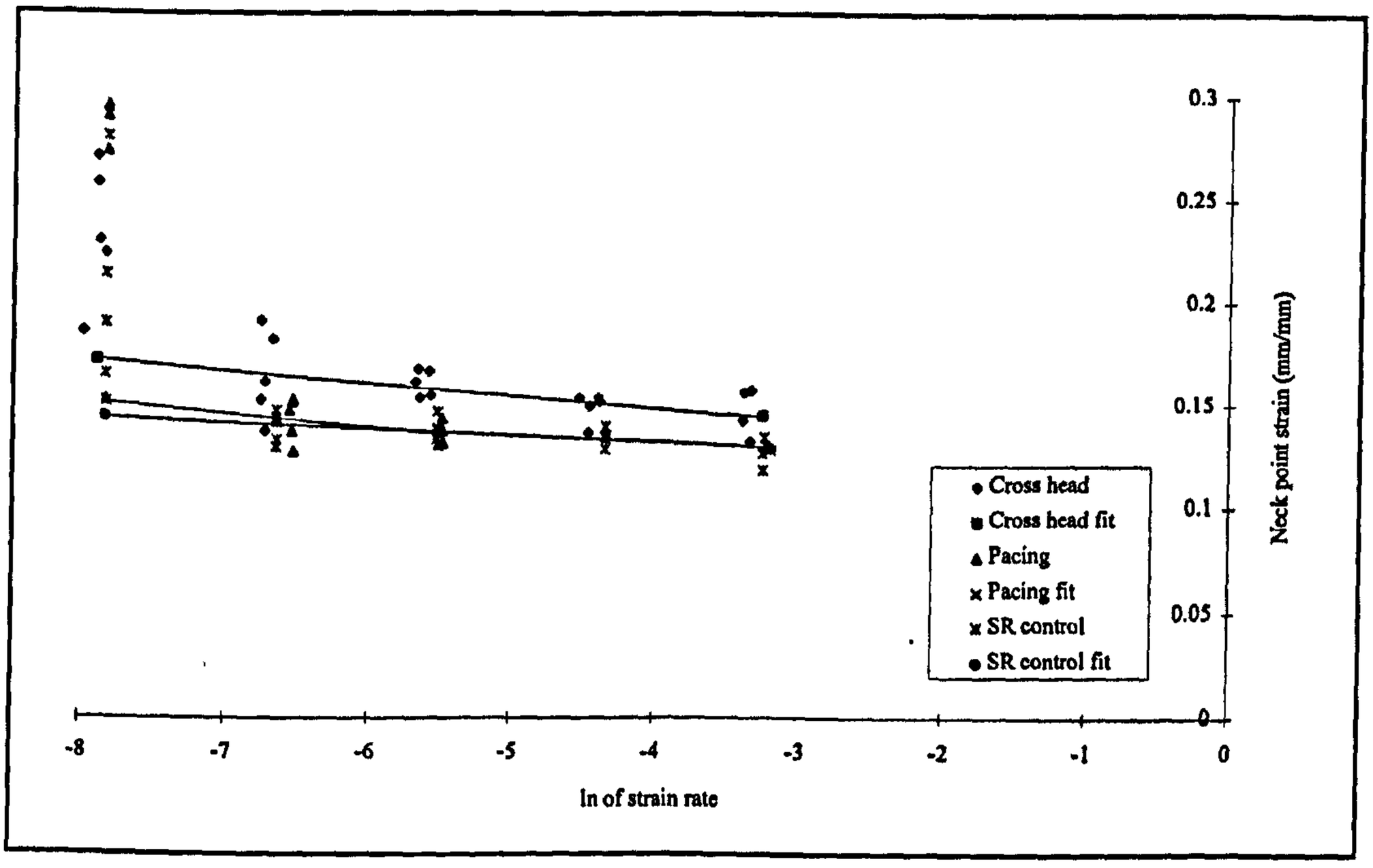

Figure 6.8 Effect of strain rate on neck point strain

If the material property under consideration is not sensitive to strain rate then it is unlikely to be affected by the test method. From the test results it was apparent that the material properties (E, υ, ε_n) are affected by the method used to control the applied deformation rate. The low strain at which the 0.2% secant modulus and Poisson's ratio are measured is where the relative accuracy of the stress-strain curve is at its worst. Hence there is a significant amount of scatter in the test results. The 0.2% modulus is affected by the applied strain rate whereas the Poisson's ratio does not appear to be. Figures 6.5 and 6.6 shows that there was a slight difference in the 0.2% modulus and Poisson's ratio measurements by the test methods, with the "control" (closed loop) method resulting in slightly higher values. The measurements for neck point stress for the three methods are very similar and there does not appear to be any significant difference between the test methods. The measurements of neck point

	0.2% Modulus		
	Crosshead fit	Pacing fit	Control fit
Gradient	41.2853	31.2466	54.7866
Intersection	773.147	736.591	907.647
	% change		
Gradient	1	-24.315	32.7026
Intersection	1	-4.7282	17.3965
	0.2% Poisson's ratio		
	Crosshead fit	Pacing fit	Control fit
Gradient	-0.0033	-0.0051	-0.0018
Intersection	0.45617	0.45524	0.49997
	% change		
Gradient	1	56.2094	-43.978
Intersection	1	-0.203	9.60177
	Neck point stress		
	Crosshead fit	Pacing fit	Control fit
Gradient	0.84543	1.01295	1.21848
Intersection	18.3291	19.7663	20.4109
	% change		
Gradient	1	19.8159	44.1266
Intersection	1	7.84125	11.3581
	Neck point strain		
	Crosshead fit	Pacing fit	Control fit
Gradient	-0.0059	-0.0065	-0.0033
Intersection	0.12542	0.10001	0.11788
	% change		
Gradient	1	11.7936	-43.005
Intersection	1	-20.26	-6.0098

Table 6.5 Material parameters effected by strain rate and test method

strain show a large amount of scatter at the slowest of the five test deformation rates. Once these data points have been removed from the data set, for the curve fit of the data with respect to the natural logarithm of strain rate, it was found that the "control"

(closed loop) method resulted in consistently higher values than the "crosshead" method.

6.4 Comparison of test methods

Due to the poor range of available deformation and data sampling rates and inability of the user to control the system response the "pacing" method is not a suitable method for the investigation of strain rate sensitive material properties and will not be discussed further. The response of the "control" (closed loop) method is especially sensitive to the controller settings which must be optimised for each desired deformation rate if a consistent set of normalised tensile test specimen strain rate responses are to be obtained. If this is not done then the method is not suitable for measurement of strain rate sensitive material properties especially those associated with accumulated strain. This optimisation of control settings was not possible for the tests undertaken at the IMC using the Instron 4505 due to mechanical resonance problems. Overcoming these mechanical resonance is an area for further work. There may be a number of methods to overcome the mechanical resonance which include: using the controller's built-in low pass filters (10 and 25 Hz) to prevent the controller exciting the mechanical resonance; or changing the system response by using a different extensometer.

Due to the large differences in measured strain rate sensitivity, shown in Table 6.5, and the fact that all the three methods investigated did not subject the tensile test specimen to a constant strain rate, a clear choice between the "control" (closed loop)

and "crosshead" methods could not be made. If the mechanical resonance was not present or could be controlled and the "control" (closed loop) system response optimised for each test, then this method would probably been the most suitable for the measurement of the strain rate sensitivity of material parameters. However as the desired deformation rate does not effect the normalised response of the "crosshead" method it was found to be more suitable than the "control" (closed loop) method, for investigating the effect of applied deformation rates in this series of tests. If different test machines are used to obtain strain rate dependent material data at differing strain rates, then it is of great importance that the normalised strain rate response of the different test machines are the same. If not then the two sets of data will not be comparable. During high strain rate tests it is not normally possible to control the strain rate of a test sample due to the short duration of the test event and hence, test methodologies attempt to achieve a constant crosshead rate. Therefore the most appropriate slow strain rate test control method for producing data comparable with high strain rate tests is the "crosshead" method.

6.5 Effect of displacement control - Conclusions

1) The stress-strain curve and strain rate sensitive materials properties are effected by the method used to control the applied deformation rate.

2) The "pacing" method has a limited strain rate range and is not considered a suitable method for determining the effect of strain rate on material properties.

3) If the system resonant response was not present or could be controlled and the "control" (closed loop) system response optimised for each test, then this

method would probably have been the most suitable for the measurement of the strain rate sensitity of material properties.

4) For the series of tests undertaken, the "crosshead" method was found to be the most suitable method for investigating the effect of applied deformation rates as the desired deformation rate does not effect the normalised response.

Chapter 7

Measurement and extrapolation of stiffness data

To investigate the effect of applied deformation on the mechanical performance of a thermoplastic over a wide range of strain rates ($3x10^{-4}$ to 20 s^{-1}) it was necessary to use two types of tensile test machines. These were a screw driven Lloyds M30K, for the slow strain rates, and a servohydraulic Instron 1343, for the high strain rates. The crosshead control method was used for both machines such that a consistent strain rate versus strain profile was achieved for both machines.

7.1 Test sample preparation

A high density polyethylene used for vehicle fuel tanks (Lupolene 4261A supplied by BASF) was injection moulded, in accordance with the suppliers recommended processing conditions [90], to form rectangular plaques of dimensions 196 x 137 mm with thicknesses of 3 and 5 mm. Also a limited number of samples were cut from a prototype Rover fuel tank made from the same material such that the properties of the injection moulded material could be compared with that obtained from a blow moulded component. To remove residual stresses, caused by manufacture, the samples were annealed whilst being held flat. This was done by heating overnight in an oven at 110° C and then slowly cooling the oven during the following day at 10° C/hour.

The same test geometry, but differing sample dimensions, was used for the slow strain rate (SSR) and high strain rate (HSR) tests. This was due to limitations of the available test equipment. For the high strain rate tests the samples needed to be small and light to achieve the desired 1m/s crosshead velocity. However at slow strain rates the load to break the small samples would not be sufficient compared with the full scale deflection of the 5 kN load cell on the available tensile testing machine in the

Advanced Technology Centre. The test specimen geometry used for the samples is defined as method 320C of BS 2782 part 3 [31], for the slow strain rate tests, and sample type B1 of ISO 6239 [91], for the high strain rate tensile tests. These test geometries are shown in Figures 7.1 and 7.2.

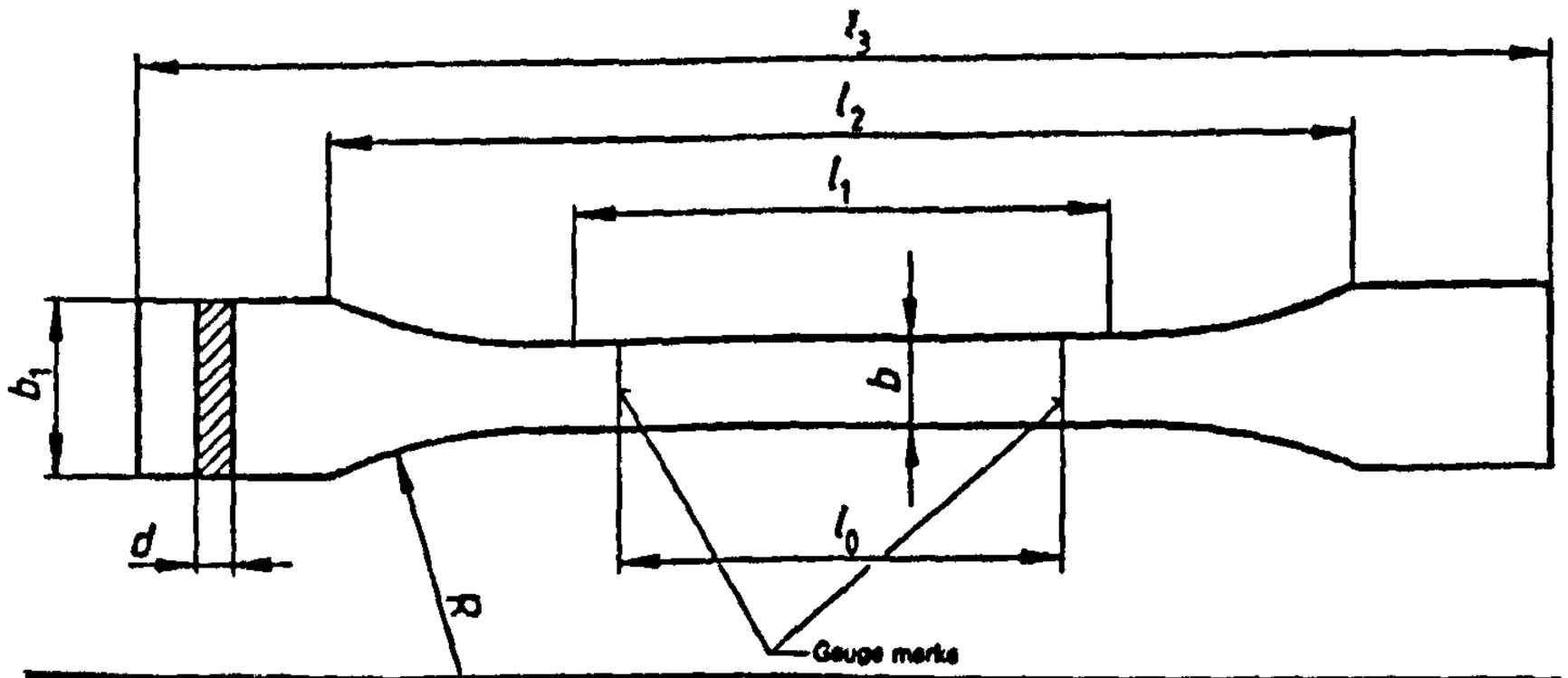

Dimensions in mm

l_3	Overall length	150 min	R	Radius	60 min
b_1	Width at ends	20 ± 0.2	d	Thickness	4 ± 0.2
l_1	Length of narrow parallel portion	60 ± 0.5	l_0	Distance between gauge marks	50 ± 0.5
b	Width of narrow parallel portion	10 ± 0.2	l_2	Initial distance between grips	115 ± 5

Figure 7.1 Slow speed tensile test sample geometry

For the slow strain rate tensile tests single samples were cut, using a standard die, from the centre of each of the 5 mm thick plaques. The samples were aligned with the material injection flow and labelled as "along" or "cross" flow. Similarly for the high strain rate tensile tests single samples were cut, using a laser, as a suitable cutting die was not available, from the centre of each of the 3 mm thick plaques. For the high strain rate tensile test specimens the surface finish of the gauge length was not satisfactory and all the samples were trimmed by hand using a sharp knife and trimming guides to ensure good quality samples.

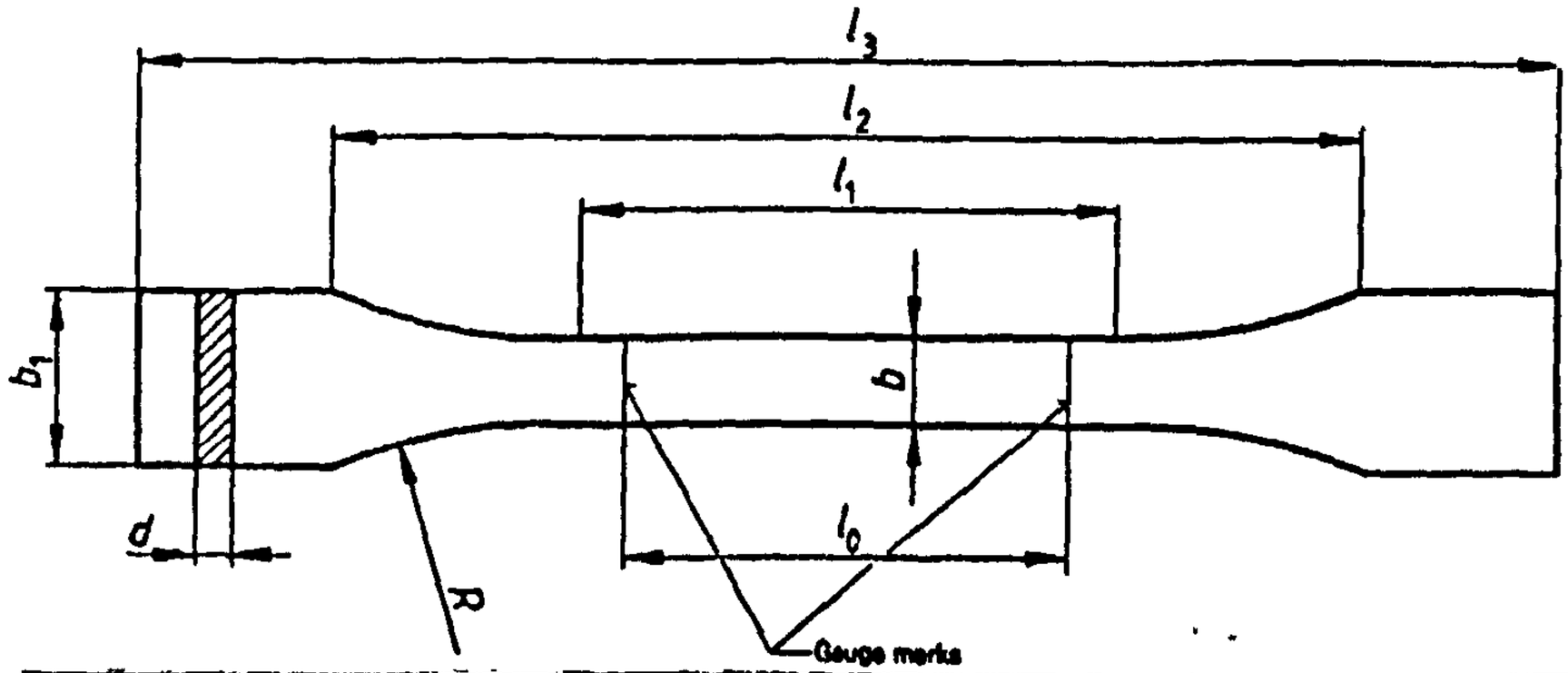

Dimensions in mm					
l_0	Overall length	75 min	R	Radius	30 min
b_1	Width at ends	10 ± 0.5	d	Thickness	2 min
l_1	Length of narrow parallel portion	30 ± 0.5	l_g	Distance between gauge marks	25 ± 0.5
b	Width of narrow parallel portion	5 ± 0.2	l_t	Initial distance between grips	58 ± 2

Figure 7.2 High speed tensile test sample geometry

7.2 Testing of samples

7.2.1 Slow strain rate testing

Crosshead rate (mm/min)	Data acquisition rate (Hz)
100	100
50	100
10	10
5	10
1	1

Table 7.1 Slow speed cross head and data sampling rates

Slow strain rate tensile tests were carried out at 23° C using a Lloyds M30K screw driven tensile testing machine at the ATC. The crosshead rates used were 1 to 100

mm/min. Strain was measured using an RDP-Howden linear-variable displacement transducer (LVDT) extensometer type V25/10. The tensile test machine load and extensometer displacement were simultaneously recorded using a PC based data acquisition system (DAQWARE version 1.1 from National Instruments Corporation). The test crosshead rates and data sampling rates used are listed in Table 7.1.

7.2.2 High strain rate testing

Temperature	23° C	0° C	-40° C
Crosshead velocity (m/s)	Data acquisition rate (Hz)		
1.0	20.48	20.48	20.48
0.1	2.048	2.048	2.048
0.01	0.2048	0.2048	0.2048

Table 7.2 High speed cross head and data acquisition rates

As a high strain rate tensile testing machine was not available at the University of Warwick, high strain rate tensile tests were carried out for the author by the National Physical Laboratory (NPL) at Teddington [92]. The tests were done using an Instron 1343 high speed servo hydraulic tensile testing machine fitted with light weight grips. The test force, measured by a quartz load cell type 9041, and crosshead ram displacement were recorded using a Gould DSO1605 storage oscilloscope. This data was then transferred to a Hewlet Packard 308 system and converted into MS-DOS ASCII formatted files. The test crosshead rates and data acquisition rates used are listed in Table 7.2.

7.3 Slow strain rate material property measurements

Having recorded the displacement and load during the tests these were converted into engineering stress-strain curves. Material properties were extracted from these stress-strain curves as defined in [31] i.e. 0.2% modulus (E) and the stress (σ_n) and strain (ε_n) at maximum load. The engineering stress-strain curves were then converted into true stress-strain curves by assuming a constant volume process. A comparison between the true stress-strain curve obtained assuming υ=0.5 and using a variable value from test showed that there was little significant difference between the two curves. The true stress-strain curves were then approximated by a bi-linear curve fit using the least squares method. The parameters of the bi-linear curve fit are: initial modulus (m_1), yield stress (σ_y) and secondary modulus (m_2).

7.3.1 Results of the tensile test

The material properties measured from the tensile test data are listed in Appendix B (Tables B1 to B6). Graphs of the tabulated results were created by plotting the material properties against the natural logarithm of the applied strain rate as shown in Figures 7.3 to 7.5. These Figures also include the least squares curve fit of the test data with respect to the natural logarithm of strain rate.

The data for the engineering measures of 0.2% modulus (E) and the neck point stress (σ_n) and strain (ε_n) show the expected test results i.e. as strain rate is increases so does 0.2% modulus and neck point stress with there being a corresponding decrease in neck point strain. Also the data for the Rover fuel tank samples lies between the bounds

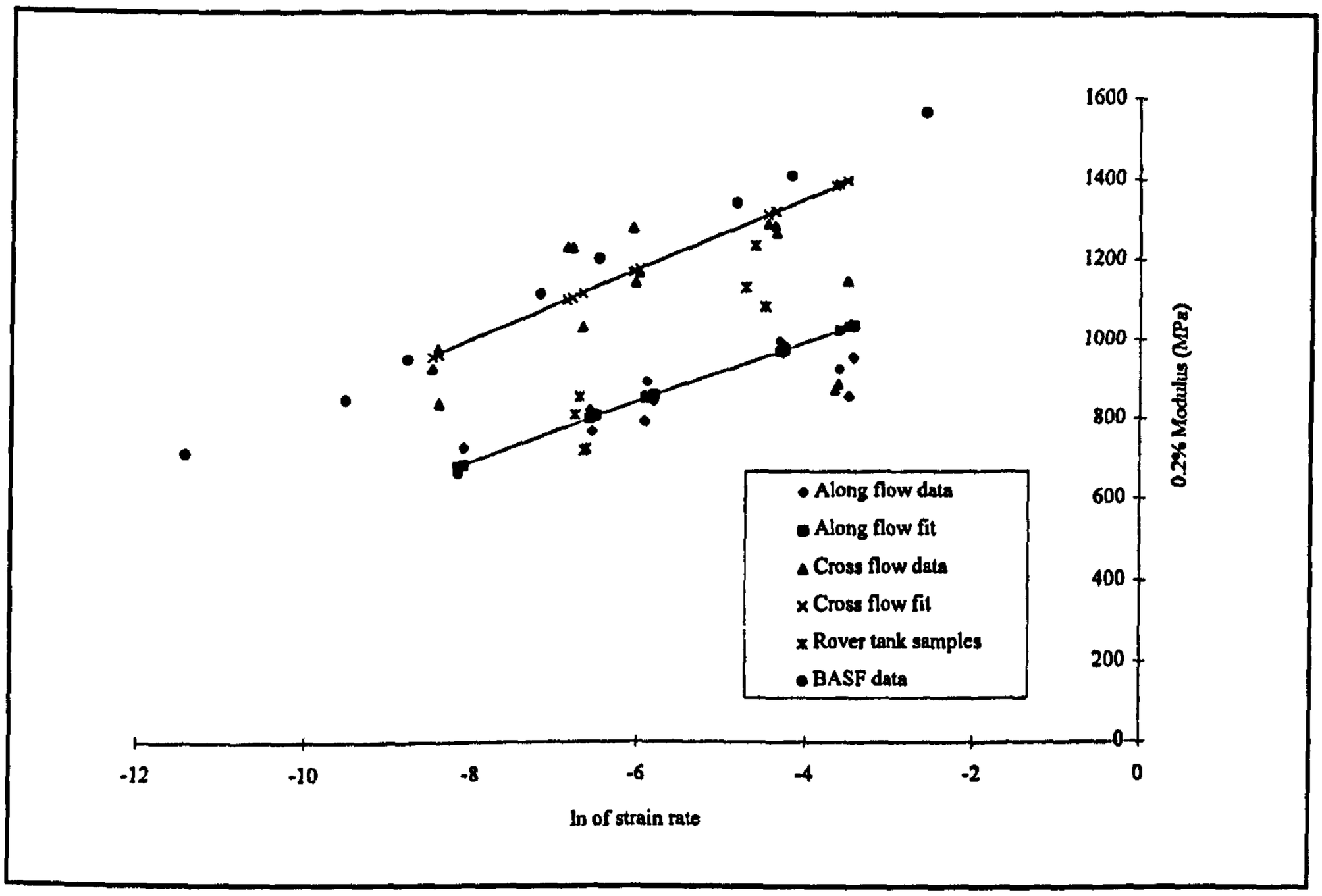

Figure 7.3 Slow speed test fit of E data

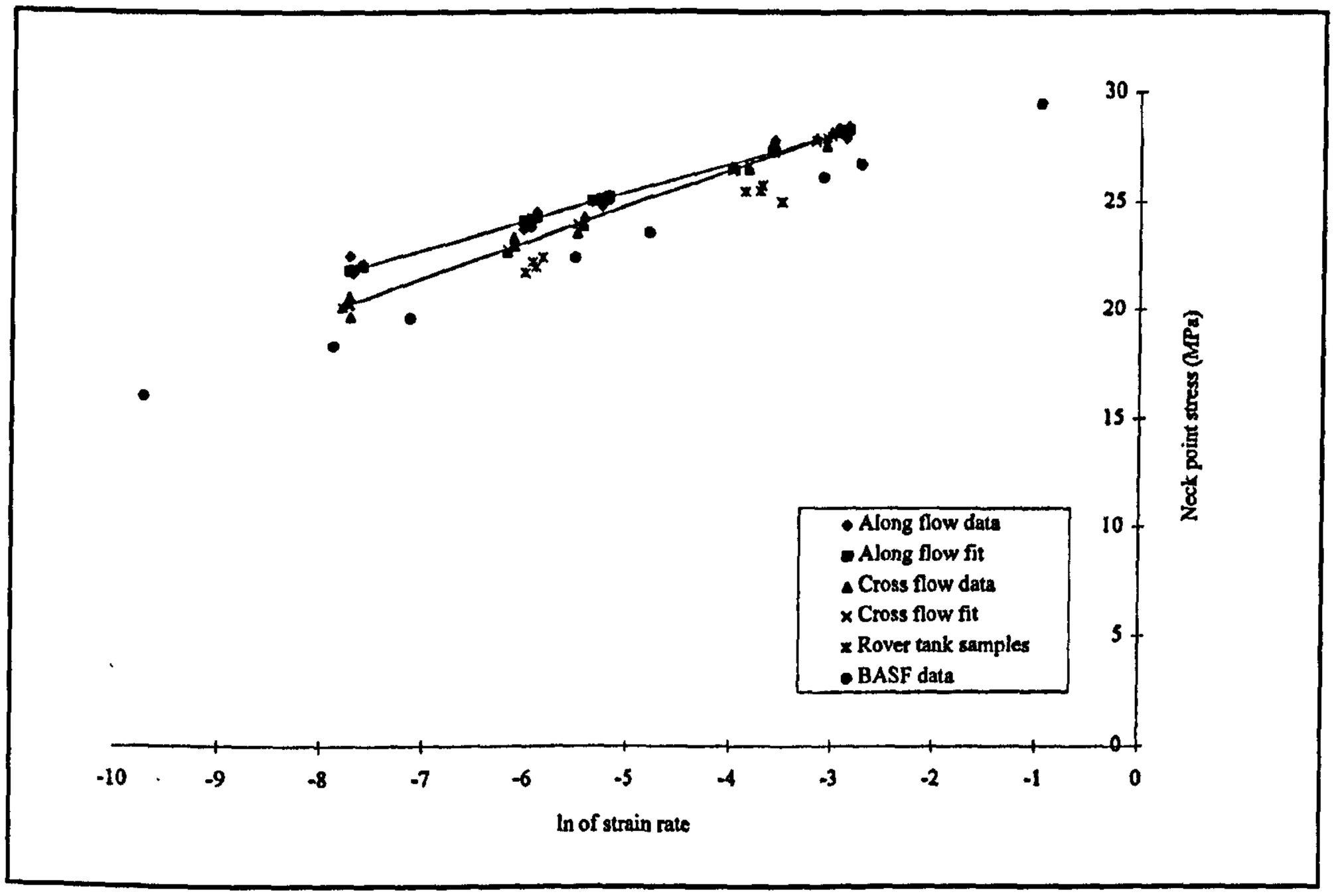

Figure 7.4 Slow Speed test fit of σ_n data

of the "along" and "cross" flow material measurements. Figure 7.3 shows that as the

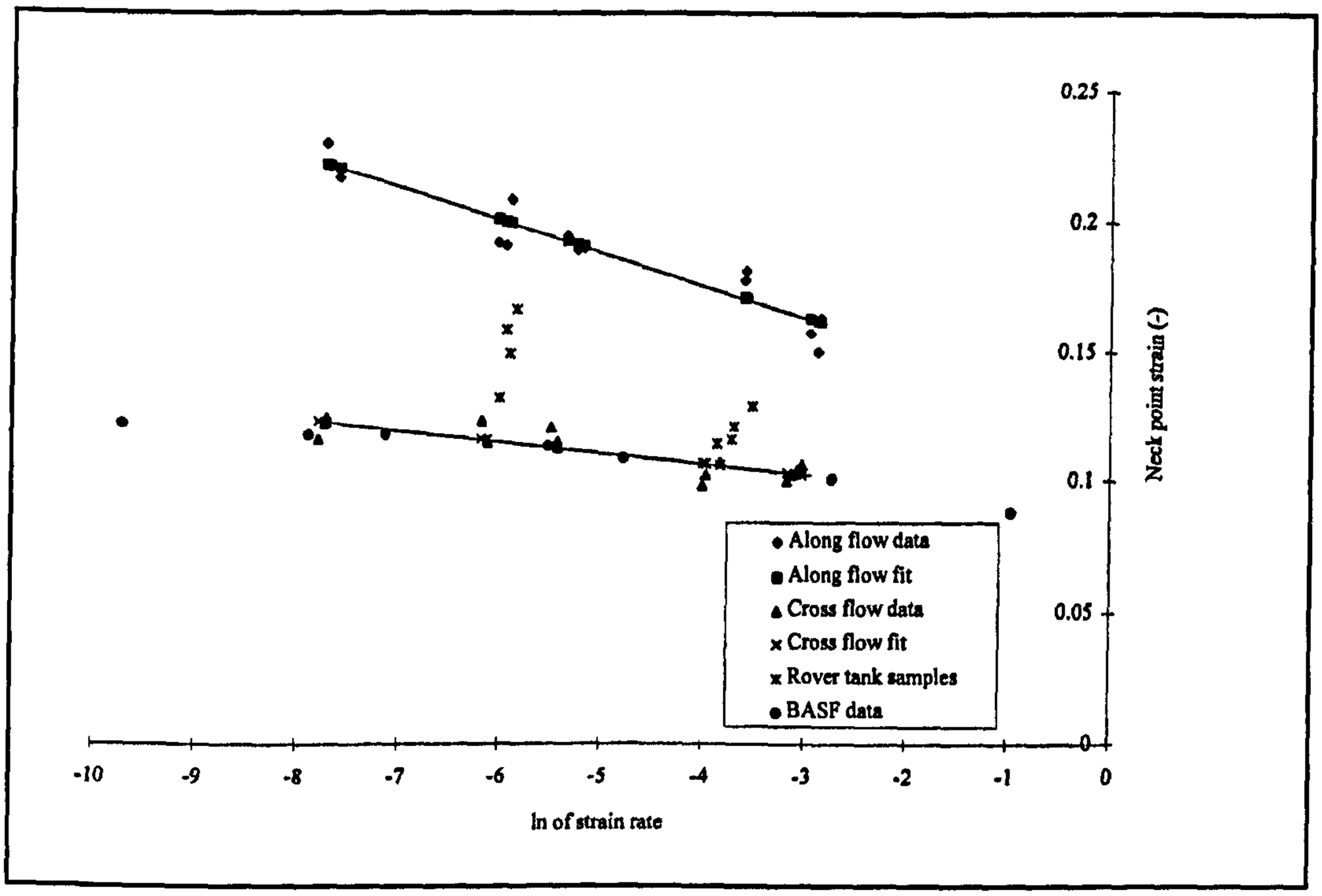

Figure 7.5 Slow speed test fit of ε_n data

strain rate increases so does the material 0.2% modulus with the "cross" flow material being significantly stiffer than the material taken from "along" flow direction. As the strain rate increases there does not appear to be a significant difference in the strain rate sensitivity of the "along" and "cross" flow materials i.e. the least squared curve fit of the data appear to be parallel. At the start of the tensile test the desired test rate is not achieved as the crosshead must accelerate, in a finite time, from rest to the desired crosshead rate. Thus as the desired test crosshead rate is increased the transient inertial response must also increase. It is probable that the apparent drop in material modulus at the 100 mm/min crosshead rate test speed may be due to such an effect with the tensile tester not being able to achieve the desired 100 mm/min crosshead rate immediately. Figure 7.4 shows that as the strain rate increases so does the stress at which the samples begin to neck. It is of interest to note that although

the "along" flow material has a lower initial stiffness than the "cross" flow material, the "along" flow material has a larger stress and strain to neck. As for the modulus data, the neck point stress data indicates that as the strain rate increases there does not appear to be a significant difference in the strain rate sensitivity of the "along" and "cross" flow materials i.e. the least squared curve fit of the data appear to be parallel. As the neck point stress increases with strain rate there is a corresponding drop in the strain to neck as shown in Figure 7.5. Unlike the two previous Figures, Figure 7.5 indicates that as strain rate increases the differing strain to neck points of the "along" and "cross" flow materials appear to be converging. This effect can also be seen when the strain rate dependent neck point stress and strain are plotted against each other in Figure 7.6.

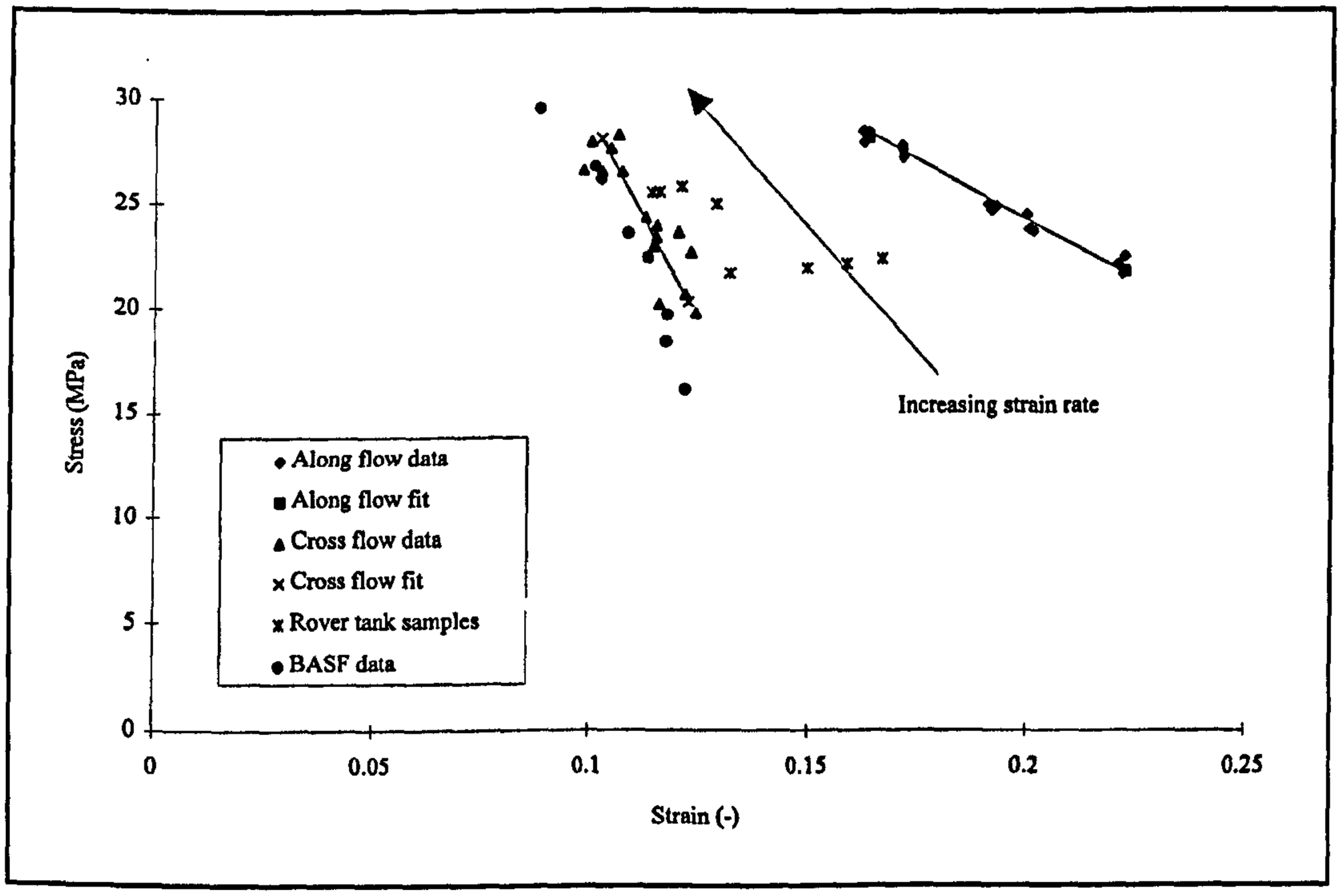

Figure 7.6 Slow speed test fit of neck point data

7.3.2 Comparison with published data

The measured material properties were compared with those supplied by the material manufacturer BASF [57]. The parameters of the curve fits of material properties with respect to the natural logarithm of strain rate, shown in Figures 7.3 to 7.5, are listed in Table 7.3 and show good agreement.

BASF data					
E	=	75.74598	ln(ε̇)	+	1300.056
σ_n	=	1.328207	ln(ε̇)	+	32.10314
ε_n	=	-0.01231	ln(ε̇)	+	0.126824
Along flow samples					
E	=	88.77061	ln(ε̇)	+	1709.775
σ_n	=	1.652864	ln(ε̇)	+	33.03201
ε_n	=	-0.00424	ln(ε̇)	+	0.089651
Cross flow samples					
E	=	98.77293	ln(ε̇)	+	1824.384
σ_n	=	1.561754	ln(ε̇)	+	30.98868
ε_n	=	-0.00368	ln(ε̇)	+	0.089411
Units					
E MPa, σ_n MPa, ε_n -, ε̇ (/s)					

Table 7.3 Slow strain rate curve fit parameters for E σ_n ε_n

When comparing the test results it should be noted that although the results are for the same material subjected to the same test conditions the test samples were made by two different manufacturing methods. Therefore it is expected that there would be differences between the two sets of data due to material orientation effects. The test data supplied by BASF was for isotropic compression moulded samples [57] whereas the injection moulded samples were anisotropic. From the comparison it can be seen

that the BASF supplied data lies closer to the "cross" flow material property measurements that for the "along" flow measurements.

7.3.3 Bi-linear curve fit data

The true stress-strain curves from the test were fitted using a bi-linear approximation such that this data could be entered into an explicit finite element program such as OASYS LS-DYNA3D [19]. On the assumption that the bi-linear fit of the test data follows the same trend as the 0.2% modulus (E) and onset of necking (σ_n , ε_n) the parameters (m_1, ε_y, σ_y and m_2) were plotted versus the natural logarithm of the strain rate in Figures B1 to B4. The trends of the least squares curve fits of the "along" flow, "cross" flow and Rover tank samples for m_1, ε_y, σ_y and m_2 follow the same trend of increased material stiffness and strength with reduced ductility as the applied strain rate increases. The effect of strain rate on the results are summarised in Table 7.4 and the parameters of the curve fits for the m_1 ,σ_y and m_2 data versus ln $\dot{\varepsilon}$ are listed in Table 7.5.

Material property	Effect of strain rate on along and cross flow measurements
m_1	slow convergence of curves
σ_y	curves virtually the same
ε_y	definite convergence of curves
m_2	divergence of curves
neck point	definite convergence of curves

Table 7.4 Effect of strain rate on slow test bi-linear results

Along flow samples					
m_1	=	64.98067	ln(ε)	+	859.1459
σ_y	=	1.19036	ln(ε)	+	25.19834
m_2	=	5.028208	ln(ε)	+	77.91187
Cross flow samples					
m_1	=	57.63525	ln(ε)	+	1041.254
σ_y	=	1.305748	ln(ε)	+	25.50496
m_2	=	8.86011	ln(ε)	+	134.3747
Units					
m_1 MPa, σ_y MPa, m_2 MPa, ε (/s)					

Table 7.5 Slow strain rate bi-linear curve fit parameters for m_1 σ_y m_2

These measurements indicate that there are definite trends. As strain rate increases the difference in the bi-linear material curve fit data for the "along" and "cross" flow material orientations becomes less.

7.4 High strain rate material property measurements

Material properties were extracted from the test force and displacement traces using the MATLAB mathematical analysis program [88]. Similarly to the slow strain rate tests the material properties that were determined were: onset of neck formation (σ_n, ε_n) and the parameters of the bi-linear curve fit using the least squares method (m_1, σ_y, m_2).

7.4.1 Determination of strain

Due to the high speed nature of the tests it was impracticable to use an extensometer. Several tests were performed at a crosshead rate of 0.01 m/min to determine a calibration factor to convert from the crosshead displacement to the effective strain in the gauge length of the test specimen. Previous test work indicated that the value for this factor was 0.4 [93]. The time-displacement traces for both the crosshead and an Instron 2620-602 clip-on extensometer with a 25 mm gauge length were compared. It was found that there was a direct linear relationship between the crosshead displacement and the strain as measured on the test samples used. The calibration factor was determined to be 0.4438 by using a least squares approach. Due to the coarse resolution of the crosshead ram transducer, the accuracy of this measurement approach for determination of specimen gauge length displacement, and hence strain, was poor. Typical displacement-time measurements, and the corresponding force-time measurements, are shown in Appendix B Figures B6, B8, B10 and Figures B7, B9 and B11 respectively for the three different test speeds. These Figures show both unfiltered and filtered test data. Figures B6, B8, B10 clearly show the coarseness of the strain measurement and Figures B9 and B11 clearly show dynamic force oscillations at test crosshead rates of 0.1 and 1.0 m/s.

7.4.2 Filtering of the force response

At test speeds of 0.1 and 1 m/s dynamic oscillations were observed in the force traces. It was believed by NPL that the oscillations were due to a mechanical resonance of the tightening mechanism in the grips used and their standard method to overcome this was to filter the test data. The justification for this will be discussed later. The filters

used in the analysis of the test data were fourth order Butterworth filters. Changes in the shape of the displacement and force time history responses were minimised by setting the filter frequency at 2.5% of the data acquisition frequency and changes to the phases of the responses were minimised by filtering the data both in the forward and then the backward directions. Examples of typical force-time and displacement-time measurements are presented in Appendix B Figures B6 to B11. Figures B7, B9 and B11 show the magnitude of the force oscillations and the effect of the filtering used.

7.4.3 Results of the tensile tests

Examples of the bi-linear curve fits are shown in Appendix B Figures B12 to B14. These show that the bi-linear approximation is satisfactory for the tests at 0.01 and 0.1 m/s but not at 1.0 m/s where Figure B14 shows that despite the careful use of filtering the high frequency loading has effected the shape of the stress-strain curve. The results of the curve fitting of the tensile test data are listed in Tables B7 to B10 and are shown graphically in Figures B15 to B22 of Appendix B. All the high speed test results show a much higher amount of scatter than that experienced for the slow speed tests. It was impossible to accurately determine the material modulus (E) as defined in the literature [31] due to the inaccurate way in which displacement was measured.

7.5 Comparison of material property measurements

The comparison of the material property measurements of σ_n, ε_n, m_1 ,σ_y, ε_y and m_2 at high strain rates with the extrapolated data from the slow strain rate tests show a large

amount of scatter which is normally associated with poor testing methods. Table 7.6 and Table 7.7 show the deviation of the high strain rate material properties measurements from the extrapolated slow strain trends.

	0.01 m/s	0.1 m/s	1.0 m/s
σ_n	+10.3549	+7.3706	-3.064
ε_n	-3.636	+18.215	+6.9826
m_1	-16.816	-28.831	+84.2473
σ_y	+9.83	+8.1038	-13.13
m_2	+16.8094	+7.1379	+63.471

Table 7.6 Average % error for "along" flow HSR data

	0.01 m/s	0.1 m/s	1.0 m/s
σ_n	-1.48	-3.543	-12.104
ε_n	-11.785	-11.109	-14.223
m_1	-22.35	-21.96	+62.9281
σ_y	+1.8247	-1.949	-16.685
m_2	+29.2571	+39.1055	+48.4121

Table 7.7 Average % error for "cross" flow HSR data

7.5.1 Neck point

The neck point (σ_n, ε_n) extrapolation from the slow strain rate test data to high strain rate tests appears to show adequate correlation when viewed as individual parameters (e.g. Figure B15 and Figure B16) but not when viewed as the neck point in Figure B17. This is probably due to the inaccurate way of converting from the ram crosshead displacement to sample strain.

7.5.2 Bi-linear curve fit

The high strain rate data appeared to be consistent with the slow strain rate test trends but there was poor correlation between the slow strain rate and high strain rate material measurements of m_1, σ_y, ε_y and m_2. It can be clearly seen in Figure B18 to Figure B22 that the 1.0 m/s test results deviate significantly from the other high strain rate tests and the slow strain rate trends. There are thought to be two principal reasons for this:

1) the strain measurement system (crosshead ram movement) is not a very accurate way of measuring strain. Thus low strain measurements are less accurate than high strain measurements and strain derivative measurements are likely to be significantly less accurate; and

2) if the observed force oscillations represent high frequency shock loads in the test specimens, this would invalidate the principle of observing the quasi static response of samples at different strain rates.

7.5.3 Determination of inadvertent shock loading

By constructing a band pass Butterworth filter it is possible to isolate the well defined decaying sinusoidal component of the tests at crosshead rates of 1 m/s. From these the resonant frequency (f_n) and logarithmic decay rate of the mechanical damping (Δ) were estimated. These are shown in Table 7.8. The average of these measurements are: f_n = 1.7 kHz and Δ = 0.9. The value of Δ is significantly higher than the damping which could be expected from metallic materials, aerodynamic or radiation modes as quoted in the literature [94]. Indeed the value for Δ is considerably higher than the value of 0.136 published [59] for the low strain DMA test results for this

Along flow		
Sample no.	f_n	Δ
12	1.74	0.93
13	1.69	0.93
14	1.47	0.93
15	1.63	0.91
Cross flow		
Sample no.	f_n	Δ
62	1.68	0.88
63	1.63	0.89
64	1.68	0.91
65	1.75	0.90

Table 7.8 Estimated damping during HSR testing at 1.0 m/s

material. The observed value for Δ and the values quoted in the literature [59] are in line with the observed behaviour of metals [94]: i.e. the damping in metals increases with applied strain. Thus it can reasonably be assumed that the observed dynamic force oscillations can be associated with large strain deformation modes of the test specimens and the desired pure quasi static loading was not achieved. Thus the unfiltered force-time measurements correspond to the true load experienced by the test specimens and the filtering of the test results, based on the premise that the observed dynamic oscillations are not experienced by the test samples, is invalid.

Having established that the dynamic oscillations at the 1.0 m/s tests correspond to the true loading of the test specimen it should be established whether these oscillations are present at slower test speeds. Due to the nature of the tests the data acquisition speed

was varied for the three test speeds (see Table 7.2). The measurement data acquisition frequencies mean that high strain rate dynamic oscillations could not be measured during the 0.01 m/s testing, due to the low frequency data acquisition rate, and that at 0.1 m/s the measurement of these oscillations will be aliassed. The aliassed high frequency oscillation in Figure B8 implies that the dynamic mode has been less well excited and is of less significance than at the higher test speed (1.0 m/s). On this evidence of reduction in magnitude of oscillations (1.0 to 0.1 m/s test speeds) and no vibration of the grips noticed by NPL at the 0.01 m/s crosshead rate, it is thought that it was unlikely that shock loading occurred at the 0.01 m/s test speed.

7.6 Effect of temperature

Due to the problem of unintentional shock loading, poor correlation was noted for the comparison of slow strain rate and high strain rate measurements at room temperature. Whereas the slow strain rate 23° C data could be directly extrapolated up to high strain rates for a comparison, additional scale temperature factors were required for the comparison of the slow strain rate 23° C data with the high strain rate sub-ambient data at 0° C and -40° C.

7.6.1 Published trends

Figure 7.7 compares the temperature dependence of material modulus data, made by a range of methods (tensile test, DMA, ultrasonic) [38,57,59,95], and Figure 7.8 the temperature dependence of neck point stress [57,59] these show an approximately linear dependence of these material measurements on temperature.

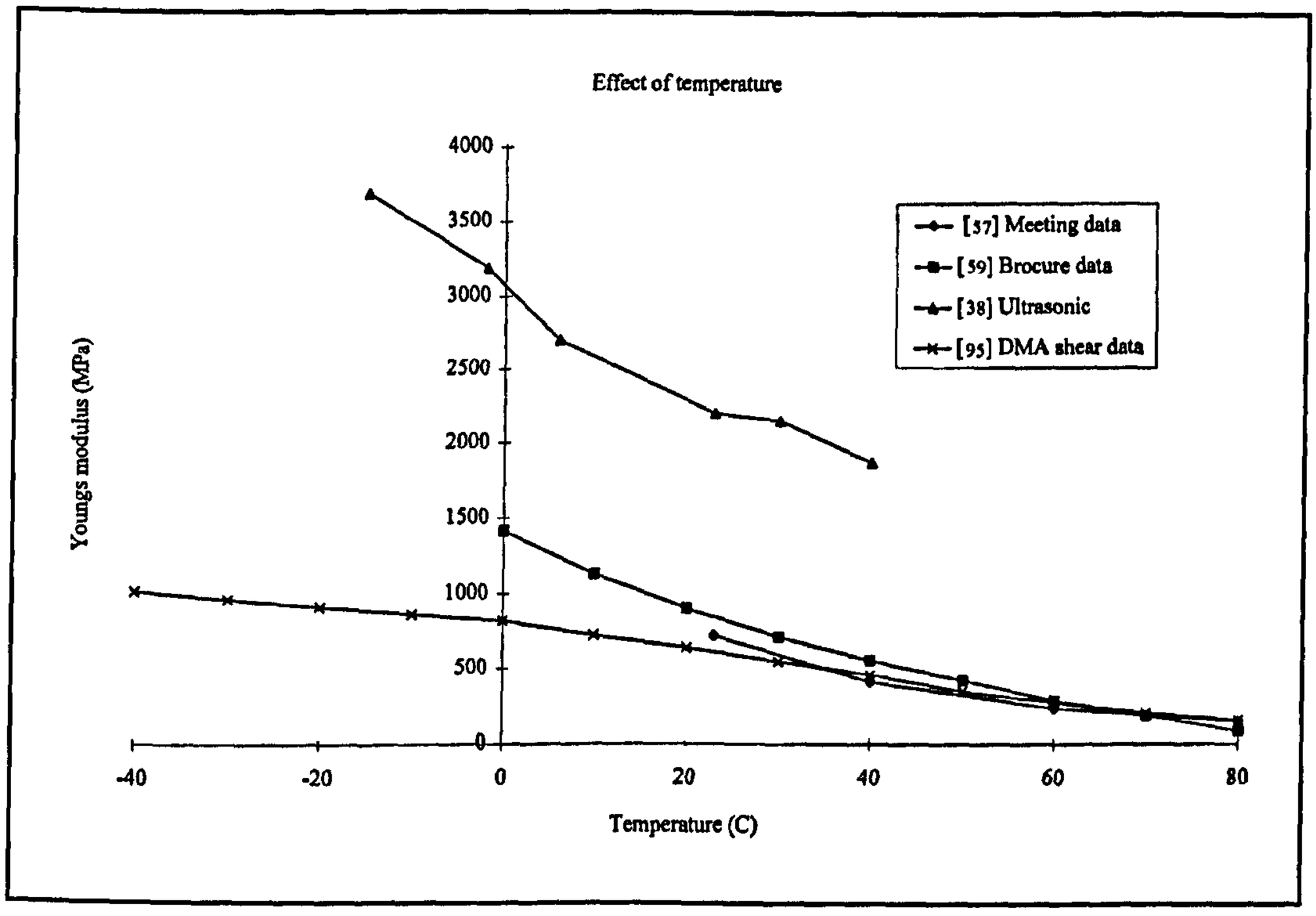

Figure 7.7 Modulus measurements at varying temperatures

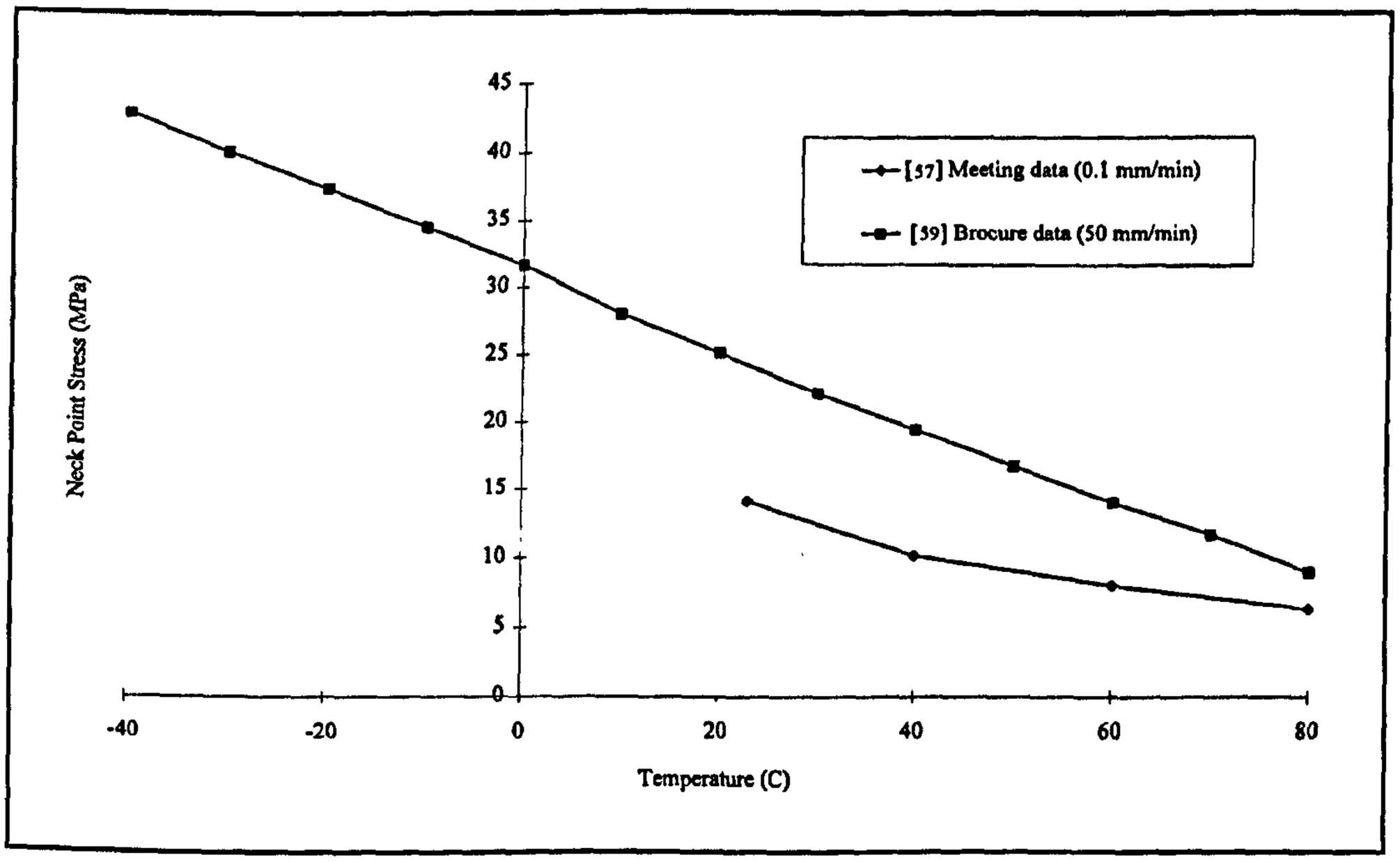

Figure 7.8 Neck point stress measurements at varying temperatures

A linear dependence of material property on temperature was assumed for the high strain rate results and the curve fit of the material properties with respect to temperature obtained using a least squared curve fit approach. These curve fits were then divided by the curve fit value for the material property at 23° C to obtain normalised scaling factors with nominal value of 1 at 23° C. The scaling factors for the effect of temperature on material property are calculated factors for 23°, 0° and -40° C are shown in Table 7.9 and Table 7.10 respectively.

Temperature range (° C)	20 to 80	0 to 80	-15 to 40	-40 to 80
Source	[38]	[57]	[59]	[95]
23° C	0.904171	1.057901	1.12177	0.954398
0° C	1.214766	1.413407	1.401522	1.192196
-40° C	1.75493	2.12442	2.000211	1.667792

Table 7.9 Modulus versus temperature scaling factors

Temperature range (° C)	20 to 80	-40 to 80
Source	[57]	[59]
23° C	0.94487	1.017984
0° C	1.16064	1.248837
-40° C	1.535893	1.710542

Table 7.10 Neck point stress versus temperature scale factors

7.6.2 Measured trends

The HSR material properties were averaged at each of the three test crosshead velocities and normalised linear scaling factors obtained for the effect of temperature.

These normalised temperature scaling factors are shown in Table 7.11. The "along" flow and "cross" flow scaling factors are consistent with each other and compare well with those of Table 7.9 and Table 7.10. There was very little difference between the effect of temperature on the "along" and "cross" flow material property measurements. The measured linear temperature scaling factors compare well with published test data and can be used with a good degree of confidence.

	ε_n	σ_n	m_1	ε_y	σ_y	m_2
23°C						
Along flow	0.95407	0.99156	1.1134	0.96285	0.97137	0.989
Cross flow	0.98139	1.01057	1.03619	0.98193	1.024	0.95959
0°C						
Along flow	0.82978	1.20286	1.49852	0.90325	1.21983	1.49066
Cross flow	0.88717	1.25977	1.45222	0.91538	1.27455	1.45889
-40°C						
Along flow	0.61363	1.57035	2.16831	0.7996	1.65193	2.3631
Cross flow	0.7233	1.69316	2.17574	0.79964	1.71027	2.32725

Table 7.11 HSR temperature factors

7.6.3 Comparison of low temperature HSR test data with temperature factored SSR data

Due to the method of strain measurement, it would be expected that as the strain increased its relative accuracy would increase. Thus a greater degree of correlation

was expected for the neck point as opposed to yield point. Also it was expected that the stiffness measurements, which are the first derivative of the stress-strain measurements, would show a worse degree of correlation than the stress or strain measurements. For a single set of test parameters, i.e. constant temperature and crosshead velocity, the average error between extrapolated data and test measurement was less for the neck point as opposed to the yield point. However, the deviation between modulus measurements and the extrapolated data was not significantly worse than that for the yield and neck points. The low temperature high strain rate test data was compared with the temperature factored slow strain rate data. Tables B19 to B21 of Appendix B lists the errors between the two sets of data and show that the errors for the sub-ambient HSR data is consistent with the errors for the ambient HSR data. As for the ambient temperature HSR test data the sub-ambient HSR test data had a large amount of scatter indicative of a poorly controlled test configuration. The expected trends of increasing stiffness and strength with reducing ductility with increasing strain rate and decreasing temperature were observed and were consistent with the extrapolated SSR test data although correlation was poor.

7.7 Comparison of data with published SHPB data

The data in [38] was collated and is enclosed in Tables C1 and C2 of Appendix C. The straight line plots of flow stress with respect to the natural logarithm of strain rate at a particular strain and temperature can by written as:

$$\sigma_f = A + B \ln \dot{\epsilon} \tag{10}$$

where A and B are temperature and strain dependent constants.

The temperature dependence of A and B were established through linear curve fits of A and B at the nominal strains of 5%, 10% and 15%. The effect of strain on these linear curve fits of A and B with respect to temperature was then established by plotting the curve fit parameters with respect to flow strain. Thus the data for the flow stresses at different temperatures and strain rates was found to fit the empirical relationship:

$$\sigma_f = (a_1 T + (a_2 |\epsilon| + a_3)) + (b_1 T + (b_2 \epsilon + b_3)) \ln \dot{\epsilon} \qquad (11)$$

where a_i and b_i are constants.

The values of a_i and b_i for HDPE and MDPE in the above equation are given in Table C3 of Appendix C. The comparison of the flow stress parameters and the curve fits show that the difference between the measured flow stress and the curve fit of Equation (11) is very small (-4.667 to 6.149%) as shown in Tables C4 and C5 respectively. By comparing the results of the MDPE SHPB tests with those for HDPE, taking those of HDPE as a reference, a worst case % tolerance can be determined, Table C6, as a benchmark for the comparison of the HDPE SHPB data with the HDPE high strain rate tensile test results.

7.7.1 Tensile test flow stress measurements

Tensile test flow stresses were extracted from the slow and high strain rate tensile test data for HDPE (BASF Lupolene 4261A). These are listed in Appendix C Tables C7 to C15. The slow strain rate tensile and high strain rate tensile results were combined to find the constants for Equation (11) and are given in Table C16.

7.7.2 Comparison of tensile and SHPB data

The value for a_2 in Equation (11) was found to be dependent on the direction of the applied strain, and thus the fit of the tensile test data must be compared with the fit of the SHPB data. The tensile results are compared in Figures C1 to C4 of Appendix C. The comparison of the data for the two different materials (BASF Lupolene 4261A and BP Rigidex 002/55), as a percentage error of the tensile test results from the compressive SHPB test results curve fit, is shown in Tables 7.11 and 7.12.

	Temperature °C		
Strain rate	-40	0	23
		5% strain	
$1x10^{-4}$	-21.99	-21.00	-19.50
$1x10^{+4}$	- 5.15	- 6.31	- 7.38
		10% strain	
$1x10^{-4}$	-15.07	- 9.79	- 2.05
$1x10^{+4}$	- 1.28	- 1.22	- 3.13
		15% strain	
$1x10^{-4}$	- 8.58	0.32	12.78
$1x10^{+4}$	- 2.30	3.37	2.47

Table 7.12 Comparison of SHPB and tensile test flow stress - "along" flow samples (% difference)

	Temperature °C		
Strain rate	-40	0	23
		5% strain	
$1x10^{-4}$	- 3.92	- 3.16	- 1.99
$1x10^{+4}$	- 3.08	- 1.31	0.33
		10% strain	
$1x10^{-4}$	0.48	3.97	9.07
$1x10^{+4}$	- 0.14	2.43	2.60
		15% strain	
$1x10^{-4}$	4.61	10.40	18.50
$1x10^{+4}$	2.59	5.79	6.62

Table 7.13 Comparison of SHPB and tensile test flow stress - "cross" flow samples (% difference)

Comparing Tables 7.12 and 7.13 with Table C6, the % difference between the SHPB and tensile testing is on average less than the difference between the SHPB HDPE and MDPE test results. The numbers highlighted in Table 7.12 indicate those measurements for which the % error is greater for the tensile test comparison as for the MDPE compressive comparison. Taking into consideration the fact that the two sets of data are for different material grades with different flow orientations, this shows that there is a very good correlation between the flow orientated tensile testing and compressive SHPB testing.

7.8 Measurement of stiffness data - Conclusions

1) The high strain rate data appeared to be consistent with the slow strain rate test trend data but there was poor correlation between the slow strain rate and high strain rate material measurements of σ_n, ε_n, m_1, σ_y and m_2.

2) The large experimental scatter of the high strain rate tensile test results and poor correlation with the slow strain rate extrapolated data was due to inadvertent shock loading and inadequate accuracy of the strain measurement. Thus the high strain rate tensile tests at the NPL were not suitable for accurate determination of the strength and stiffness of small thermoplastic samples.

3) There was very little difference between the effect of temperature on the "along" and "cross" flow material property measurements. The measured linear temperature scaling factors compare well with published test data and can be used with a good degree of confidence.

4) The compressive SHPB and tensile test results show a strong degree of agreement for both the flow directions. Thus the assumption of a logarithmic relationship between strain rate and flow stress can be made for the tensile test flow stress of HDPE.

5) Despite the poor correlation between slow strain rate and high strain rate test data it is probable that slow strain rate tensile test data can be extrapolated to high strain rates assuming a linear relationship with respect to the natural logarithm of the strain rate.

Chapter 8

Impact performance simulation of beam and disc samples

The object of the experimental testing was to create a typical impact event that could be instrumented for correlation with a numerical simulation. Geometric models of the impact of a simply supported beam and disc are relatively simple and contain many of the nonlinear effects that occur during impact events:

1) variable, high strain rates;

2) plasticity;

3) gaps with closure, sliding and large differences in material stiffnesses;

4) large deformations and the formation of hinges.

The data that can be readily measured in the beam and disc impact tests are the low frequency responses of the load cell that the striker is mounted on. Only the low frequency response can be used as load cells are normally statically calibrated and not dynamically calibrated with the striker attached. Thus the test data that was collected, for correlation, was the low frequency component of the force time history of the measurement load cell used.

8.1 Beam and disc sample material

Beam and disc samples were cut from the same flow orientated material plaques (HDPE - BASF Lupolene 4261A) as were used to measure material properties in Chapter 7. This data is listed in Table 7.5. The beam and discs were cut from the centre of annealed plaques and in the case of the beams were orientated with the flow directions.

8.2 Coupon sample impact testing

The jigs used to simply support the coupon samples were manufactured from steel and mounted in an ICI instrumented impact tester. Figure 8.1 [96] shows the schematic of the test operating system.

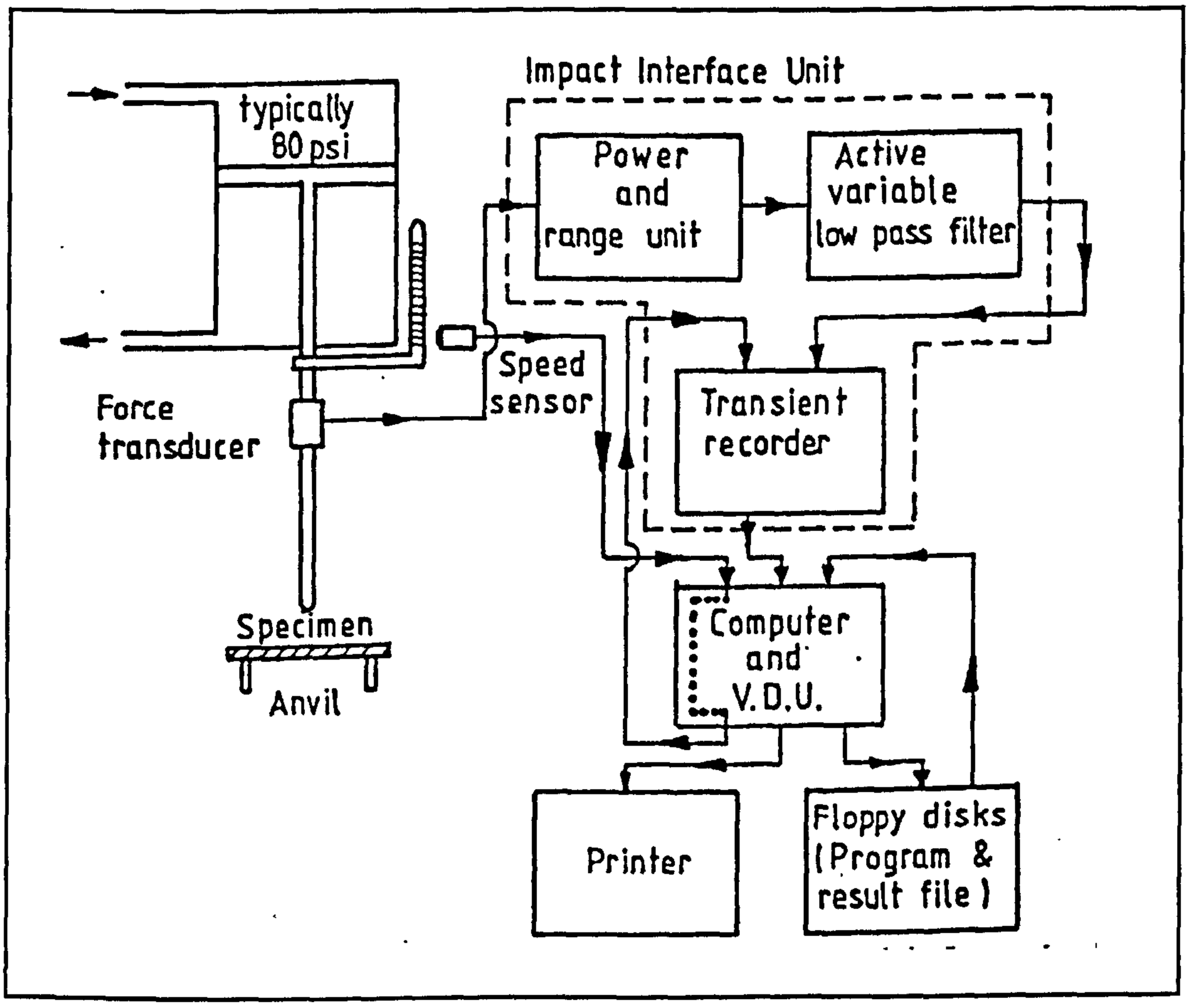

Figure 8.1 Schematic layout of instrumented impact test [96]

The standard steel striker, with a hemispherical end, was used for the disc test and special light weight aluminium striker made for the bending test. The test configurations are shown in Figures 8.2 and 8.3 with the details of the striker masses and load cell stiffnesses listed in Table 8.1.

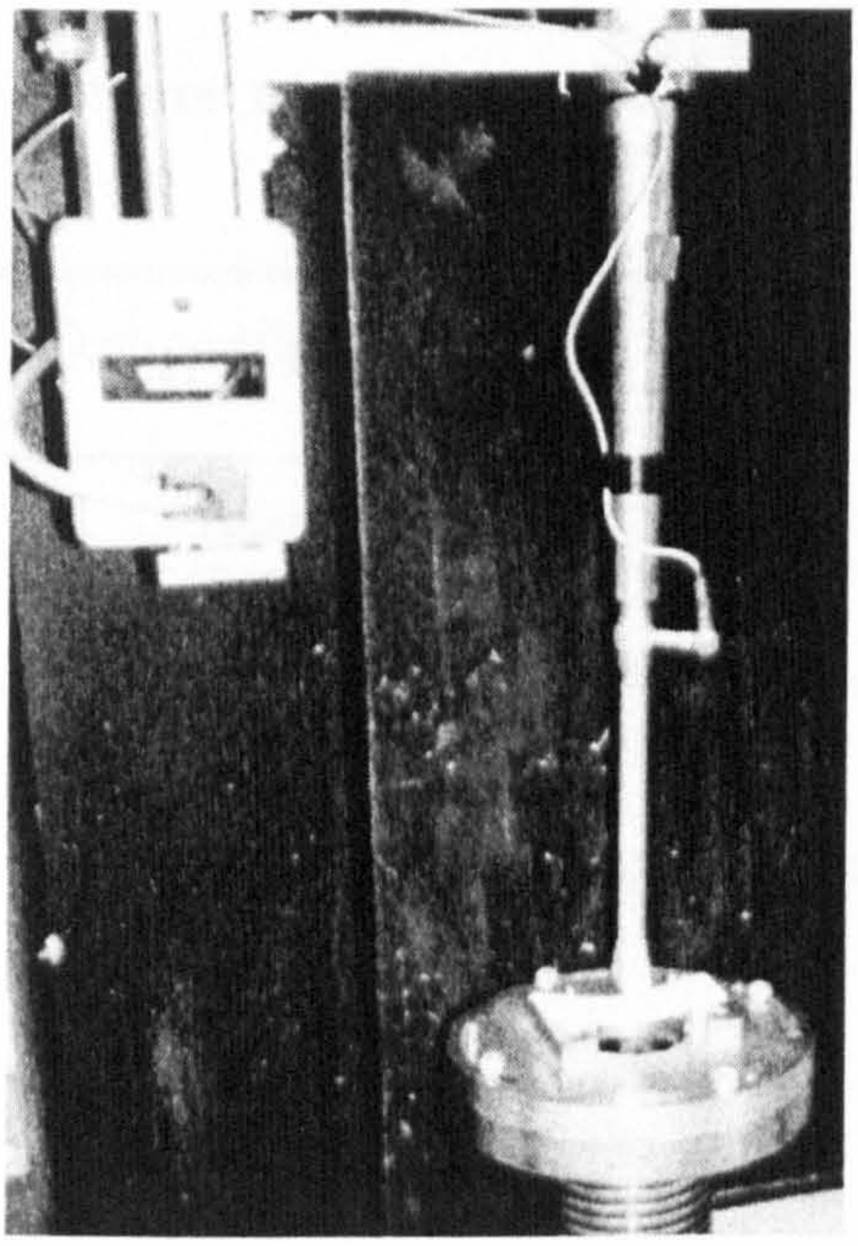

Figure 8.2 Beam impact test configuration

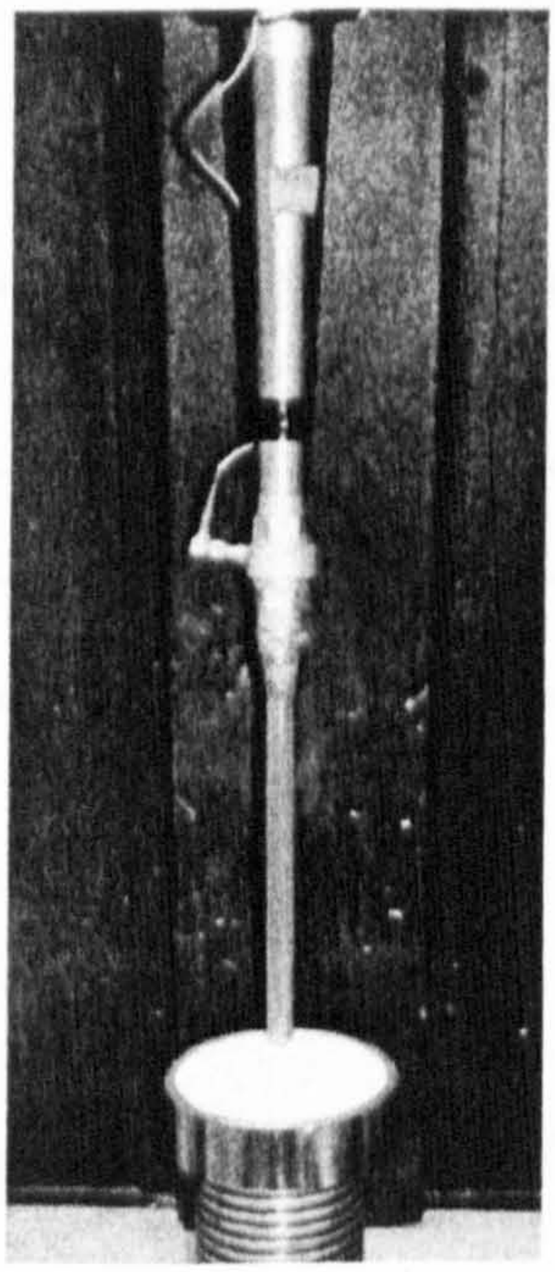

Figure 8.3 Disc impact test configuration

	Test configuration	
	Beam	Disc
Load cell model No. (PCB piezotronics)	221A03	223
Load cell mass (g)	26.7	118.7
Load cell stiffness (N/m)	$3.5x10^{+9}$	$7.0x10^{+9}$
Striker mass (g)	36.8	198.1

Table 8.1 Beam and disc test load cell and striker mass and stiffness details

The pneumatic air pressure of the tester was adjusted such that the impacting velocity was 4 m/s. The time history of the load cell impact response was recorded using the systems PC based data acquisition system. The sensitivity of the data acquisition

system was 1024 points in the time domain and 256 points in the force domain. The force and time resolution of the system for the tests are shown in Table 8.2.

Test configuration	Time resolution (s)	Force resolution (N)
Beam	$1x10^{-5}$	1.348
Disc	$1x10^{-5}$	19.26

Table 8.2 Experimental test measurement resolution

The force-time histories of the impact events were converted from the software package's internal turbo PASCAL binary format into DOS ASCII files and transferred to a UNIX system. The force-time histories were then formatted as OASYS LS-DYNA3D time history curve files and manipulated to zero load and time axes such that they could be directly compared with numerical predictions.

8.3 Analytical material models used

As the jigs and strikers used in the impact tests were only subjected to elastic strains they were modelled using an isotropic linear elastic material model with appropriate constants for the steel and aluminium parts. The stress-strain curve of high density polyethylene (HDPE) is known to be:

1) nonlinear;

2) strain rate dependent;

3) temperature dependent; and

4) history dependant.

The non inclusion of nonlinearity and strain rate stiffening are known to lead to significant deviations between test and numerical simulations [45,97]. Whereas numerical simulations of the impact of metal components have included nonlinear and strain rate effects, e.g. the use of Cowper Symonds strain rate hardening [98], it has been argued that the inclusion of rate dependency in the simulation of the impact of thermoplastic components is not feasible [74]. This is certainly the case for implicit finite element simulations, because polymers do not have a time independent modulus which is required for the analytical method, but not so for explicit finite element simulations. Three observed trends were used to determine the type of material model to be used [99]. These were:

1) the stiffness and strength of HDPE appears to follow an Eyring type strain rate dependency;

2) as the strain rate increases the material stress-strain curve becomes increasingly similar to a bi-linear approximation;

3) as the strain rate increases the flow orientation effects are reduced.

Thus the material stiffness was approximated as an isotropic bi-linear representation at high strain rates. The material model used in the impact analyses was the OASYS LS-DYNA3D material model number 19 [98]. This bi-linear isotropic material model was chosen as it had the ability to include load curves to define the strain rate dependence of the elastic modulus, yield stress, yielding modulus and failure stress.

8.4 Finite element analysis

NISA/Display III software was used to create solid models for the beam and disc impact tests. Solid models were created as through-thickness effects and changes in geometric contact were important. The finite element models were then converted into analytical models for solution in ÓASYS LS-DYNA3D by the OASYS NCODE software [100].

Normally five through thickness integration points are used in the formulation of shell elements with elastic-plastic capabilities to adequately define the through-thickness strain distribution in nonlinear analyses. In the solid models of the beam and disc coupon test samples eight integration points through the thickness of the samples were used (four solid elements with two integration points per dimension). Due to the nature of the analyses whereby line and point loadings were applied to solid elements, Gaussian quadrature [101] elements were to be used instead of the default single integration point elements in order to avoid "hour glassing" problems and solution numerical instabilities associated with single integration point elements [98].

In explicit finite element solutions a critical factor in the use of strain rate dependent material models is the control of the solution time step. Most analyses use a fixed time step and if this time step is too large then the solution will converge on the wrong solution. In order to converge on the correct solution it is necessary to use a smaller time step than the minimum time step associated with the speed of sound through all the model elements. This is so that wave propagation effects can be tracked. Obviously if the stiffness of an element is changing then the speed of sound

in that element must also. This is not a problem for elastic-plastic steel analyses as the local stiffness decreases during plasticity, with a corresponding decrease in the speed of sound, as opposed to strain rate dependent thermoplastics where increasing strain rates cause the material to stiffen. A stiffening element requires the time step to be decreased in order to track wave propagation effects. Time step problems, due to the strain rate effects were not encountered as solid elements of both HDPE coupon samples and steel/aluminium jigs were used with similar sizes. Thus the solution minimum time step was set by the solid element of the jigs which had high stiffness and used an elastic material model without the ability to change its stiffness.

8.4.1 Beam analysis

Shown in Figure 8.4, a finite element model was created to simulate the impact of a beam (dimensions 80 x 25 x 3 mm) simply supported at a pitch of 50 mm and impacted, with a incident velocity of 4 m/s, at its centre.

The salient features of the model are:

1) quarter symmetry was used to reduce analysis execution time;

2) the impacted beam was modelled using solid elements with a typical length of 0.75 - 1.5 mm, using four elements through the beam thickness to model through-thickness effects;

3) the steel support was modelled using solid elements with a typical element length of 1 mm, consistent with that for the beam;

4) the 10 mm diameter cylindrical face of the aluminium striker modelled using solid elements and attached to the shaft, modelled using beam elements, with a constraint equation;

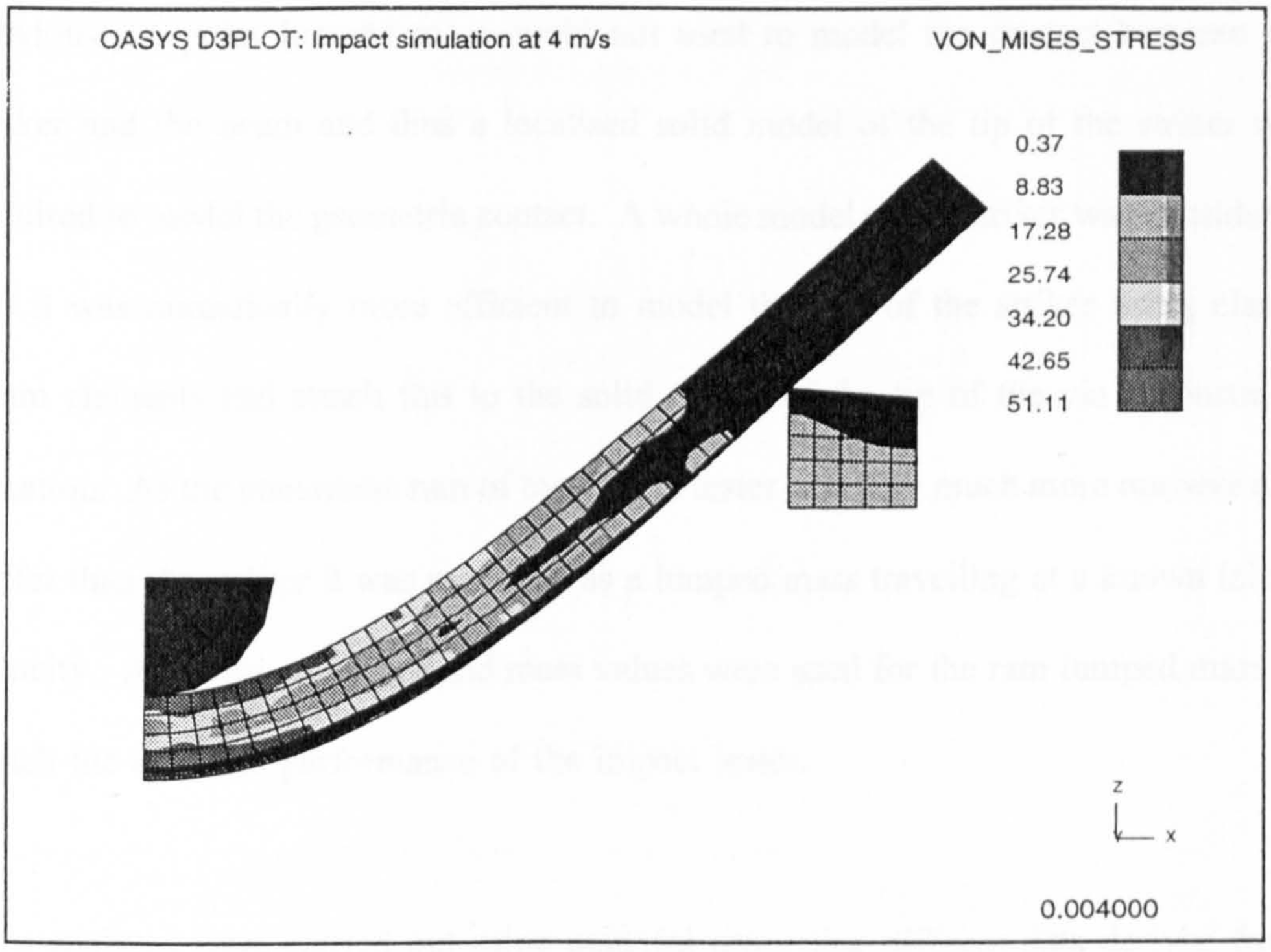

Figure 8.4 Beam impact simulation - "along" flow data

5) load cell modelled as a spring;

6) pneumatic ram modelled as a lumped mass with initial velocity.

For the analyses it was important to keep the finite element model as small as possible such that the elapsed execution time would not be excessive. Thus quarter symmetry was used. It was necessary to model the load cell and striker as a step input will excite, to some extent, the fundamental resonance of any system. Instrumented impact tests are well known to have problems with dynamic resonances of their measurement systems [44,72,73]. To a first approximation the dynamic characteristics of the measurement can be considered to be a single degree of freedom system mass and spring system. The load cell acts as a spring with the striker acting as a lumped mass. The spring stiffness for the load cell used was obtained from manufacturers data.

Obviously a point lumped mass could not used to model the contact between the striker and the beam and thus a localised solid model of the tip of the striker was required to model the geometric contact. A whole model of the striker was considered but it was numerically more efficient to model the rest of the striker using elastic beam elements and attach this to the solid model of the tip of the via a constraint equation. As the pneumatic ram of the impact tester was very much more massive and stiffer than the striker it was modelled as a lumped mass travelling at a known initial velocity. Appropriate energy and mass values were used for the ram lumped mass to match the dynamic performance of the impact tester.

Two analyses were carried out using material properties stiffness data derived from oriented material tensile tests (Table 7.5). The time steps used in the analyses were in the order of $6x10^{-8}$ s and the impact event duration of $5x10^{-3}$ s. The analyses took approximately four elapsed days on a Silicon Graphics R4000 workstation. The difference between the "cross" flow predicted load cell force time history and that of the predicted contact pressure between the striker and beam is shown in Figure 8.5. This Figure shows that for this configuration although the low frequency content of the load cell and contact force time responses show good agreement there was a significant difference in the high frequency content of the applied load. These differences are due to dynamic wave propagation effects within the striker.

8.4.2 Disc analysis

Following the same methodology as for the beam impact test configuration a finite element model, shown in Figure 8.6, was created to simulate the impact of a disc (80

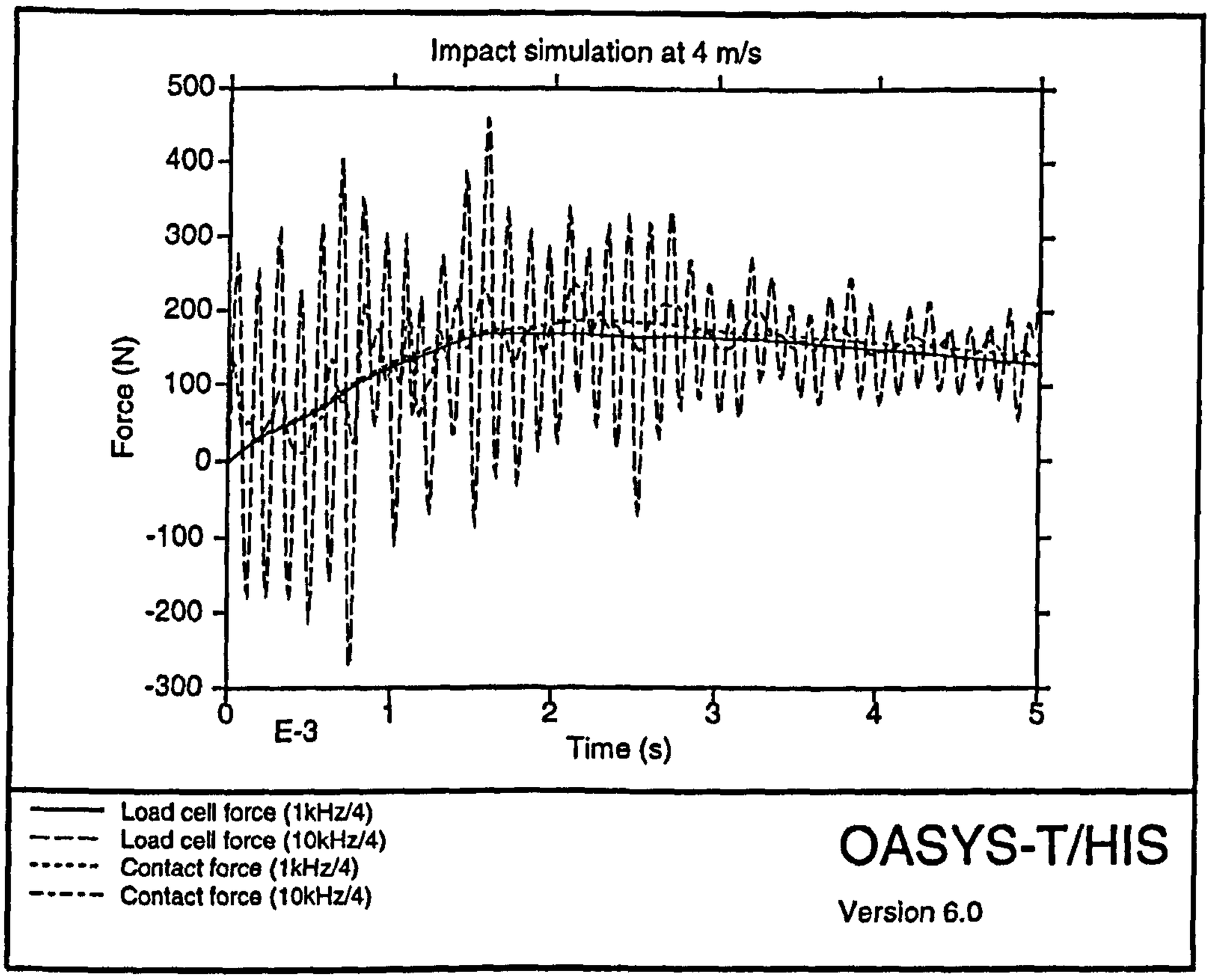

Figure 8.5 Predicted beam contact force and load cell force comparison

mm diameter x 3 mm thick) simply supported at a diameter of 50 mm and impacted, with a velocity of 4 m/s, at its centre.

The salient features of the model are:

1) quarter symmetry used;

2) impacted beam was modelled using solid elements with a side lengths of 0.75 - 3 mm, using four elements through the disc thickness;

3) steel support modelled using solid elements with a typical element length of 1 mm;

4) 10 mm diameter hemispherical face of the aluminium striker modelled using solid elements and attached to the shaft, modelled using beam elements, with

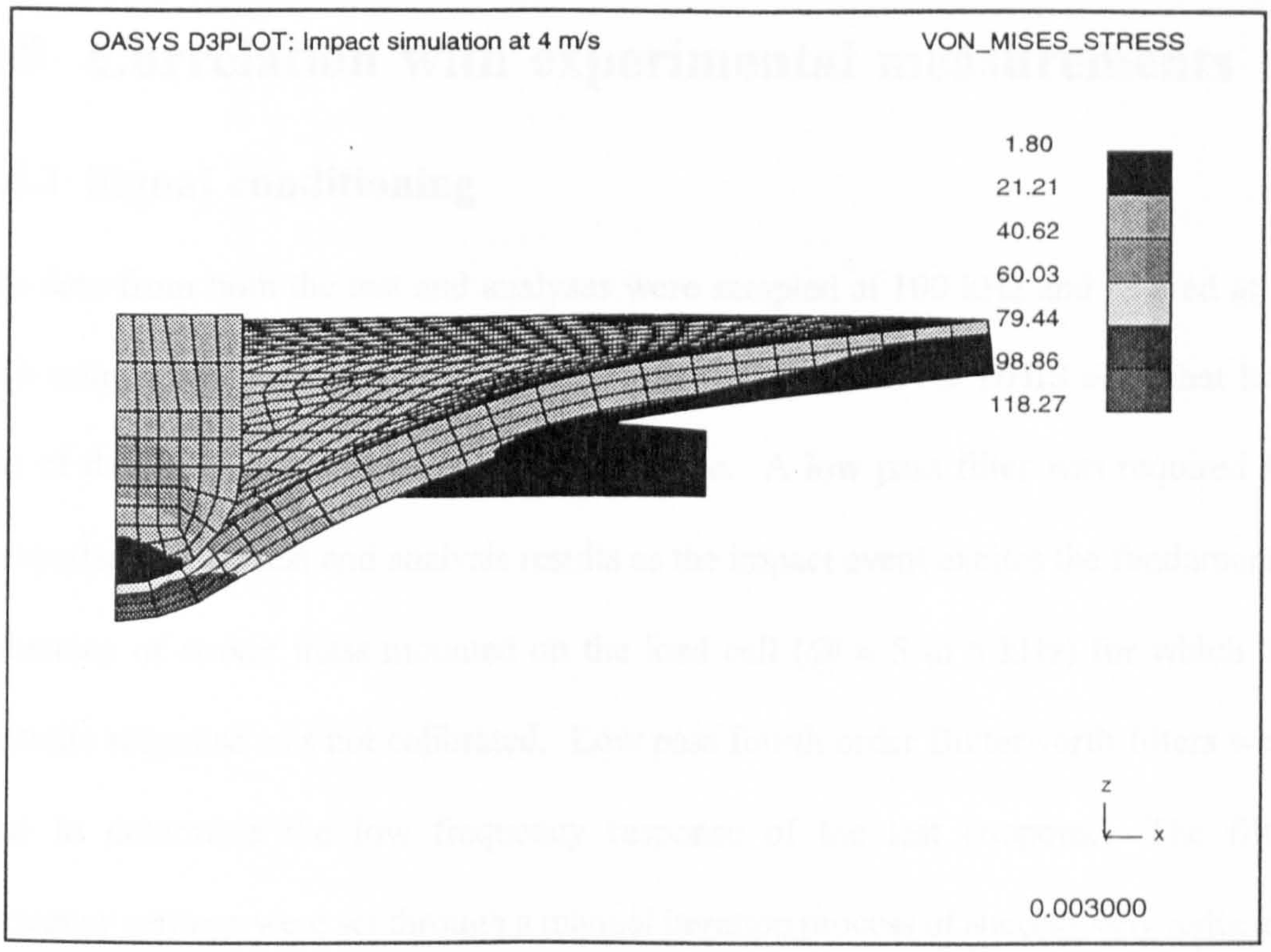

Figure 8.6 Disc impact simulations - average data

a constraint equation;

5) load cell modelled as a spring;

6) pneumatic ram modelled as a lumped mass with initial velocity.

Three analyses were carried out using average material properties derived from oriented material tensile tests (Tables 7.3 and 7.5). The time steps used in the analyses were in the order of $5x10^{-8}$ s and the impact event duration of $5x10^{-3}$ s. The analyses assumed various failure criteria which were:

1) no failure;

2) failure at the onset of the neck point of the tensile test; and

3) failure at three times the onset of the neck point of the tensile test.

8.5 Correlation with experimental measurements

8.5.1 Signal conditioning

The data from both the test and analyses were sampled at 100 kHz and filtered at 10 kHz using a low pass first order Butterworth filter in OASYS T/HIS such that both sets of data conformed to a consistent base line. A low pass filter was required for comparison of the test and analysis results as the impact event excites the fundamental resonance of striker mass mounted on the load cell (@ ≈ 5 to 6 kHz) for which the dynamic response was not calibrated. Low pass fourth order Butterworth filters were used to determine the low frequency response of the test coupons. The filter frequency settings were set through a manual iteration process of successively reducing the filter frequency until the high frequency response of the load cell-striker had been removed. In the case of the beam samples the filtering frequency was 1 kHz and in the case of the disc samples 2.5 kHz.

8.5.2 Beam comparison

The excellent correlation between the low frequency response of the analyses and experimental results can be seen in Figures 8.7 and 8.8. These Figures show the comparison of the simulated and measured low frequency responses of the piezo electric load cell used in the tests.

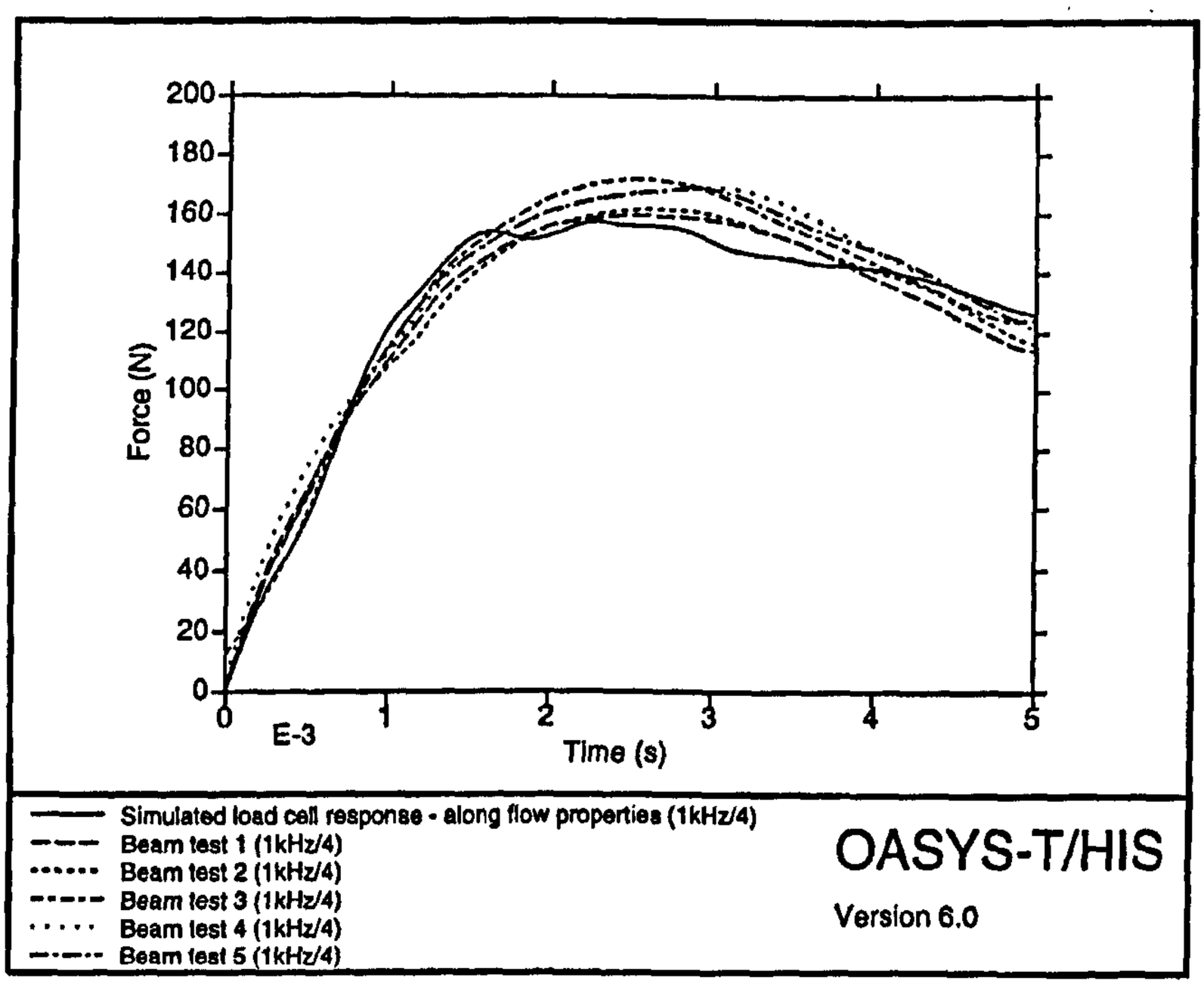

Figure 8.7 "Along" flow low frequency response comparison

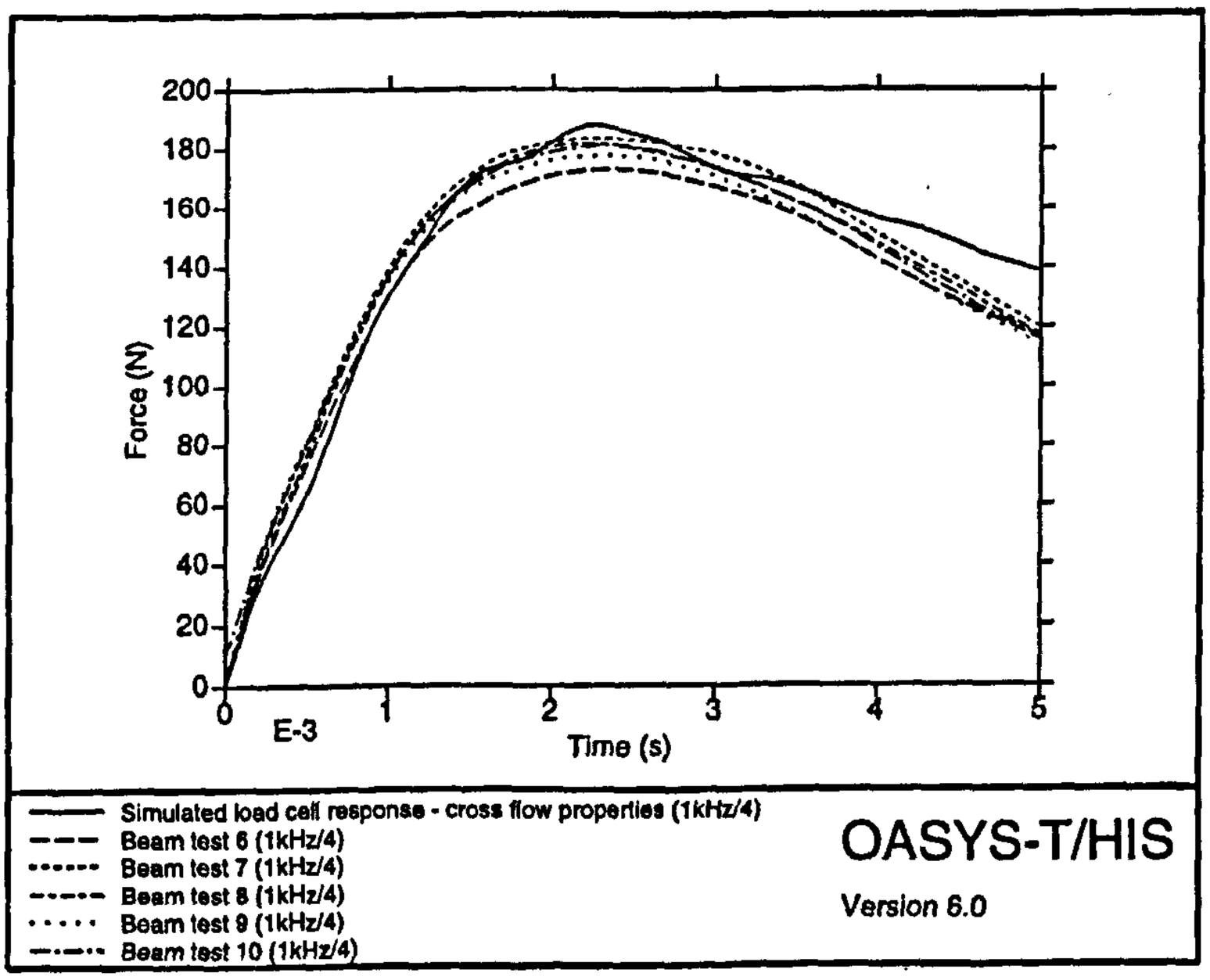

Figure 8.8 "Cross" flow low frequency response comparison

The shape of the force-time history response shows good agreement with the

experimental measurements. When the predicted force was divided by the measured force then the agreement was within ±20% as shown in Figures 8.9 and 8.10. There was little difference in the loads predicted and measured between "along" and "cross" flow material orientations. Thus it was concluded that material orientation effects were not important for this test configuration.

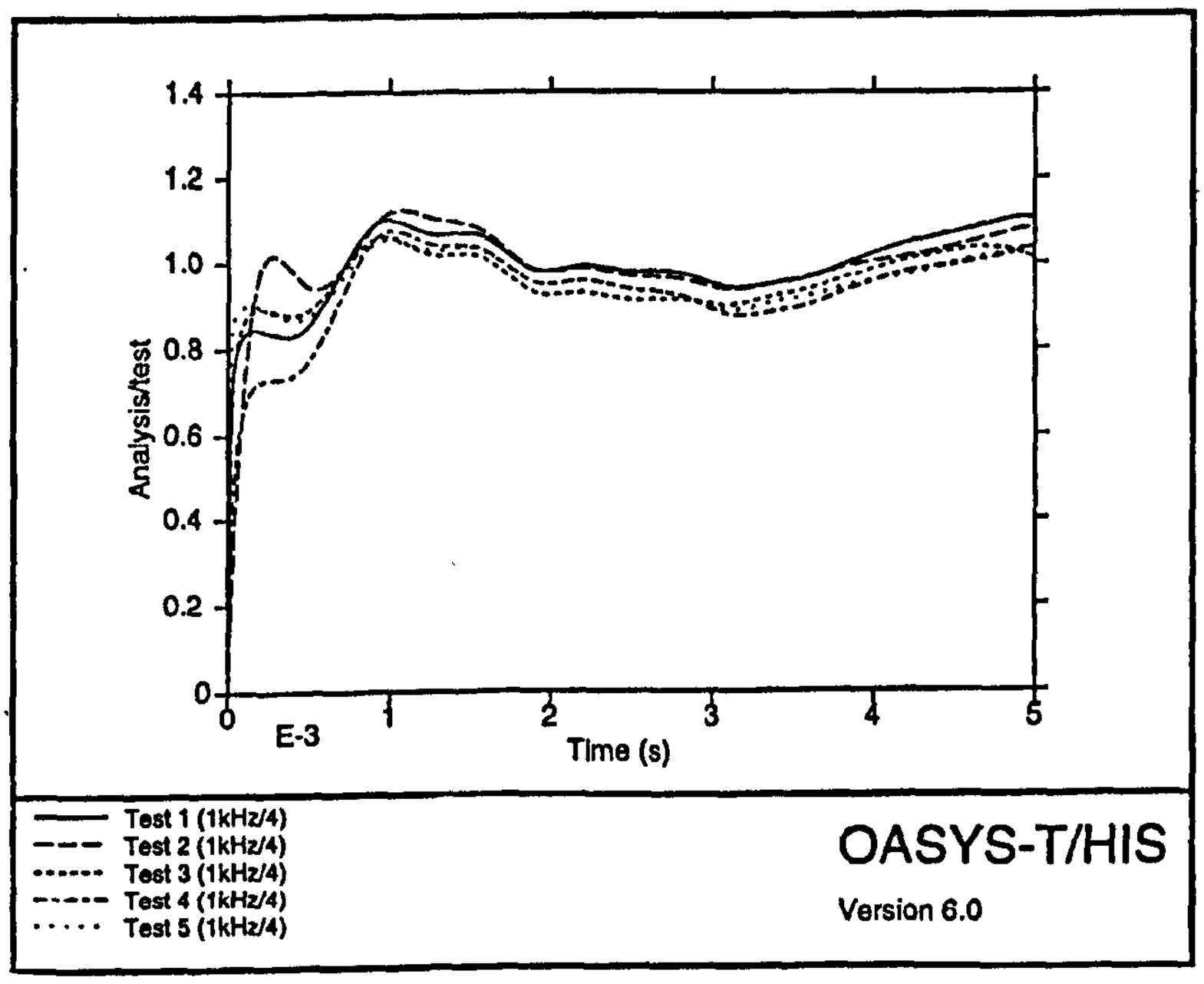

Figure 8.9 "Along" flow force-time history comparison

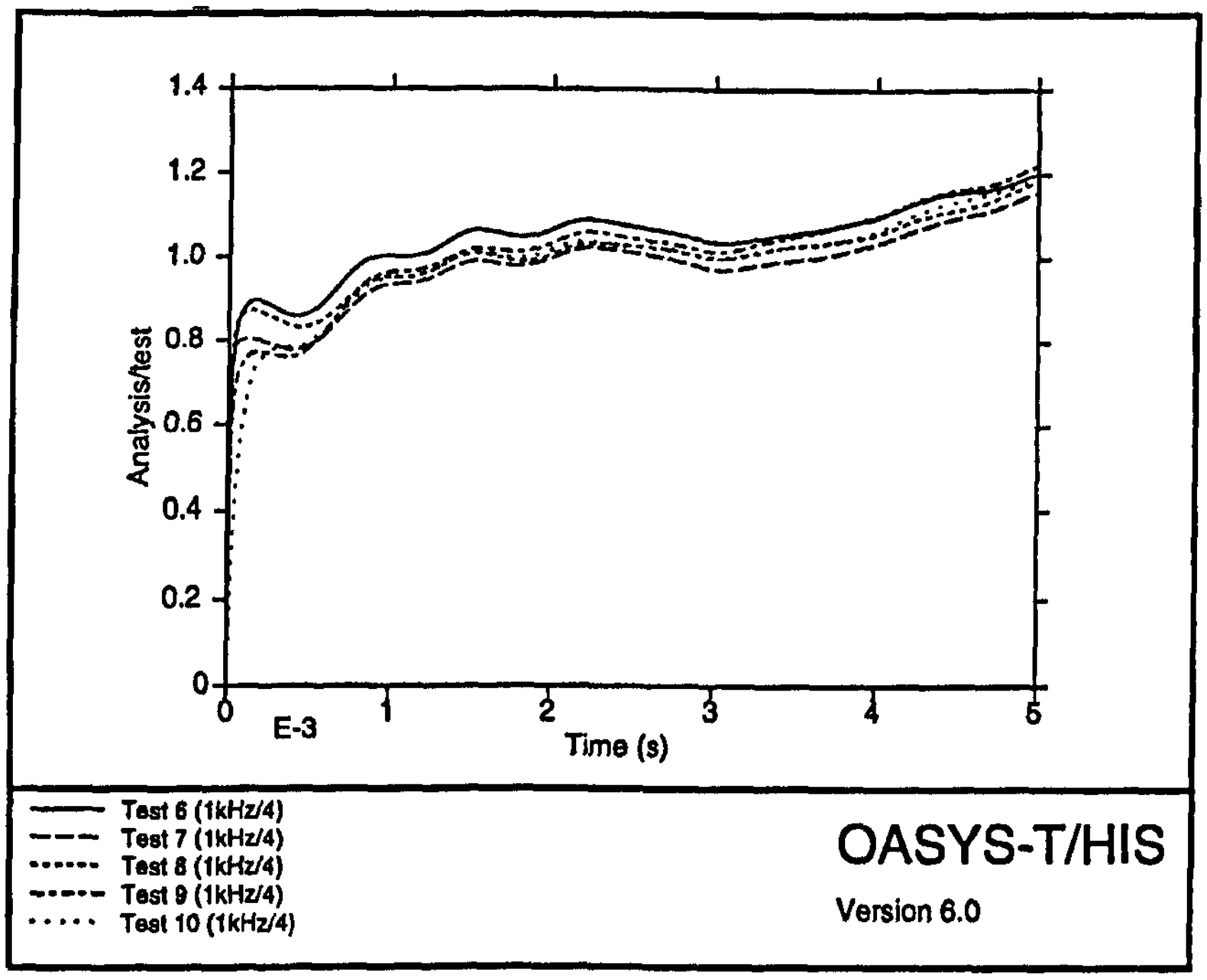

Figure 8.10 "Cross" flow force-time history comparison

8.5.3 Disc comparison

The comparison of the predicted force-time histories and those measured are shown in Figure 8.11. From the Figure it can be seen that:

1) the analytical model is too stiff;

2) the material can withstand significantly higher loads and deformations than those indicated by failure defined as the onset of the neck point of the tensile test;

3) a von Mises failure equivalent stress failure criterion at a level higher that the tensile test neck point does not adequately represent the ductile disc failure mode.

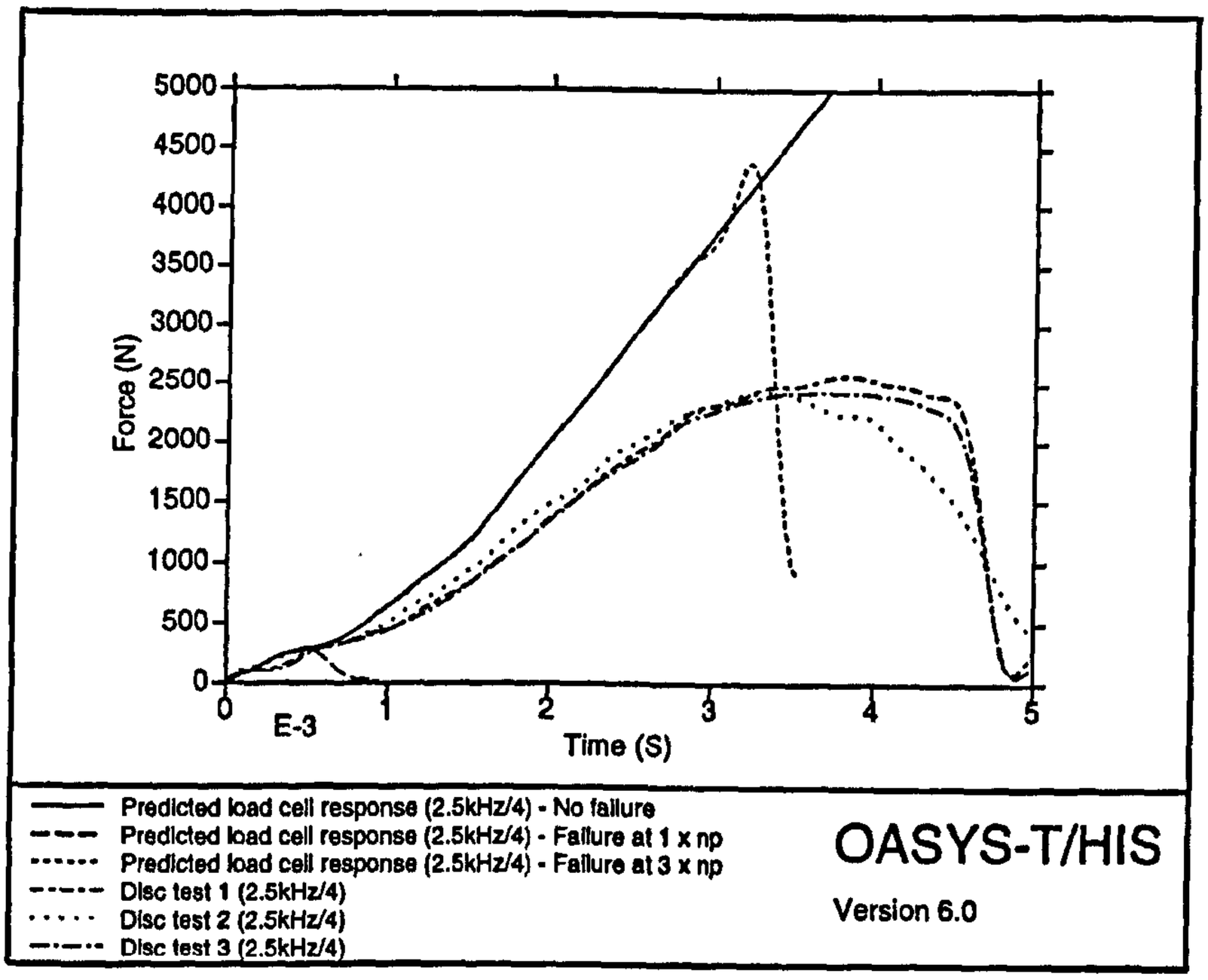

Figure 8.11 Disc low frequency response comparison

By dividing the predicted force of the 'no failure' analysis by the experimentally measured force this high-lights where the differences between the test and analysis occur. This is shown in Figure 8.12. Yield of HDPE occurs very early (≈ 0.3 ms) during the impact and the effect of the bi-linear idealisation can be observed clearly in Figure 8.12.

At the onset of yield there is a significant spike in the error between test and analysis. This would be expected as this is the point where the deviation between the bi-linear idealisation and the true stress-strain curve is greatest. The onset of necking, as measured in the tensile test, is predicted at approximately 0.5 ms and at loads beyond this the disc analyses predicted significantly higher loads (≈ 20 to 50%) than those measured from test. The following analytical modelling effects were investigated to

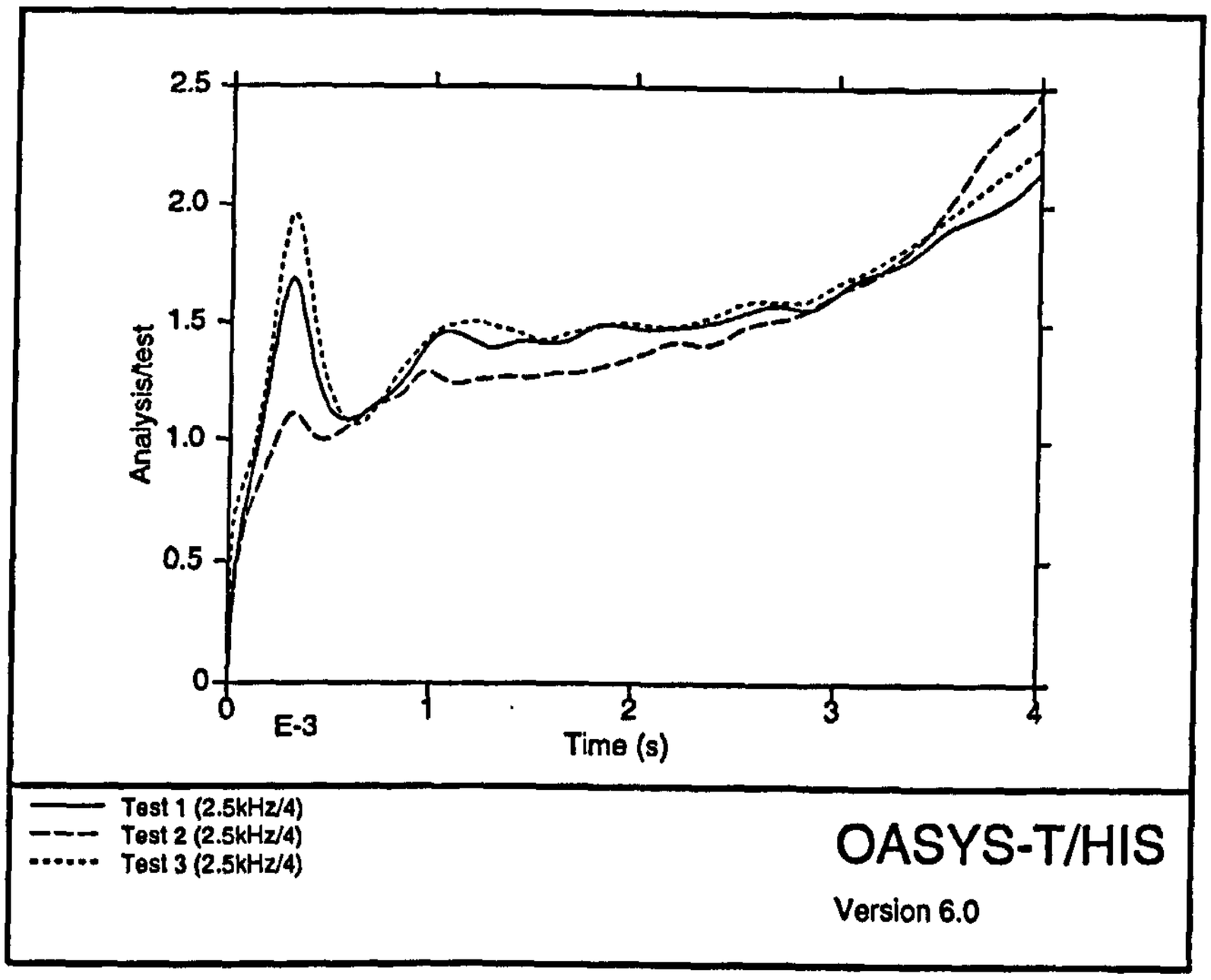

Figure 8.12 Disc force/time history comparison

try and resolve the differences between the test and analyses:

1) mesh density (doubled);

2) solution time step (halved);

3) velocity profile of the impact simulation compared to the test data (identical);

4) coefficient of friction (0 - 0.4);

5) contact algorithm stiffness (halved/doubled);

6) profile of striker (checked using coordinate measuring machine).

None of these made any significant difference to the finite element predictions. This indicated that either incorrect values for the material flow stiffness were used or there must be an additional material softening process involved that was not included in the finite element analyses. As the stress-strain curves obtained from the tensile test data

was limited to below the onset of necking this may result in errors when the bi-linear approximation is extrapolated beyond this point. The post yield secondary modulus (m_2) values were compared with those indicated by the flow stress extrapolations (section 7.7). The comparison of the two methods for extrapolating the stress-strain data beyond the onset of necking in the tensile test is shown in Table 8.3.

$\dot{\varepsilon}$	σ_y bi-linear method	σ_y flow stress method	m_2 bi-linear method	m_2 flow stress method
0.0001	13.86	12.02	42.18	67.77
0.001	16.73	15.30	58.17	72.57
0.01	19.60	18.76	74.16	77.37
0.1	22.48	22.27	90.15	82.18
1	25.35	25.80	106.1	86.98
10	28.23	29.35	122.1	91.78
100	31.10	32.90	138.1	96.58
1000	33.97	36.46	154.1	101.4
10000	36.85	40.02	170.1	106.2
100000	39.72	43.58	186.1	111.0
1000000	42.59	47.15	202.1	115.8

Table 8.3 Post yield bi-linear and flow stress flow data comparison

The bi-linear extrapolation data was from Table 7.5 and the flow stress extrapolation data from Equation 11 and Table C16. Table 8.3 shows that the two methods result in very similar data for the material model and thus the data is likely to be accurate. The flow stress extrapolation data was used in a further analyses with the material failure point set at approximately the same strain (50% ≡ 2.5 x tensile test neck point

stress). The comparison of the two analyses and the test results are shown in Figure 8.13.

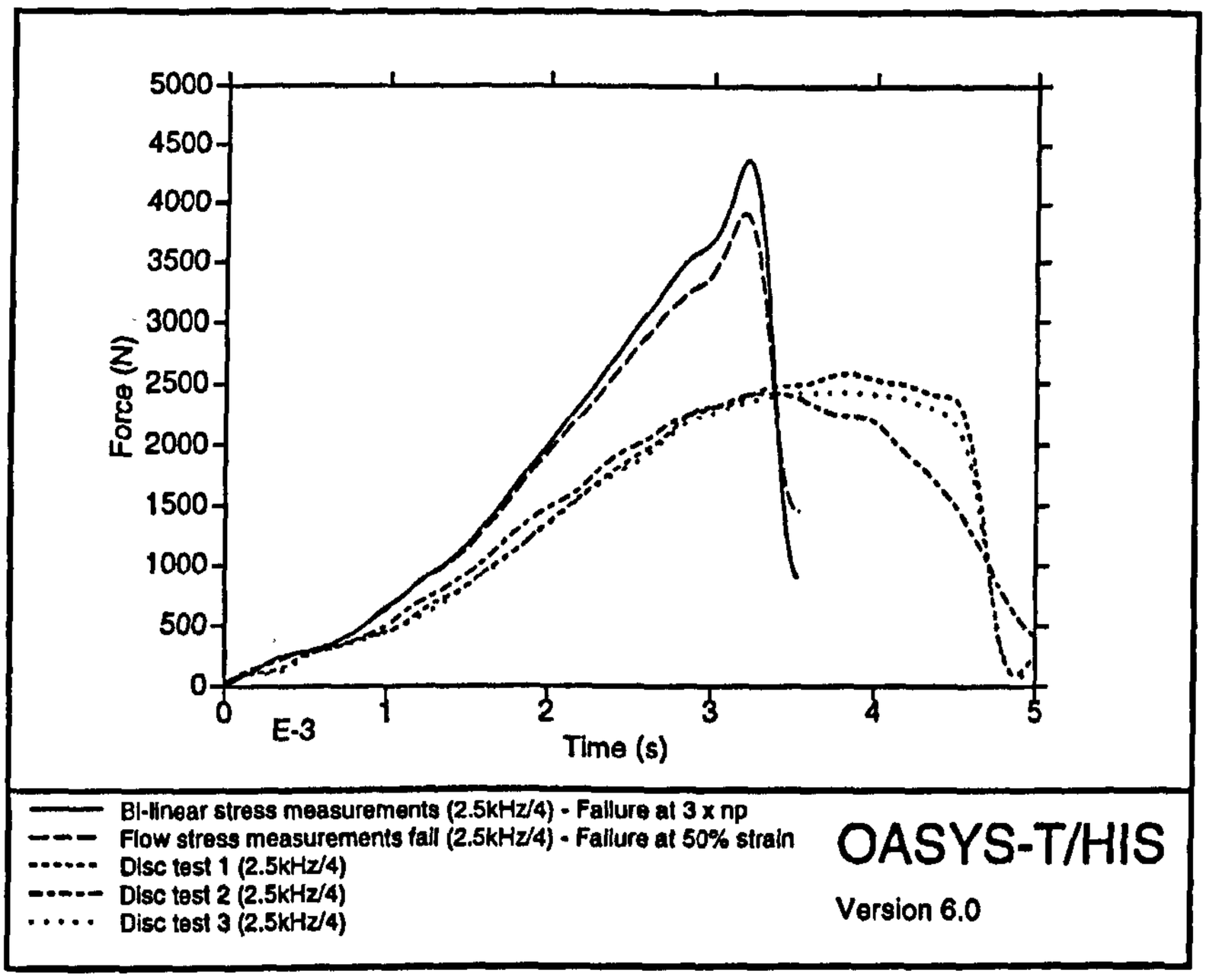

Figure 8.13 Disc prediction - bi-linear and flow stress data comparison

Having concluded that the higher stiffness prediction was not due to test measurements or errors in the analytical modelling it was concluded that an additional material deformation process must be involved. This could be a thermal process which is known to occur during tensile and compressive testing at high strain rates. At high strain rates a temperature rise is generated in the material which has two mechanical effects. The first is the expansion of the material and the second is a softening of the material. If the observed softening in the disc impact test were attributed to a thermal process then the increase in material temperature would be in the order of 15 to 25° C based on the temperature dependence of the flow stress (Equation 11). A significant

bulk temperature rise of this order was not observed immediately after the disc impact tests. Therefore a non thermal softening effect must be responsible.

At 3 ms the onset of material failure in the disc occurs and in the case of the 'no failure' model analysis the deviation between test and analysis sharply increases. In the analytical model the failure criteria was that of a maximum allowable von Mises equivalent stress. Once a particular element has exceeded the allowable stress it is deleted from the solution. This type of failure model results in a rapid drop in the predicted force time history typical of a brittle type failure with no constant load drawing phase. Thus this type of failure model does not represent the true failure characteristics of this type of material. A material model which progressively degrades the material stiffness as it fails is required to model the failure of ductile thermoplastics. This failure model was not available to the author at the time of the analyses.

8.5.4 Comparison between beam and disc geometries

The predicted strains in the beam analyses are less than those which would cause a tensile test specimen to neck as apposed to the disc analyses where the material was strained beyond this point and to failure. Despite the fact that there was good correlation between the extrapolation of the slow strain rate data and the reported SHPB data at moderately large strains of 5, 10 and 15% strain this method over predicted the material stiffness, as observed by the disc impact test, at large strains (up to 50%). The difference in correlation between the two test configurations was due to the differing maximum strain levels experienced by the beam and disc samples. At

loads beyond the tensile test neck point the extrapolation of slow strain rate bi-linear material data predicts higher values for the material stiffness than that observed by the disc impact tests. The difference in correlation between the two test configurations is based on the maximum strain generated in the two configurations. At large strains beyond the tensile test neck point (≈ 20%) a significant softening effect was observed in the disc impact test. This limits the strain range up to which this proposed methodology can be used. This softening effect is not well understood. It is probably not a thermal softening process and requires further research if finite element simulations are to accurately predict events at these high strains (>20%).

8.6 Impact simulation of beam and discs - Conclusions

1) For the beam test configuration the material orientation effects were not important for this test configuration.

2) The difference in correlation between the beam and disc test configurations is based on the maximum strain generated in the two configurations.

3) At large strains beyond the tensile test neck point (≈ 20%) a significant softening effect was observed in the disc impact test. This limits the strain range up to which this proposed methodology can be used.

4) Current material model assumptions using a maximum allowable von Mises equivalent stress and deletion of elements are inadequate to model the failure of ductile thermoplastics and further research is required in this area.

Chapter 9

Fuel tank impact simulation

The successful prediction of the impact performance of an automotive thermoplastic fuel tank and correlation with experimental test results had not been previously achieved prior to the author's publication [102]. The component that was chosen to achieve this was a Rover blow moulded fuel tank (vehicle model PR3, part number WFE 105220). This was chosen as a typical blow moulded thermoplastic component which could be required to withstand significant impact loads. Also a three dimensional CAD model and manufactured parts were available. The tests and analyses described in this Chapter were undertaken for research purposes only and not for homologation or legislative requirements. The impact test facility that was available to test the fuel tank was the swinging head impact pendulum at Rover's Gaydon site which was modified to provide an impact similar to that specified in EEC Regulation No. 34 Annex 5 [18]. A test jig was designed and manufactured to support the fuel tank in the same attitude that it would be in a vehicle and using the in-vehicle securing straps.

9.1 Impact tests

The reason for the tests was to supply experimental data to correlate with OASYS LS-DYNA3D impact simulations of a thermoplastic fuel tank for research purposes only. The tests were carried out on the swinging head impact pendulum at Gaydon on 16 August 1995 and 20 November 1995, with the hemi-spherical head replaced by a steel square based pyramid with equilateral faces. A section through the pyramid is shown in Figure 9.1.

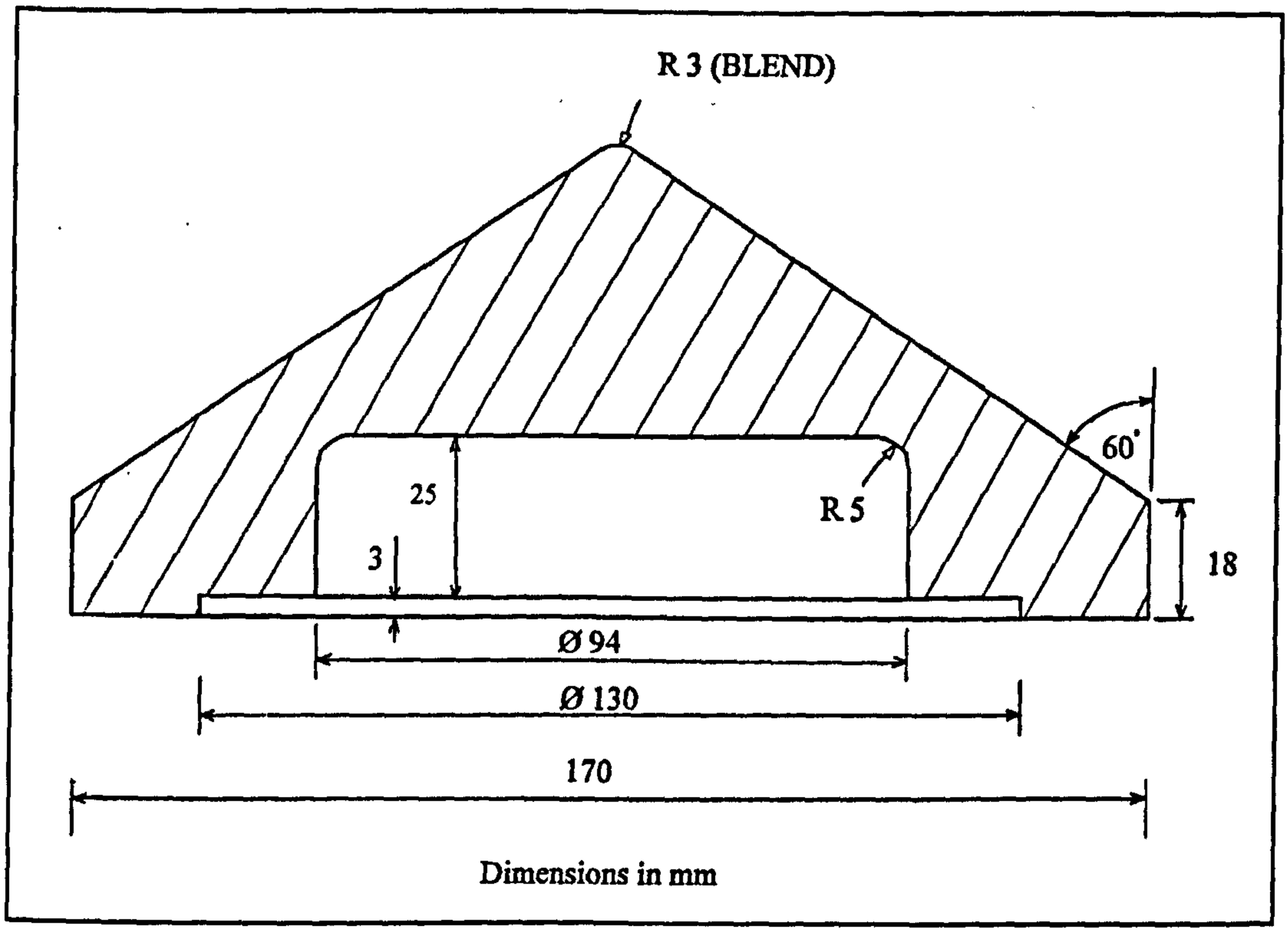

Figure 9.1 Pyramid head form section for impact pendulum

The inertial requirement for the test was that the pendulum should have an effective mass of 15 kg @ 1 m. The replacement steel square based pyramid was designed such that the pendulum would meet this requirement. However because the internal space in the pyramid head was insufficient for the accelerometers, a 14.38 mm thick aluminium spacing ring was needed to achieve the required internal space. This increased the effective mass of the pendulum to 16.63 kg @ 1 m.

9.1.1 Initial test configuration

The configuration for test 1 is shown in Figure 9.2, with the configuration for tests 2 and 3 being very similar except for changes in lateral alignment of the fuel tank relative to the pendulum.

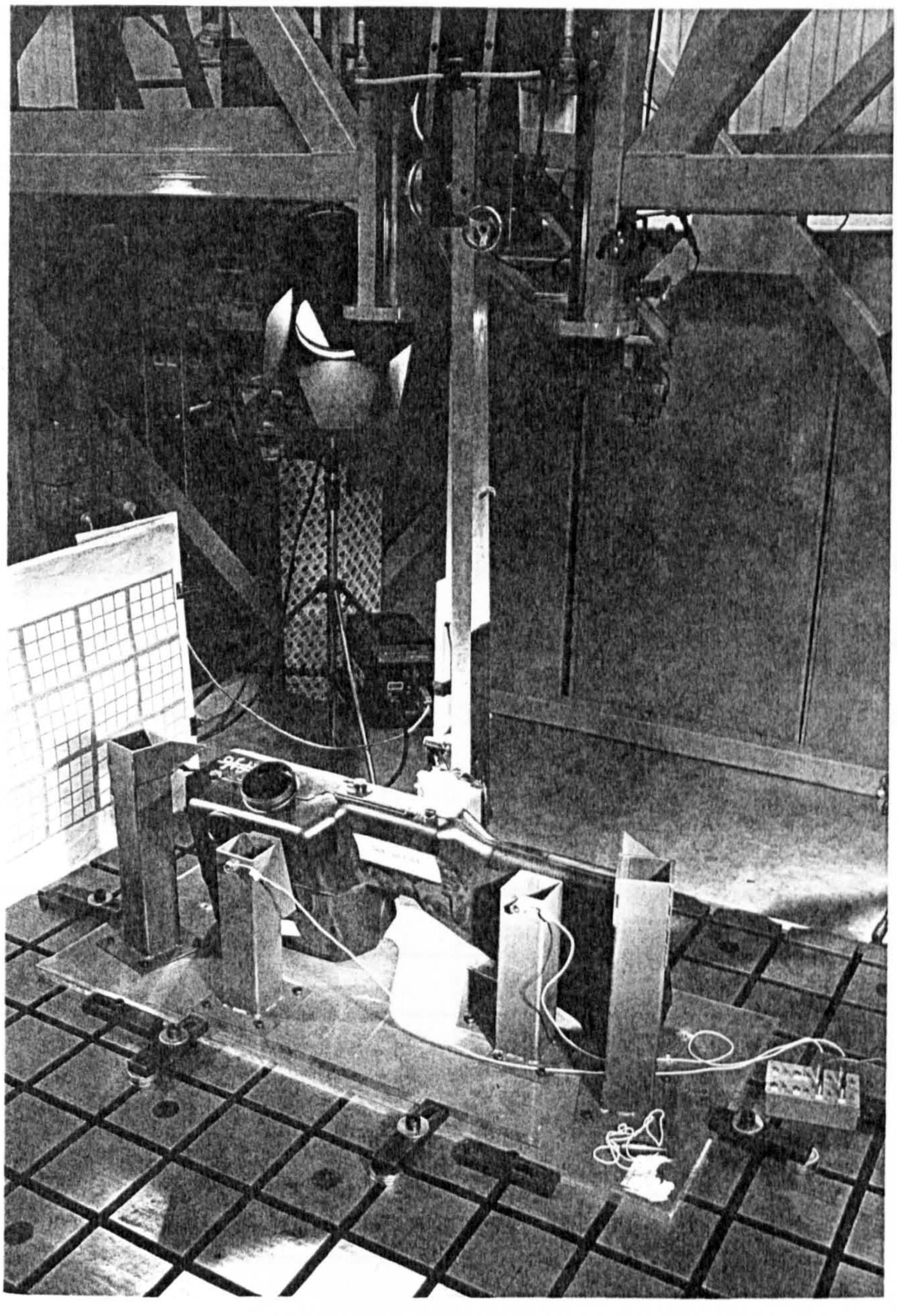

Figure 9.2 View of impact test configuration

The fuel tank support jig consisted of a 1" thick aluminium base plate to which four steel brackets were bolted. These were arranged to provide the appropriate mounting features and points for the fuel tank in-vehicle securing straps. These brackets were

manufactured from 4" square by 3/16" thick steel box section and 3/16" thick steel plate. To resist the securing and impact loads two reaction pillars were used. These were made from 4" square by 3/16" thick steel box section and bolted to the base plate. One of the reaction pillars required a 30° aluminium wedge to achieve a flush mating face with the fuel tank. The fuel tank was secured against the reaction pillars by the in-vehicle straps.

The incident velocity of the modified pendulum was set at 12 kph such that energy of the impact should have been 30 Nm. However due to an error in the initial calculations and the additional mass of the spacing ring the fuel tank was tested with a greater incident energy (66.4 Nm). The mass and energy of the initial test configuration are shown in Table 9.1.

	Desired	Test
Mass (kg)	18.30	19.91
Inertia about the pivot point (kg m^2)	20.72	22.83
Effective mass @ 1 m (kg)	15	16.63
Incident velocity (kph)	8.4	12
Incident energy (Nm)	30.0	66.4

Table 9.1 Inertia and energy of the test pendulum for the initial tests

Three initial tests were carried out with the pendulum striking the fuel tank at different positions. The position of the fuel tank on the base plate relative to the swinging

pendulum at rest was adjusted to achieve the dimensions shown in Table 9.2 and Figure 9.3.

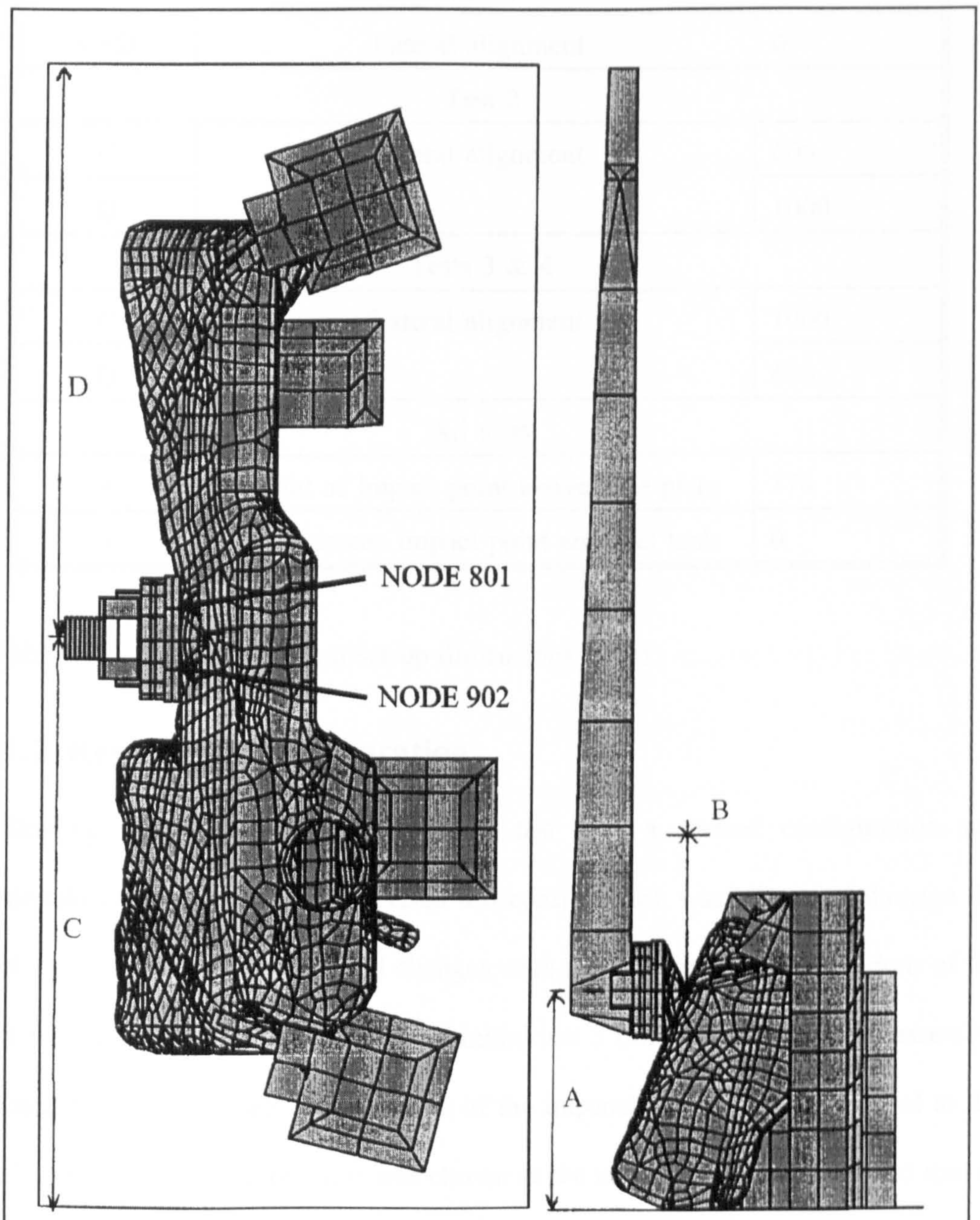

Figure 9.3 Position of the tank relative to the impact pendulum

Dimension	Description	Value (mm)
Test 1		
C=D	Lateral alignment	0
Test 2		
C	Lateral alignment	600
D		1000
Tests 3 & 4		
C	Lateral alignment	1000
D		600
All tests		
A	Height of impact point above base plate	374
B	Gap between impact point and fuel tank	0

Table 9.2 Tank/pendulum set up dimensions (mm)

9.1.2 Revised test configuration

Following the first three tests a fourth test with a revised configuration was undertaken. The object of the revised test configuration was to try and damage the fuel tank. To achieve this several changes were made. The set up dimensions of the test were chosen to be the same as for initial test 3 but with the fuel tank assembly rotated through 30° such that the point of the impacting pyramid was normal to the fuel tank surface. Position three was chosen as the initial test results indicated that of the three initial test positions, position number three had the stiffest response and thus the fuel tank strain rates during the impact would be the highest. The test rig was modified by placing it on a frame at 30° to the horizontal. The incident velocity of

the pendulum was increased to 24 kph, close to the maximum attainable from the swinging pendulum, i.e. an increase in impact energy to 245 Nm.

9.1.3 Test instrumentation

The test data that could be directly compared with the analytical simulations was the acceleration response of the pendulum. The steel square based pyramid was instrumented internally with two accelerometers. Also both reaction pillars were instrumented with accelerometers for all the tests as shown in Figure 9.2. Typical accelerometer calibration plots are shown in Appendix D Figures D1 and D2. The reaction pillars were instrumented to check whether they were subject to significant deformations during the test. The data acquisition system was set up using a scrap fuel tank to maximise the resolution of test data. The resulting sampling frequency was 10 kHz, the maximum available. As well as digitally recording the acceleration data, the initial series of tests (1 to 3) were recorded visually by a NAC (HSV-400) high speed colour video. Due to the fact that the lights for the high speed video caused the temperature of the fuel tank to rise significantly (10.5° C), the revised test (4) was not filmed.

9.1.4 Measured test results

For the comparison of the test and analysis data the OASYS T/HIS software was used. The acceleration test data, digitally recorded at Rover Gaydon, was converted via LOTUS 1-2-3 spread sheets into OASYS LS-DYNA3D time history curves. The test data was then manipulated to zero the time and acceleration axes and convert the data units to seconds and millimetres per second squared for comparison with the analytical

data. Typical acceleration test results are shown in Appendix D Figures D3 and D4. For all the tests there was no significant difference in the response of the two accelerometers mounted in the steel pyramid. Figure 9.4 shows the comparison of the first three impact tests and from this the relative stiffnesses of the three positions can be seen.

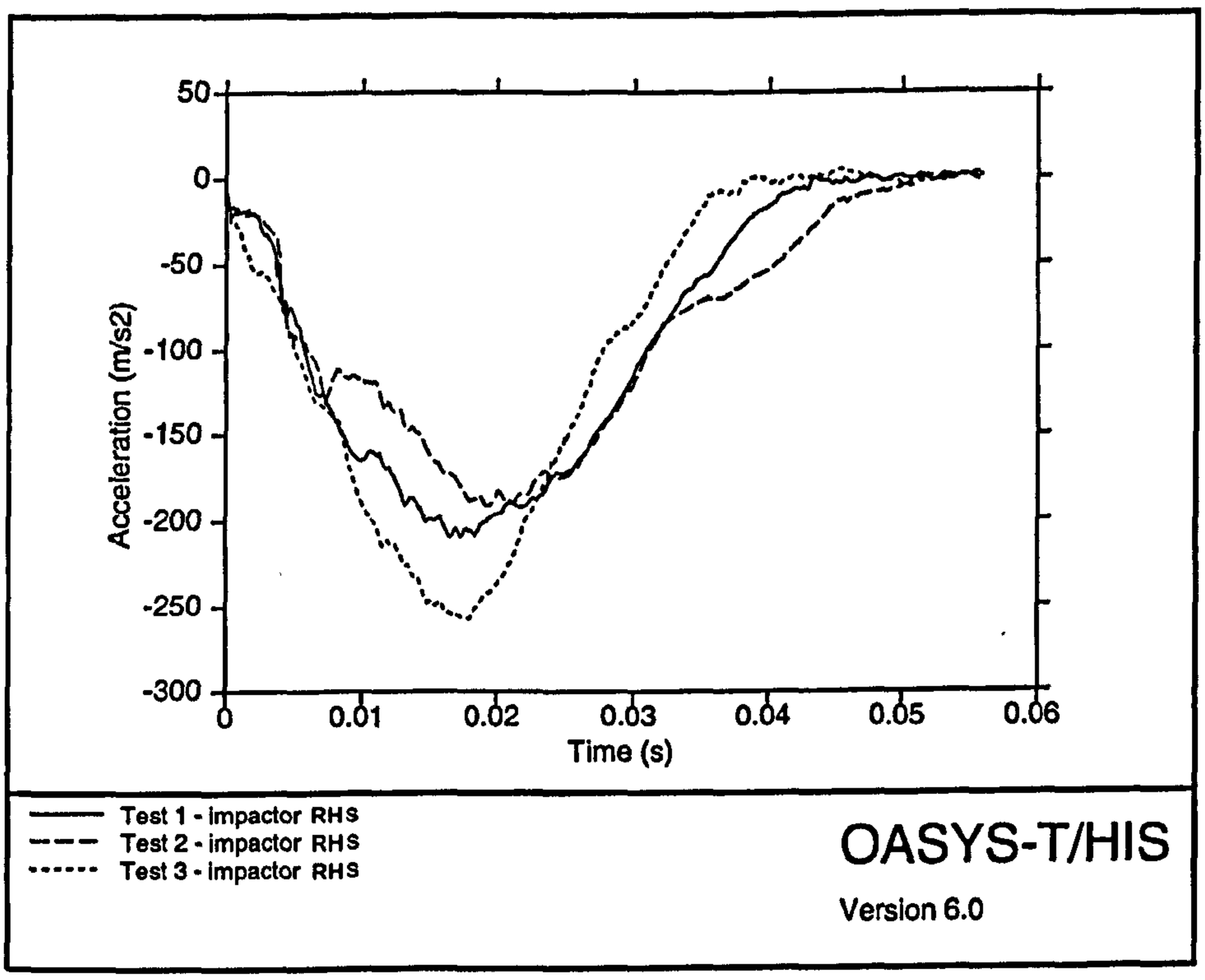

Figure 9.4 Pendulum response for initial tests

The high speed video of the impact tests was recorded at a slow speed on to standard VHS video tape such that it could be replayed on a domestic video recorder. During the initial three tests the background temperature and humidity were 27.5° C and 46%. Four spot lights were used to illuminate the fuel tank and this had the effect of raising the fuel tank surface temperature to approximately 38° C (measured immediately after the test by a contacting thermocouple). The acceleration responses of the reaction

pillars indicated that the deformation of the pillars was not significant and this was confirmed by the high speed video. After each test the fuel tank was visually inspected for damage. Apart from minor scuffing, at the impact point, there was no visible damage to the fuel tank for the first three tests. Therefore the same fuel tank was used for all four tests. The background temperature and humidity were 23.4° C and 38% for the fourth test. After the fourth test the fuel tank was visually inspected and there was a significant dent in the fuel tank surface at the point of impact. Due to the viscous nature of the fuel tank material, the size of the dent could be seen to reduce visibly in size immediately after the test.

9.2 Predictive analyses

A three dimensional model of the fuel tank, created in Pro/Engineer, was available from the supplier, Solvay Automotive, and the surface geometry of this was transferred as IGES curves into the EMRC software NISA/Display III which was used as the pre-processor to define the model of the impact test. The curves were converted into a surface model and meshed with shell elements. During the development of the fuel tank there had been a blow moulding simulation undertaken to predict the tank wall thickness distribution [15]. However use of the simulation thickness distribution results were not possible for the following reasons:

1) there had subsequently been significant changes in the design of the fuel tank;

2) the finite element mesh used for the simulation consisted of triangular elements which were not suitable for the impact analysis software.

As an accurate blow moulding simulation of the fuel tank was not available at the time of the impact analyses, the fuel tank wall thickness distribution (3 to 10 mm) was measured using an ultrasonic thickness gauge and entered into the FEM in 1 mm steps.

The fuel tank boundary conditions were defined by the in-vehicle mounting straps securing the fuel tank to the test supporting jig. The fuel tank restraining straps were imported from a Rover supplied ComputerVision CADDS-5X model via IGES and, similarly to the fuel tank external surface these were converted to a surface model and meshed with shell elements. The reaction pillars and the brackets to which the fuel tank was secured by straps was modelled and meshed with shell elements in NISA/Display III. The interfaces between the fuel tank, straps and the reaction pillars were modelled using contact surfaces and the strap pre-load was modelled as an applied displacement boundary condition.

The swinging pendulum was modelled using a mixture of shell and solid elements, as appropriate to the geometry of its components, and then checked to ensure that its mass and inertia coincided with the known measured values for the test pendulum. The impact analyses were initiated by defining the pendulum to be rotating at a known angular velocity at the moment of impact. The impact simulation model for test 1 is shown in Figure 9.5.

Two impact simulation configurations were analyzed. These were tests 1 and 4. Isotropic elastic models were used for all the metallic parts of the analytical model with the material data as listed in Appendix D Table D1. The HDPE fuel tank was

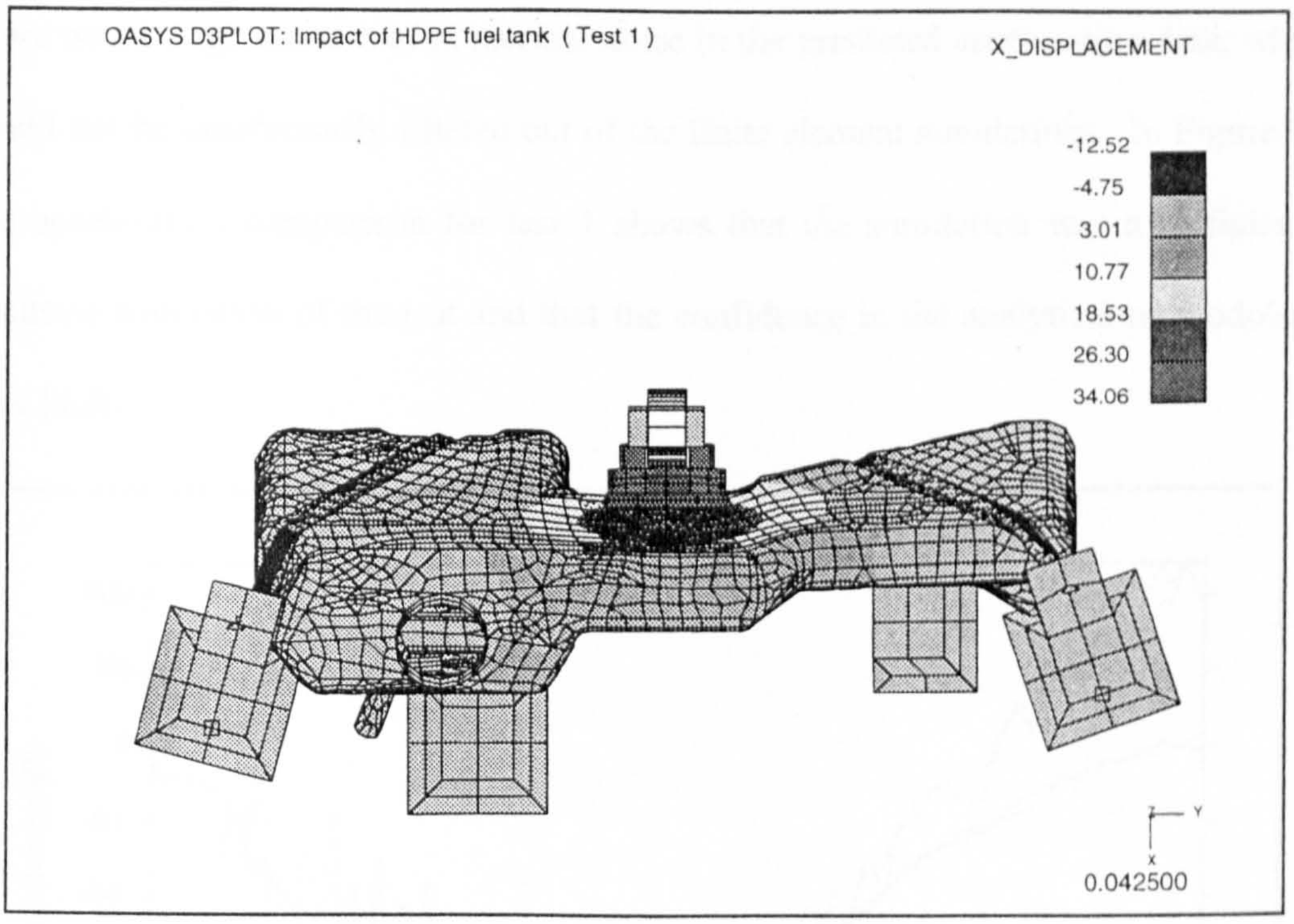

Figure 9.5 Impact simulation at 42.5×10^{-3} s

modelled using an isotropic elastic-plastic model with load curves to account for strain rate effects. As the ambient temperatures for the first three tests (1 to 3) and last test (4) were different, two sets of data were used. These were based on the average data for "along" and "cross" flow material property measurements as listed in Tables 7.5 and 7.11. The data used is listed in Appendix D Tables D2 and D3.

9.3 Correlation of force time history

The correlation of the impact simulations and tests were ascertained by comparing the measured and predicted acceleration responses of the accelerometers mounted in the square based pyramid. In the comparisons the two accelerometers on the pendulum (right hand side and left hand side) corresponded to nodes 801 and 902 of the finite element model. Node positions 801 and 902 are shown in Figure 9.3. Unfortunately

there was a large amount of numerical noise in the predicted acceleration data, which could not be satisfactorily filtered out of the finite element simulations. In Figure 9.6 the acceleration comparison for test 1 shows that the simulation was a sufficiently accurate simulation of the test and that the confidence in the analytical methodology was high.

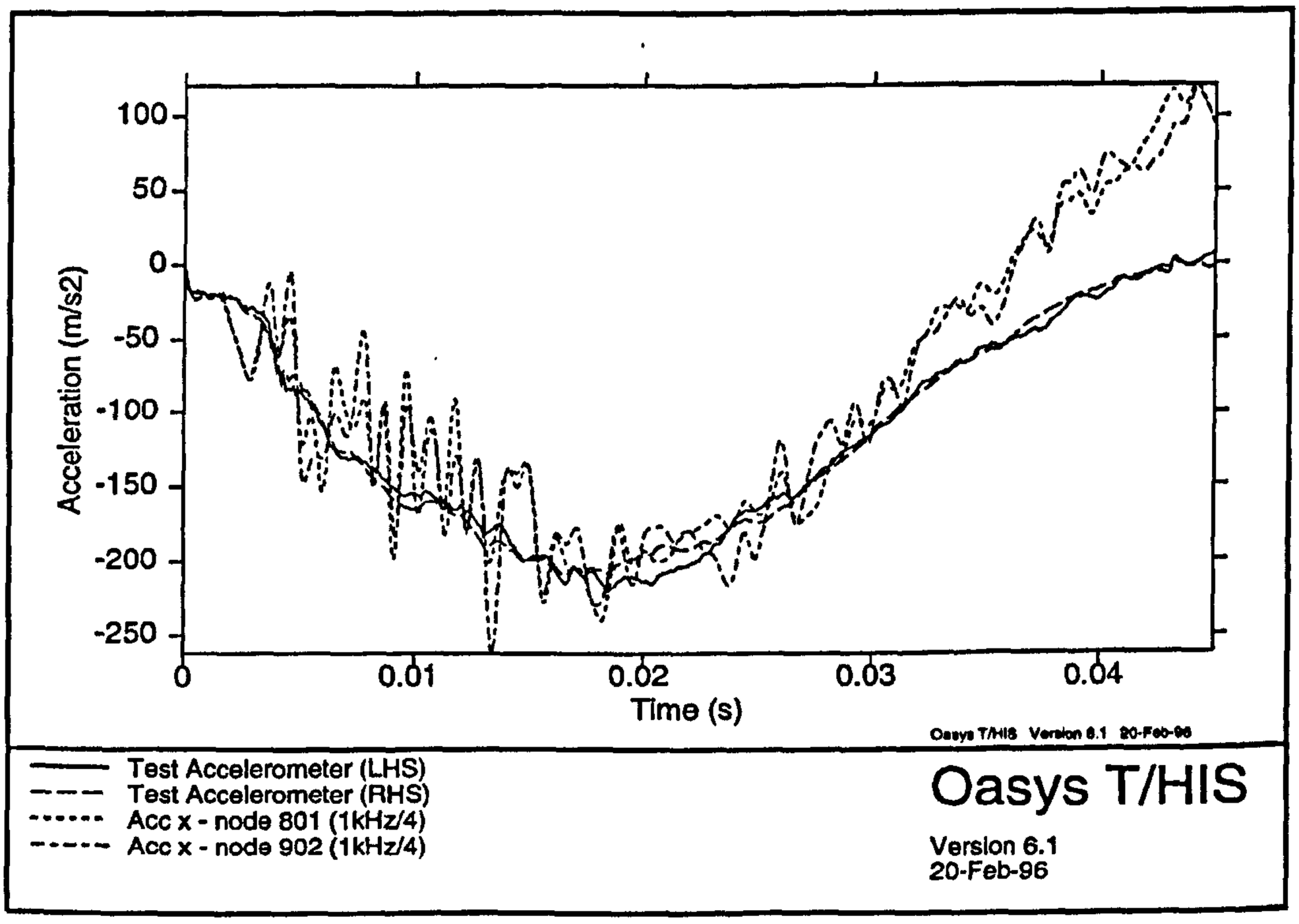

Figure 9.6 Test 1 Comparison of pendulum acceleration

During test 4 the pendulum was used at the maximum velocity of which it was capable as the test was intended to induce permanent deformation of the fuel tank. Figure 9.7 shows the acceleration comparison for test 4. This shows that the simulation under predicted the fuel tank stiffness but still was sufficiently close to provide confidence in the analytical methodology.

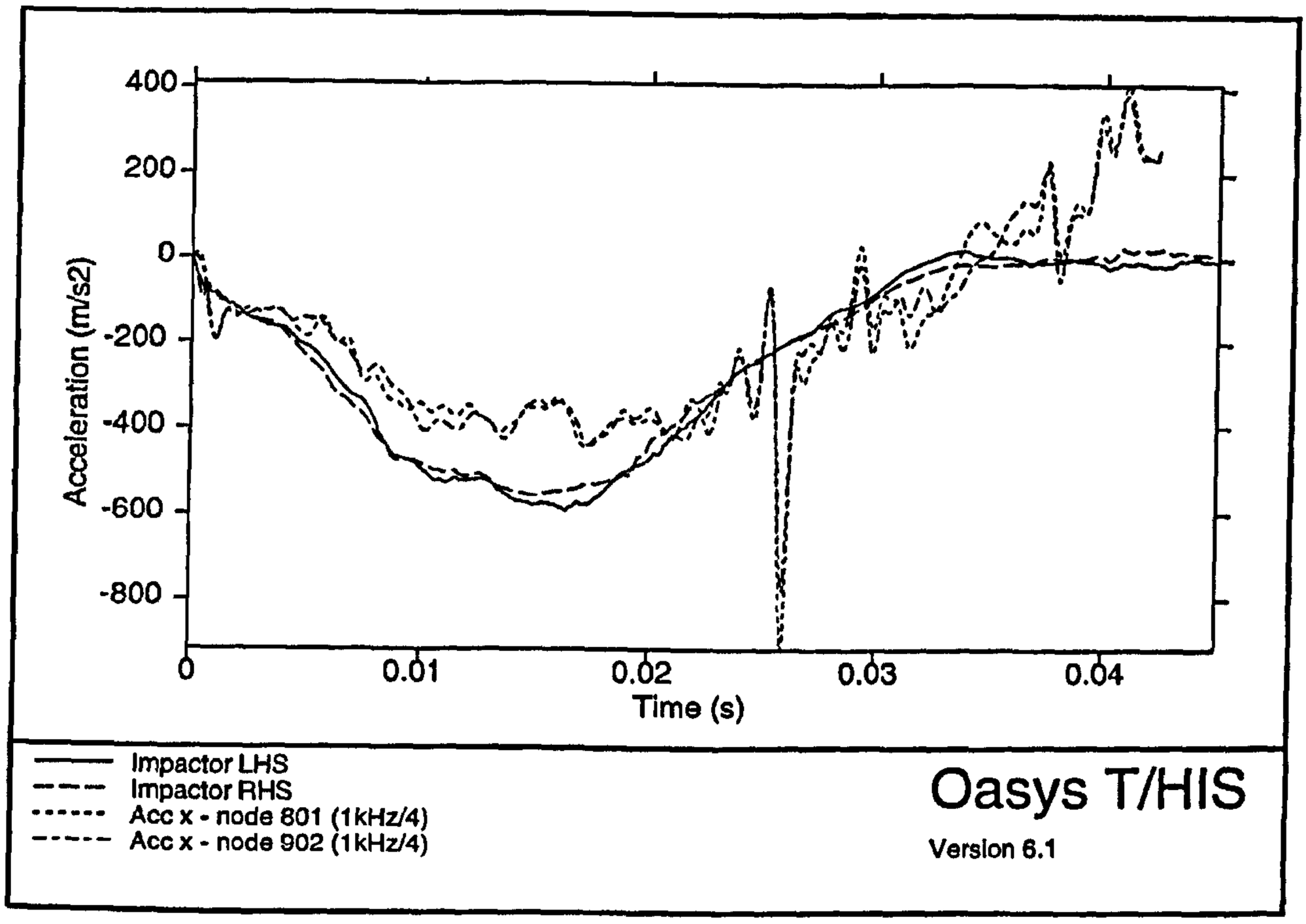

Figure 9.7 Test 4 comparison of pendulum acceleration

In test 1 the fuel tank deformation is essentially an elastic large deformation mode of the whole fuel tank with a face of the impacting pyramid striking the fuel tank. As such the use of distributed wall thickness or average wall thickness makes no significant difference in the predicted acceleration of the pendulum. Test 4 was intended to induce local plastic deformation of the fuel tank with the point of the impacting pyramid striking the fuel tank. In order to do this the fuel tank was hit by the pendulum at its maximum attainable velocity and at the point where tests 1, 2 and 3 had shown the fuel tank to be stiffest (position 3). Unfortunately at the local impact point on the fuel tank the wall thickness distribution and gradient were large. Hence although test 1 correlated well with a global mode of the fuel tank the correlation of test 4 did not correlate so well with the local mode of the fuel tank excited in test 4. This was probably due to the inaccurate modelling of local wall thickness, especially

along the parison parting line. Whereas it may be theoretically possible to refine the finite element mesh and wall thickness distribution, it was not practical to do this due to the following reasons:

1) it was not possible to accurately measure the wall thickness distribution with the available ultrasonic wall thickness gauge due to its transducer dimensions;

2) the relative dimensions of the fuel tank wall thickness to shell element length would not be appropriate for a finer finite element mesh;

3) if a finer finite element mesh had been created the resulting analysis time would be excessive on the available hardware. (The analyses were being run on a Silicon Graphics Indigo R4000 and taking approximately 6 days to solve).

9.4 Sensitivity of simulation to input data

9.4.1 Effect of material supplier

The work detailed in Chapter 7 on obtaining the material properties of HDPE was carried out on the BASF material Lupolene 4261A. The data for this material was used for the impact simulation work on the Rover fuel tank which was manufactured from a different grade of HDPE. The fuel tank was made from the Solvay material Eltex RSB 714. To establish whether this was valid, back to back comparison analyses were performed using data for both material grades. The data for the Solvay material was obtained by undertaking slow speed strain rate controlled tensile tests at 35° C and fitting the true stress-strain curves with a bi-linear representation, as discussed in Chapter 7. The effect of using the two different sets of data is shown in Figure 9.8 and Table 9.3 which compare the predictions with the test data.

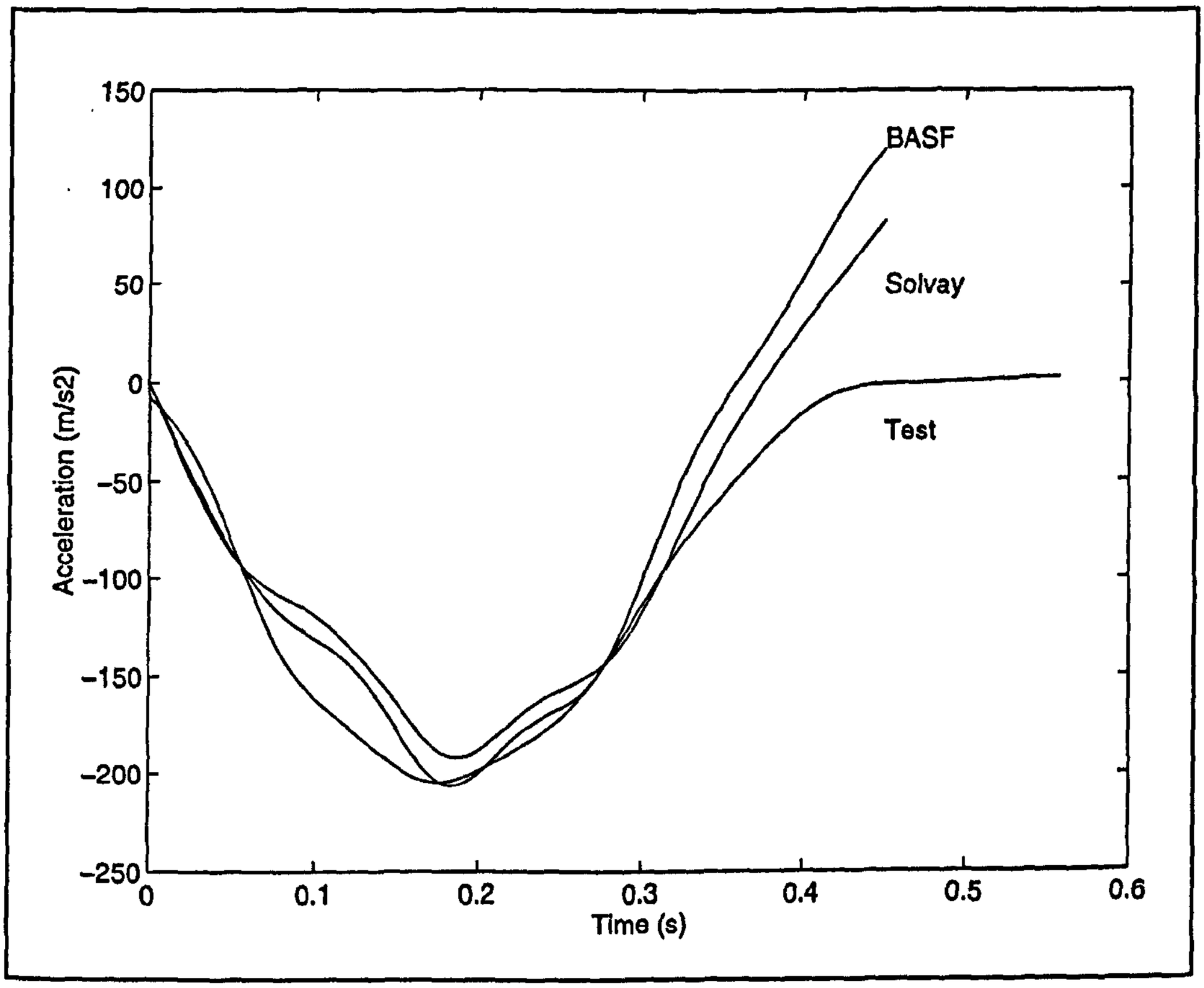

Figure 9.8 Effect of different material data

	Peak acceleration		Time to peak	
Test node/ accelerometer position	801/rhs	902/lhs	801/rhs	902/lhs
BASF	1.01	0.914	1.04	0.9950
Solvay	0.937	0.853	1.07	0.966

Table 9.3 Effect of different material data on test versus analysis comparison

There is little difference in the predicted acceleration of the pendulum, with the BASF data producing slightly better correlation. The two materials have very similar

stiffnesses but the different test methods used may be the reason why the two differing strain rate sensitivities for the two materials. (The BASF data was obtained from crosshead controlled tests and the Solvay data was obtained from strain rate controlled tests). Of the two sets of data, the data obtained for the BASF material is a more reliable measure of the strain rate sensitivity of HDPE, due to the reasons given in Chapter 6, and should be used in preference to the data obtained for the Solvay material.

9.4.2 Sensitivity of test 1 FEA

The sensitivity of analysis to input data was determined by varying the input parameters of material stiffness, wall thickness and pendulum velocity by a factor of two and determining their effect on the time to peak acceleration and the magnitude of peak acceleration. Figures 9.9 to 9.11 show the effect of varying material stiffness, fuel tank wall thickness and pendulum impact velocity by factors of 2.0 and 0.5 compared to the base line analysis (1.0).

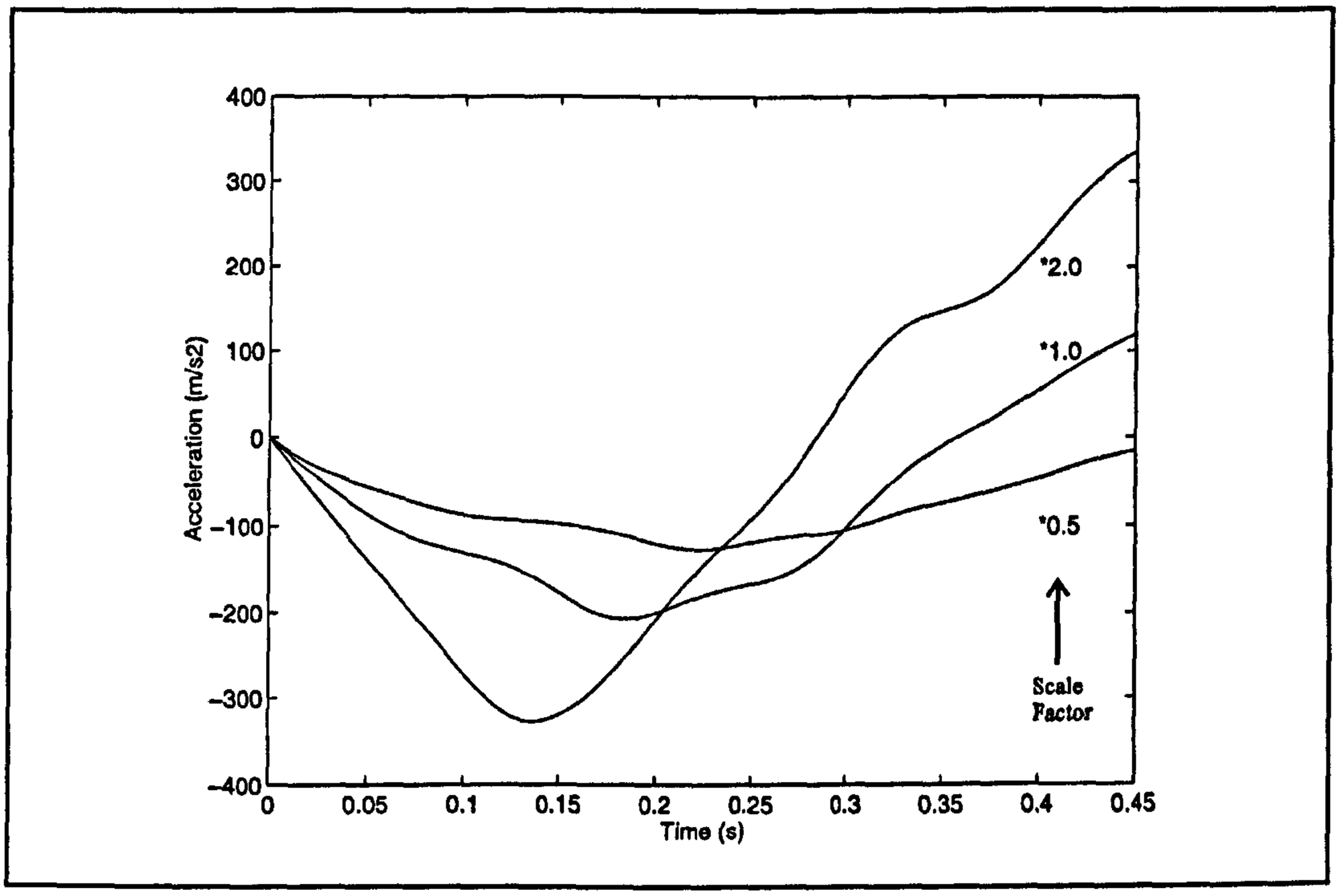

Figure 9.9 Effect of material stiffness - prediction at node 801

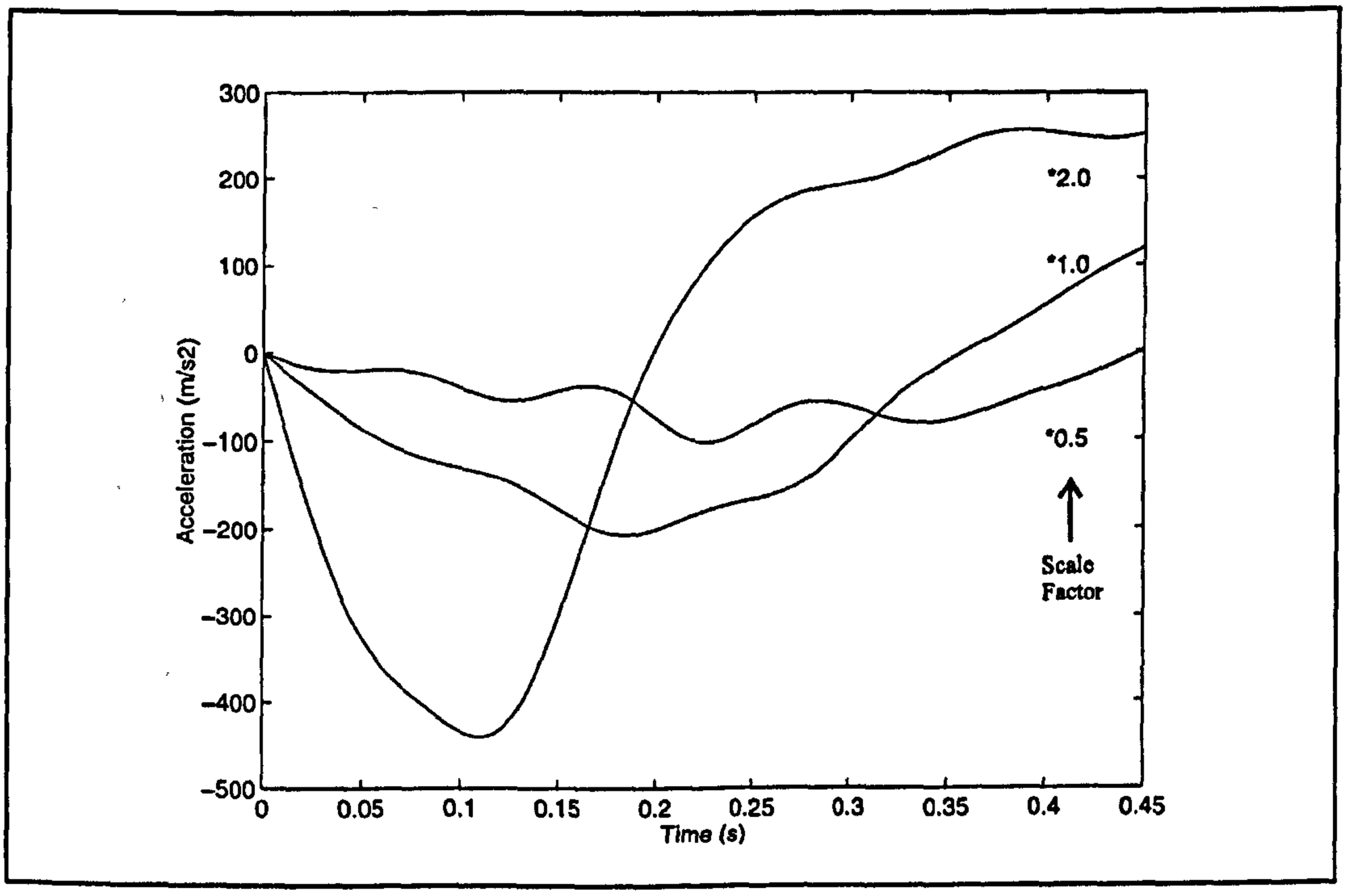

Figure 9.10 Effect of tank wall thickness - prediction at node 801

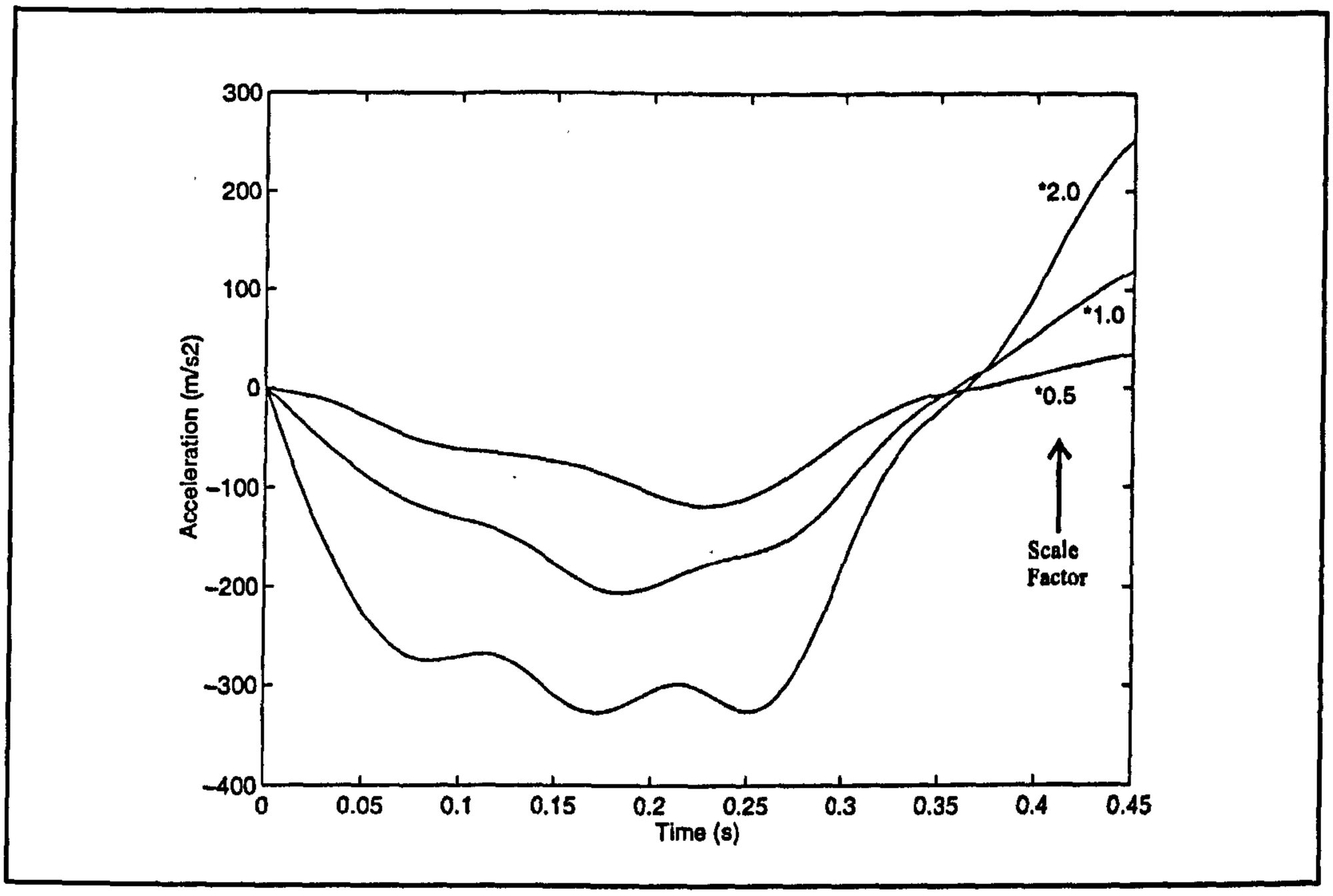

Figure 9.11 Effect of pendulum velocity - prediction at node 801

Table 9.4 shows the relative sensitivity of the peak acceleration and time to peak acceleration on the input parameters of material stiffness, fuel tank wall thickness and pendulum impact velocity. As well as changing the magnitude of the pendulum acceleration and time to peak acceleration the different parameters result in differing acceleration pulse shapes for the pendulum. From the comparison of Figures 9.9 to 9.11 and in Table 9.4 the relative effects of the different parameters can be determined for the Test 1 configuration. The effect of varying each of the three parameters did not produce identical effects (e.g. acceleration pulse shape and magnitude) therefore the following list of relative importance is to some extent subjective.

	Peak acceleration			Time to peak acceleration		
	Material stiffness					
Factor	0.50	1.00	2	0.50	1.00	2
node 801	0.616	1.00	1.54	1.21	1.00	0.771
node 902	0.650	1.00	1.66	1.15	1.00	0.726
	Tank wall thickness					
Factor	0.50	1.00	2	0.50	1.00	2
node 801	0.496	1.00	2.13	1.23	1.00	0.599
node 902	0.517	1.00	2.25	1.19	1.00	0.577
	Pendulum velocity					
Factor	0.50	1.00	2.00	0.50	1.00	2
node 801	0.574	1.00	1.58	1.24	1.00	0.933
node 902	0.654	1.00	1.73	1.21	1.00	1.01

Table 9.4 Sensitivity of Test 1 analyses

For the three parameters and the test configuration considered the relative order of importance was:

1) fuel tank wall thickness;

2) pendulum impact velocity;

3) material stiffness.

9.5 The use of finite element analysis to aid the design of thermoplastic structures

Knowing what features effect the mechanical performance of a fuel tank is the beginning of the design process. Previous work has highlighted the fact that thermoplastic fuel tanks are safer than steel fuel tanks [103]. However in order to achieve these safety benefits it is necessary to use an integrated approach such as that suggested for injection moulded components [104]. This should reduce the risk of the tank failing during qualification testing or in-service. The design of thermoplastic fuel tanks requires a team approach from the designer, material supplier and manufacturer [105]. The design of automotive fuel tanks cannot be considered in isolation to the vehicle and the whole of the fuel system is considered for permeation tests. The development of a blow moulded thermoplastic automotive fuel tank should include the activities of structural performance prediction (creep deformation and impact resistance) and manufacturing assessment (blow moulding simulation). Finite element analyses can be used for structural performance predictions [17,102] and manufacturing assessment [15] but their greatest benefit comes through understanding the underlying effects behind the analytical predictions.

Through the prediction and correlation with experimental test results of a blow moulded automotive fuel tank, a methodology has been developed whereby the mechanical performance of thermoplastic materials can be assessed and used to predict the high strain rate performance of structures made from these types of materials. This methodology is not limited to HDPE or thermoplastic fuel tanks but is generic

and can be applied to general three dimensional objects made from materials with similar mechanical characteristics.

Having shown how the strain rate dependent stiffness of HDPE could be measured and used to predict the impact performance of components this work should be extended to other materials with strain rate dependent stiffnesses. Dioh [56] and Johnson et al. [64] have shown that MDPE and polypropylene both have similar trends for material properties with respect to the natural logarithm of strain rate. It would be of particular interest to establish the degree of correlation between simulations and impact tests of components made from these materials. The application of the proposed methodology to other materials (e.g. polymer matrix composites) is an area of ongoing research at the University of Warwick [106].

9.6 Fuel tank impact simulation - Conclusions

1) The correlation of test 1 showed that the finite element analysis simulation was an accurate simulation of the test and that the confidence in the methodology was high.

2) The correlation of test 4 was not nearly as good as test 1 and this was thought to be due to inaccurate modelling of local wall thickness, especially along the parison parting line.

3) Of the three parameters that were investigated the relative order of importance were: fuel tank wall thickness; pendulum impact velocity and material stiffness.

4) Having shown good agreement between impact simulations and test results it was concluded that the proposed methodology (Chapter 5) can be used to

predict the performance of HDPE fuel tanks at the design stage; thus providing a strategic economic advantage in eliminating test failures and a reduction in product development time. The author is not aware that this had been achieved prior to the author's publication [102].

Chapter 10

Conclusions

10.1 Stress-strain measurements and the effect of displacement control

1) The stress-strain curve and strain rate sensitive material properties are effected by the method used to control the applied deformation rate.

2) The "pacing" method has a limited strain rate range and was not considered a suitable method for determining the effect of strain rate on material properties.

3) If the system resonant response was not present or could be controlled and the "control" (closed loop) system response optimised for each test, then this method would probably have been the most suitable for the measurement of the strain rate sensitity of material properties.

4) For the series of tests undertaken, the "crosshead" method was found to be the most suitable method for investigating the effect of applied deformation rates as the desired deformation rate does not effect the normalised response.

10.2 Measurement and extrapolation of stiffness data

1) The high strain rate data appeared to be consistent with the slow strain rate test trend data but there was poor correlation between the slow strain rate and high strain rate material measurements of σ_n, ε_n, m_1, σ_y and m_2.

2) The large experimental scatter of the high strain rate tensile test results and poor correlation with the slow strain rate extrapolated data was due to

inadvertent shock loading and inadequate accuracy of the strain measurement. Thus the high strain rate tensile tests at the NPL were not suitable for accurate determination of the strength and stiffness of small thermoplastic samples.

3) There was very little difference between the effect of temperature on the "along" and "cross" flow material property measurements. The measured linear temperature scaling factors compare well with published test data and can be used with a good degree of confidence.

4) The compressive SHPB and tensile test results show a strong degree of agreement for both the flow directions. Thus the assumption of a logarithmic relationship between strain rate and flow stress can be made for the tensile test flow stress of HDPE.

5) Despite the poor correlation between slow strain rate and high strain rate test data it is probable that slow strain rate tensile test data can be extrapolated to high strain rates assuming a linear relationship with respect to the natural logarithm of the strain rate.

10.3 Impact performance of beam and disc samples

1) For the beam test configuration the material orientation effects were not important for this test configuration.

2) The difference in correlation between the beam and disc test configurations is based on the maximum strain generated in the two configurations.

3) At large strains beyond the tensile test neck point (≈ 20%) a significant softening effect was observed in the disc impact test. This limits the strain range up to which this proposed methodology can be used.

4) Current material model assumptions using a maximum allowable von Mises equivalent stress and deletion of elements are inadequate to model the failure of ductile thermoplastics and further research is required in this area.

10.4 Fuel tank impact simulation

1) The correlation of test 1 showed that the finite element analysis simulation was an accurate simulation of the test and that the confidence in the methodology was high.

2) The correlation of test 4 was not nearly as good as test 1 and this was thought to be due to the inaccurate modelling of local wall thickness, especially along the parison parting line.

3) Of the three parameters that were investigated the relative order of importance were: tank wall thickness; pendulum impact velocity and material stiffness.

4) Having shown good agreement between impact simulations and test results it was can be concluded that the proposed methodology (Chapter 5) can be used to predict the performance of HDPE fuel tanks at the design stage; thus providing a strategic economic advantage in eliminating test failures and a reduction in product development time. The author is not aware that this had been achieved prior to the authors publication [102].

Chapter 11

Recommendations for further work

The response of the "control" (closed loop) method is especially sensitive to the controller settings which must be optimised for each desired deformation rate if a consistent set of normalised tensile test specimen strain rate responses are to be obtained. If this is not done then the method is not suitable for measurement of strain rate sensitive material properties especially those associated with accumulated strain. This was not possible for the tests undertaken at the IMC using the Instron 4505 due to mechanical resonance problems. Overcoming these mechanical resonance is an area for further work. There may be a number of methods to overcome this which include: using the controllers existing built-in low pass filters (10 and 25 Hz) to prevent the controller exciting the mechanical resonance; or changing the system response by using a different extensometer.

At large strains beyond the tensile test neck point (≈ 20%) a significant softening effect was observed in the disc impact test. This limits the strain range up to which this proposed methodology can be used. This softening effect is not well understood. It is probably not a thermal softening process and requires further research if finite element simulations are to accurately predict events at these high strains (>20%).

In this work the finite element analyses assumed isotropic material performance with no dependence of behaviour on the hydrostatic component of stress. Further work is desirable to determine the effect of applied deformation rate on these assumptions.

As the methodology for the measurement of strain rate dependent stiffness is independent of application, the material data measured should be applicable to other

components made from the same material. However it is well known that processing conditions for thermoplastics can have a significant effect on the resultant material properties of the finished component. Therefore further research is required to quantify the effects of processing on strain rate dependent material properties.

Having shown how the strain rate dependent stiffness of HDPE could be measured and used to predict the impact performance of components this work should be extended to other materials with strain rate dependent stiffnesses. Dioh [56] and Johnson et al. [64] have shown that MDPE and polypropylene both have similar trends for material properties with respect to the natural logarithm of strain rate. It would be of particular interest to establish the degree of correlation between simulations and impact tests for components made from these materials.

This thesis has concentrated on how the stiffness of thermoplastics can be represented in simulations of impact events. An obvious extension of this work could be the inclusion of damage and failure mechanisms. As mentioned previously, the use of an effective stress based failure criterion has been discounted as a suitable approach for modelling ductile failure [51,74,77] with the suggestion that failure modelling needs to be characterised by a fracture mechanics [74] or damage approach [77].

References

1 Anon. Plastics meet fuel tank challenge, European Plastics News, pp 26-29, May 1992.

2 H Guyot, Plastics industry faces strong environmental opposition, European Plastics News, pp 34-35, March 1994.

3 Berlin technical control board (TUEV-Berlin), Guidelines - Fire protection of vehicles, The ministerial committee's special subcommittee on vehicle fire safety (FKT), 45 StVZO, Federal Republic of Germany 1969.

4 D I Wimpenny, Material property characterisation for nonlinear finite element analysis of thermoplastic pressure vessel, M.Sc. thesis, University of Warwick, 1991

5 A Moffat, Design performance assessment of plastic pressure vessels using nonlinear finite element analysis, M.Sc. Thesis, University of Warwick, 1991

6 J P J Coulton, Developing an analytical method for the creep analysis of plastic fuel tanks, NAFEMS Benchmark magazine, pp 20-22, September 1992

7 J P J Coulton, Nonlinear design analysis of thermoplastic fuel tanks, 4th International Conference on Quality Assurance and Standards in Finite Element and Associated Technologies, Brighton, pp 184-195, May 1993

8 M Rashidy, Developments in the mathematical modelling of vehicle crashworthiness, Automotive Design Engineering, pp 230-237, 1990.

9 R Q Riley, Alternative cars in the 21st century: a new personal transportation paradigm, Chapter 7 - Safety and low-mass vehicles, SAE Warrendale USA, 1994.

10 Government PNGV secretariat, Partnership for a new generation of vehicles: program plan, US Department of Commerce Washington USA, 1994

11 P T Davies, Innovative manufacturing initiative, Report to the management committee on the case for a research programme in the manufacturing of land transport (road vehicles), Dec 1994.

12 K Schweizerhof L Nilson J O Hallquist, Crashworthiness analysis in the automotive industry, International Journal of Computer Applications in Technology, 1991.

13 P S Bulson, Project definition study on structural Impact, prepared for the SERC and DoE, Job No. 266.1 Ref. AME/266.1/R/01.1 August 1990.

14 C Hauck, Blow-molded articles with optimum wall thickness - BASF develops new calculation program for simulating the blow-molding procedure, K '92 2/03 - e, BASF Aktiengesellschaft, Ludwigshafen June 1992.

15 D Assaker P Evrard, Finite element analysis of a fuel tank blow moulding - Rover PR3 project, LC 6 - DAR-PEV/BLM, Laboratoire central Solvay SA, July 1993

16 M Ryan, Mould makers make the most of computer technology ... and CAD companies rally to their aid, British Plastics and Rubber Weekly, p19, April 1994

17 J P J Coulton, Non-linear design analysis of plastic fuel tanks, M.Sc. Thesis, University of Warwick September 1992.

18 UN Agreement, Concerning the adoption of uniform conditions of approval and reciprocal recognition of approval for motor vehicle equipment and parts, Addendum 33. Uniform provisions concerning the approval of vehicles with regard to the prevention of fire risks, ECE regulation no. 34, January 1979.

19 OASYS LS-DYNA3D, an explicit finite element simulation available from Ove Arup and Partners, 13 Fitzroy street London.

20 PAMCRASH , an explicit finite element analysis program supported by PSI, 20 rue Saarinen Silic 303 France.

21 ABAQUS explicit, a finite element program available from Hibbitt Karleson and Sorenson Inc. Providence USA.

22 Physical testing of plastics - correlation with end-use performance, Conference proceedings, American Society for testing and materials, ASTM publication no. 04-73600-19, June 1979.

23 R Brown, Choosing properties, Engineering, pp 23-24, Sept 1994.

24 W Bartholomeyzik, Important physical properties of plastics and aspects of plastics technology, BASF Atiengesellschaft Ludwigshafen Germany, Nov 1988.

25 Designing with plastic: the fundamentals, Design guide TDM-1, Hoechst Celanese, Chatham USA, 1991.

26 D Müller, Review of mathematical design methods for thermoplastic machine parts, BASF Atiengesellschaft Ludwigshafen Germany, July 1982.

27 A F Johnson G D Sims, Design procedures for plastic panels, National Physical Laboratory, ISBN 0 946754 06 3, 1987

28 F J Locket, Polymer data for engineering design: nature and status, Polymer Engineering Group and British Plastics Federation, May 1995.

29 J Bannantine, Fundamentals of metal fatigue analysis, Prentice-Hall, 1990.

30 D R Askeland, The science and engineering of materials, Chapman and Hall, 1990.

31 Mechanical properties - Methods 320A to 320F tensile strength, elongation and elastic modulus, Methods for testing plastics, BS 2782 part 3.

32 T Nicholas, Tensile testing of materials at high rates of strain, Experimental Mechanics, Volume 21 pp 177-185, May 1981

33 P Gaucher R François Séguéla, Scrutinizing the tensile necking of polyethylene by means of video-controlled extensometry, 9th International Conference on Deformation Yield and Fracture of Polymers, Churchill College Cambridge, paper 27, April 1994

34 C G'Sell A Dahoun M Aboulfaraj, Modelling of the large-strain behaviour of amorphous and semi-crystalline polymers, POLYMAT '94, Imperial College London, pp 224-227, September 1994.

35 Method 335A Determination of flexural properties of rigid plastics, Methods for testing plastics, BS 2782 part 3.

36 Plastics - Determination of tensile creep, International standard ISO 899-1981 (E)

37 Methods 354A and 354B Determination of tensile-impact strength, Methods for testing plastics, BS 2782 part 3.

38 N N Dioh, High strain rate behaviour of polymers at various temperatures, PhD thesis Imperial College of Science and Technology, 1993.

39 G R Johnson W H Cook, A constitutive model and data for metals subjected to large strains, high strain rates and high temperatures, Seventh International Symposium on Ballistics c/o KIvI, The Hague the Netherlands, April 1983.

40 Method 359 Determination of Charpy impact strength of rigid materials, Methods for testing plastics, BS 2782 - part 3.

41 Method 350 Determination of Izod impact strength of rigid materials, Methods for testing plastics, BS 2782 - part 3.

42 M Bramuzzo, Dynamic elastic modulus in bending: a new determination technique in impact and rebound conditions, Polymer Testing Volume 5 pp 439-454, 1985.

43 Method 353B Determination of multi-axial impact behaviour by the instrumented puncture test, Methods for testing plastics, BS 2782 part 3.

44 Anon. Misleading claim for falling weight test, British Plastics and Rubber, p 12, Sept 1994.

45 M A Wheel, High speed double torsion testing of pipe grade polyethylenes, PhD thesis Imperial College of Science and Technology, September 1991

46 N Shaikh, Ultrasonic characterisation of structural polymers, Characterisation of mechanical properties of materials, MD - vol. 33 pp 17-31, ASME 1992.

47 Plastics - determination of dynamic mechanical properties - Part 1 general principals, ISO/DIS 6721-1

48 Anon. Thermal analysis of polymers, seminar, Netsch mastermix Ltd., Forte Posthouse Hotel Birmingham, July 1994.

49 J D Lear P S Gill, Theory of operation of the Du Pont 982 Dynamic Mechanical Analyzer, Du Pont Wedgewood Way Stevenage.

50 I M Ward, Review: the yield behaviour of polymers, Journal of Material Science, Volume 6 pp 1397-1417, 1971.

51 G Trantina R Nimmer, Structural analysis of thermoplastic components, McGraw-Hill 1994

52 S I Krishnamachari, Applied stress analysis of plastics: a mechanical engineering approach, Van Nostrand Reinhold, 1994.

53 L E Nielson R F Landel, Mechanical properties of polymers and composites, Marcel Dekker, 1994

54 S S Sternstein L Ongching, Yield criteria for plastic deformation of glassy high polymers in general stress fields, Polymer Preprints, American Chemical Society, Division of Polymer Chemistry, Vol. 10 No. 2, 1969

55 A F Johnson G D Simms, The short time behaviour of thermoplastics, Plastics and Rubber Processing and Applications, Volume 1 pp 63-71, 1981.

56 A Ebenhau, private communication, BASF Aktiengesellschaft D-6700 Ludwigshafen Germany, 13:6:91

57 A Ebenhau, private communication with D I Wimpenny (University of Warwick) upon a visit to, BASF Aktiengesellschaft D-6700 Ludwigshafen, 24:9:91

58 H Kolsky, The measurement of the material damping of high polymers over ten decades of frequency and its interpretation, M^3D: Mechanics and mechanisms of material damping, ASTM publication code no. 04-011690-23, pp 4-27, Sept 1992.

59 Anon. Lupolen 4261A - brochure, BASF Aktiengesellschaft D-6700 Ludwigshafen Germany.

60 S D Batterman J L Bassani, Yielding, anisotropy and deformation processing of polymers, Mechanics of plastics and plastic composites, ASME AMD Vol 104 pp 13-27, Dec 1989.

61 E M Arruda M Boyce, Anisotropic effects on the finite strain deformation behaviour of glassy polymers, Plastics and plastic composites: material properties, part performance and process simulation, ASME AMD Vol 29 pp 1-12, 1991.

62 J Ameodo D Lee, Modelling the uniaxial rate and temperature dependent behaviour of amorphous and semicrystalline polymers, Plastics and plastic composites: material properties, part performance and process simulation, ASME AMD Vol 29 pp 13-31, 1991.

63 M C Boyce E L Montagut A S Argon, The effects of thermomechanical coupling on the cold drawing process of glassy polymers, Plastics and plastic composites: material properties, part performance and process simulation, ASME AMD Vol 29 pp 47-75, 1991.

64 P Krishnaswamy M E Tuttle A F Emery, Finite element modelling of the time dependent behaviour of nonlinear ductile polymers, Plastics and plastic composites: material properties, part performance and process simulation, ASME AMD Vol 29 pp 77-99, 1991.

65 W Bruijs, Pendulum impact simulation on TPS bumper beams, POLYMAT '94, Imperial College London, Addendum not bound in conference proceedings, September 1994.

66 M M Matsco, Nonlinear finite element analysis in plastics design, Mobay Co. Plastics and fibres division Pittsburgh USA, Ref 216 3M 4/91.

67 R P Nimmer O A Bailey T W Paro, Analysis techniques for the design of thermoplastic bumpers, SAE paper 870107, 1988.

68 D Hertema, Property characterisation of PC/ABS blends for use in energy management applications, SAE paper 910402, Feb 1991.

69 M E Vickers H Fisher, Real-time in-situ X-ray diffraction study of polyethylene deformation, Deformation yield and fracture of polymers, Churchill College, Cambridge, April 1994.

70 B Harper V Sura, Nonlinear thermoviscoelastic behaviour of thermide films, Time dependent failure of polymers: Experimental study, ASME AMD Vol 155 pp 5-14, 1992.

71 N N Dioh P S Levers J G Williams, Thickness effects in split Hopkinson pressure bar tests, Polymer, Vol. 34 No. 20 pp 4230-4234, 1993.

72 P E Reed, Developments in instrumented impact testing of plastics and composites, Progress in rubber and plastics technology, Volume 5, No. 2. pp 157-172, RAPRA technology Ltd..

73 L M Carapellucci R P Nimmer A F Yee, Some problems associated with puncture testing of plastics, Proc of Society of Plastics Engineers Annual Technical Conference, ANTEC pp 622-628, 1986.

74 B A Crouch, Numerical modelling of yield and fracture in plastics, Proc of Society of Plastics Engineers Annual Technical Conference, ANTEC pp 1571-1573, 1989.

75 G Sala M Angehileri, Analytical and experimental evaluation of finite element models for crash analysis, Structures under shock and impact II, Proceedings of the 2nd International Conference pp 155-173, Portsmouth, June 1992.

76 Y Germain J P Moulin, Constitutive equations for polymer part design, POLYMAT '94 pp 426-429, Imperial College of Science and Technology, September 1994.

77 D J Bammann M L Chiesa A McDonald W A Kawahara J J Dike V D Revelli, Prediction of ductile failure in metal structures, ASME AMD Volume 107 pp 7-12, November 1990.

78 K Grøstad A Syre T Bach, Influence of surface topography and morphology on impact resistance of PP-copolymer studied by falling weight impact testing, Deformation yield and fracture of polymers, paper 53, Churchill College Cambridge, April 1994.

79 C B Bucknall, The relevance of impact testing in the materials science of polymers, Plastics rubber and composites processing and applications, Volume 17 No 3 pp 141-145, 1992.

80 C L Rohn, Dynamic mechanical measurement yields a better HDPE fuel tank, Modern Plastics, Vol 66 pp 129-132, Oct 1989.

81 J P J Coulton, Analysis of rotor moulded PR3 fuel tank, Rover Advanced Technology Centre - University of Warwick, internal report, April 1992

82 J P J Coulton, Initial pressure analysis of the R8M16 and P2001 expansion tanks, Rover Advanced Technology Centre - University of Warwick, internal report, July 1992

83 J P J Coulton, Nonlinear pressure analysis of polypropylene expansion tanks", Rover Advanced Technology Centre - University of Warwick, internal report, Aug. 1992

84 J P J Coulton, Creep analysis of HDPE fuel tanks, Rover Advanced Technology Centre - University of Warwick, internal report, Oct. 1992

85 S Mizunaga N Saek H Watanabe, Development of blow-molded bumper beam, SAE paper no. 900834

86 F Jensen D Negrelli, Fluid filled vessels under acceleration, ANSYS Users Conference pp 8.61-8.71, ANSYS Inc 210 Johnson Road Houston PA 15342-1300 USA, 1987.

87 A O Bolukbasi, Analysis of crash-resistant fuel systems and airframe structure interaction in a crash environment, American Helicopter Society, 47th Annual Forum Proceedings, Phoenix USA, Vol 1 pp 587-597, May 1991.

88 386-MATLAB for 80386 based MS-DOS Personal Computers, The MathWorks Inc, USA.

89 D J Ewins, Modal testing; theory and practice, Research Studies Press, 1984.

90 BASF Plastics, Lupolene - product line properties and processing, BASF Atkiengesellschaft D-6700 Ludwigshafen Germany, September 1991.

91 ISO 6239,` Plastics- determination of tensile properties by use of small specimens

92 A Pearce, Tensile testing of a high molecular weight polyethylene over a range of strain rates and temperatures, NPL report DMM(D)221, September 1994

93 M W Money, Tensile testing of POCAN S1506 over a range of strain rates and temperatures, Report for the Rover Group, NPL reference NPK 2/233 DMA(D)662

94 C M Harris C E Crede, Shock and vibration hand book, McGraw-Hill, 1976

95 CAMPUS database, supplied by BASF Aktiengesellschaft Ludwigshafen Germany.

96 Anon., Instrumented impact tester operations manual, p/n 8-00-99-0010 ICI Australia Operations Pty. Ltd., Australia.

97 Wai-Nang Chung, Fracture toughness and creep fracture studies of polyethylenes, Ph.D. Thesis Imperial College of Science and Technology, January 1991.

98 J O Halquist, OASYS LS-DYNA3D Volume 4 Theoretical Manual, Ove Arup and Partners,13 Fitzroy Street London.

99 J P J Coulton, Measurement and use of polymeric material stiffness data for impact simulations, 1994 DYNA3D user group conference, Nottingham, Sept 1994

100 J P J Coulton, Measurement and use of material stiffness data to predict the performance of impact events, POLYMAT '94 - Polymer properties for CAD/CAM 2, pp 439-442, London, Sept. 1994

101 Anon, A finite element primer, NAFEMS, 1987.

102 J P J Coulton, The determination and use of polymeric material stiffness data for use in the impact analysis of HDPE fuel tanks, 3rd International LS-DYNA3D Conference, Kyoto Japan, session 2 paper 8, Nov 1995.

103 G Heufer, Plastic fuel tanks - a contribution to vehicle safety, European Plastic News, pp 68-71, May 1974

104 P S Nagarasheth, An integrated system approach for the injection moulded plastic part from design to fabrication, Proc of Society of Plastics Engineers, ANTEC pp 220-223, 1989.

105 L D Liehe, Plastic fuel tanks in the Federal Republic of Germany and Europe, SAE paper 880686, 1987.

106 O I Okoli G F Smith, Overcoming inertial problems in the high strain rate testing of a glass/epoxy composite, Proc of Society of Plastics Engineers Annual Technical Conference, ANTEC Vol 2 pp 2998-3002, May 1995.

Bibliography

B1 Anon. Guide to examinations for higher degrees by research, The University of Warwick, September 1995

B2 W Brostow R D Corneliussen, Failure of thermoplastics, Hanser, 1986

B3 W Browstow M Fleissner W F Müller, Slow crack propagation in polyethylene: analysis and prediction, ANTEC 1989.

B4 R J Crawford, Rotational moulding of plastics, John Wiley and Sons, 1992

B5 G N Gaeman J C Phelps K C Rusch, Plastics in automotive applications, SAE, 1989

B6 Y K Godovsky, Theromphysical properties of polymers, Springer-Verlag, 1992

B7 P Hen, Tensile testing, ASM Int, 1992

B8 R W Hertzberg J A Manson, Fatigue of engineering thermoplastics, Academic Press, 1980

B9 E Hinton, NAFEMS introduction to nonlinear finite element analysis, NAFEMS, 1992

B10 D Hitchings, A finite element dynamics primer, NAFEMS, 1992

B11 A I Isayev, Modelling of polymer processing - recent developments, Hanser, 1991

B12 K Kadota A Chudnovsky, Analysis of the fatigue process zone in polyethylene, Plastics and plastic composites: material properties, part performance, and process simulation, ASME MD Volume 29, December 1991.

B13 P Krishnaswamy M E Tuttle A F Emery J Ahmad, Finite element modelling of crack-tip behaviour in ductile polymers: stationary and growing cracks, Time dependent failure of polymers: Experimental study, AMD-Vol. 155, ASME 1992.

B14 B N Leis P Krishnaswamy S K Naboulsi, Effect of finite crack of notch-tip radius on time-dependent stress fields in ductile polymers, Time dependent failure of polymers: Experimental study, AMD-Vol. 155, ASME 1992.

B15 F J Lockett, Nonlinear viscoelastic solids, Academic Press, 1972

B16 F J Lockett, Engineering design basis for thermoplastic products, Her Majesty's Stationary Office, 1982

B17 E A Muccio, plastic part technology, ASM Int, 1991

B18 E A Muccio, plastic processing technology, ASM Int, 1994

B19 L E Nielsen, Mechanical Properties of polymers and composites, Marcel Dekker, 1974

B20 M C Pfeil C H Popelar V H Kenner, Determination of critical J for the polyethylene butt fusion joints, Time dependent failure of polymers: Experimental study, AMD-Vol. 155, ASME 1992.

B21 S F Popelar C H Popelar V H Kenner, Creep crack growth in joints of a thermoplastic, International Journal of Fracture, Volume 50 1991.

B22 SAE, Plastics in automobile bumper systems and exterior panels, SAE, 1990

B23 SAE, New developments in exterior body panels and bumper systems, SAE, 1991

B24 SAE, Automotive body panel and bumper system materials and design, SAE, 1992

B25 J J Strebel V Chellappa A A Moet K Sehanobish, Measurement of fracture toughness from fatigue studies, ANTEC 1991, Society of Plastics Engineers

B26 S Turner, Mechanical testing of plastics, George Goodwin, 1983

B27 I M Ward, Mechanical properties of solid polymers, Wiley-Interscience, 1971

B28 J G Williams, Stress analysis of polymers, Ellis Horwood Ltd, 1980

B29 J G Williams A Pavan, Impact and dynamic fracture of polymers and composites, Mechanical Engineering Publications ltd, 1993

B30 P Yala, Rapid crack propagation in polyethylene gas pipes, Ph.D. Thesis Imperial College of Science and Technology, January 1991.

Appendix A

Results of tensile test control

A series of tests were undertaken, on a linear polyethylene for rotational moulding, (NCPE 8627/NCPE 8628 supplied by NESTE Chemicals which is used for plastic fuel tanks), using the three control methods available for an Instron 4505 tensile tester at the University of Warwick's International Manufacturing Centre (IMC). The aim was to compare the effect of tensile test control methods on the material properties that the test methods propose to measure as illustrated by those defined in [31] i.e. the engineering measures of 0.2% secant modulus (E) and Poisson's ratio (υ) and the stress (σ_n) and strain (ε_n) at maximum load. The results from the three sets of tests, as listed in Table 6.4 are shown in the following Tables A1 to A3. Figures A1 to A5 show the comparisons of the typical strain rate versus tensile strain plots measured for the three methods.

E (MPa)	υ (-)	$\dot{\varepsilon}$ (s^{-1})	σ_n (MPa)	ε_n (-)	$\dot{\varepsilon}$ (s^{-1})
$\dot{\delta}$ = 200 mm/min					
6.33e+02	4.35e-01	8.71e-02	1.49e+01	1.45e-01	3.87e-02
6.86e+02	4.70e-01	7.64e-02	1.59e+01	1.42e-01	3.38e-02
6.01e+02	4.39e-01	5.84e-02	1.52e+01	1.57e-01	3.57e-02
6.50e+02	5.02e-01	5.14e-02	1.52e+01	1.32e-01	3.55e-02
7.10e+02	4.98e-01	7.59e-02	1.61e+01	1.56e-01	3.41e-02
$\dot{\delta}$ = 65 mm/min					
6.08e+02	4.68e-01	8.96e-03	1.45e+01	1.36e-01	1.15e-02
6.25e+02	4.90e-01	8.94e-03	1.47e+01	1.53e-01	1.08e-02
5.58e+02	4.64e-01	9.10e-03	1.44e+01	1.53e-01	1.23e-02
5.92e+02	4.53e-01	9.39e-03	1.50e+01	1.49e-01	1.16e-02
5.35e+02	4.29e-01	1.01e-02	1.46e+01	1.51e-01	1.24e-02
$\dot{\delta}$ = 20 mm/min					
4.67e+02	4.49e-01	2.69e-03	1.33e+01	1.66e-01	3.75e-03
5.83e+02	5.25e-01	2.26e-03	1.39e+01	1.54e-01	3.80e-03
5.10e+02	4.82e-01	2.47e-03	1.36e+01	1.61e-01	3.43e-03
5.40e+02	4.75e-01	2.25e-03	1.37e+01	1.67e-01	3.48e-03
6.03e+02	5.10e-01	2.24e-03	1.41e+01	1.53e-01	3.53e-03
$\dot{\delta}$ = 6.5 mm/min					
4.66e+02	4.43e-01	9.14e-04	1.24e+01	1.91e-01	1.16e-03
6.25e+02	6.18e-01	7.12e-04	1.26e+01	1.37e-01	1.20e-03
5.03e+02	5.23e-01	8.18e-04	1.24e+01	1.52e-01	1.16e-03
4.08e+02	3.94e-01	9.84e-04	1.22e+01	1.61e-01	1.20e-03
4.15e+02	4.35e-01	9.53e-04	1.22e+01	1.82e-01	1.26e-03
$\dot{\delta}$ = 2 mm/min					
4.18e+02	4.53e-01	2.67e-04	1.21e+01	1.86e-01	3.40e-04
4.42e+02	5.30e-01	2.56e-04	1.18e+01	2.24e-01	3.97e-04
3.82e+02	4.24e-01	2.74e-04	1.13e+01	2.71e-01	3.72e-04
4.75e+02	5.19e-01	2.44e-04	1.18e+01	2.30e-01	3.79e-04
3.72e+02	4.43e-01	2.82e-04	1.18e+01	2.58e-01	3.74e-04

Table A1 Crosshead method test results

E (MPa)	υ (-)	$\dot{\varepsilon}$ (s^{-1})	σ_n (MPa)	ε_n (-)	$\dot{\varepsilon}$ (s^{-1})
$\dot{\varepsilon}$ = 24 %/min					
4.83e+02	4.33e-01	2.59e-03	1.46e+01	1.30e-01	4.03e-03
5.85e+02	4.95e-01	2.23e-03	1.42e+01	1.39e-01	4.09e-03
5.72e+02	4.83e-01	2.72e-03	1.45e+01	1.43e-01	4.13e-03
5.73e+02	5.22e-01	2.31e-03	1.43e+01	1.37e-01	4.12e-03
5.59e+02	5.07e-01	2.66e-03	1.39e+01	1.31e-01	4.16e-03
$\dot{\varepsilon}$ = 7.8 %/min					
5.09e+02	4.91e-01	9.18e-04	1.28e+01	1.47e-01	1.42e-03
4.70e+02	4.70e-01	9.14e-04	1.26e+01	1.52e-01	1.45e-03
5.20e+02	4.85e-01	9.19e-04	1.33e+01	1.51e-01	1.44e-03
5.49e+02	5.23e-01	9.16e-04	1.33e+01	1.37e-01	1.44e-03
5.02e+02	4.69e-01	9.42e-04	1.28e+01	1.27e-01	1.46e-03
$\dot{\varepsilon}$ = 2.4 %/min					
4.67e+02	4.14e-01	3.01e-04	1.24e+01	1.52e-01	3.99e-04
4.99e+02	5.00e-01	2.91e-04	1.20e+01	2.96e-01	4.00e-04
4.87e+02	5.19e-01	2.99e-04	1.17e+01	2.74e-01	4.00e-04
4.75e+02	5.04e-01	3.04e-04	1.17e+01	2.91e-01	4.00e-04
5.02e+02	5.50e-01	2.94e-04	1.18e+01	2.95e-01	4.00e-04

Table A2 Pacing method test results

E (MPa)	υ (-)	$\dot{\varepsilon}$ (s^{-1})	σ_n (MPa)	ε_n (-)	$\dot{\varepsilon}$ (s^{-1})
$\dot{\varepsilon}$ = 240 %/min					
6.63e+02	4.45e-01	9.34e-02	1.63e+01	1.28e-01	4.11e-02
6.98e+02	4.86e-01	1.76e-02	1.73e+01	1.34e-01	3.92e-02
6.55e+02	4.64e-01	2.28e-02	1.67e+01	1.30e-01	3.95e-02
6.67e+02	5.03e-01	1.45e-02	1.65e+01	1.26e-01	3.88e-02
7.52e+02	5.21e-01	1.52e-02	1.64e+01	1.18e-01	3.89e-02
$\dot{\varepsilon}$ = 78 %/min					
6.83e+02	5.11e-01	9.31e-03	1.51e+01	1.35e-01	1.31e-02
5.85e+02	5.76e-01	6.42e-03	1.47e+01	1.34e-01	1.29e-02
6.88e+02	5.01e-01	7.07e-03	1.54e+01	1.28e-01	1.30e-02
7.45e+02	5.67e-01	6.37e-03	1.50e+01	1.33e-01	1.30e-02
6.19e+02	4.75e-01	6.31e-03	1.50e+01	1.39e-01	1.30e-02
$\dot{\varepsilon}$ = 24 %/min					
5.57e+02	4.95e-01	2.92e-03	1.33e+01	1.46e-01	4.00e-03
5.98e+02	5.03e-01	2.34e-03	1.36e+01	1.33e-01	3.98e-03
6.35e+02	6.15e-01	2.27e-03	1.40e+01	1.38e-01	4.00e-03
6.66e+02	6.94e-01	2.30e-03	1.33e+01	1.37e-01	4.00e-03
6.19e+02	5.63e-01	2.24e-03	1.37e+01	1.35e-01	4.00e-03
$\dot{\varepsilon}$ = 7.8 %/min					
5.66e+02	4.78e-01	1.40e-03	1.24e+01	1.47e-01	1.30e-03
5.00e+02	4.51e-01	1.30e-03	1.16e+01	1.41e-01	1.30e-03
4.97e+02	4.91e-01	1.21e-03	1.17e+01	1.29e-01	1.30e-03
5.10e+02	4.97e-01	1.34e-03	1.24e+01	1.43e-01	1.30e-03
4.59e+02	4.28e-01	1.26e-03	1.24e+01	1.33e-01	1.30e-03
$\dot{\varepsilon}$ = 2.4 %/min					
3.81e+02	4.36e-01	3.07e-04	1.12e+01	1.90e-01	3.98e-04
4.50e+02	4.98e-01	2.85e-04	1.10e+01	2.14e-01	3.98e-04
4.32e+02	5.01e-01	2.93e-04	1.07e+01	2.81e-01	3.99e-04
5.33e+02	5.75e-01	2.92e-04	1.14e+01	1.65e-01	3.98e-04
4.57e+02	4.94e-01	3.06e-04	1.12e+01	1.90e-01	3.98e-04

Table A3 Closed loop method test results

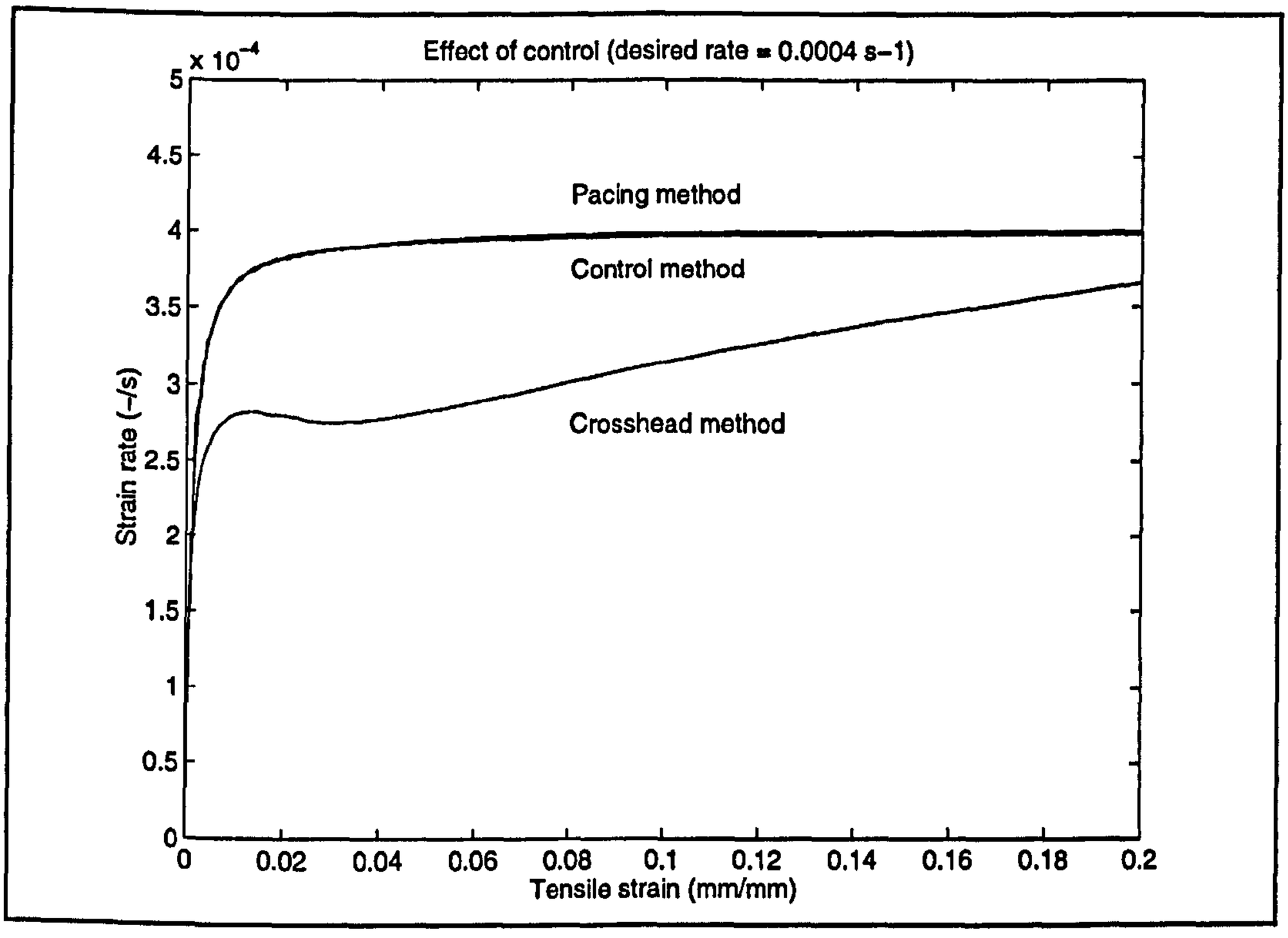

Figure A1 Effect of desired deformation rate 0.0004 s^{-1}

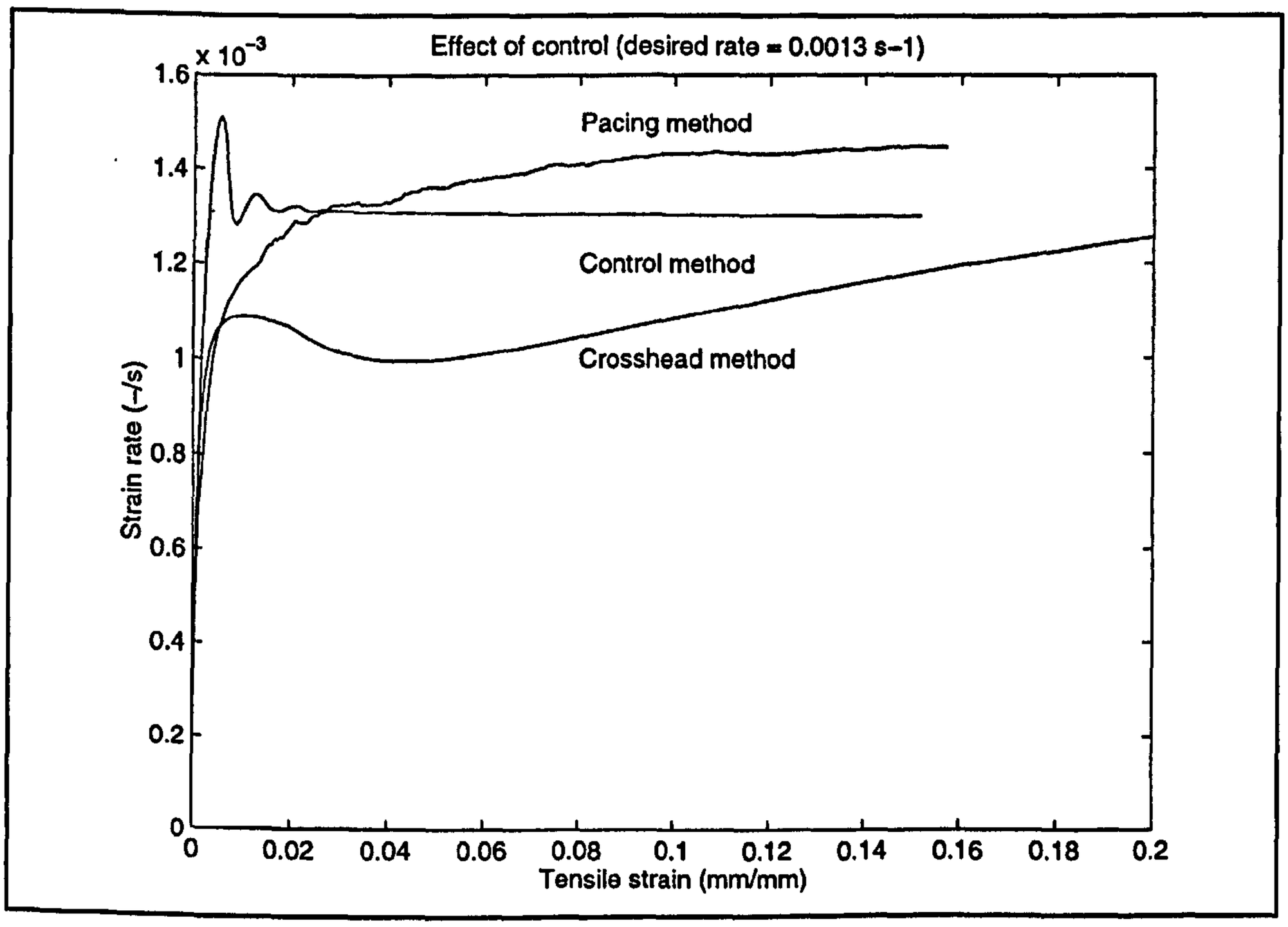

Figure A2 Effect of desired deformation rate 0.0013 s^{-1}

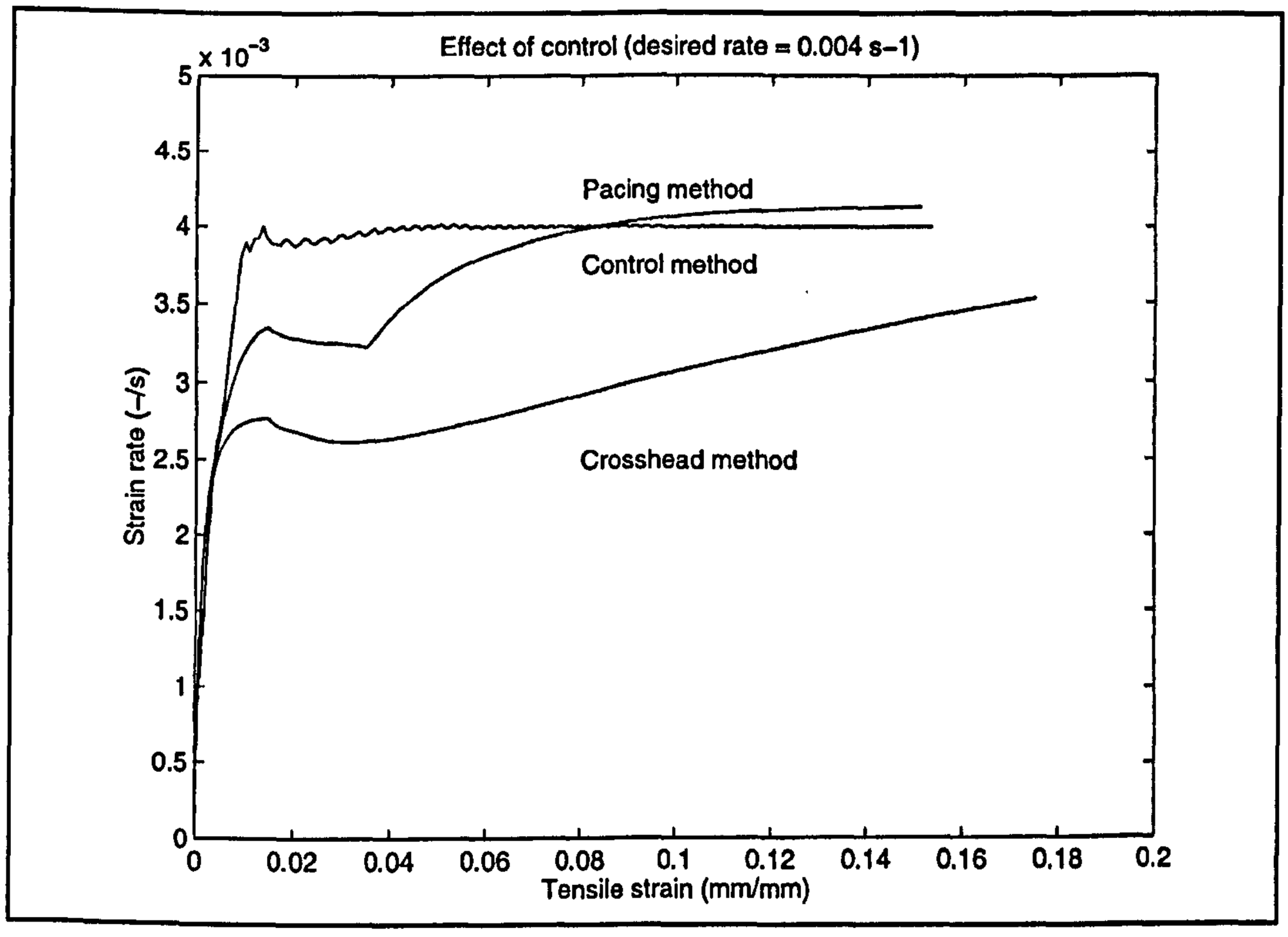

Figure A3 Effect of desired deformation rate 0.004 s^{-1}

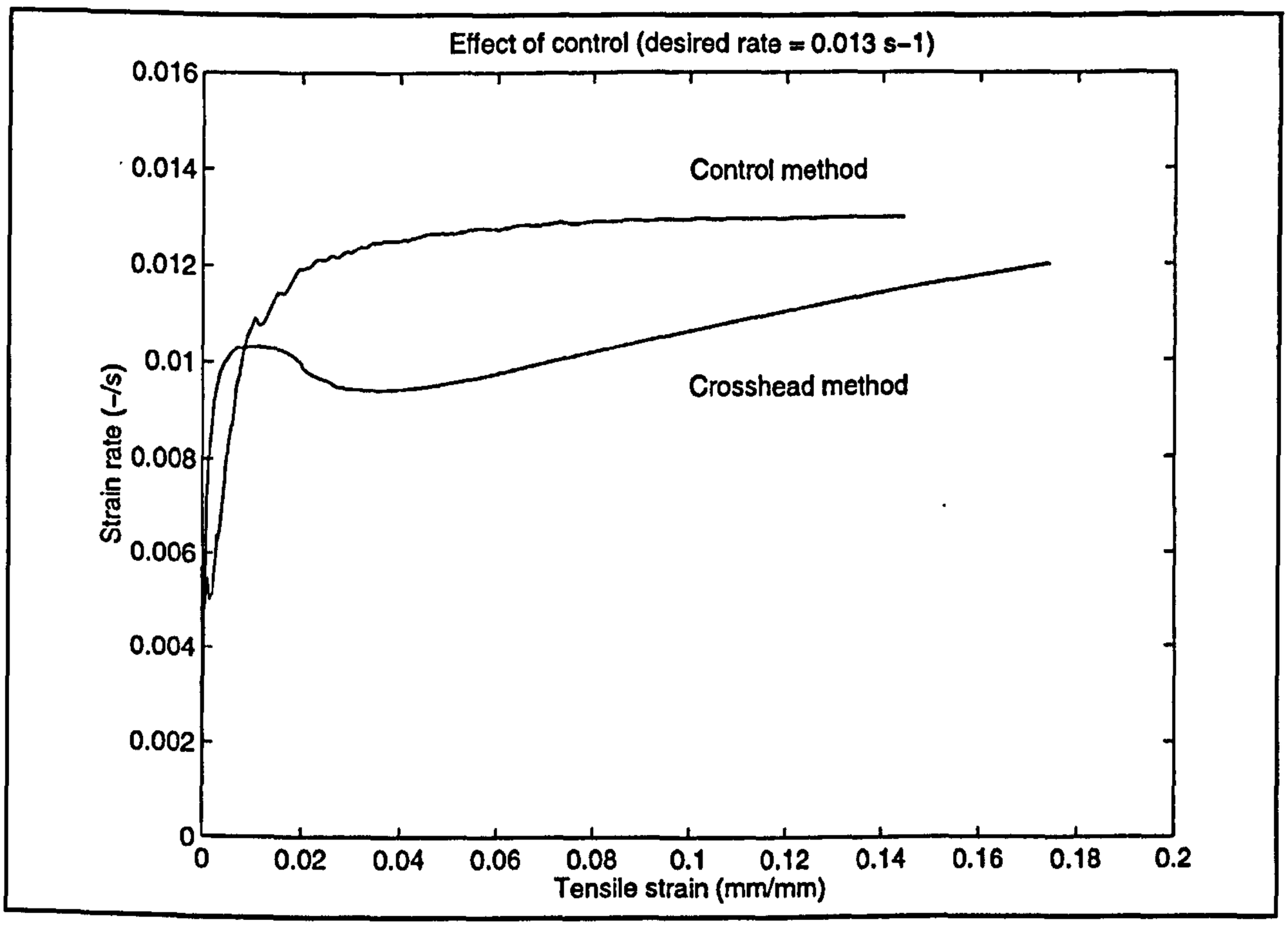

Figure A4 Effect of desired deformation rate 0.013 s^{-1}

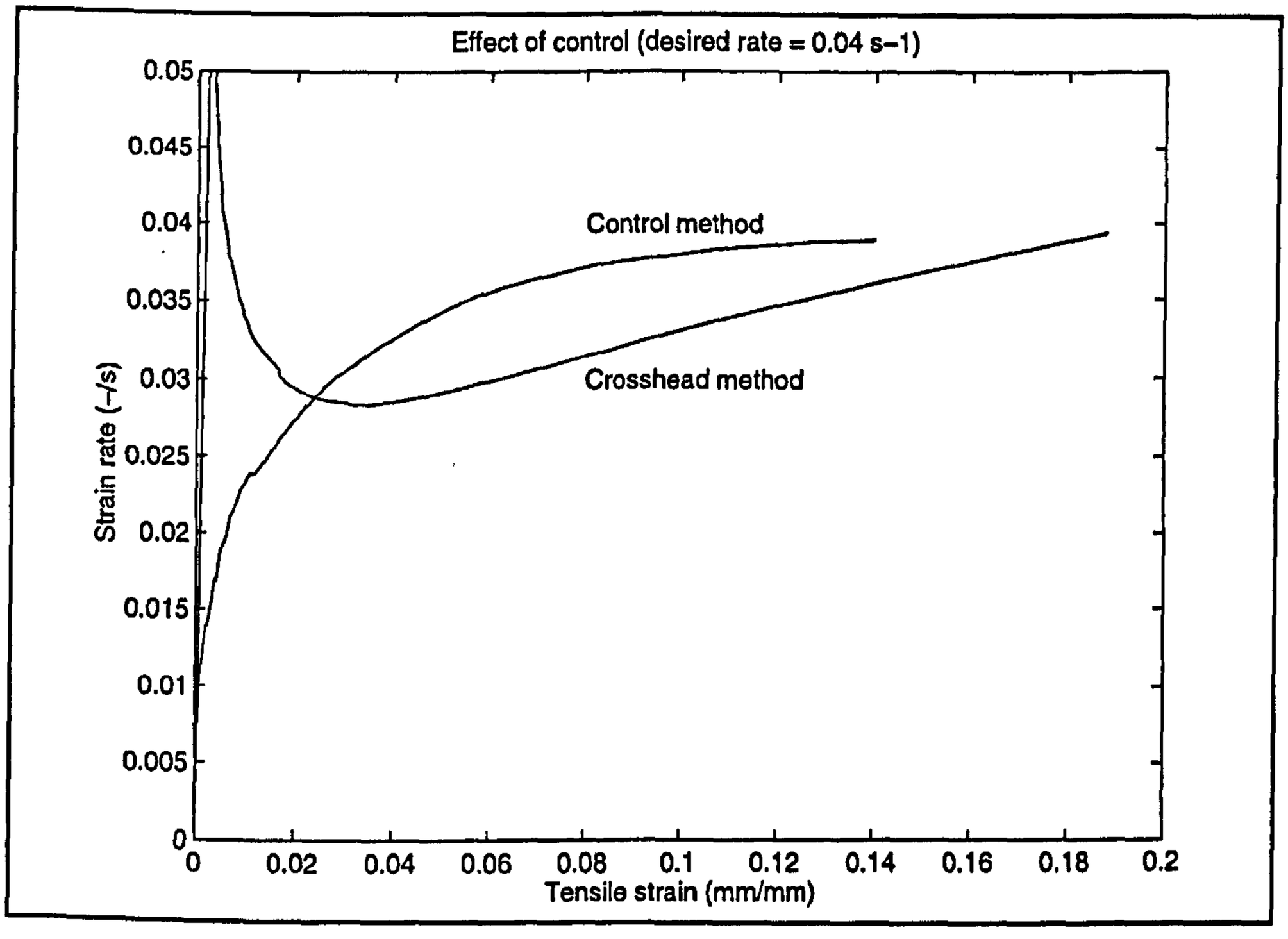

Figure A5 Effect of desired deformation rate 0.04 s^{-1}

Appendix B

Results of tensile tests

A series of slow strain rate and high strain rate tests were undertaken, on a HDPE for blow moulding, (Lupolene 4261A supplied by BASF which is used for plastic fuel tanks), using the crosshead control method. A total of thirty eight samples were tested. The injection moulded samples were labels 1-15 for the "along" flow direction and 51-65 for the "cross" flow direction. Eight samples were cut from a prototype fuel tank and were labelled Rover tank samples 1-8.

B.1 Results of SSR tensile tests at 23° C

The slow strain rate tests were carried out on a Lloyds M30K tensile tester at the University of Warwick's Advanced Technology Centre. The results of the tensile tests are listed in Tables B1 to B6. Tables B1 to B3 list the engineering material properties, as defined by BS 2782 part 3 Methods 320A to 320F [31]. Tables B4 to B6 list the results of the bi-linear curve fits. The bi-linear results are presented graphically in Figures B1 to B5.

Sample No.	C/H velo (mm/min)	$\dot{\varepsilon}$ (s^{-1})	E (Mpa)	$\dot{\varepsilon}$ (s^{-1})	σ_n (MPa)	ε_n (-)
1	50	0.01124	1084.9	0.02968	21.8818	0.1373
2	50	0.00989	1237.4	0.02418	22.6655	0.1227
3	50	0.0089	1132.6	0.021	22.6639	0.1208
4	50	0.01116	1085	0.02461	22.7488	0.1283
5	5	0.00123	855.19	0.00246	18.9261	0.1408
6	5	0.00117	810.405	0.00272	18.8097	0.1609
7	5	0.0013	721.191	0.0029	18.8296	0.1811
8	5	0.00134	725.651	0.00262	18.8176	0.1716

Table B1 Rover tank samples standard data

Sample No.	C/H velo (mm/min)	$\dot{\varepsilon}$ (s^{-1})	E (Mpa)	$\dot{\varepsilon}$ (s^{-1})	σ_n (MPa)	ε_n (-)
1	100	0.03215	957.25	0.05191	24.0994	0.1708
2	100	0.02708	927.541	0.0574	23.9906	0.1776
3	100	0.03046	857.124	0.05611	23.89	0.1622
4	50	0.01383	968.082	0.02721	22.6166	0.1945
5	50	0.01407	987.235	0.02766	22.9701	0.1987
6	50	0.01336	996.346	0.02742	22.885	0.1947
7	10	0.00299	845.414	0.00522	20.2795	0.2082
8	10	0.00277	892.218	0.00557	20.4606	0.209
9	10	0.00271	792.614	0.00474	20.3068	0.2151
10	5	0.0015	811.016	0.00259	19.4845	0.2102
11	5	0.00139	821.891	0.00272	19.656	0.2314
12	5	0.00144	769.03	0.0024	19.3669	0.2116
13	1	2.84e-04	664.286	4.53e-04	17.161	0.2474
14	1	3.03e-04	683.849	4.97e-04	17.6052	0.2419
15	1	3.02e-04	727.713	4.38e-04	17.608	0.2585

Table B2 "Along" flow samples standard data

Sample No.	C/H velo (mm/min)	$\dot{\varepsilon}$ (s^{-1})	E (Mpa)	$\dot{\varepsilon}$ (s^{-1})	σ_n (MPa)	ε_n (-)
51	100	0.02702	889.041	0.04815	25.2906	0.1121
52	100	0.02588	875.274	0.04158	25.1697	0.1054
53	100	0.02985	1149.1	0.04609	24.79	0.1102
54	50	0.01273	1270.1	0.01884	23.9109	0.1078
55	50	0.01157	1291.2	0.02155	23.7482	0.1129
56	50	0.01254	1288.2	0.01829	24.0401	0.1032
57	10	0.0025	1168	0.00437	21.2201	0.1219
58	10	0.00231	1280.8	0.00436	21.6355	0.1191
59	10	0.00237	1145.3	0.00409	20.8264	0.1276
60	5	0.00105	1234	0.00219	20.3845	0.1212
61	5	0.00112	1232.9	0.00218	20.7514	0.122
62	5	0.00127	1033.3	0.00205	19.9655	0.1307
63	1	2.20e-04	976.739	0.00044	18.2059	0.1294
64	1	2.06e-04	927.595	4.10e-04	17.9042	0.1228
65	1	2.23e-04	837.705	4.43e-04	17.364	0.1321

Table B3 "Cross" flow samples standard data

Sample No.	C/H velo (mm/min)	$\dot{\varepsilon}$ (s^{-1})	m_1 (MPa)	σ_y (MPa)	$\dot{\varepsilon}$ (s^{-1})	m_2 (MPa)
1	100	0.03036	649.303	21.2971	0.04124	63.8685
2	100	0.0286	642.633	21.0783	0.04383	63.4325
3	100	0.03099	636.951	20.6372	0.04442	70.1186
4	50	0.01478	579.773	20.0601	0.01996	55.1769
5	50	0.01492	580.624	20.6702	0.02023	53.5026
6	50	0.01446	585.26	20.367	0.02031	55.7717
7	10	0.00302	462.018	18.0187	0.00391	48.637
8	10	0.00301	482.273	18.2299	0.00406	48.6316
9	10	0.00292	448.429	18.0268	0.00368	48.6171
10	5	0.00158	440.18	17.211	0.00197	47.3757
11	5	0.00154	431.202	17.6362	0.002	44.5794
12	5	0.0015	437.199	17.1819	0.00188	46.597
13	1	0.00029	331.321	15.307	0.00036	39.3704
14	1	0.00032	360.917	16.0608	0.00038	41.0253
15	1	0.00032	342.88	15.8754	0.00036	38.4677

Table B4 "Along" flow samples bi-linear fit data

Sample No.	C/H velo (mm/min)	$\dot{\varepsilon}$ (s^{-1})	m_1 (MPa)	σ_y (MPa)	$\dot{\varepsilon}$ (s^{-1})	m_2 (MPa)
51	100	0.02861	762.79	20.9767	0.04033	107.542
52	100	0.02785	770.146	20.7939	0.03669	113.73
53	100	0.02953	810.797	20.4321	0.04047	106.334
54	50	0.01287	816.839	19.9309	0.0165	98.4582
55	50	0.01243	844.041	19.835	0.01763	93.1339
56	50	0.01265	885.255	19.9182	0.01645	102.94
57	10	0.00261	705.744	17.7142	0.00356	78.3185
58	10	0.00244	743.271	17.9872	0.0035	81.9847
59	10	0.00252	651.337	17.4558	0.00339	75.7245
60	5	0.00119	712.292	16.7389	0.00172	78.347
61	5	0.00123	706.547	17.1691	0.00171	78.1412
62	5	0.0013	599.859	16.796	0.00169	70.6093
63	1	0.00035	547.036	14.9888	0.00035	68.6789
64	1	0.00023	582.136	14.5534	0.00033	70.7188
65	1	0.00025	499.066	14.423	0.00035	64.3274

Table B5 "Cross" flow samples bi-linear fit data

Sample No.	C/H velo (mm/min)	$\dot{\varepsilon}$ (s^{-1})	m_1 (MPa)	σ_y (MPa)	$\dot{\varepsilon}$ (s^{-1})	m_2 (MPa)
1	50	0.01313	679.453	18.2093	0.02084	77.0148
2	50	0.01215	778.561	18.6855	0.01883	85.947
3	50	0.01111	748.634	18.641	0.0171	89.1104
4	50	0.01305	703.415	19.0625	0.01879	82.9243
5	5	0.00137	528.85	15.9184	0.00185	64.7655
6	5	0.00136	496.844	16.0977	0.00193	57.1216
7	5	0.00147	447.318	16.6402	0.00198	50.3606
8	5	0.00132	446.805	15.6829	0.00186	53.7368

Table B6 Rover tank samples bi-linear fit data

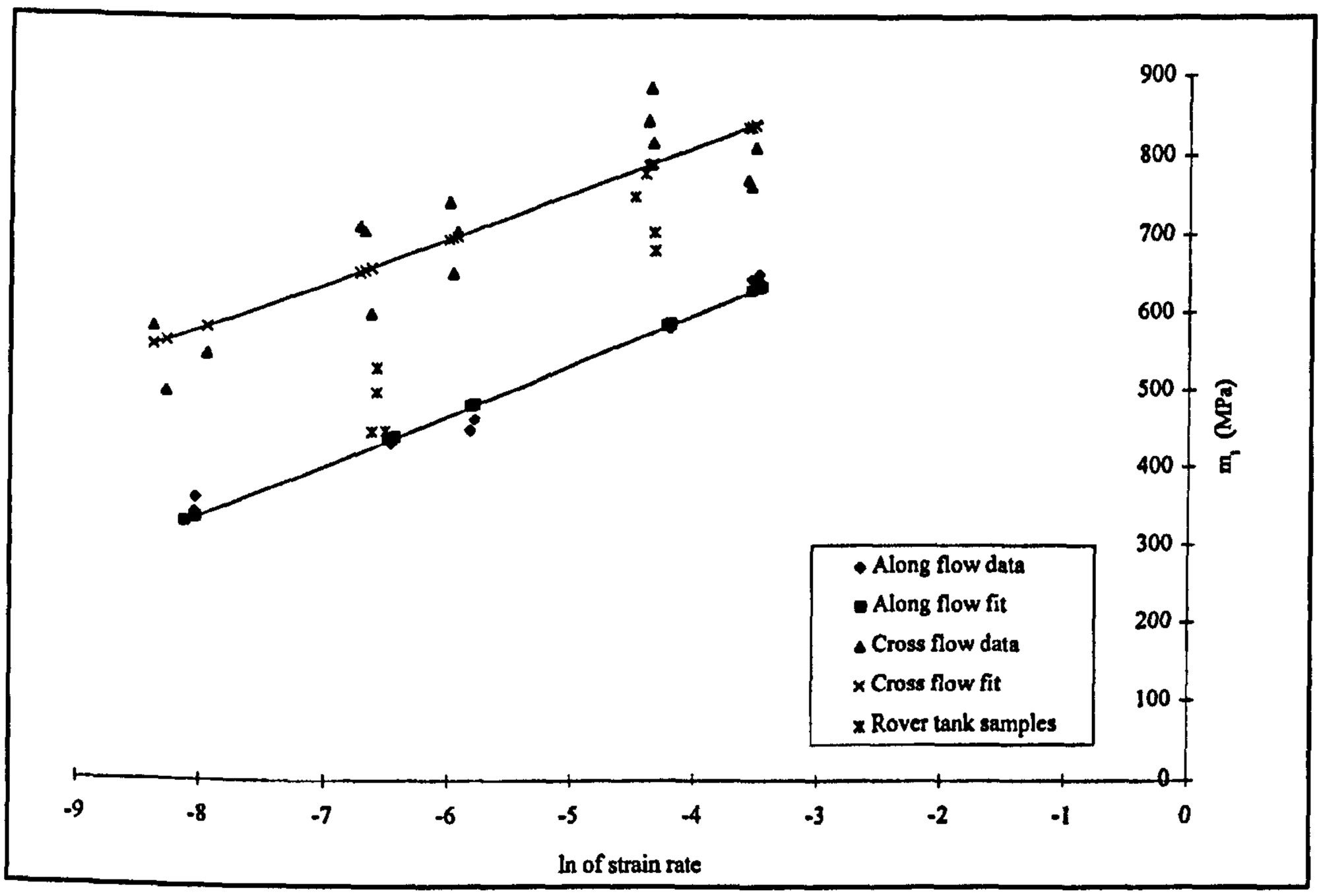

Figure B1 Comparison of m_1 trends - slow tests

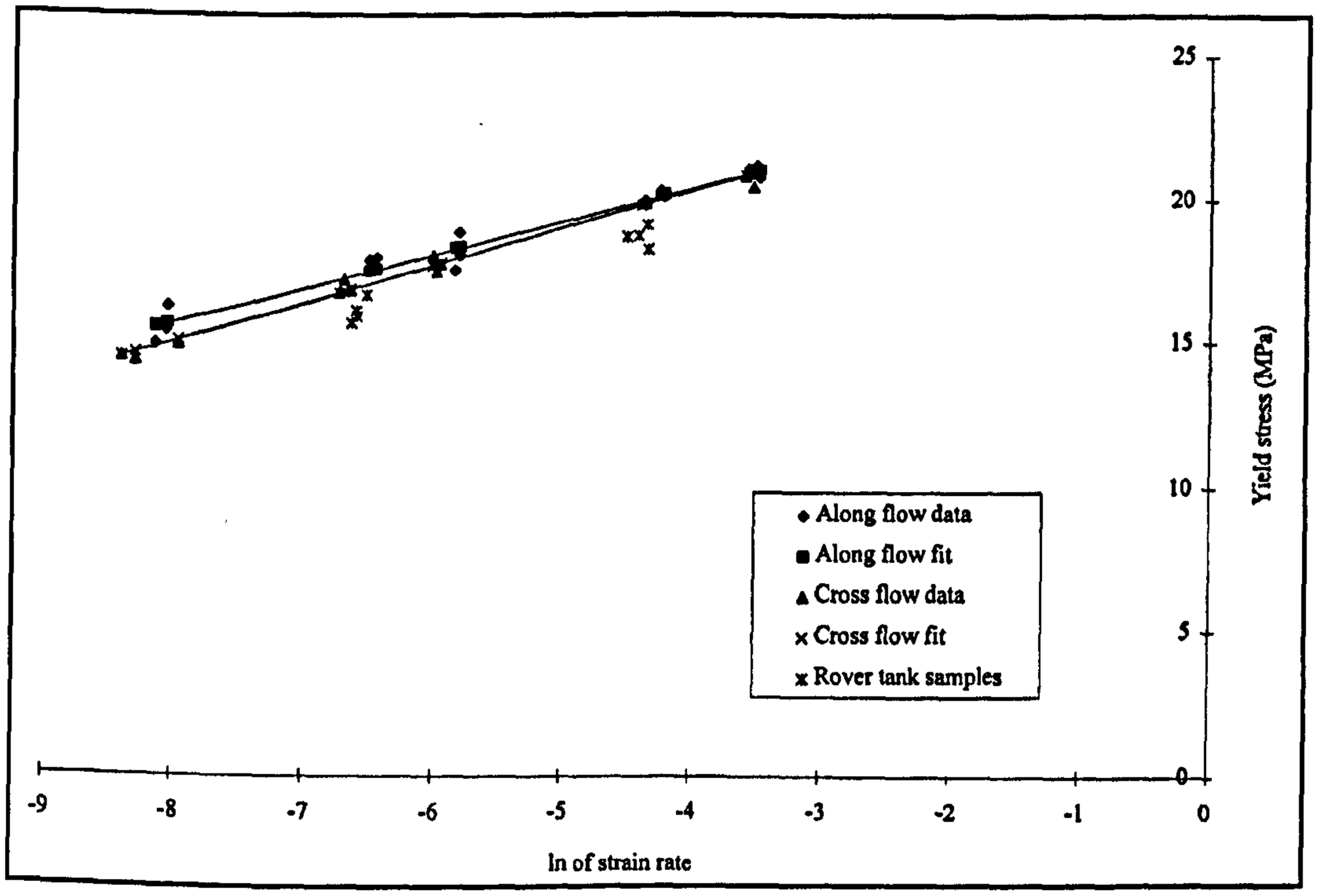

Figure B2 Comparison of σ_y trends - slow tests

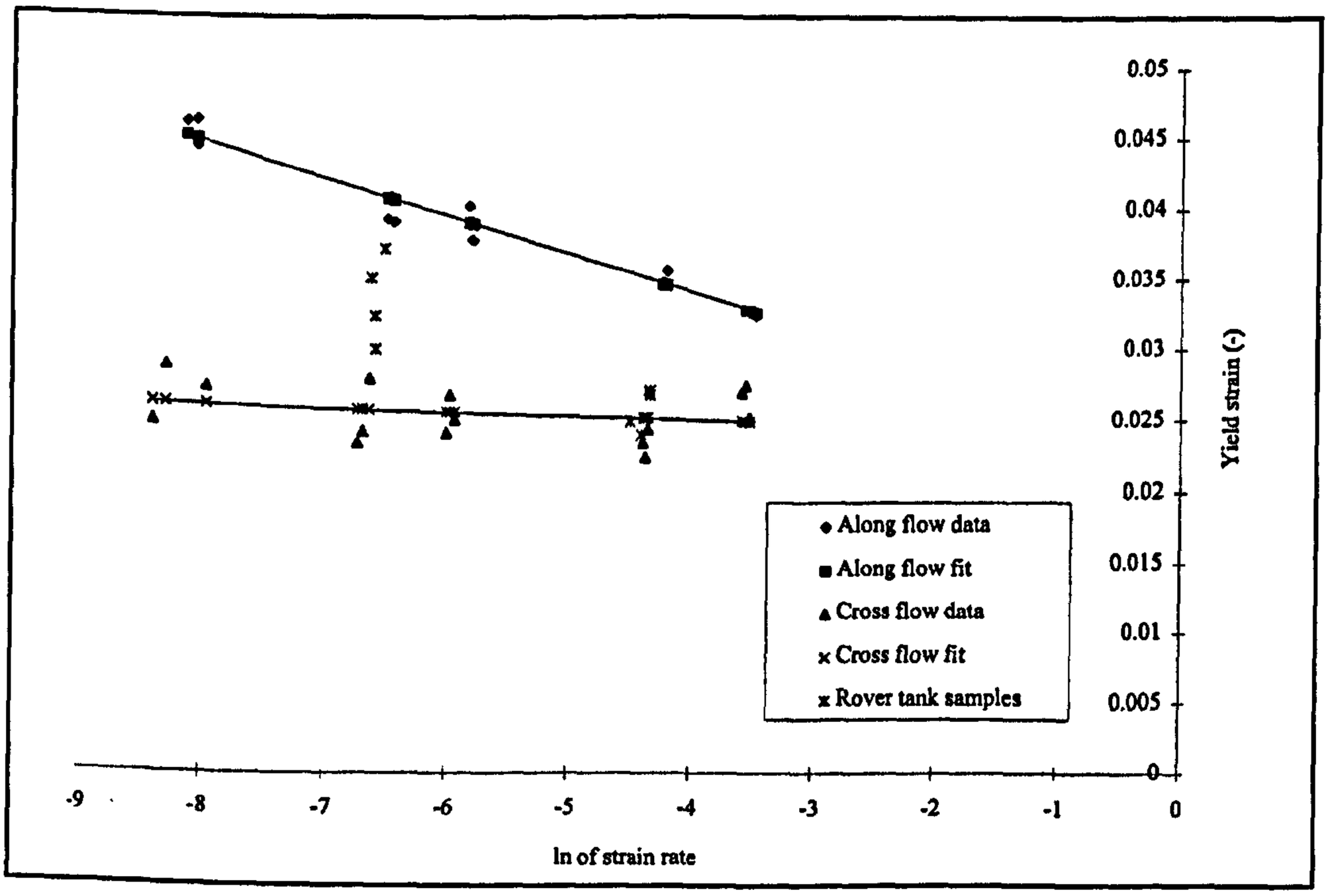

Figure B3 Comparison of ε_y trends - slow tests

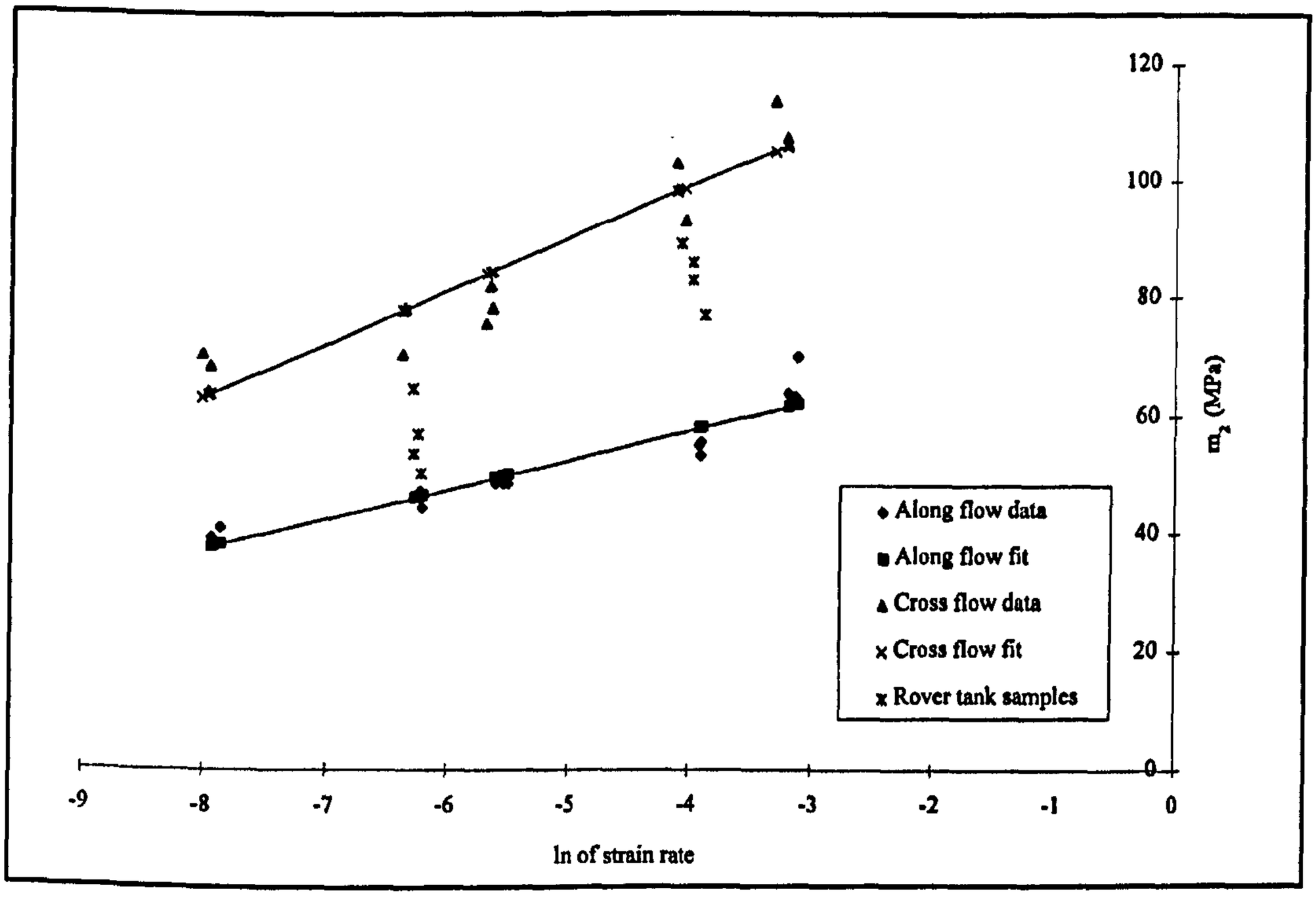

Figure B4 Comparison of m_2 trends - slow tests

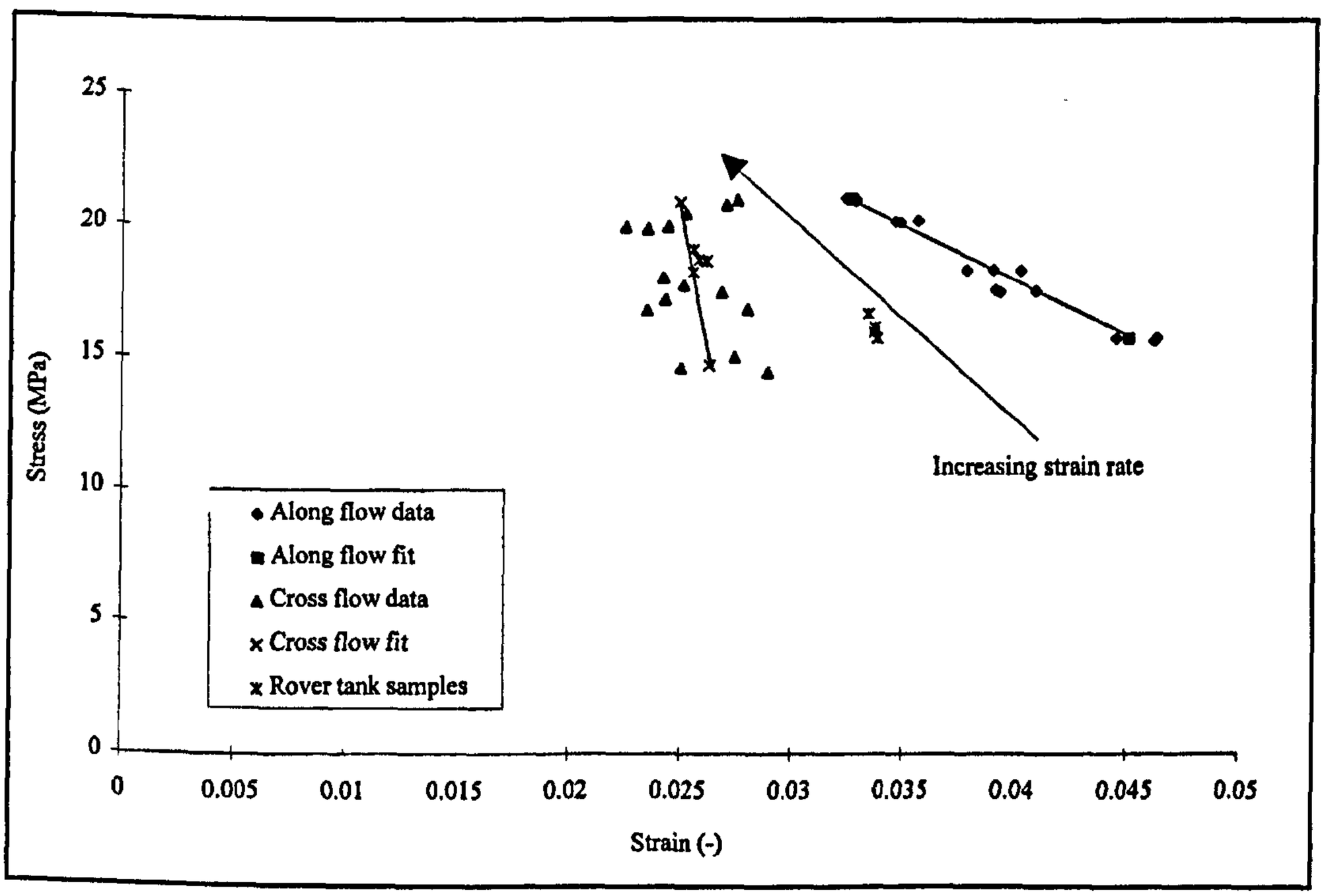

Figure B5 Comparison of yield point trends - slow tests

B.2 Results of HSR tensile tests at 23° C

The high strain rate tests were carried out for the author by the National Physical Laboratory (NPL) at Teddington [92] using an Instron 1343 high speed servo hydraulic tensile testing machine. A total of ninety samples were tested. The injection moulded samples were labelled 1-45 for the "along" flow direction and 51-95 for the "cross" flow direction. Samples 1-15 and 51-65 were tested at 23° C. Typical displacement-time and force-time traces for the high strain rate tests are shown in Figures B6 to B11 and typical bi-linear curve fits are shown in Figures B12 to B14. The results of the tensile tests are listed in Table B7 to Table B10. Table B7 and Table B8 list the neck point true stress and strain. Table B9 and Table B10 list the bi-linear curve fit parameters of the "along" and "cross" flow tests respectively. The bi-linear results are presented graphically in Figures B15 to B22.

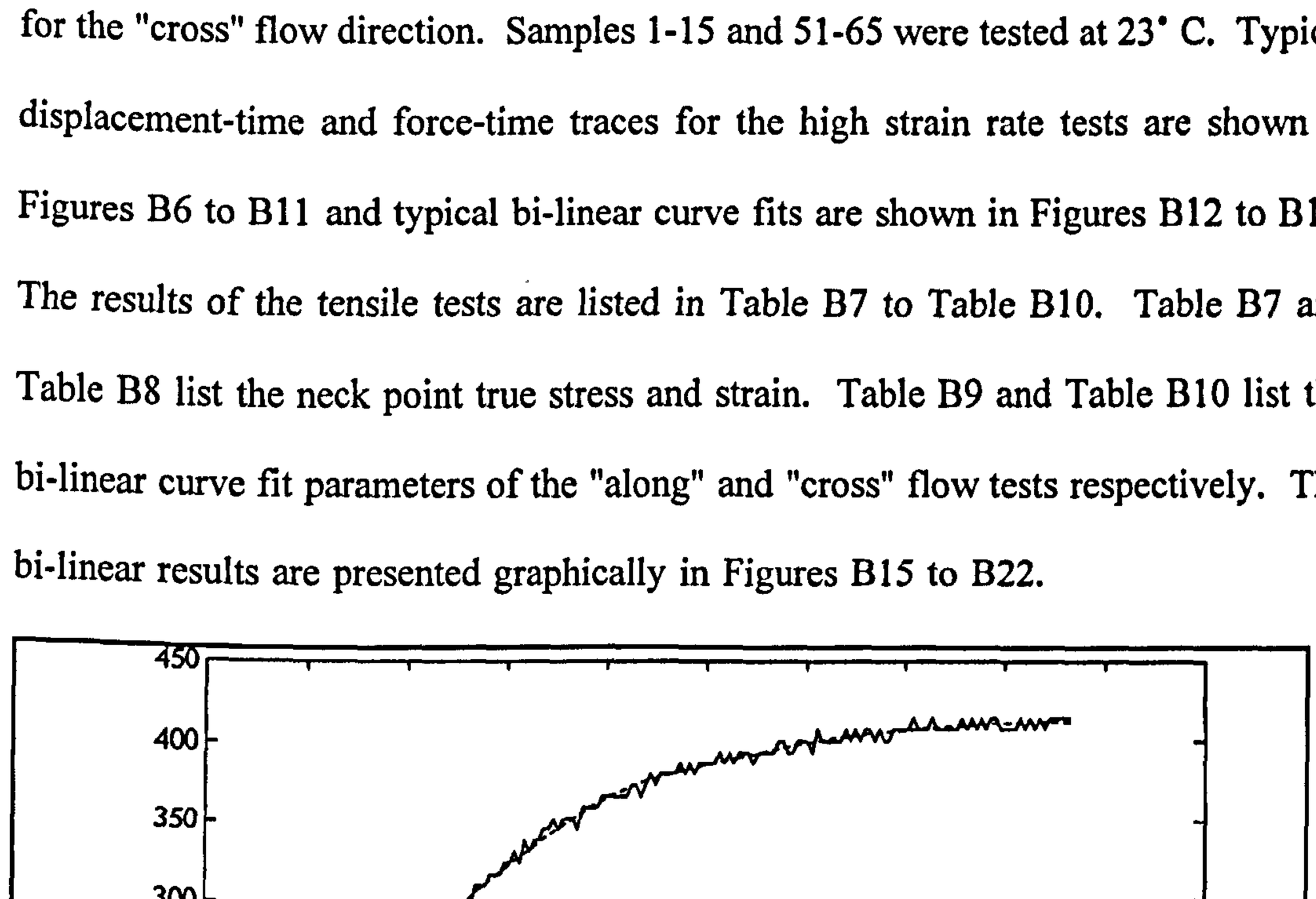

Figure B6 Typical force-time trace at 0.01 m/s

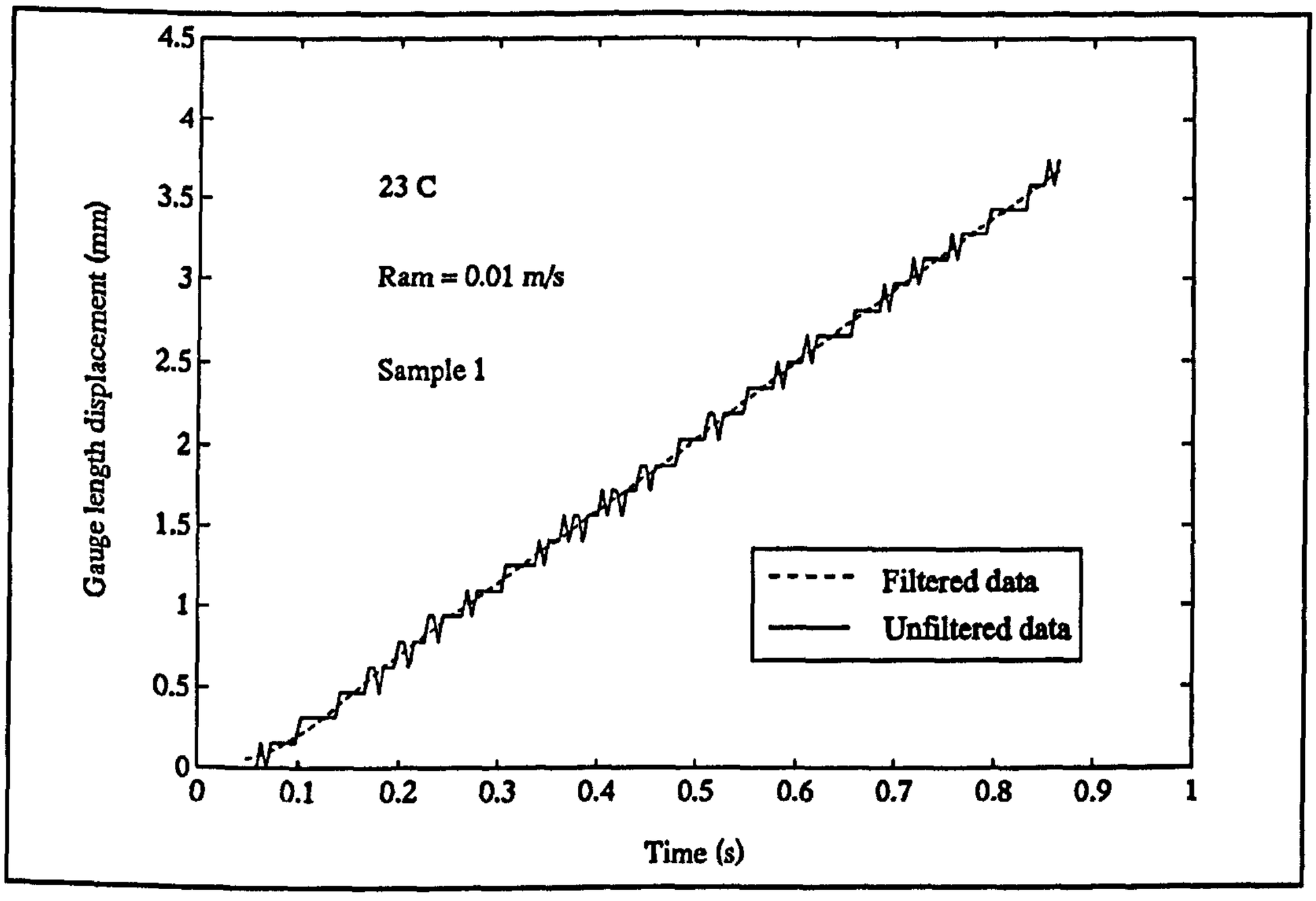

Figure B7 Typical displacement-time trace at 0.01 m/s

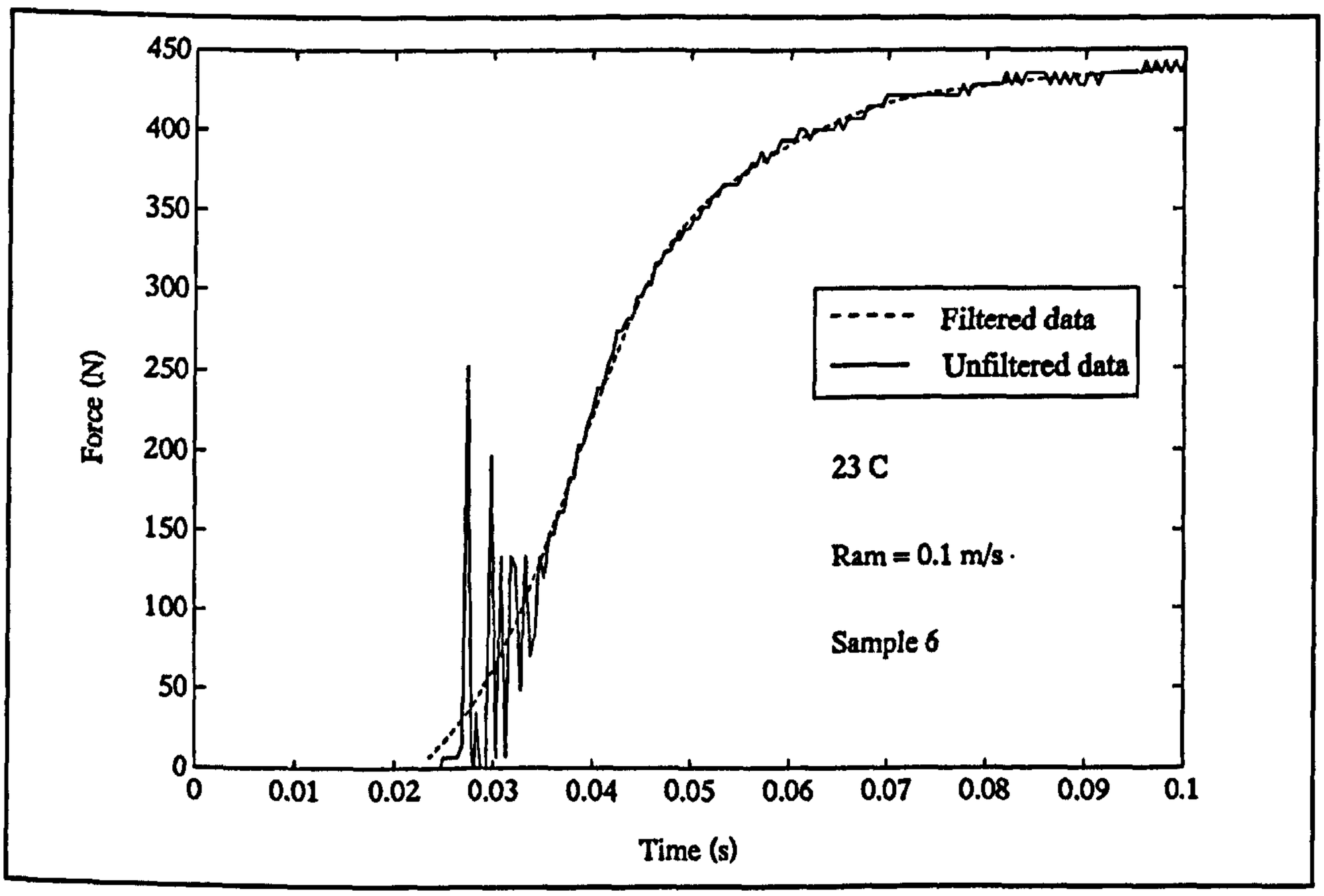

Figure B8 Typical force-time trace at 0.1 m/s

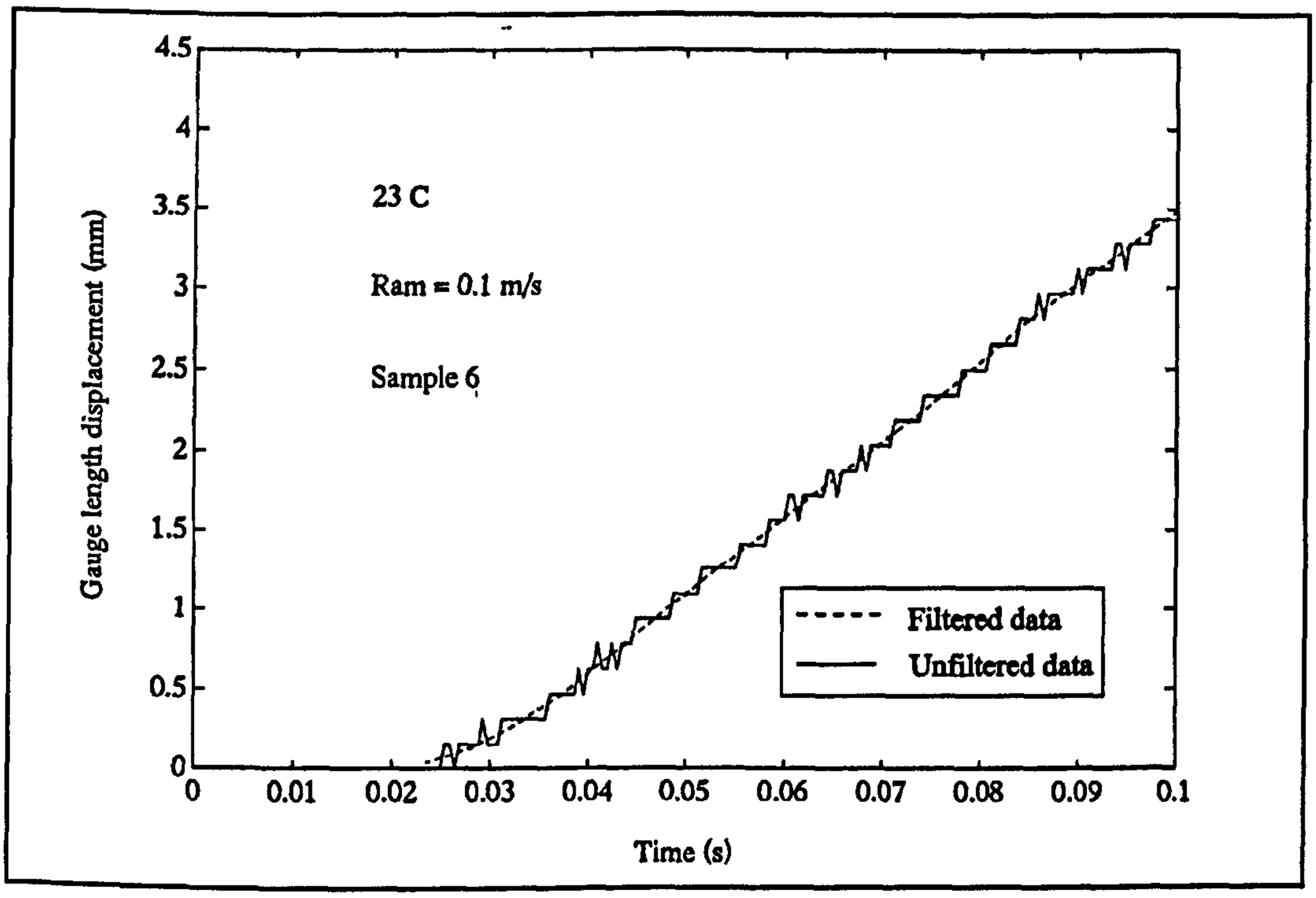

Figure B9 Typical displacement-time trace at 0.1 m/s

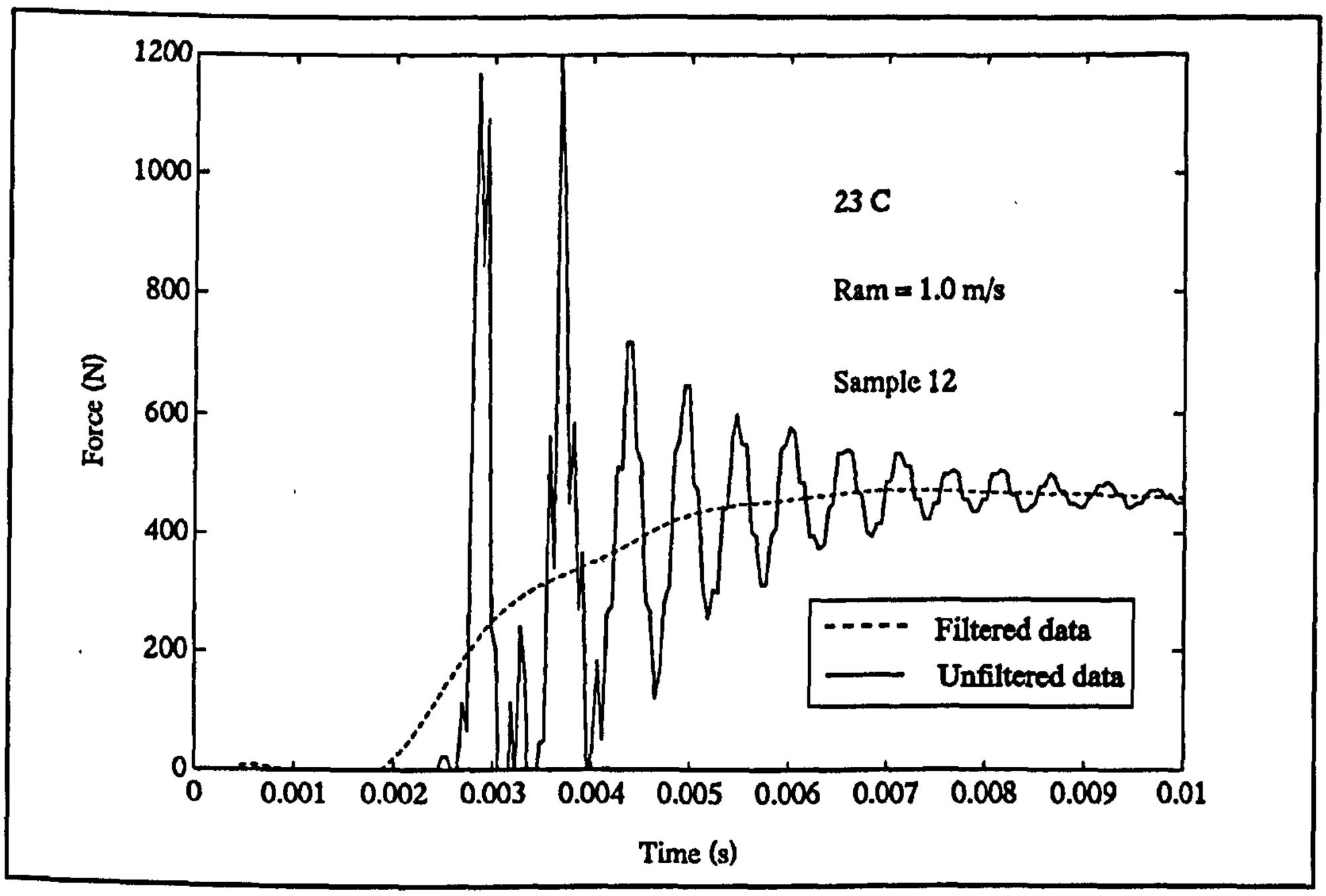

Figure B10 Typical force-time trace at 1.0 m/s

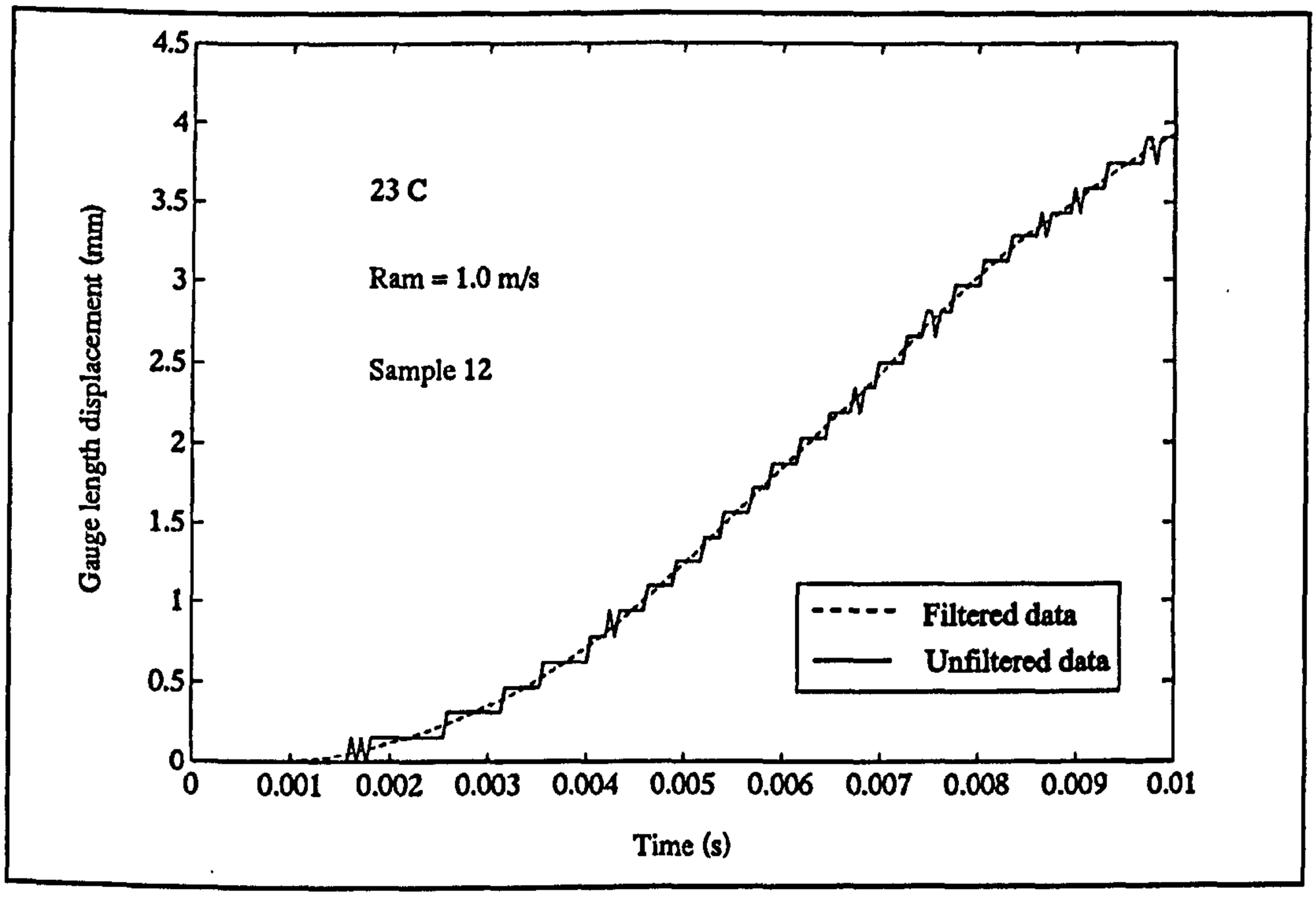

Figure B11 Typical displacement-time trace at 1.0 m/s

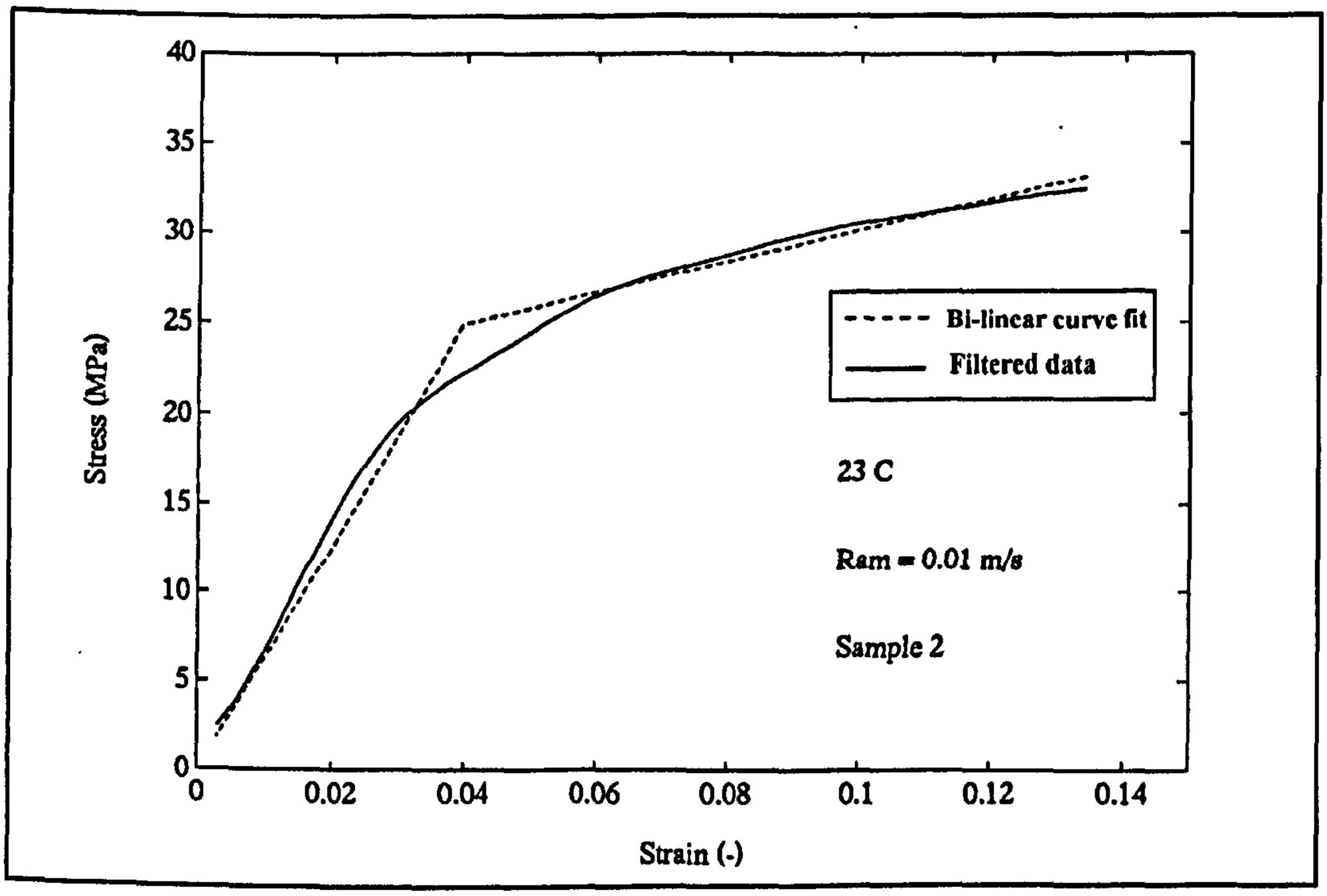

Figure B12 Typical bi-linear curve fit at 0.01 m/s

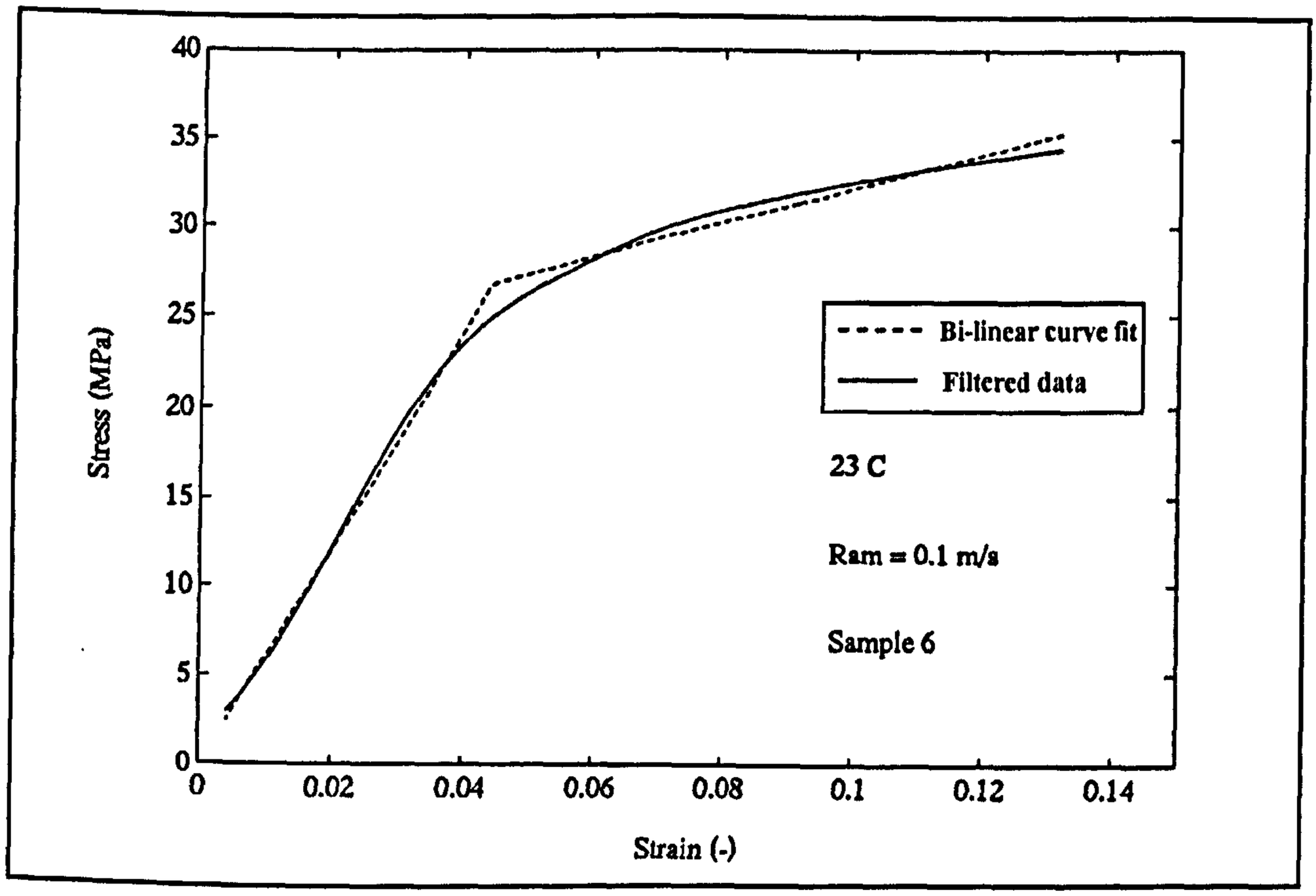

Figure B13 Typical bi-linear curve fit at 0.1 m/s

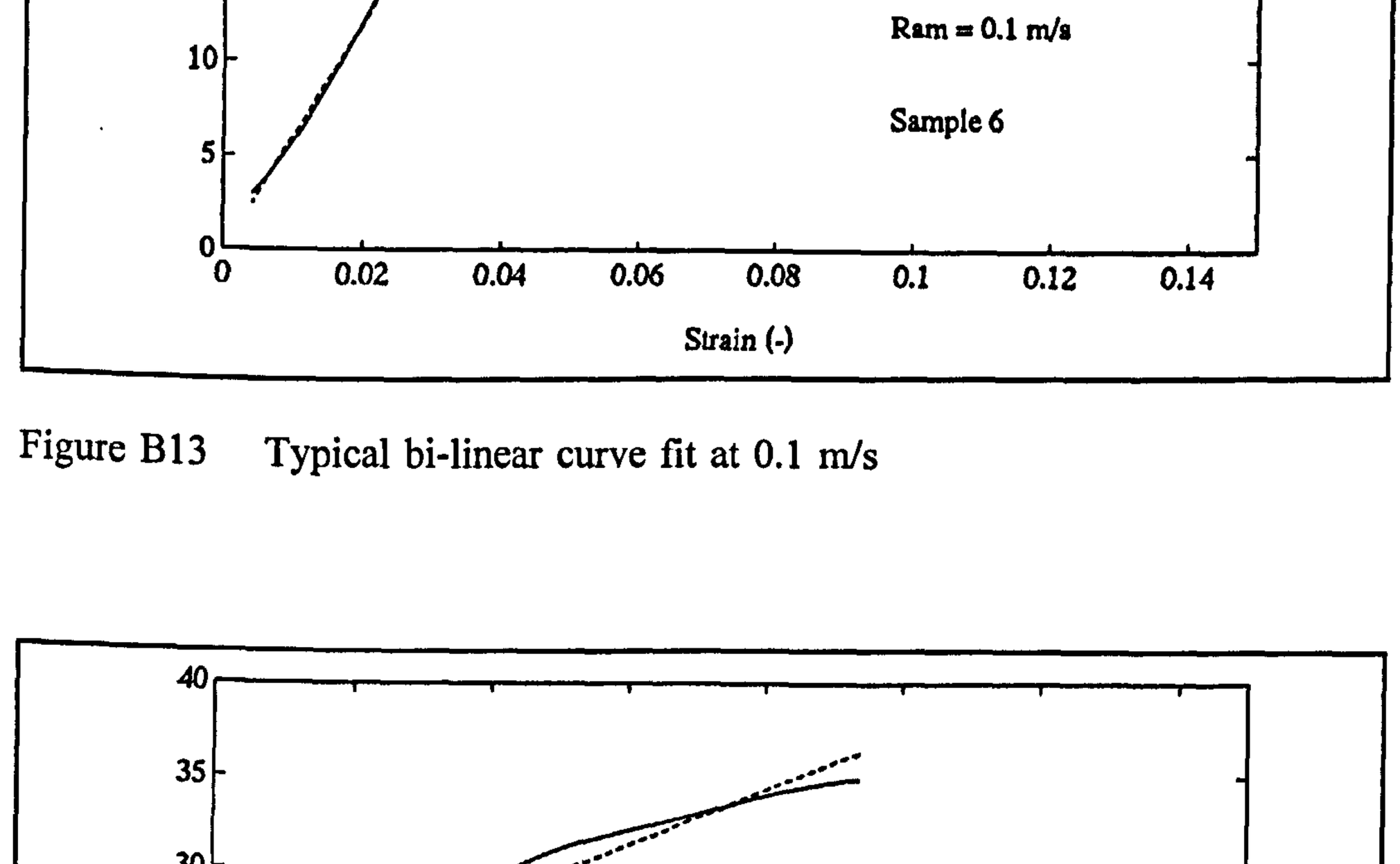

Figure B14 Typical bi-linear curve fit at 1.0 m/s

Sample No.	C/H Velo (m/s)	$\dot{\varepsilon}$ (s^{-1})	σ_n (MPa)	ε_n (-)
1	0.01	0.1607	32.2062	0.1348
2	0.01	0.159	32.4272	0.134
3	0.01	0.1563	33.3548	0.1496
4	0.01	0.1567	32.5143	0.1479
5	0.01	0.1554	33.0925	0.1544
6	0.1	1.6433	34.449	0.1317
7	0.1	1.6573	34.3913	0.1371
8	0.1	1.5734	35.2126	0.1437
9	0.1	1.5083	36.9233	0.1613
10	0.1	1.5432	34.6446	0.1425
11	1			
12	1	21.8248	34.8775	0.0936
13	1	21.5993	36.1319	0.0996
14	1	21.8363	34.5846	0.0989
15	1	22.5998	34.793	0.0937

Table B7 "Along" flow samples standard data - HSR

Sample No.	C/H Velo (m/s)	$\dot{\varepsilon}$ (s^{-1})	σ_n (MPa)	ε_n (-)
51	0.01	0.1862	30.1998	0.0872
52	0.01	0.1776	30.0743	0.0894
53	0.01	0.1724	30.8748	0.0911
54	0.01	0.1812	30.0019	0.0895
55	0.01	0.1707	29.5005	0.0705
56	0.1	1.6985	32.8465	0.0777
57	0.1	1.7363	33.1699	0.0799
58	0.1	1.6486	31.5639	0.0758
59	0.1	1.6968	33.3589	0.0754
60	0.1	1.7926	32.6663	0.0795
61	1	23.3905	33.0137	0.0555
62	1	22.7398	33.0252	0.0715
63	1	24.8725	33.4829	0.0733
64	1	24.4182	34.1065	0.0557
65	1	23.7146	34.5723	0.0709

Table B8 "Cross" flow samples standard data - HSR

Sample No.	C/H velo. (m/s)	$\dot{\varepsilon}$ (s^{-1})	m_1 (MPa)	σ_y (MPa)	$\dot{\varepsilon}$ (s^{-1})	m_2 (MPa)
1	0.01	0.1397	623.234	24.6801	0.164	86.7011
2	0.01	0.1372	628.702	24.8337	0.1654	87.3478
3	0.01	0.1406	605.59	25.7981	0.1624	77.2984
4	0.01	0.1357	602.002	25.1637	0.1646	75.4157
5	0.01	0.1367	578.548	25.514	0.1626	75.1582
6	0.1	0.8709	605.057	26.7435	1.7732	97.7849
7	0.1	0.8634	649.124	27.6527	1.7605	79.7495
8	0.1	0.9616	531.833	27.4426	1.7292	92.7559
9	0.1	0.8843	602.163	28.8436	1.7073	77.702
10	0.1	0.8693	641.264	26.9331	1.7592	84.3955
11	1					
12	1	4.3692	1643.31	24.4853	20.6617	149.656
13	1	3.7301	2010.73	24.5309	21.0682	149.836
14	1	3.4591	1968.35	23.0297	20.7846	156.062
15	1	4.9096	1372.75	24.7094	20.9491	153.788

Table B9 "Along" flow samples bi-linear fit data - HSR

Sample No.	C/H velo. (m/s)	$\dot{\varepsilon}$ (s^{-1})	m_1 (MPa)	σ_y (MPa)	$\dot{\varepsilon}$ (s^{-1})	m_2 (MPa)
51	0.01	0.1268	702.266	23.4557	0.1693	147.134
52	0.01	0.1179	747.953	23.7101	0.1713	130.681
53	0.01	0.1206	765.201	24.3334	0.1711	131.796
54	0.01	0.1391	676.548	23.4085	0.1704	141.687
55	0.01	0.1496	693.74	22.2691	0.1671	215.519
56	0.1	0.6775	812.647	25.0295	1.8498	193.44
57	0.1	0.7138	824.251	25.5518	1.8538	184.011
58	0.1	0.7152	794.09	23.8227	1.8007	200.342
59	0.1	0.7066	853.166	25.9362	1.8077	198.148
60	0.1	0.7985	704.643	25.5785	1.809	195.695
61	1	3.3217	2100.84	23.1092	18.5772	251.178
62	1	3.9987	1764.35	23.4658	19.2487	213.394
63	1	4.2307	1652.69	24.2945	20.0035	197.343
64	1	3.7849	1814.67	22.8649	18.7741	307.781
65	1	4.1001	1782.38	24.2404	19.553	221.587

Table B10 "Cross" flow samples bi-linear fit data - HSR

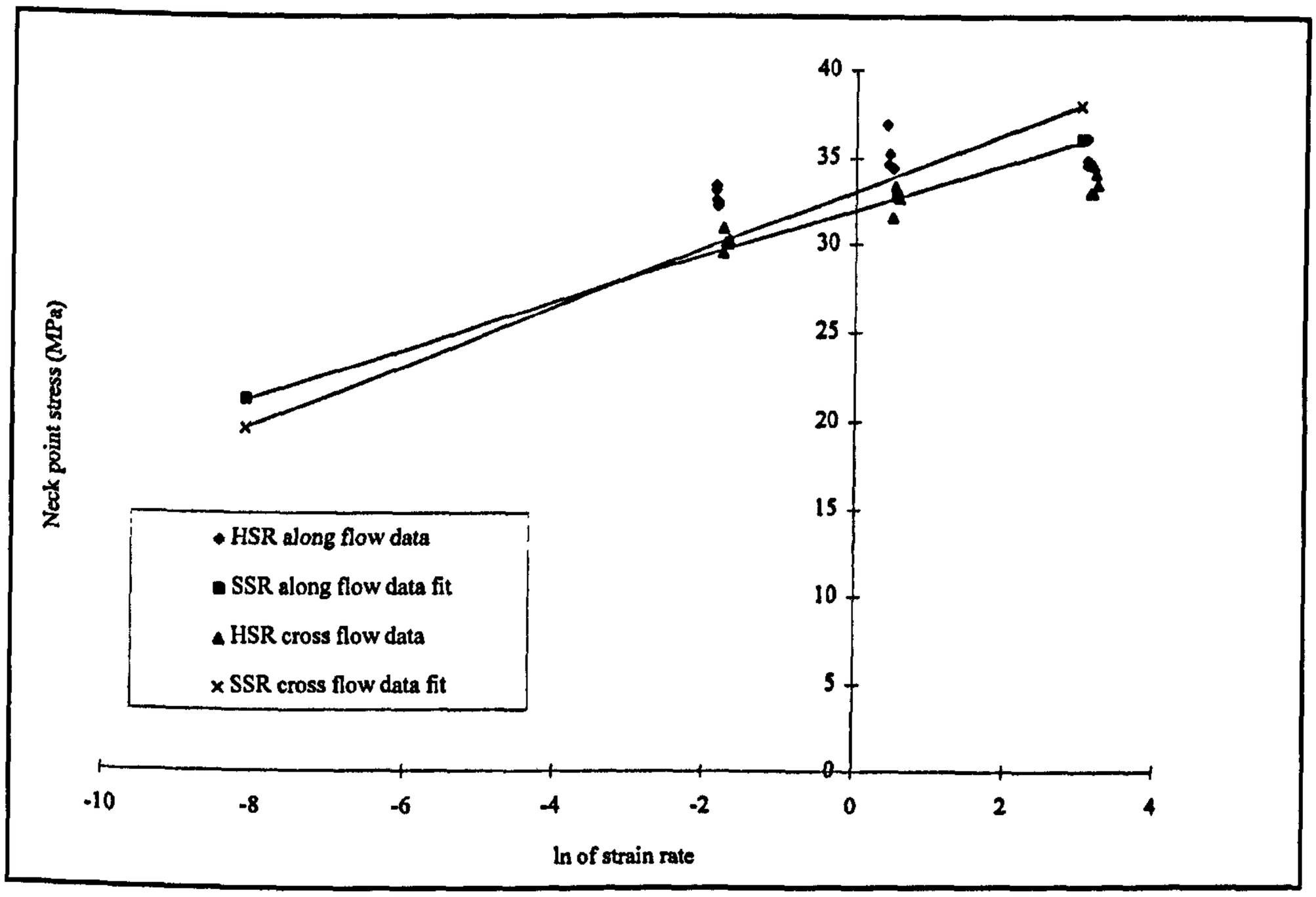

Figure B15 Comparison of σ_n trends - HSR tests

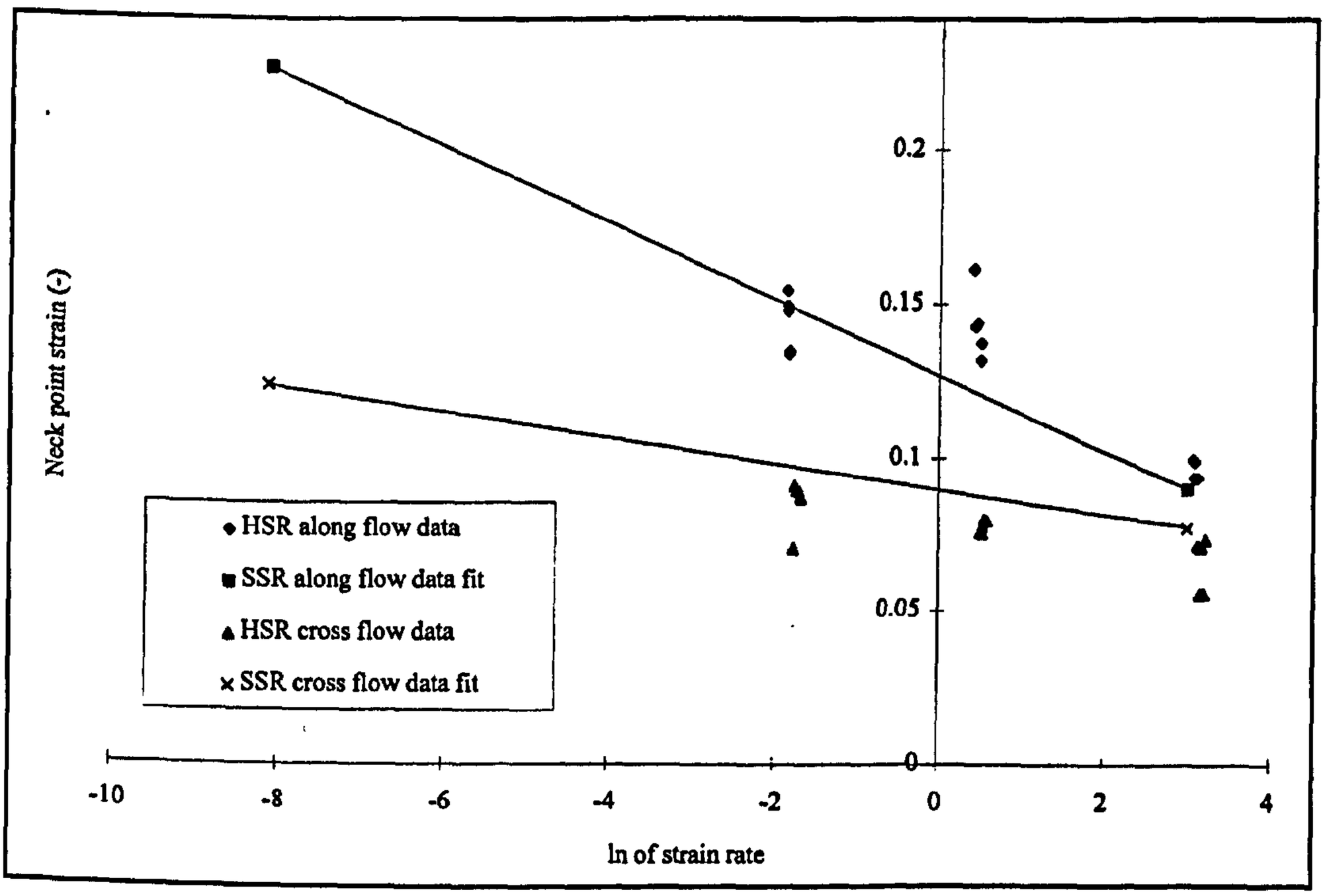

Figure B16 Comparison of ε_n trends - HSR tests

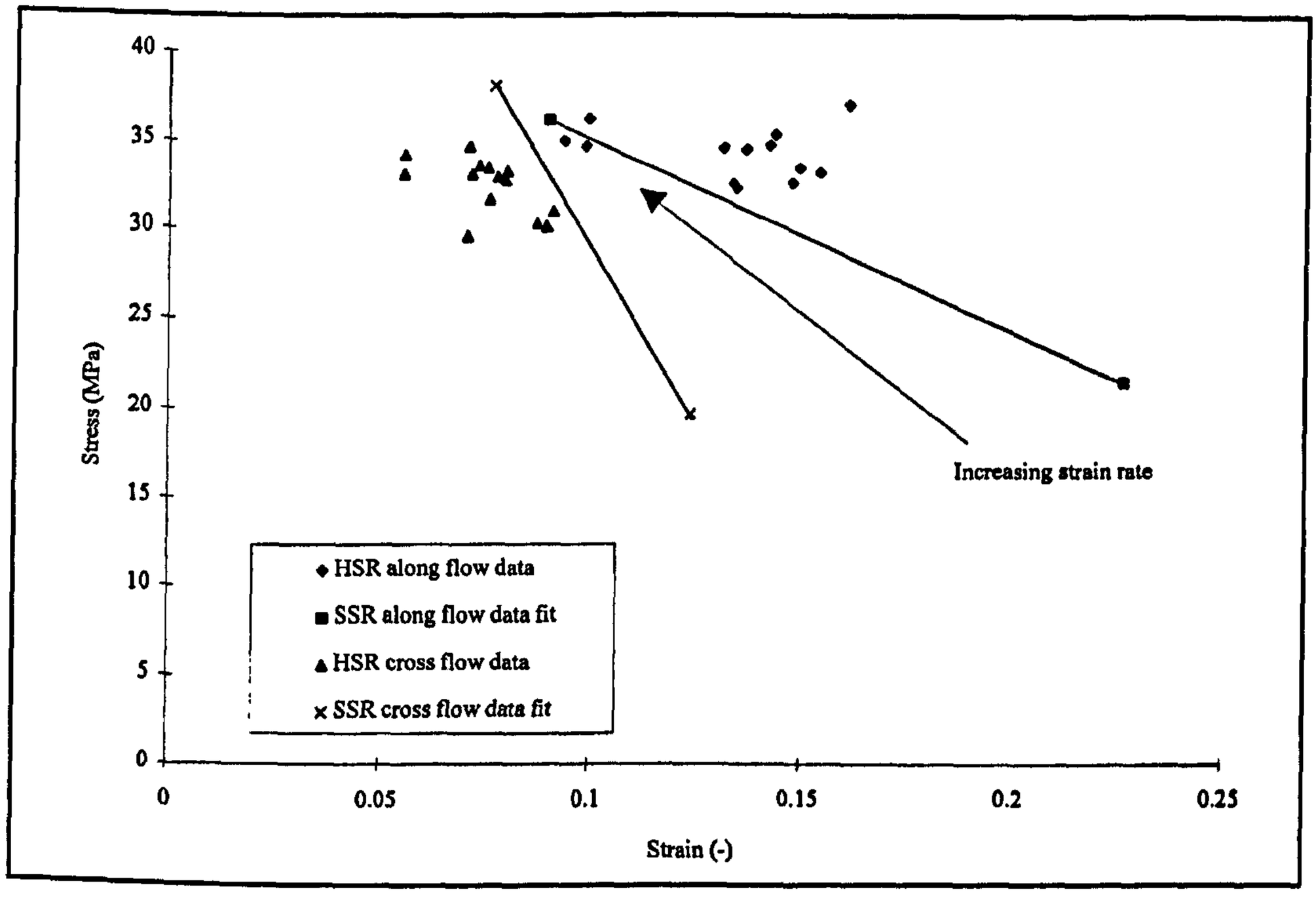

Figure B17 Comparison of neck point trends - HSR tests

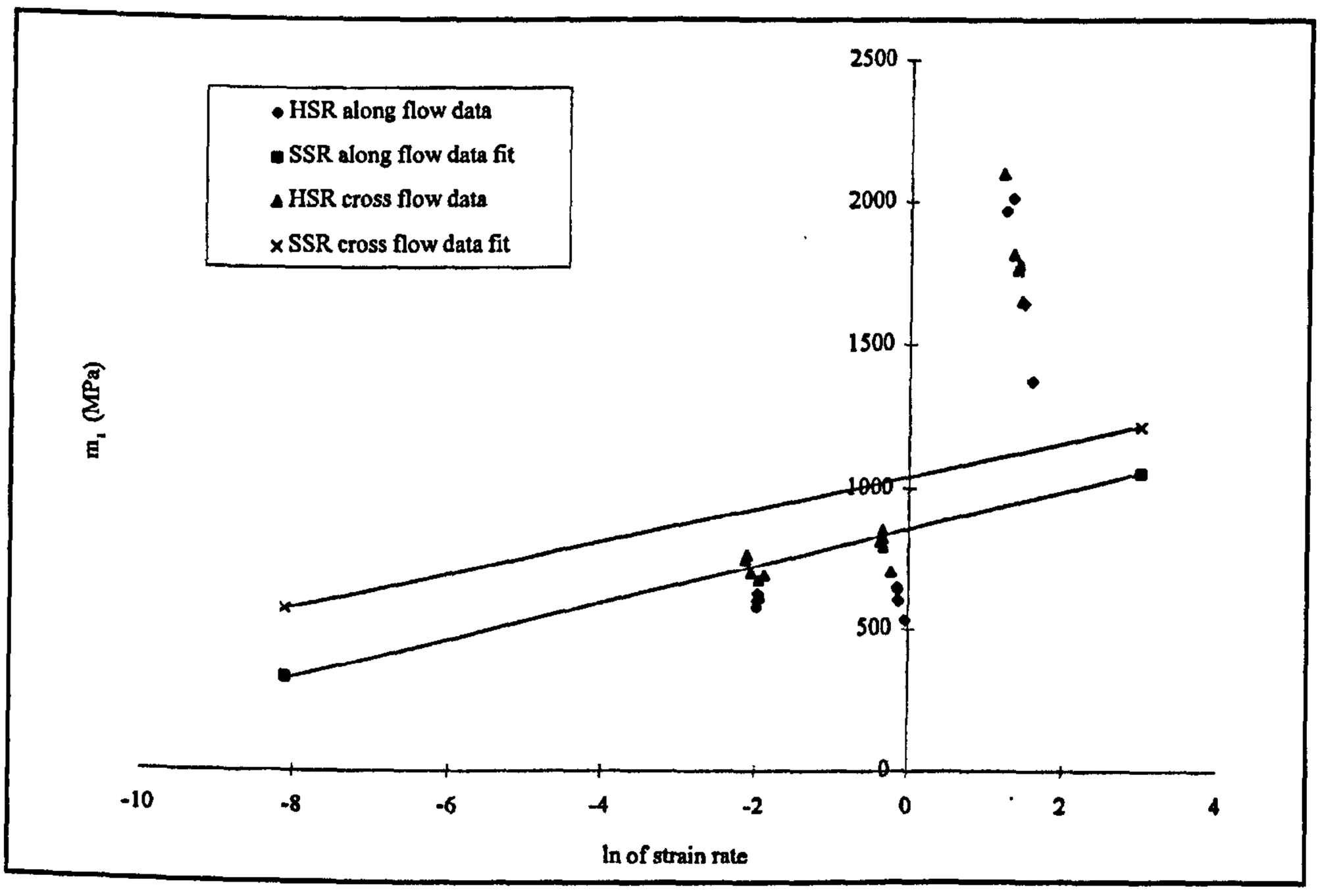

Figure B18 Comparison of m_1 trends - HSR tests

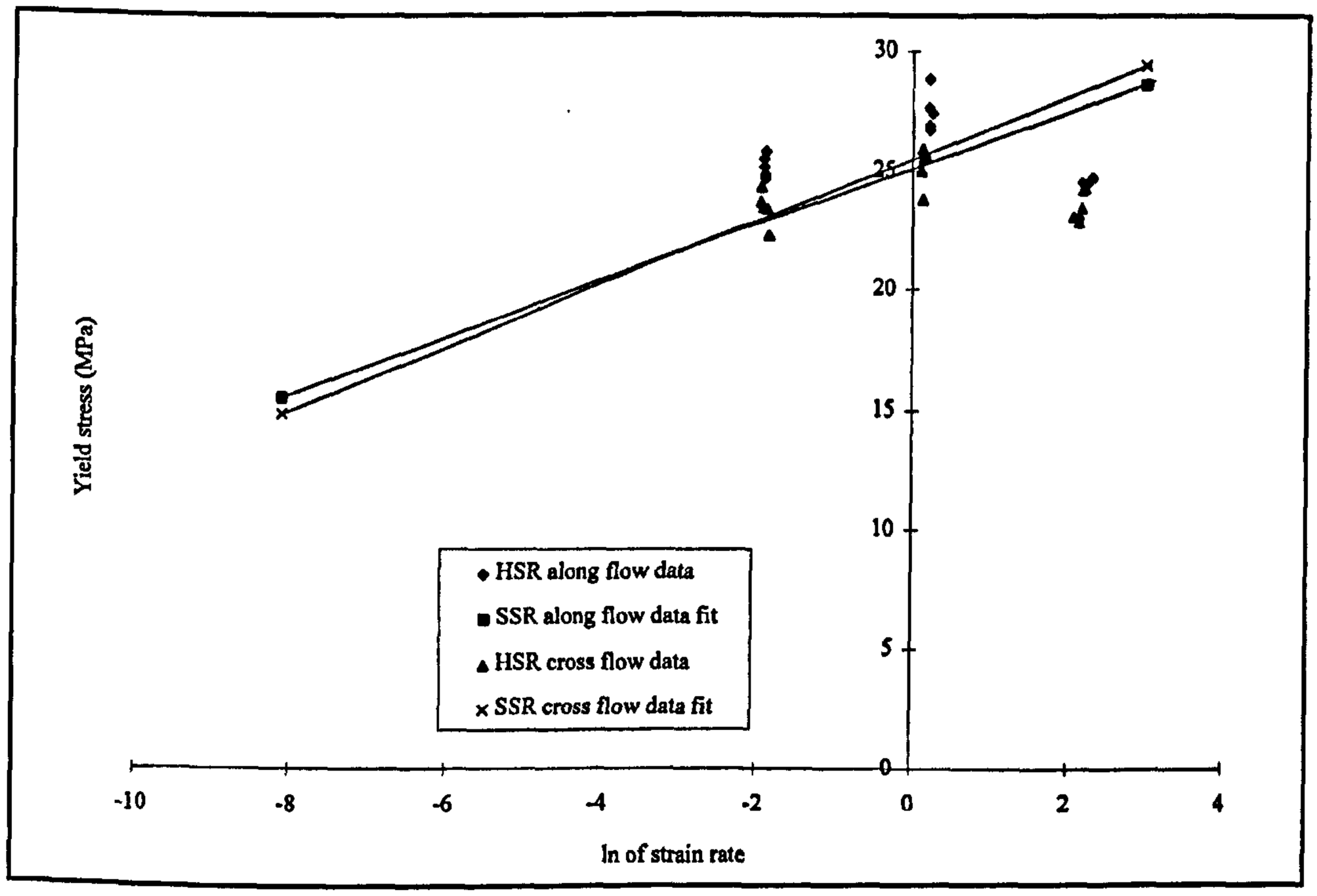

Figure B19 Comparison of σ_y trends - HSR tests

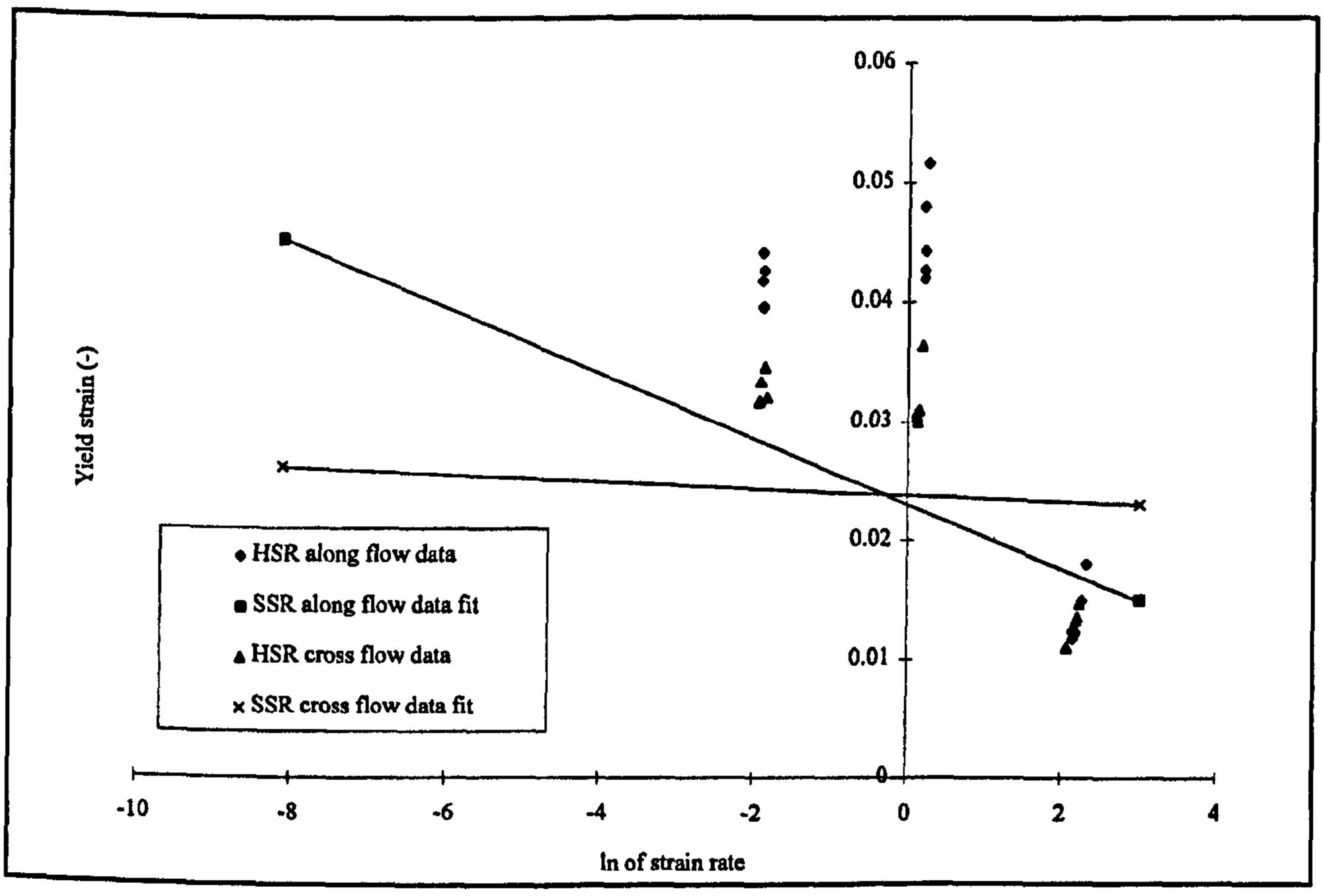

Figure B20 Comparison of ε_y trends - HSR tests

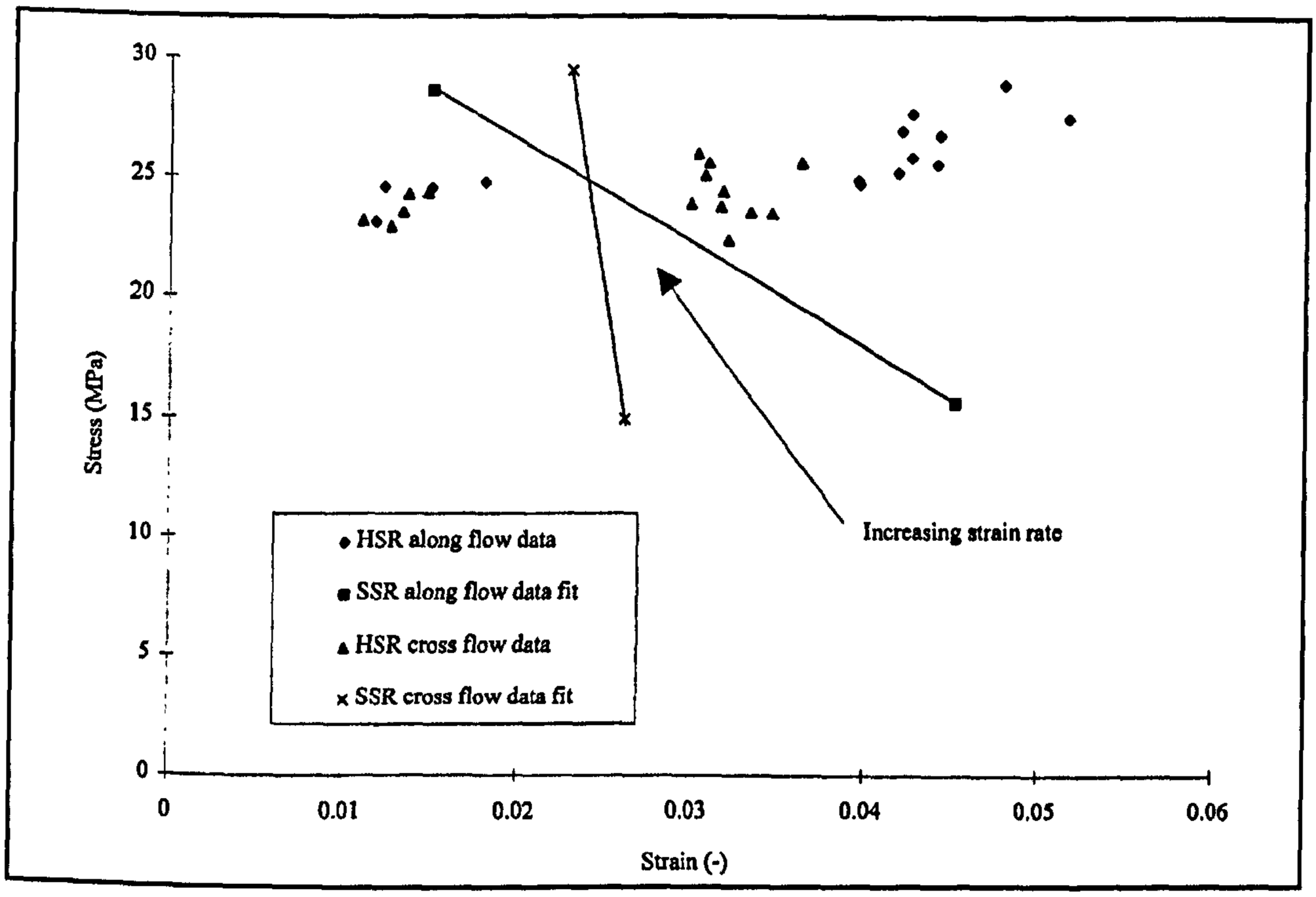

Figure B21 Comparison of yield point trends - HSR tests

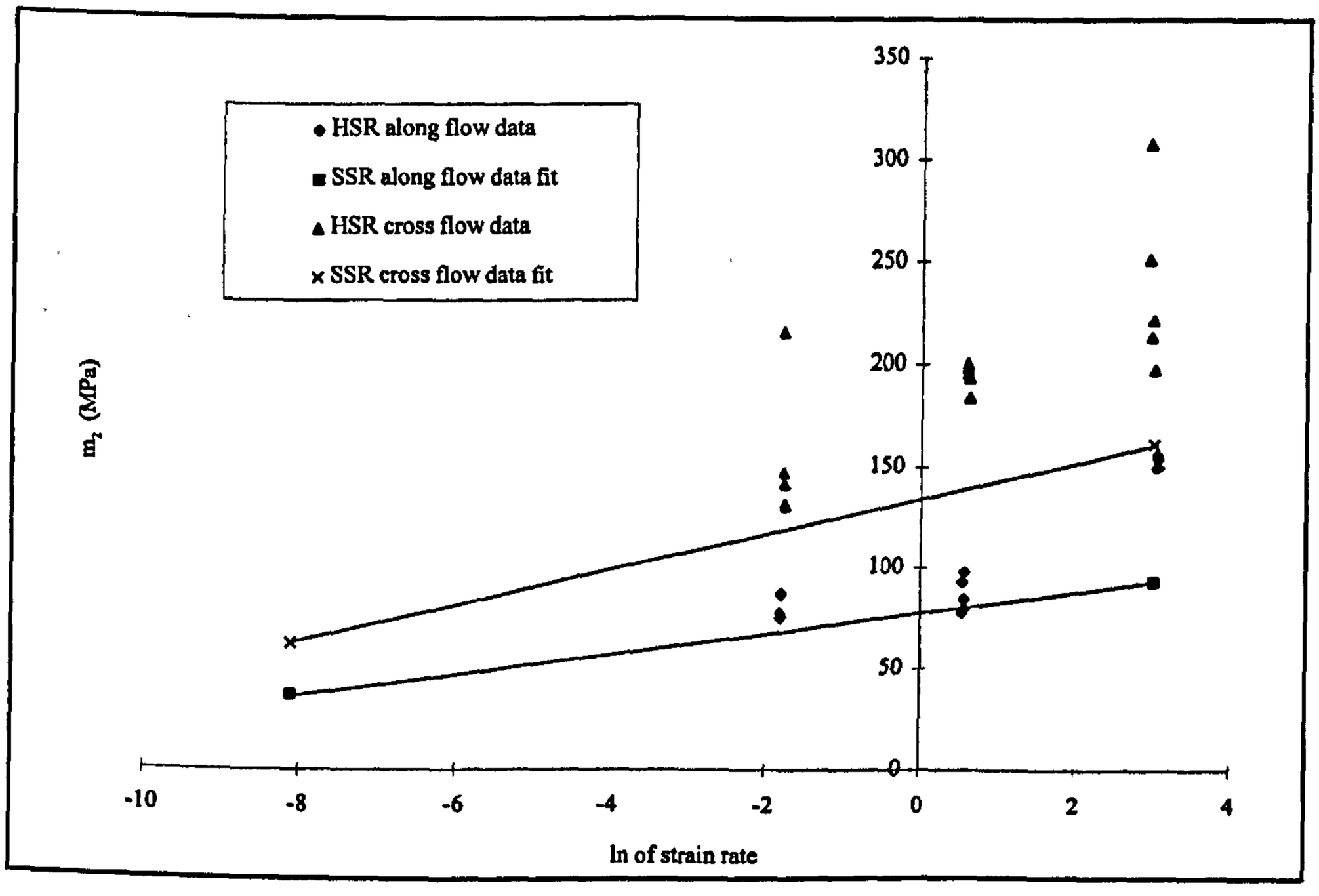

Figure B22 Comparison of m_2 trends - HSR tests

B.3 Subambient HSR tensile tests results

The results of subambient tensile tests at 0° and -40° C are listed in Table B11 to Table B18. Table B11 to Table B14 list the neck point true stress and strain and Table B15 to Table B18 list the bi-linear curve fit parameters of the "along" and "cross" flow tests respectively.

Sample No.	C/H velo (m/s)	$\dot{\varepsilon}$ (s^{-1})	ε_n (-)	σ_n (MPa)
16	0.01	0.166	0.1164	39.7231
17	0.01	0.1606	0.1137	37.3819
18	0.01	0.1597	0.1325	40.3164
19	0.01	0.1664	0.117	40.4638
20	0.01	0.1626	0.1166	39.7778
21	0.1	1.5661	0.0996	41.0015
22	0.1	1.1195	0.0842	39.1542
23	0.1	1.6717	0.1139	40.8334
24	0.1	1.6892	0.1102	40.7239
25	0.1	1.6657	0.0845	39.3723
26	1	24.5775	0.0962	43.9571
27	1	23.9431	0.0494	41.3598
28	1	23.6585	0.0698	42.6538
29	1			
30	1	22.9301	0.0769	42.6617

Table B11 0°C HSR "along" flow samples neck point data

Sample No.	C/H velo (m/s)	$\dot{\varepsilon}$ (s^{-1})	ε_n (-)	σ_n (MPa)
66	0.01	0.1746	0.0692	37.8839
67	0.01	0.1816	0.07	38.9533
68	0.01	0.1711	0.0688	37.5782
69	0.01	0.1674	0.067	38.7106
70	0.01	0.1653	0.0661	40.4316
71	0.1			
72	0.1	1.7747	0.0711	40.4494
73	0.1	1.5832	0.0634	40.9278
74	0.1	1.681	0.0666	39.9376
75	0.1	1.6476	0.0771	41.2061
76	1	21.3962	0.0576	43.6485
77	1	21.6526	0.0573	43.1962
78	1	20.4924	0.0578	44.6286
79	1			
80	1			

Table B12 0°C HSR "cross" flow samples neck point data

Sample No.	C/H velo (m/s)	$\dot{\varepsilon}$ (s^{-1})	ε_n (-)	σ_n (MPa)
31	0.01	0.1547	0.1186	52.1739
32	0.01	0.1748	0.1004	51.4416
33	0.01	0.1843	0.0838	52.6751
34	0.01	0.1775	0.0823	50.7158
35	0.01			
36	0.1			
37	0.1	1.6168	0.0901	58.4075
38	0.1	1.6615	0.0901	53.5919
39	0.1	1.7412	0.1056	53.2015
40	0.1	1.7183	0.0943	53.4842
49	1	23.0727	0.0678	55.1991
42	1	21.4602	0.0486	59.1204
43	1			
44	1	22.8333	0.0501	52.1232
45	1	21.6391	0.0607	56.4092

Table B13 -40°C HSR "along" flow samples neck point data

Sample No.	C/H velo (m/s)	$\dot{\varepsilon}$ (s^{-1})	ε_n (-)	σ_n (MPa)
81	0.01	0.1542	0.0535	50.6454
82	0.01	0.1496	0.052	51.4382
83	0.01	0.1634	0.0559	49.5829
84	0.01	0.1886	0.0627	53.0176
85	0.01	0.1681	0.064	52.0648
86	0.1	1.6505	0.0634	54.6102
87	0.1	1.5305	0.0619	52.2841
88	0.1	1.6524	0.0614	55.5469
89	0.1	1.626	0.0538	52.7689
90	0.1	1.492	0.0616	55.0536
91	1	21.1004	0.0476	56.6456
92	1	21.4386	0.0556	57.701
93	1	20.4364	0.047	57.7658
94	1	19.5634	0.0469	58.0532
95	1	20.6413	0.0482	56.6286

Table B14 -40°C HSR "cross" flow samples neck point data

Sample No.	C/H velo (m/s)	$\dot{\varepsilon}$ (s^{-1})	m_1 (MPa)	σ_y (MPa)	$\dot{\varepsilon}$ (s^{-1})	m_2 (MPa)
16	0.01	0.0709	884.143	31.5639	0.167	112.812
17	0.01	0.1644	1034.79	30.2159	0.1676	92.2829
18	0.01	0.0688	872.374	31.9289	0.1636	95.4197
19	0.01	0.0685	813.441	29.9346	0.1658	144.955
20	0.01	0.06	940.622	32.2633	0.1654	103.184
21	0.1	0.08664	915.04	32.1179	1.7389	154.502
22	0.1	0.7614	996.556	29.797	1.154	216.15
23	0.1	0.6789	735.157	32.935	1.7276	123.795
24	0.1	0.6165	830.917	33.486	1.7234	117.905
25	0.1	0.524	933.51	30.5258	1.767	194.687
26	1	3.0073	2600.98	33.2925	22.4773	151.516
27	1	41.2839	4429.86	28.7941	19.2746	316.956
28	1	11.9922	4204.03	29.4282	18.4808	248.799
29	1					
30	1	11.5656	3308.86	32.0959	19.8934	183.168

Table B15 0°C HSR "along" flow samples bi-linear data

Sample No.	C/H velo (m/s)	$\dot{\varepsilon}$ (s^{-1})	m_1 (MPa)	σ_y (MPa)	$\dot{\varepsilon}$ (s^{-1})	m_2 (MPa)
66	0.01	0.0583	961.224	30.0863	0.1723	235.451
67	0.01	0.0627	906.48	31.6362	0.1633	247.385
68	0.01	0.0516	1013.48	29.3909	0.1701	237.289
69	0.01	0.0517	1075.46	30.4355	0.1722	245.305
70	0.01	0.0505	1114.37	31.3139	0.1727	272.998
71	0.1	0	0	0	0	0
72	0.1	0.6369	995.577	32.854	1.7762	239.03
73	0.1	1.0078	1294.38	31.324	1.8237	288.101
74	0.1	1.3197	1156.83	31.003	1.805	286.011
75	0.1	1.074	1190.11	32.4899	1.7715	205.937
76	1	16.7586	2889.39	32.0722	17.3721	306.587
77	1	12.13	3798.44	29.6278	17.2289	328.337
78	1	12.9107	2392.44	34.9296	17.8067	265.457
79	1	0	0	0	0	0
80	1	0	0	0	0	0

Table B16 0°C HSR "cross" flow samples bi-linear data

Sample No.	C/H velo (m/s)	$\dot{\varepsilon}$ (s^{-1})	m_1 (MPa)	σ_y (MPa)	$\dot{\varepsilon}$ (s^{-1})	m_2 (MPa)
31	0.01	0.1564	1337.16	42.3881	0.1665	122.365
32	0.01	0.1559	1486.28	42.9536	0.1711	132.688
33	0.01	0.1563	1392.96	40.3957	0.1722	252.74
34	0.01	0.1539	1588.01	41.6059	0.171	183.377
35	0.01	0	0	0	0	0
36	0.1	0	0	0	0	0
37	0.1	1.3657	1391.63	46.8981	1.7608	213.008
38	0.1	1.307	1414.2	44.406	1.788	181.716
39	0.1	1.5134	1176.54	44.4731	1.744	149.921
40	0.1	1.3156	1340.02	44.7567	1.7431	166.987
49	1	4.5472	2577.54	42.014	19.4065	322.913
42	1	6.7179	4488.45	43.0891	16.7687	514.743
43	1	0	0	0	0	0
44	1	4.2309	2554.69	37.5539	17.1063	519.987
45	1	4.9135	2445.95	42.315	17.9261	410.312

Table B17 -40°C HSR "along" flow samples bi-linear data

Sample No.	C/H velo (m/s)	$\dot{\varepsilon}$ (s^{-1})	m_1 (MPa)	σ_y (MPa)	$\dot{\varepsilon}$ (s^{-1})	m_2 (MPa)
81	0.01	0.136	1793.73	38.9238	0.1691	430.587
82	0.01	0.1676	1789.44	39.5467	0.1683	461.63
83	0.01	0.0889	1788.18	38.8034	0.1713	373.643
84	0.01	0.092	1552.04	42.3708	0.165	365.842
85	0.01	0.1156	1598.35	42.1965	0.1687	318.229
86	0.1	1.1122	1746.36	43.6591	1.756	349.19
87	0.1	1.1667	1647.17	41.3439	1.7449	357.08
88	0.1	0.9977	1980.38	43.1723	1.8107	382.688
89	0.1	0.9172	2050.46	38.5487	1.7901	482.542
90	0.1	0.9196	1968.48	42.7159	1.8561	368.193
91	1	4.2756	3021.67	38.9796	16.1514	635.473
92	1	4.8312	2609.15	43.051	17.4042	479.265
93	1	3.9518	3062.06	40.4191	16.474	642.819
94	1	3.7747	3537.47	39.2659	15.5308	648.852
95	1	3.5519	3569.52	39.2647	16.2497	586.371

Table B18 -40°C HSR "cross" flow samples bi-linear data

B.4 Error between SSR tensile test data extrapolation and HSR test data

The HSR test data was compared with the temperature factored SSR data and Table B19 to Table B21 list the errors between the two sets of data.

	C/H velocity (m/s)		
	0.01	0.1	1
Along flow			
m_1	-0.16816	-0.28831	0.84247
ε_y	0.46842	1.02845	-0.16586
σ_y	0.09830	0.08104	-0.13130
m_2	0.16809	0.07138	0.63471
ε_n	-0.03636	0.18215	0.06983
σ_n	0.10355	0.07371	-0.03064
Cross flow			
m_1	-0.2235	-0.2196	0.62928
ε_y	0.33877	0.32911	-0.43956
σ_y	0.01825	-0.01949	-0.16685
m_2	0.29257	0.39106	0.48412
ε_n	-0.11785	-0.11109	-0.14223
σ_n	-0.00148	-0.03543	-0.12104

Table B19 HSR 23°C average errors

	C/H velocity (m/s)		
	0.01	0.1	1
Along flow			
m_1	-0.12806	-0.32927	1.15067
ε_y	0.31660	0.89929	-0.37371
σ_y	0.13003	0.05410	-0.10412
m_2	0.06872	0.43894	0.60410
ε_n	-0.03659	-0.02285	-0.08108
σ_n	0.10679	0.02356	-0.02335
Cross flow			
m_1	-0.20046	-0.23293	0.74864
ε_y	0.29033	0.94537	-0.10952
σ_y	0.06836	-0.03186	-0.13117
m_2	0.43054	0.25125	0.28812
ε_n	-0.20812	-0.11366	-0.06188
σ_n	0.02019	-0.05652	-0.03374

Table B20 HSR 0°C average errors

	C/H velocity (m/s)		
	0.01	0.1	1
Along flow			
m_1	-0.09347	-0.30226	0.36751
ε_y	0.29033	0.94537	-0.10952
σ_y	0.09934	0.06215	-0.20383
m_2	0.05940	-0.06772	0.67770
ε_n	0.08768	0.21458	0.02606
σ_n	0.11285	0.02406	-0.02297
Cross flow			
m_1	-0.14630	-0.17122	0.29534
ε_y	0.21891	0.18106	-0.30496
σ_y	0.02999	-0.05429	-0.16792
m_2	0.41299	0.19458	0.61654
ε_n	-0.18108	-0.04740	-0.11709
σ_n	0.00933	-0.05543	-0.10931

Table B21 HSR -40°C average errors

Appendix C

Tensile and compressive HSR flow stress measurements

The curve fits of the SHPB flow stress measurements in Dioh's thesis [38] are collated in Tables C1 and C2. The SHPB flow stress curve fit constants, for Equation (11), are shown in Table C3. The accuracy of the curve fit can be seen in Tables C4 and C5 where the deviation between the empirical equation and the experimental curve fits can be seen to be -5.161 to 6.149% for HDPE and -2.723 to 2.002% for MDPE. The comparison of the HDPE and MDPE SHPB flow stress is shown in Table C6.

	Temperature °C		
Strain rate	-20	0	23
	5% strain		
$1x10^{-4}$	32.8	25	15.3
$1x10^{+4}$	60.8	52.2	41.9
	10% strain		
$1x10^{-4}$	36.2	29.5	20.2
$1x10^{+4}$	61.7	54	44.1
	15% strain		
$1x10^{-4}$	38.1	31.1	21.4
$1x10^{+4}$	62.8	55	44.7

Table C1 HDPE SHPB flow stress data (MPa) [38]

	Temperature °C		
Strain rate	-20	0	23
	5% strain		
$1x10^{-4}$	28.4	20.2	11.9
$1x10^{+4}$	53.5	43.9	34.8
	10% strain		
$1x10^{-4}$	31.7	23.9	15.0
$1x10^{+4}$	56.1	47.2	37.8
	15% strain		
$1x10^{-4}$	34.2	25.8	17.2
$1x10^{+4}$	57.2	48.3	39.7

Table C2 MDPE SHPB flow stress data (MPa) [38]

a_1	a_2	a_3	b_1	b_2	b_3
HDPE					
-0.40677	41.8333	147.6487	-0.00184	1.791465	2.056386
MDPE					
-0.40526	49.5	140.9123	-0.00179	0.669537	1.825317

Table C3 SHPB flow stress curve fit constants

	Temperature °C		
Strain rate	-20	0	23
	5% strain		
$1x10^{-4}$	0.618	0.826	6.149
$1x10^{+4}$	-0.241	-0.040	1.274
	10% strain		
$1x10^{-4}$	-0.775	-4.667	-5.161
$1x10^{+4}$	0.357	-1.026	-0.906
	15% strain		
$1x10^{-4}$	1.932	-0.194	3.150
$1x10^{+4}$	0.616	-0.523	0.597

Table C4 HDPE SHPB flow stress fit (% difference)

	Temperature °C		
Strain rate	-20	0	23
	5% strain		
$1x10^{-4}$	0.441	2.722	-0.771
$1x10^{+4}$	-0.580	1.948	0.733
	10% strain		
$1x10^{-4}$	-1.235	-1.535	-2.723
$1x10^{+4}$	-1.325	-0.590	-1.530
	15% strain		
$1x10^{-4}$	-0.316	2.002	1.017
$1x10^{+4}$	0.565	1.632	-0.785

Table C5 MDPE SHPB flow stress fit (% difference)

	Temperature °C		
Strain rate	-20	0	23
	5% strain		
$1x10^{-4}$	-13.57	-17.68	-27.29
$1x10^{+4}$	-12.31	-14.23	-17.39
	10% strain		
$1x10^{-4}$	-12.84	-16.32	-23.83
$1x10^{+4}$	-10.60	-12.21	-14.83
	15% strain		
$1x10^{-4}$	-12.22	-15.22	-21.29
$1x10^{+4}$	-8.96	-10.28	-12.41

Table C6 Comparison of MDPE and HDPE curve fit data (% difference)

The following Tables C7 to C9 and C10 to C15 contain the flow stress measurements that were extracted from the slow strain rate and high strain rate tensile data measured at the ATC and NPL. The curve fit parameters for this data in Equation (11) are shown in Table C16. Figures C1 to C4 show the comparison of the tensile test data with the SHPB data.

Sample No.	C/H velocity (mm/min)	Stress (MPa) @ 5% strain	Strain rate (s^{-1})	Stress (MPa) @ 10% strain	Strain rate (s^{-1})
1	50	20.0042	0.01907	23.9657	0.02365
2	50	21.2374	0.01821	25.0246	0.02106
3	50	21.1253	0.01655	25.0616	0.01884
4	50	21.047	0.01788	25.0594	0.02115
5	5	16.9577	0.00173	20.6871	0.00205
6	5	16.5818	0.00175	20.3964	0.00206
7	5	16.2745	0.0017	20.3038	0.00202
8	5	16.4288	0.00164	20.3823	0.002

Table C7 SSR tensile flow stress data @ 23°C - Rover tank samples

Sample No.	C/H velocity (mm/min)	Stress (MPa) @ 5% strain	Strain rate (s^{-1})	Stress (MPa) @ 10% strain	Strain rate (s^{-1})
1	100	21.5474	0.03973	26.0996	0.04216
2	100	21.3555	0.04106	25.9087	0.04515
3	100	21.2184	0.04239	25.8591	0.04681
4	50	19.8248	0.0181	24.1714	0.02031
5	50	20.1736	0.01803	24.5793	0.02015
6	50	20.0305	0.01841	24.5385	0.02069
7	10	17.0448	0.00353	21.3912	0.00391
8	10	17.3416	0.00365	21.5922	0.00409
9	10	16.8289	0.00341	21.2727	0.00373
10	5	16.1832	0.00173	20.4061	0.00196
11	5	16.2422	0.00179	20.5097	0.00197
12	5	16.1619	0.00169	20.3395	0.00189
13	1	13.4491	0.00033	17.4891	0.00036
14	1	14.3626	0.00036	18.4672	0.00038
15	1	13.9312	0.00036	17.857	0.00037

Table C8 SSR tensile flow stress data @ 23°C - "along" flow samples

Sample No.	C/H velocity (mm/min)	Stress (MPa) @ 5% strain	Strain rate (s^{-1})	Stress (MPa) @ 10% strain	Strain rate (s^{-1})
51	100	23.9441	0.03987	28.0692	0.0497
52	100	24.0296	0.03759		
53	100	23.5457	0.04117	27.4585	0.04152
54	50	22.9255	0.01664	26.4902	0.01752
55	50	22.7762	0.01772	26.2849	0.01986
56	50	23.2968	0.01691	26.7394	0.01706
57	10	19.8835	0.00345	23.3995	0.00391
58	10	20.4006	0.00345	23.9063	0.00393
59	10	19.2659	0.00333	22.9758	0.00366
60	5	19.085	0.00169	22.5005	0.00195
61	5	19.3879	0.00166	22.9147	0.00192
62	5	18.2532	0.00166	21.9927	0.00183
63	1	16.5644	0.00034	20.001	0.00038
64	1	16.4894	0.00032	19.7669	0.00037
65	1	15.6752	0.00033	19.1046	0.00039

Table C9 SSR tensile flow stress data @ 23°C - "cross" flow samples

Sample No.	C/H velocity (m/s)	Stress (MPa) @ 5% strain	Strain rate (s^{-1})
1	0.01	24.2643	0.1723
2	0.01	24.4741	0.1734
3	0.01	24.3587	0.1737
4	0.01	24.0135	0.1725
5	0.01	23.7923	0.1743
6	0.1	26.3002	1.8277
7	0.1	27.0502	1.8202
8	0.1	25.384	1.8175
9	0.1	26.6465	1.8102
10	0.1	26.3009	1.8255
11	1		
12	1	31.0663	22.1067
13	1	31.7991	22.552
14	1	31.1234	22.2914
15	1	30.911	21.8303

Table C10 HSR tensile flow stress data @ 23°C - "along" flow samples

Sample No.	C/H velocity (m/s)	Stress (MPa) @ 5% strain	Strain rate (s^{-1})
51	0.01	26.282	0.1654
52	0.01	26.5256	0.1698
53	0.01	27.0795	0.1727
54	0.01	25.8536	0.1681
55	0.01	26.5036	0.1671
56	0.1	29.4423	1.9254
57	0.1	29.974	1.9194
58	0.1	28.7268	1.8639
59	0.1	30.7109	1.8488
60	0.1	29.0989	1.8493
61	1	32.6368	22.6299
62	1	32.3597	21.6348
63	1	32.3623	22.3326
64	1	33.7716	23.3845
65	1	33.3039	21.9567

Table C11 HSR tensile flow stress data @ 23°C - "cross" flow samples

Sample No.	C/H velocity (m/s)	Stress (MPa) @ 5% strain	Strain rate (s^{-1})
16	0.01	32.6204	0.1745
17	0.01	32.0321	0.174
18	0.01	32.3207	0.1721
19	0.01	31.0544	0.1716
20	0.01	33.4392	0.1703
21	0.1	34.7557	1.8296
22	0.1	34.0936	1.1755
23	0.1	33.2611	1.819
24	0.1	34.5238	1.7941
25	0.1	34.6954	1.8392
26	1	40.9185	23.9129
27	1	41.38	24.0539
28	1	40.3931	20.986
29	1		
30	1	40.2465	22.001

Table C12 HSR tensile flow stress data @ 0°C - "along" flow samples

Sample No.	C/H velocity (m/s)	Stress (MPa) @ 5% strain	Strain rate (s^{-1})
66	0.01	34.9559	0.1724
67	0.01	35.9883	0.1598
68	0.01	34.8118	0.1713
69	0.01	36.1575	0.172
70	0.01	37.7556	0.1734
71	0.1		
72	0.1	37.8614	1.7996
73	0.1	39.4785	1.8362
74	0.1	37.8614	1.7996
75	0.1	39.4785	1.8362
76	1	43.2518	19.9889
77	1	42.3369	20.3192
78	1	43.9202	20.1197
79	1		
80	1		

Table C13 HSR tensile flow stress data @ 0°C - "cross" flow samples

Sample No.	C/H velocity (m/s)	Stress (MPa) @ 5% strain	Strain rate (s^{-1})
31	0.01	44.5285	0.1739
32	0.01	46.3289	0.1706
33	0.01	46.5262	0.1692
34	0.01	46.8305	0.169
35	0.01		
36	0.1		
37	0.1	51.9615	1.8203
38	0.1	48.8272	1.8423
39	0.1	46.6972	1.766
40	0.1	48.3409	1.7583
49	1	53.5582	21.5873
42	1	59.2002	21.6183
43	1		
44	1	52.1161	22.8027
45	1	55.4176	20.4

Table C14 HSR tensile flow stress data @ -40°C - "along" flow samples

Sample No.	C/H velocity (m/s)	Stress (MPa) @ 5% strain	Strain rate (s^{-1})
81	0.01	50.1937	0.1586
82	0.01	51.3086	0.1528
83	0.01	49.0286	0.1666
84	0.01	51.5772	0.1688
85	0.01	50.7361	0.1663
86	0.1	53.1073	1.7829
87	0.1	50.6939	1.7525
88	0.1	54.5924	1.8251
89	0.1	52.4838	1.7206
90	0.1	53.5734	1.8599
91	1	56.7554	21.5535
92	1	57.2086	20.6245
93	1	57.8944	20.873
94	1	58.1594	19.9204
95	1	56.7243	20.8854

Table C15 HSR tensile test flow stress data @ -40°C - "cross" flow samples

a_1	a_2	a_3	b_1	b_2	b_3
Along flow					
-0.35791	94.03057	127.5293	-0.00647	1.997534	3.394904
Cross flow					
-0.37844	79.92594	137.2861	-0.00091	2.173466	1.78557

Table C16 Tensile test flow stress curve fit constants

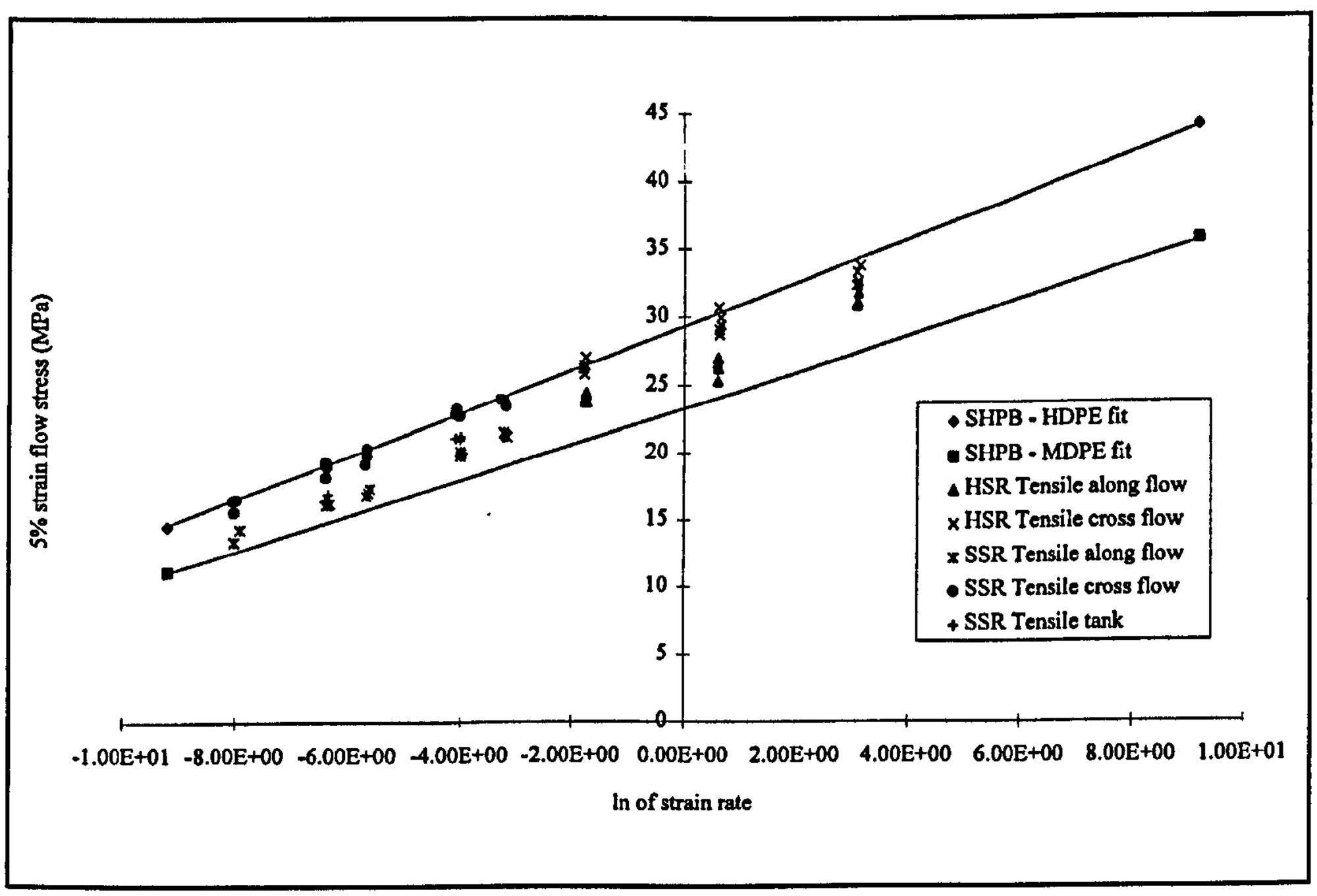

Figure C1 Tensile test/SHPB flow stress comparison @ 5% strain, 23°C

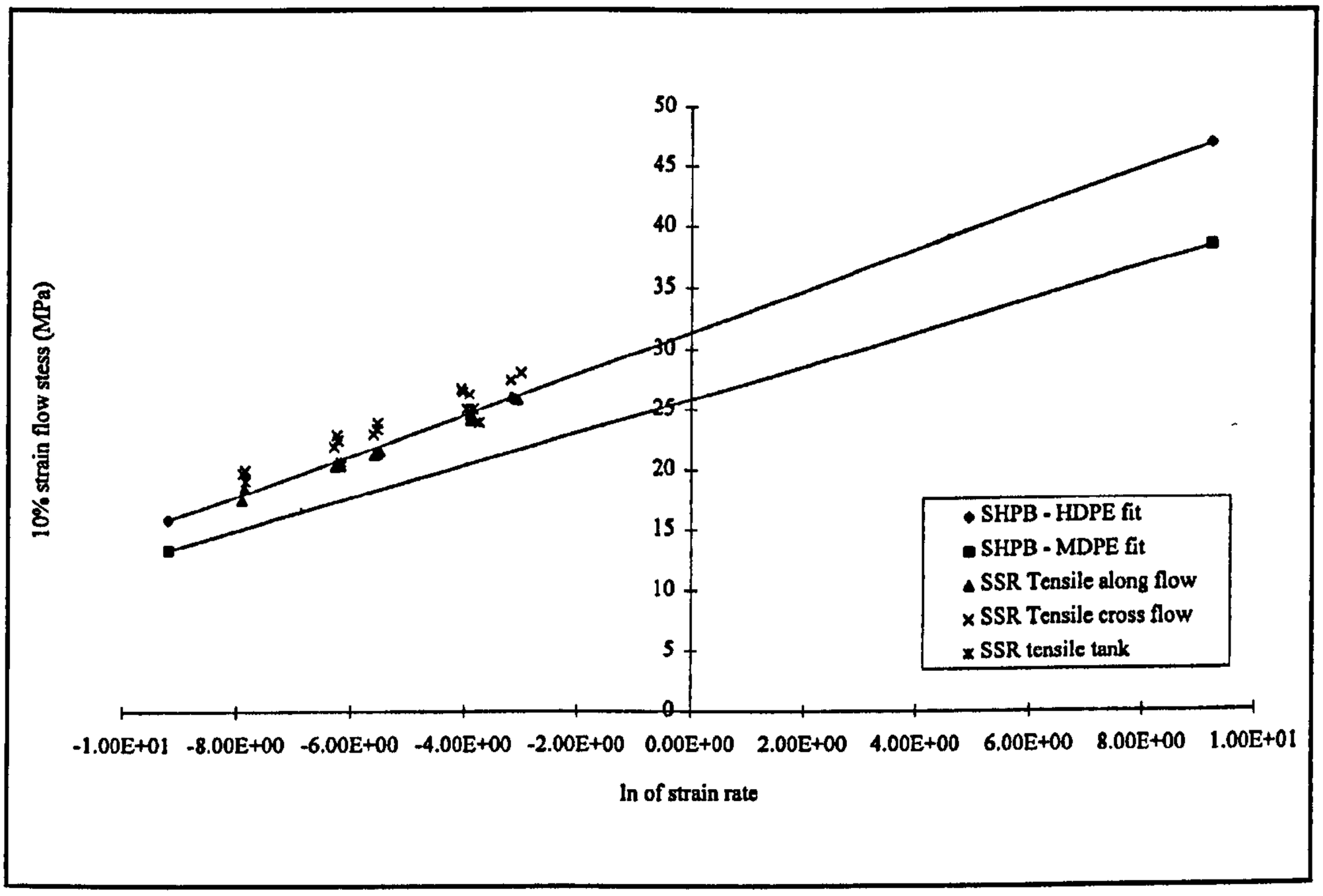

Figure C2 SSR tensile test/SHPB flow stress comparison @ 10% strain, 23°C

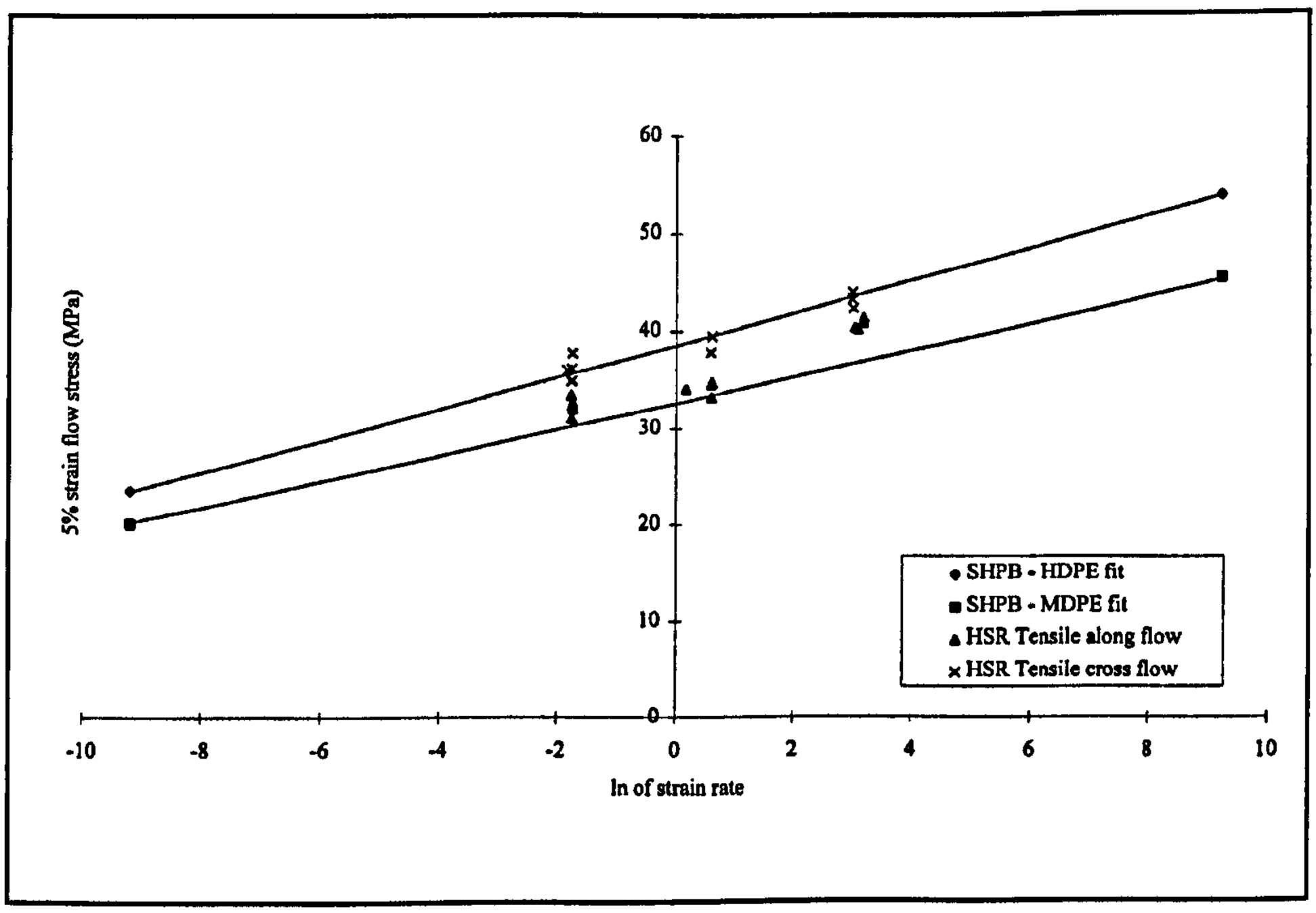

Figure C3 HSR tensile test/SHPB flow stress comparison @ 5% strain, 0°C

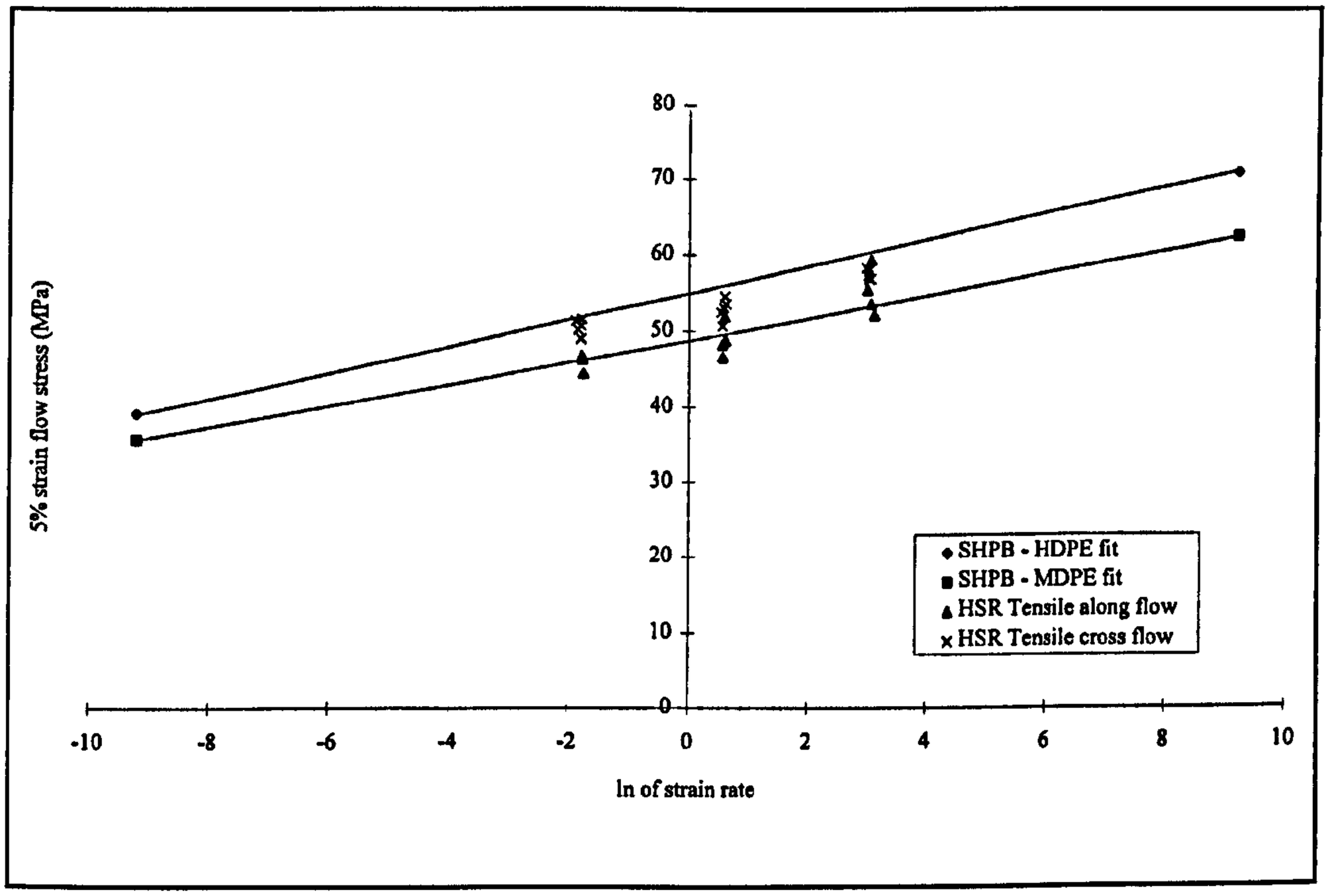

Figure C4 HSR tensile test/SHPB flow stress comparison @ 5% strain, -40°C

Appendix D

Fuel tank test and analysis data

D.1 Typical accelerometer calibration plots

Figures D1 and D2 show typical calibration plots for the accelerometers used for instrumenting the impact test of the thermoplastic fuel tank. The stiffness data used in the impact simulations is shown in Tables D1 to D3. Table D1 lists the elastic constants used for the jig and swinging pendulum. These stiffness were assumed not to vary with temperature. Tables D2 and D3 list the material stiffness data used for the impact simulations of impact tests 1 and 4 respectively. Two sets of data were used due to the different temperatures of the two tests.

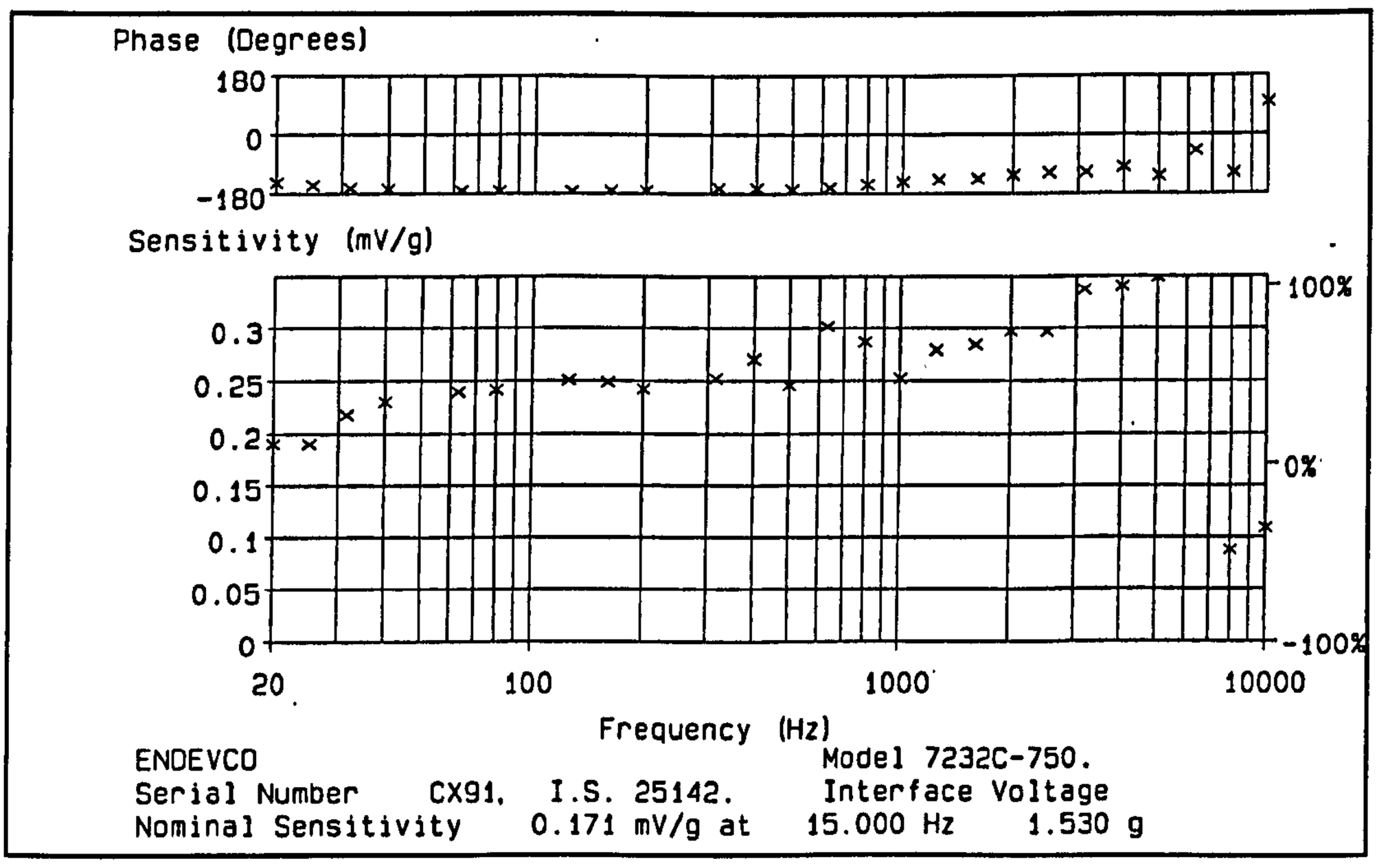

Figure D1 Pendulum accelerometer - calibration plot

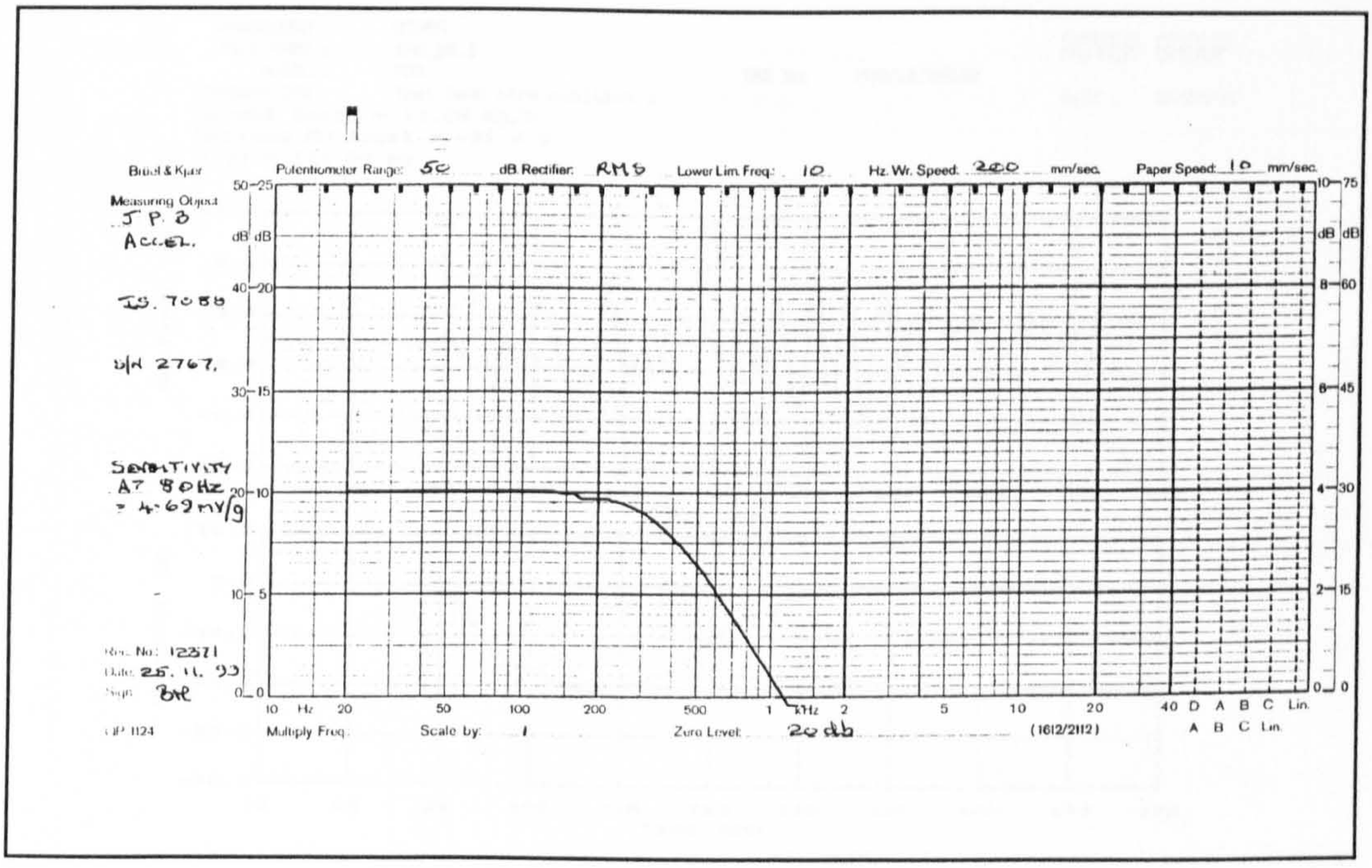

Figure D2 Reaction pillar accelerometer - calibration plot

D.2 Typical impact test acceleration plots

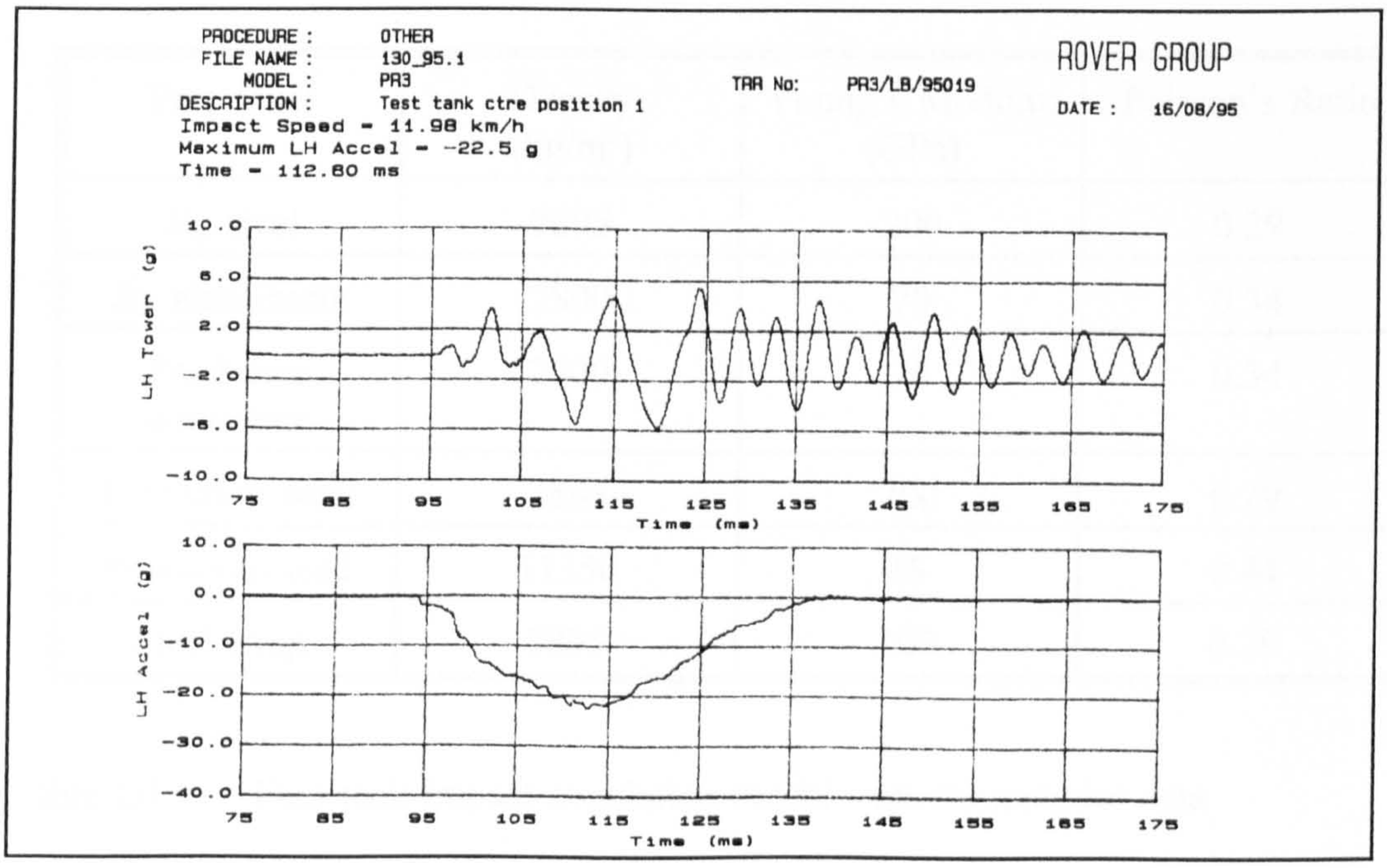

Figure D3 Test 1 - Rover test results plot 1

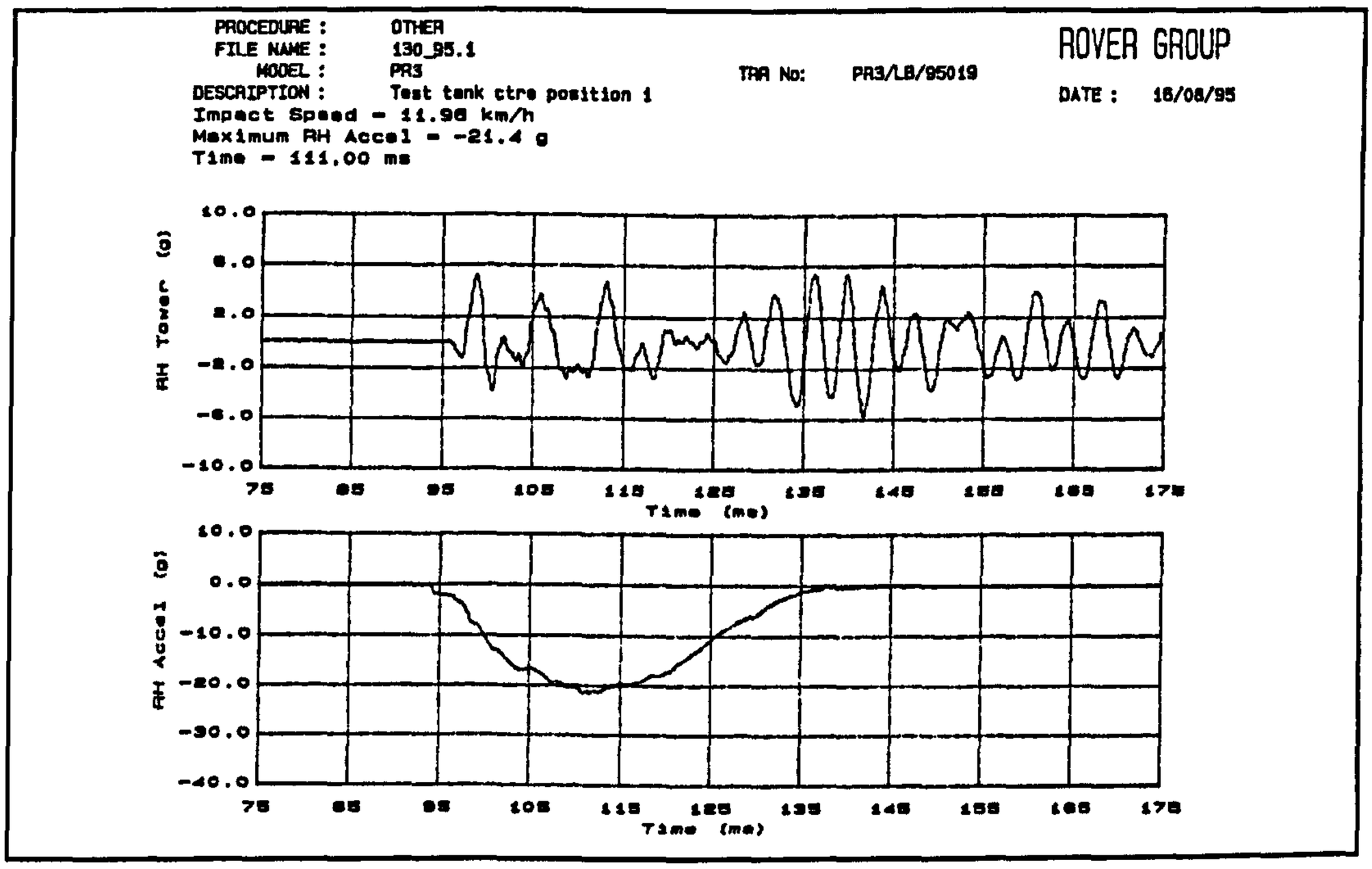

Figure D4 Test 1 - Rover test results plot 2

D.3 Impact simulation material data

Part name	Density (kg/m^3)	Young's Modulus (GPa)	Poisson's Ratio
Jig steel	7895	200	0.29
Jig aluminium	2800	70	0.34
Pendulum aluminum	2800	70	0.34
Pendulum steel	7895	200	0.29
Pendulum lead	11350	18	0.44
Steel straps	7895	200	0.29

Table D1 Fuel tank impact simulation model - elastic material data

Non strain rate dependent properties			
Density = 945 kg/m^3		Poisson's Ratio = 0.465	
Strain rate dependent properties			
Strain rate	Yield stress	Young's Modulus	Hardening modulus
0.0001	12.011	327.97	29.935
0.001	14.508	450.58	41.277
0.01	17.004	573.20	2.618
0.1	19.500	695.81	63.960
1.0	21.997	818.43	75.301
10.0	24.493	941.05	86.642
100.0	26.99	1063.7	97.984
1000.0	29.486	1186.3	109.33
10000.0	31.983	1308.9	120.67
100000.0	34.479	1431.5	132.01
1000000.0	36.976	1554.1	143.35

Table D2 Test 1 impact simulation model - HDPE material data

Non strain rate dependent properties			
Density = 945 kg/m^3		Poisson's Ratio = 0.465	
Strain rate dependent properties			
Strain rate	Yield stress	Young's Modulus	Hardening modulus
0.0001	13.860	385.50	42.180
0.001	16.730	526.70	58.170
0.01	19.600	667.90	74.160
0.1	22.480	809.00	90.150
1.0	25.350	950.20	106.10
10.0	28.230	1091.0	122.10
100.0	31.100	1233.0	138.10
1000.0	33.970	1374.0	154.10
10000.0	36.850	1515.0	170.10
100000.0	39.720	1656.0	186.10
1000000.0	42.590	1797.0	202.10

Table D3 Test 4 impact simulation model - HDPE material data